



UNIVERSITY OF CASSINO AND SOUTHERN LAZIO

Ph.D. in Methods, models and technologies for Engineering  
Civil Engineering curriculum

Cycle XXXIV

# **New approaches for road safety assessment of vulnerable users**

SSD: ICAR-04



**Daniela Santilli**



UNIVERSITY OF CASSINO  
AND SOUTHERN LAZIO

Ph.D. in  
Methods, models and technologies for Engineering  
Civil Engineering curriculum  
Cycle XXXIV

**New approaches for road safety assessment  
of vulnerable users**

SSD: ICAR-04

**Coordinator**

Prof. Fabrizio Marignetti

**Ph.D. Student**

Daniela Santilli

**Supervisor**

Prof. Mauro D'Apuzzo

**A.A.2019/2020**



# **ACKNOWLEDGEMENTS**

# ABSTRACT

The increasingly frequent natural disasters, summed to the pandemic event, have led countries to reorganize their cities, habits, moves. The first step was to implement solutions to limit urban congestion by inducing citizens to prefer more sustainable and active ways. To discourage the use of motorized transport, more and more routes or areas for active users, as pedestrian or cyclists, should be dedicated. In order to conceive a safe and comfortable environment, specific studies and high budget, are needed. Due to the current economical constraints and the increasing need of physical distancing due to the pandemic situation, private and public road managers need procedures that maximize the resources to implement effective and sustainable interventions. It must be said that all the measures and actions implemented so far in the road sector are aimed at reducing the danger of the motorized component, but little has been done for vulnerable users. Unfortunately, in Italy there are still few regulations that can support technicians in the decision-making process. The most common way to solve the safety problem is the use of a systemic approach and this PhD thesis has the main objective of presenting a preliminary methodology for assessing the safety of vulnerable road users. In particular, the framework of the proposed procedure accompanies the sequence of the Chapters, which can be summarized as follows:

- *Introduction*: this chapter presents the need to convert citizens' habits towards sustainability in order to respond to European demands. This requires the evaluation of road safety which can be pursued with different methods proposed in the literature; the one chosen in this study is based on risk analysis.
- *Chapter 1*: deals with risk-based engineering analyzes, created mainly to activate forecasting and prevention measures in response to the damage generated by natural disasters. This made it possible to obtain a general definition of risk which was then extended to many other sectors such as the road sector. Then the different risk factors were identified (then examined in detail in the following chapters).
- *Chapter 2*: notes the relationship between road safety and vehicle speed. a predictive model was developed to estimate the average speed of vehicles (which represents the vehicle exposure factor) as a function of the urban, rural and “transition” environment. This model starts from a recalibration and re-adaptation of the literature models using Floating Car Data (FCD).

- *Chapter 3*: to assess the risk to which users are subjected in a road section, it is necessary to know not only the anthropometric data of the average user but also the exposure of vulnerable users, therefore the pedestrian and cycle flow. To estimate these flows, a hybrid methodology was defined which blends the purely configurational approach with the characteristics of the examination area and a demand-driven methodology.
- *Chapter 4*: to prevent accidents at a site and predict the related consequences, since the data is not always available, a methodology has been proposed that enriches the existing vulnerability functions with the kinematic parameters of multibody simulations.
- *Chapter 5*: once the risk factors were defined, a synthetic index was created. The latter allows to identify and classify the sites providing a prioritization of interventions. To choose the type of countermeasure to be implemented, it is necessary to take into account the characteristics of the road, flows, speeds, the surrounding space, the hierarchy of the roads but also the available economic resources. Then, the most common countermeasures for the safety of pedestrians and cyclists were identified, their estimated average costs were considered and decision-making matrices of choice were proposed. This should allow the designer to have a procedure that, starting from the context and the risk factor, identifies the most convenient and effective countermeasure.
- *Chapter 6*: among the many countermeasures, the one most used in urban areas to reduce the speed of vehicles is traffic calming. In this chapter, attention was focused on altimetric devices, analyzing the effects they produce on the human body (whether used temporarily or permanently, single or in series) using simplified models.

# TABLE OF CONTENTS

ABSTRACT.....	II
List of Figures.....	VIII
List of Tables.....	XVIII
INTRODUCTION.....	20
Sustainable Mobility concept.....	23
Road safety estimation and accident statistics.....	28
References.....	32
CHAPTER 1.    Introduction to risk assessment in road safety for vulnerable users	
35	
1.1    Risk definition.....	35
1.1.1    Risk analysis.....	40
1.2    Road safety risk.....	44
1.2.1    Exposure.....	49
1.2.2    Hazard.....	51
1.2.3    Vulnerability.....	52
1.3    Conclusion.....	53
References.....	54
CHAPTER 2.    Vehicular flows exposure.....	56
2.1    Literature review.....	57
2.1.1    Free flow conditions (or isolated vehicle).....	59
2.1.2    Conditions under traffic.....	63
2.2    Driver behaviour in transition urban-rural area.....	65
2.3    Proposed method for the speed evaluation.....	67
2.4    Results.....	70
2.4.1    Speed analysis in free-flow conditions.....	71
2.4.2    Speed analysis under traffic.....	74
2.5    Statistics.....	76
2.5.1    Descriptive statistics.....	76
2.5.2    Analysis tools.....	77
2.5.3    Removals of outliers.....	81

2.5.4	Influence of buildings and site factors on traffic .....	83
2.6	Conclusion .....	86
	References.....	88
CHAPTER 3.	Pedestrian flows exposure .....	92
3.1	Counting and estimating technologies for non-motorized travel: state of the art 94	
3.1.1	Direct measurement .....	94
3.1.2	Forecasting models.....	99
3.2	Pedestrian flow estimation: configurational approach .....	103
3.2.1	Description of the procedure .....	106
3.2.2	Pedestrian survey .....	119
3.2.3	Results of the forecast analysis .....	126
3.2.4	Comparison between real and forecast data.....	128
3.2.5	Data purification.....	129
3.2.6	Corrective weights .....	130
3.2.7	Generalization of the model .....	139
3.3	The variation of non-motorized flows .....	143
3.4	Estimated cycle/pedestrian flow: demand driven model.....	146
3.4.1	Model of generation or emission.....	149
3.4.2	Distribution model .....	150
3.4.3	Modal choice model.....	150
3.4.4	Route assignment or choice model .....	152
3.5	Conclusions .....	158
	References.....	159
CHAPTER 4.	Road user vulnerabilities .....	167
4.1	Dynamic vehicle-pedestrian collisions .....	168
4.1.1	Pedestrian-vehicle collisions .....	168
4.1.2	Types of free trajectories.....	169
4.1.3	Vehicles characteristics .....	172
4.1.4	Pedestrian's characteristics .....	175
4.2	Proposed Methodology for pedestrian injuries evaluation .....	176
4.2.1	Injury scales .....	179
4.2.2	Conversion of injury thresholds to AIS scale .....	186
4.3	Damage to the vehicle .....	186
4.3.1	Correlations between vehicle damage and collision speed .....	188
4.4	Euro NCAP.....	189

4.4.1	Pedestrian crash tests carried out by Euro NCAP .....	191
4.4.2	The dummies used in crash tests .....	193
4.5	Calibration of numerical multi-body model for the reconstructions of vehicle-pedestrian impacts .....	194
4.6	Software calibration and parametric analysis .....	198
4.6.1	Software calibration .....	198
4.6.2	Other simulations .....	202
4.6.3	Parametric analysis .....	204
4.7	Evaluation of injury level by existing prediction function .....	204
4.8	Conclusions .....	206
	References .....	208
<b>CHAPTER 5. COUNTERMEASURES: DESIGN CHOICES FOR THE PROTECTION OF PEDESTRIANS AND CYCLISTS .....</b>		<b>213</b>
5.1	Risk-based prioritization .....	213
5.1.1	Synthetic index based on risk analysis .....	214
5.2	The pedestrian areas .....	216
5.2.1	Pedestrian crossings .....	219
5.2.2	Total kinetic energy of the vehicular flow .....	220
5.2.3	Proposed procedure .....	221
5.2.4	Pedestrian crossing categories .....	222
5.2.5	Benefit-cost analysis .....	231
5.3	Cycling network design .....	232
5.3.1	Types of cycling path layouts .....	233
5.3.2	Choice of the specific cycling path layout to be adopted .....	236
5.4	Conclusions .....	239
	References .....	239
<b>CHAPTER 6. Punctual countermeasures: traffic calming .....</b>		<b>241</b>
6.1	State of art .....	241
6.1.1	Experimental studies .....	242
6.1.2	Theoretical studies .....	243
6.2	Vibrations' effects on the human body .....	244
6.3	Simulation models .....	250
6.3.1	Input data .....	251
6.3.2	Model validation with irregular profile .....	258
6.3.3	Case study .....	261
6.4	Conclusions .....	285

References.....	286
Appendix A.....	294
Appendix B.....	296
B.1 Historical excursus.....	296
B.2 Effects of frequency on the human body.....	302
B.2.1 International standard relating to exposure to vibrations.....	311
B.3 Exemplary models of vehicles.....	312
B.3.1 Description of mathematical models.....	315
B.3.2 Comparison between the 5 dof model and the decoupled 4 + 1 dof...	324
References.....	329

## LIST OF FIGURES

Figure I.0.1 Symbols of the eight MDGs.....	20
Figure I.0.2 The key concepts of the 2030 agenda .....	21
Figure I.0.3 Sustainable Development Goals (SDGs) .....	22
Figure I.0.4 Allocation of resources for Missions .....	23
Figure I.0.5 Operation diagram of a multimodal service.....	25
Figure I.0.6 Data of deaths in the EU (European Transport Safety Council, 2021)..	29
Figure I.0.7 Dead and injured 2000 to 2020 according to Istat .....	30
Figure I.0.8 Graphic representation of accidents by category in 2019 (source Istat)	30
Figure I.0.9 Graphic representation of accidents by category in 2020 (source Istat)	31
Figure 1.1 Functional forms of the hazard and structural strength probabilities: a) probability density function $p_H(x)$ and probability of non-exceedance a level of structural strength $F_S(x)$ for a given value of the magnitude $x$ ; b) probability of exceedance $\phi_H(x)$ and probability density function of a structural strength $p_S(x)$ for a given value of the magnitude $x$ (modified after (UNDRO, 1979)).	38
Figure 1.2 Sample vulnerability function $\alpha(x)$ in the hypothesis of structural strength as hazard-independent variable; b) probability density function of the magnitude $x_{pH}(x)$ (modified after (UNDRO, 1979)).	39
Figure 1.3 Simplification of vulnerability curve through step function (modified after (UNDRO, 1979)).	39
Figure 1.4 Flow chart adapted from (D.Lgs n°81, 2008).	41
Figure 1.5 Risk matrix .....	43
Figure 1.6 Summary scheme of the procedure. ....	47
Figure 1.7 Possible accident scenarios .....	48
Figure 1.8 illustration of typical cases of auto accidents with bicycle- vehicle. ....	48
Figure 1.9 Possible pedestrian-vehicle impact configuration .....	48
Figure 1.10 Vehicular flow in urban areas. ....	49
Figure 1.11 Vehicular flow in rural areas. ....	49
Figure 1.12 Pedestrian flow .....	50
Figure 1.13 Cycle flow .....	50
Figure 1.14 Street in urban area.....	51

Figure 1.15 Street in rural area .....	51
Figure 1.16 Urban border.....	51
Figure 1.17 Rural border.....	51
Figure 2.1 a) Spot speed values derived from the georeferenced FCD along a selected road alignment presented in a GIS platform. b) diagram describing the speed data, aggregated on a 100 m long section basis and depicted as a function of travelled distance from the administrative urban/rural border with corresponding confidence levels thresholds. ....	66
Figure 2.2 Flowchart of the proposed methodology to develop generalised speed prediction models for two way single carriageway road layouts in urban, rural and “transition” area .....	70
Figure 2.3 The transition length concept. ....	74
Figure 2.4 OLS relationships obtained for $K_{urb}$ and $K_{rur}$ as a function of average useful road width of the road cross-section, Lu. ....	75
Figure 2.5 Comparison between the observed and estimated Time speed under congestion with optimized coefficients (a) and through the generalized calibrated model (b). ....	76
Figure 2.6 STD - Lua correlation.....	78
Figure 2.7 STD – W correlation .....	78
Figure 2.8 STD correlation - n. accesses .....	78
Figure 2.9 STD correlation - n. crossing .....	78
Figure 2.10 STD correlation -% illegal parking .....	79
Figure 2.11 STD correlation -% occupied by buildings .....	79
Figure 2.12 STD correlation - Vs .....	79
Figure 2.13 Standard deviation correlation with flow rate and relative confidence band. ....	82
Figure 2.14 Standard deviation correlation with range for all sites.....	82
Figure 2.15 Correlation between standard deviation and useful arc width. ....	83
Figure 2.16 Correlation between standard deviation and tortuosity. ....	83
Figure 2.17 Correlation between standard deviation and n. accesses.....	83
Figure 2.18 Correlation between standard deviation and n. crossings. ....	83
Figure 2.19 Correlation between standard deviation and percentage of unauthorized parking.....	83
Figure 2.20 Correlation between standard deviation and built-up percentage. ....	83
Figure 2.21 Representation of FCD data at site 5 (source: QGIS) .....	84
Figure 3.1 Carpets with pressure sensors (taken from Google Images) .....	96

Figure 3.2 Infrared sensor (taken from Google Images) .....	97
Figure 3.3 Video surveillance cameras (taken from Google Images) .....	98
Figure 3.4 Software to process and process video images (taken from Google Images) .....	98
Figures 3.5 software that recognizes and counts the movements of objects from a video (taken from Google Images) .....	98
Figures 3.6 facial recognition software (taken from Google Images) .....	98
Figure 3.7 Instant tracking with GPS.....	99
Figure 3.8 Angular variation between the sections of the network .....	105
Figure 3.9 Impedance function for pedestrian movement. ....	107
Figure 3.10 Succession of buffers from the network centroid up to 1600 m away (taken from Qgis). ....	107
Figure 3.11 Table of mean k values for each circular crown .....	108
Figure 3.12 In red the position of the municipality of Cassino in the province of Frosinone (Source: <a href="https://it.wikipedia.org/wiki/Cassino#/media/File:Map_of_city_of_Cassino_(province_of_Frosinone,_region_Lazio,_Italia)">https://it.wikipedia.org/wiki/Cassino#/media/File: Map_of_city_of_Cassino_(province_of_Frosinone,_region_Lazio,_Italia)</a> ..	109
Figure 3.13 Aerial photography Cassino center, study area .....	109
Figure 3.14 Portion of the Cassino center affected by the study. ....	109
Figure 3.15 Flow chart of the proposed methodology.....	110
Figure 3.16 Attributes of Section 1 of the Municipality of Cassino.....	111
Figures 3.17Lazio Region divided into its census sections. The sections of the Municipality of Cassino are selected in yellow .....	111
Figure 3.18 Census sections constituting the municipal territory of Cassino.....	111
Figure 3.19 Addition of the fields "_P1" (Resident Population), "_E3" (Residential Buildings), "_E4" (Commercial Buildings) .....	112
Figure 3.20 Use of Open Street Map in the construction of the pedestrian network (taken from Qgis).....	114
Figure 3.21 Use of Google Satellite in the construction of the pedestrian network (taken from Qgis).....	114
Figure 3.22 Isolated areas of the center as they do not have pedestrian crossings (taken from Qgis).....	115
Figure 3.23 Calculation of a field in the "network centroid" layer, containing as values the average of the resident population of the centroids of the sections within 100 m of each centroid of the network. There are terms of transformation of the Reference Systems (SR).....	116
Figure 3.24 Creations of the centroids of the census sections. ....	117

Figure 3.25 Centroids of the census sections (in blue) and of the sections of the network (in red) (taken from Qgis) .....	117
Figure 3.26 Removal of geometries without information on the resident population (_P1) (taken from Qgis) .....	118
Figure 3.27 ISTAT basket year 2019 (Source: <a href="https://www.istat.it/it/files//2019/02/infograficaPaniere.pdf">https://www.istat.it/it/files//2019/02/infograficaPaniere.pdf</a> - 19/8/2019).....	120
Figure 3.28 Bing Maps Aerial view; on the left, circled in red, the position of the roundabout in the Roman amphitheater area of Cassino and on the right enlarged in detail. (Source: <a href="https://www.arcgis.com/home/webmap/viewer.html?webmap=4628bbe4f10b4a81b41b520ba5cae20">https://www.arcgis.com/home/webmap/viewer.html?webmap=4628bbe4f10b4a81b41b520ba5cae20</a> ) .....	121
Figure 3.29 Google street view, roundabout in the Roman amphitheater area of Cassino, first exit viale Bonomi; second via G. Di Biasio.....	121
Figure 3.30 Pre-holiday route .....	122
Figures 3.31 Weekday route .....	122
Figure 3.32 Placement of devices on the windshield.....	123
Figure 3.33 EXCEL spreadsheet .....	125
Figure 3.34 VLC media player, panel access: Video Effects. ....	125
Figure 3.35 VLC media player, Video Effects, Geometry, Interactive Zoom. ....	125
Figure 3.36 VLC Media Player, Video Effects, Essential. ....	125
Figure 3.37 QGIS representation of pedestrians detected and present on the study path in the weekday scenario. ....	126
Figure 3.38 Thematic representation of the results of the unweighted analysis, with a legend of the Integration values based on the colors. ....	127
Figure 3.39 Thematic representation of the results of the weighted analysis with Pprox, with a legend of the Integration values based on the colors. ....	127
Figure 3.40 Resulting graphs of the survey on the working day .....	129
Figure 3.41 Graphs resulting from the survey on the day before holidays.....	129
Figure 3.42 Graph resulting from the survey on the day before holidays (a) and weekdays (b) not weighted with the singular points to be purified. ....	130
Figure 3.43 Graph resulting from the survey on the non-weighted working day without any singular points .....	130
Figure 3.44 Graph resulting from the survey on the day before a holiday, unweighted without any singular points .....	130
Figure 3.45 Identification of the attractors present in the study area .....	131
Figure 3.46 commercial businesses present on the network.....	131
Figure 3.47 Results with weighted hybrid analysis .....	133

Figure 3.48 Urban and rural transport stops in Cassino .....	134
Figure 3.49 Results with weighted hybrid analysis .....	135
Figure 3.50 Schools present in the study area .....	137
Figure 3.51 Results with weighted hybrid analysis .....	138
Figure 3.52Cassino subdivision into four quadrants with buffer 400.....	139
Figure 3.53 Qgis; Axial_map: divided cassino.....	139
Figure 3.54 Qgis; Axial_map_cassino divided into four quadrants .....	140
Figure 3.55 Resulting graphs relating to the survey on the weekday, simulation without weights. ....	140
Figure 3.56 Resulting graphs relating to the survey on the day before holidays, simulation without weights. ....	141
Figure 3.57 Comparative variability of the automobile (left)(taken from Ryuset al.,2014) and bicycle .....	144
Figure 3.58Pedestrian daily pattern(Lu, T. 2016).....	144
Figure 3.59Crossing crowding ratio .....	145
Figure 3.60 Representative quantities of the pedestrian crossing.....	146
Figure 3.61 Operation of the transport system .....	147
Figure 3.62 Four-stage model.....	149
Figure 3.63 Excel table origin-destination.....	153
Figure 3.64. Graphic rendering of the lines of desire (taken from QGIS).....	153
Figure 3.65 Representation of the 'fixed distance buffer' (taken from QGIS).....	153
Figure 3.66 Representation of the 'fixed distance buffer'. (taken from QGIS).....	154
Figure 3.67 Attribute table returned upon application of the 'intersection' geoprocessing tool.....	154
Figure 3.68 Estimated flows with zero buffer .....	155
Figure 3.69 Estimated flows with 45 m buffer .....	155
Figure 3.70 Flows estimated as the average of the flows obtained with buffers at 0 and 45 m radii .....	155
Figure 3.71 Loaded cycle network representation of flows compared with the geographical reference of the PUT: (taken from QGIS).....	157
Figure 3.72 Estimated flows with zero buffer .....	158
Figure 3.73 Estimated flows with 45 m buffer .....	158
Figure 3.74 Flows estimated as the average of the flows obtained with buffers at 0 and 45 m radii .....	158
Figure 4.1 Center of gravity and diagram of the forces acting on the pedestrian with subsequent motion.....	169

Figure 4.2 Analysis of the WAD (Taken from the text (Vangi & al., 2008)) .....	170
Figure 4.3 Geometric parameters for defining the front of the vehicle .....	172
Figure 4.4 Example of a vehicle with a low front .....	173
Figure 4.5 Example of high front vehicle .....	173
Figure 4.6 Example of a vehicle with a vertical front .....	173
Figure 4.7 Type of front with top view .....	174
Figure 4.8 Risk of death/injury based on age .....	175
Figure 4.9 Positions of the pedestrian with respect to the front of the vehicle.....	176
Figure 4.10 Conceptual scheme adopted in the numerical simulations.....	177
Figure 4.11 Pedestrian kinematics after various vehicle impacts .....	178
Figure 4.12 Percentage of AIS 2 injuries per body region in different countries....	181
Figure 4.13 Percentage of AIS injuries by body region .....	181
Figure 4.14 Impact zones in the primary impact .....	187
Figure 4.15 Example of damage due to the impact of the head on the windshield (Taken from Google images).....	188
Figure 4.16 Example of a fracture caused by the vehicle's bumper .....	188
Figure 4.17 Impact speed and a pedestrian's risk of severe injury or death .....	189
Figure 4.18 Euro NCAP rating levels .....	190
Figure 4.19 Green star rating .....	190
Figure 4.20 Example mapping of the front of the vehicle in relation to pedestrian safety passenger car (Opel corsa) b) SUV (Jeep Renegade) (taken from (EuroNCAP, <a href="https://www.euroncap.com, sd">https://www.euroncap.com, sd</a> )) .....	191
Figure 4.21 Hybrid III mannequins and features .....	191
Figure 4.22 Crash test simulation .....	192
Figure 4.23 Dummy sensors .....	193
Figure 4.24 Multibody model proposed by the software (image taken from the software).....	195
Figure 4.25 In black the parts to be selected and locked .....	196
Figure 4.26 Top view and side view of the dummy placement (Taken from the Software).....	196
Figure 4.27 Color of the single covers in the pre-impact phase and colors of the single bodies in the post-impact phase. (Taken from the software) .....	197
Figure 4.28 Characteristics of the car .....	199
Figure 4.29 Sequence of images that compare the simulated crash-test with that of the article.....	200

Figure 4.30 Graphic-analytical determination of the head’s accelerations provided by the numerical simulation .....	201
Figure 4.31 Comparison of data from simulation and those reported in (Carollo F., 2018) (teenager-SUV).....	202
Figure 4.32 Comparison of the simulation results with those reported in (Carollo F., 2018) (teenager-sedan).....	202
Figure 4.33 Example of ISS probability distribution derived from vulnerability prediction functions.....	205
Figure 4.34 ISS vulnerability model-ISSaverage comparison (teenager-adult pedestrian).....	206
Figure 5.1 Sections prioritization.....	215
Figure 5.2 Shared zone example (taken from Google Images) .....	216
Figure 5.3 Pedestrian precincts example (taken from Google Images).....	217
Figure 5.4 Living street example (taken from Google Images).....	217
Figure 5.5 Example of raised crossing (source Google Images) .....	225
Figure 5.6 Countdown device (source Google Images) .....	226
Figure 5.7 Example animated pictogram (source Google Images) .....	226
Figure 5.8 Crossing at the public transport stop on the cat carriageway .....	227
Figure 5.9 Crossing near public transport stops .....	227
Figure 5.10 Crossing near public transport stops .....	228
Figure 5.11 Crossing near public transport stops .....	228
Figure 5.12 Crossing near public transport stops .....	228
Figure 5.13 Crossing positioning in the presence of cycle paths.....	229
Figure 5.14 Crossing positioning in the presence of cycle paths.....	229
Figure 5.15 Example of an altimetrically staggered crossing (source google Maps loc. Grotte Celoni, RM) .....	230
Figure 5.16 Example of an altimetrically staggered crossing (source google Maps loc. Grotte Celoni, RM) .....	231
Figure 5.17 Example of a CMF table for installing a raised pedestrian crosswalks (from (Federal Highway Administration, 2009)).....	232
Figure 5.18 Example of sharing street space (zone 20).....	234
Figure 5.19 Visual separation of the cycle path by means of horizontal signs.....	234
Figure 5.20 physical separation of the cycle path by railing .....	234
Figure 5.21 Greenway example .....	235
Figure 5.22 Example of cycle lane .....	235
Figure 5.23 Example of one-way Protected cycle path .....	235

Figure 5.24 Example of cycle path .....	236
Figure 5.25 Example of road of 30 Km/h zone .....	236
Figure 5.26 Example of cycle track .....	236
Figure 5.27 Shared-use path example .....	236
Figure 6.1 Various types of waves.....	245
Figure 6.2 principle of superposition (taken from the Handbook of human vibration by MJGriffin) .....	247
Figure 6.3 comparison of displacement, speed and acceleration.....	248
Figure 6.4 difference between peak acceleration, peak to peak and effective value (RMS).....	249
Figure 6.5 Difference between PSD as a function of time and its representation in one-third octave band frequencies.....	253
Figure 6.6 Road profile with a bump 12 feet long and 3 inches high.....	258
Figure 6.7 Irregular profile .....	259
Figure 6.8 RMS as a function of speed for different vehicles .....	259
Figure 6.9 Speed-dependent eVDV for different vehicles .....	259
Figure 6.10 Speed hump (12 feet; 2.5 inch) .....	261
Figure 6.11 Speed hump (12 feet; 3 inch) .....	261
Figure 6.12 Speed hump (22 feet, 3 inch).....	261
Figure 6.13 Speed hump (22 feet; 3.5 inch) .....	262
Figure 6.14 Speed table (22 feet, 3 inch).....	262
Figure 6.15Graphic representation of the correlation between speed and accelerations (RMS and eVDV) on vehicle A .....	263
Figure 6.16 Graphic representation of the correlation between speed and accelerations (RMS and eVDV) on vehicle C .....	263
Figure 6.17Graphic representation of the correlation between speed and accelerations (RMS and eVDV) on vehicle D .....	264
Figure 6.18Graphic representation of the correlation between speed and accelerations (RMS and eVDV) on vehicle E .....	264
Figure 6.19Correlation between speed and accelerations (RMS and eVDV) of the different vehicles on the speed hump.....	265
Figure 6.20Correlation between speed and accelerations (RMS and eVDV) of the different vehicles on the speed hump.....	266
Figure 6.21 Correlation between speed and accelerations (RMS and eVDV) of the different vehicles on the speed hump.....	266

Figure 6.22 Correlation between speed and accelerations (RMS and eVDV) of the different vehicles on the speed hump.....	266
Figure 6.23 Correlation between speed and accelerations (RMS and eVDV) of the different vehicles on the speed table .....	267
Figure 6.24 The V-RMS and V-eVDV diagrams for each vehicle on the speed table .....	269
Figure 6.25 The V-RMS and V-eVDV diagrams for each vehicle on the speed hump .....	269
Figure 6.26 The curve that approximates the V-RMS and V-eVDV bonds is a logistic-sigmoidal.....	270
Figure 6.27 Figure 6.27 The approximation curve of V-RMS and V-eVDV.....	271
Figure 6.28 RMS on traffic calming according to V50 and V85 .....	273
Figure 6.29 Evdv on traffic calming according to V50 and V85.....	273
Figure 6.30 Speed probability distribution and the RMS probability distribution ..	276
Figure 6.31 RMS and Evdv on speed hump (12-14 feet) according to V50 and V85 .....	280
Figure 6.32 The probability distribution of RMS and eVDV .....	280
Figure 6.33 RMS and Evdv on traffic calming according to V50 and V85 .....	284
Figure B.1 Possible forms of speed humps.....	299
Figure B.2 Difference between a speed hump and a speed bump .....	299
Figure B.3 Speed bump example .....	300
Figure B.4 Speed hump example .....	300
Figure B.5 Raised crosswalks example .....	301
Figure B.6 Signal as a function of time of a sinusoid .....	303
Figure B.7 Signal as a function of frequencies for a sine wave.....	303
Figure B.8 Time domain signal for a multi-sine wave .....	304
Figure B.9 Signal in the frequency domain for a multi-sine wave .....	304
Figure B.10 Random signal as a function of time .....	305
Figure B.11 Random signal according to the frequencies .....	305
Figure B.12 Effects on the human body as a function of frequency .....	307
Figure B.13 Perception thresholds for vibrations for vertical sinusoidal oscillations as a function of frequency .....	309
Figure B.14 Perception threshold for horizontal sinusoidal vibrations as a function of frequency.....	309
Figure B.15 weighting curves for longitudinal and transverse vibrations.....	311
Figure B.16 Quarter car model diagram .....	312

Figure B.17 Half car model diagram .....	312
Figure B.18 Spring-damper diagram representing the tire .....	313
Figure B.19 Comparison of experimental moment of inertia and calculated moment of inertia.....	314
Figure B.20 quarter-car model.....	316
Figure B.21 Acceleration as a function of space-time.....	319
Figure B.22 Half-car model .....	319
Figure B.23 time-history of the movements of the masses.....	321
Figure B.24 time history of the vertical displacements of the masses.....	321
Figure B.25 acceleration as a function of time .....	322
Figure B.26 5 dof model .....	323
Figure B.27 Speed hump (12 feet, 13 inch).....	325
Figure B.28 Speed table (22 feet, 3 inch) .....	325
Figure B.29 RMS comparison between coupled and decoupled approaches .....	325
Figure B.30 eVDV comparison between coupled and decoupled approaches .....	326
Figure B.31 RMS comparison between coupled and decoupled approaches .....	326
Figure B.32 eVDV comparison between coupled and decoupled approaches .....	326
Figure B.33 RMS comparison between coupled and decoupled approaches .....	327
Figure B.34 eVDV comparison between coupled and decoupled approaches .....	327
Figure B.35 RMS comparison between coupled and decoupled approaches .....	327
Figure B.36 eVDV comparison between coupled and decoupled approaches .....	328
Figure B.37 Accelerations in the frequency domain for vehicle A on a parabolic bump at 15 km/h.....	329
Figure B.38 accelerations in the frequency domain for vehicle A over a trapezoidal bump at 15 km/h .....	329
Figure B.39 Accelerations in the frequency domain for vehicle E over a parabolic bump at 25 km/h .....	329
Figure B.40 Accelerations in the frequency domain for vehicle E over a trapezoidal bump at 25 km/h .....	329

# LIST OF TABLES

Table 1.1 Qualitative estimation scale relationship between probability and damage. .....	42
Table 1.2 Levels and Priorities of intervention definitions. ....	43
Table 1.3 Macro-objectives aimed at preventing road accidents and reducing their severity. ....	46
Table 2.1 Review of spot speed prediction models (taken from D’Apuzzo, Santilli, et al., 2021).....	61
Table 2.2 Review of running speed/average travel speed prediction models (taken from D’Apuzzo, Santilli, et al., 2021) .....	64
Table 2.3 Input data for the assessment of free- flow time mean speed in urban areas .....	72
Table 2.4 Input data for the assessment of free- flow time mean speed in rural areas .....	73
Table 2.5 Results Normal model - site 7b. ....	80
Table 2.6 Results model Beta- site 7b. ....	80
Table 2.7 Standard deviation and flow rate data for the site 1 .....	81
Table 2.8 Number of sections per site as a function of the length and number of FCD data. ....	84
Table 2.9 Site 5 data (source: QGIS, Google Earth) .....	85
Table 2.10 Parameters according to the buildings for the site 5. ....	86
Table 3.1 The most popular exposure measures .....	93
Table 3.2 Techniques used for the survey of non-motorized travel .....	95
Table 3.3 Values of k as a function of distance d .....	107
Table 3.4 Tables of road sections existing on streets and squares of the survey route. .....	122
Table 4.1 Damage related to the severity of the injury .....	180
Table 4.2 ISS levels .....	182
Table 4.3 Abbreviated Injury Scale for Head Injury .....	184
Table 4.4 HIC-AIS relationship .....	186
Table 4.5 HIC- influence of the hood (EuroNCAP, 2012) .....	191
Table 4.6 Probability of injury based on severity .....	205
Table 4.7 ISS vulnerability model-ISSaverage comparison .....	206
Table 5.1 Level of service of the sidewalk .....	218

Table 5.2 Average cost of a pedestrian crossing .....	221
Table 5.3 Choice of the type of crossing based on flow assessments .....	221
Table 5.4 Safe positioning of a marked crosswalk .....	223
Table 5.5 Average cost estimated by type of pedestrian crossing .....	231
Table 5.6 Decision matrix.....	237
Table 5.7 Cost estimates for the design of the different solutions.....	238
Table 6.1 Discretization by bands.....	252
Table 6.2 Percentage reduction of vibration compared to vehicle A.....	260
Table 6.3 Correlation between speed and accelerations (RMS and eVDV) on the vehicle A .....	262
Table 6.4 Correlation between speed and accelerations (RMS and eVDV) on the vehicle C.....	263
Table 6.5 Correlation between speed and accelerations (RMS and eVDV) on the vehicle D .....	264
Table 6.6 Correlation between speed and accelerations (RMS and eVDV) on the vehicle E.....	264
Table 6.7 Coefficients of the logistic function on the different vehicles passing through the speed table .....	271
Table 6.8 Coefficients of the logistic function on the different vehicles passing through the speed hump.....	271
Table 6.9 Coefficients of the logistic function on the different vehicles passing through the speed table .....	271
Table 6.10 Coefficients of the logistic function on the different vehicles passing through the speed hump .....	271
Table 6.11 RMS and eVDV as a function of V50 and V85 generated by vehicle A when crossing speed hump and speed table.....	272
Table 6.12 RMS and eVDV as a function of V50 and V85 generated by vehicle C when crossing speed hump and speed table.....	272
Table 6.13 RMS and eVDV as a function of V50 and V85 generated by vehicle D when crossing speed hump and speed table.....	272
Table 6.14 RMS and eVDV as a function of V50 and V85 generated by vehicle E when crossing speed hump and speed table.....	273
Table B. 1 Multiplication factors for longitudinal and transverse vibrations.....	310

# INTRODUCTION

Sustainable mobility is a hot topic that has generated numerous debates in international and national policies. In fact, governance increasingly needs to initiate policies aimed at reducing the environmental impact resulting from the mobility of people and goods.

With the advent of the new millennium, it became clear that the world was growing at an unsustainable pace. For this reason, the 193 UN member states have committed themselves to achieve, between 2000 and 2015, the Millennium Development Goals (MDG) (World Health Organization (WHO), 2017) (United Nations Organization (ONU), 2000). Eight objectives have been defined and summarized in the following figure.



*Figure I.0.1 Symbols of the eight MDGs*

Each of the objectives had specific targets and dates set for achieving them. To accelerate progress, the finance ministers of the G8 countries decided in 2005 to provide funds; these were intended for social programs to improve health and education and to alleviate poverty. Important milestones have been achieved since the MDGs were adopted, however, the set goals have not been fully achieved (UNSTATS, 2015) (United Nations Organization (UN), 2015). It is from this partial failure that the need and desire to do more arise. So in 2015, the countries of the world came together again to chart a plan for a sustainable future, focusing on complex issues (including poverty, hunger, education, health, employment, reducing inequalities, climate

change) which embrace the three dimensions of development (economy, society and environment) closely interrelated.

The novelty lies in the fact that, while the MDGs were aimed only at developing countries, these new objectives are considered universal, since they concern all countries and all inhabitants of the world (Sachs, 2012). They are also more complex and complete because they include new issues, such as climate change, sustainable consumption, innovation in all fields and the importance of ensuring peace and justice for all.

At a global level it was understood that common and shared action was necessary to improve the life of the Planet and its inhabitants, so they created the 2030 Agenda for Sustainable Development.

This is based on five key concepts:

- *People*: it consists in eliminating hunger and poverty in all forms, guaranteeing dignity and equality;
- *Prosperity*: guaranteeing prosperous and full lives in harmony with nature;
- *Peace*: promoting peaceful, just and inclusive societies;
- *Partnership*: implement the Agenda through solid partnerships;
- *Planet*: protecting the planet's natural resources and climate for future generations.



Figure I.0.2 The key concepts of the 2030 agenda

The 2030 agenda is made up of 17 Sustainable Development Goals (SDGs) divided into 169 Targets (Nations, 2015) (Alleanza Italiana per lo Sviluppo Sostenibile (ASviS), 2015); these represent a compass to put Italy and the world on a sustainable path. The process of changing the development model is monitored through Goals, Targets and over 240 indicators: with respect to these parameters, each country is periodically evaluated by the UN and by national and international public opinion.

Each Objective cannot be considered independently but must be pursued on the basis of a systemic approach, which takes into account the reciprocal interrelationships and does not have negative repercussions on other spheres of development. Only the integrated growth of all three components will allow the achievement of sustainable development.



*Figure I.0.3 Sustainable Development Goals (SDGs)*

To implement the Sustainable Development Goals it is necessary to intervene by involving all components of society (from businesses to the public sector, from civil society to philanthropic institutions, from universities and research centers, to information and culture operators) both at an international level than national. This means that resources must be made available for all countries, according to their level of development, contexts and national capacities.

Within the framework of these 2021-2027 reforms, there is the Next Generation Eu (Ngeu) plan (also known as the Recovery fund) which is seen as a tool for relaunching the EU economy after the pandemic crisis. This is a set of investments and reforms to accelerate the ecological and digital transition, improve the training of male and female workers, and achieve greater gender, territorial and generational equity. The Ngeu foresees a fund of 750 billion euros, of which 209 billion (27.8%) went to Italy. The goal is to implement reforms that increase the sustainability of individual European economies, making them more "resilient" to the changes that are looming in the years of recovery from the Covid-19 crisis. In order to explain how and where they will

spend the money coming from the EU, the various countries must submit the National Recovery and Resilience Plans (PNRR) to Brussels. These national plans must comply with predefined criteria, concentrating investment and spending projects.

The PNRR presented by Italy is divided into sixteen Components, grouped into six Missions with a breakdown of funds as shown in the following figure.

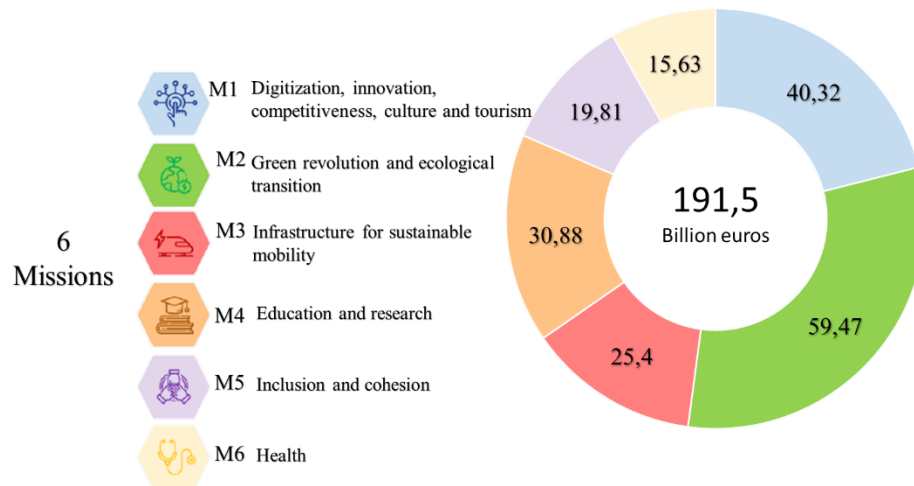


Figure I.0.4 Allocation of resources for Missions

This thesis work can be linked to the third Mission. Given the devastating effects caused by global warming, countries around the world are taking action to limit it. To do this, it is necessary to focus on the use of non-polluting and sustainable means.

## Sustainable Mobility concept

Since the 1990s in Italy there has been talk of sustainable mobility, or rather low environmental impact mobility aimed at maximizing the efficiency and speed of travel. Indeed, according to the World Business Council for Sustainable Development (2020), this mobility allows people to move freely, communicate and establish relationships without ever losing sight of the human and environmental aspects.

Thanks to a huge amount of research-driven evidences, European countries have now realized that by improving transport systems (focusing above all on public, shared and more eco-sustainable services) it is possible to make cities safe and livable by reducing negative externalities (noise pollution, smog, traffic congestion, accidents, greenhouse gas emissions or fine dust, etc).

The growing demand for mobility of road transport, especially private, often makes circulation conditions in urban and rural contexts very critical. Due to the unbalanced

interaction between supply and demand, the decline in service levels and the increase in emissions of greenhouse gases, nitrogen oxides and fine particles are observed (Fioravanti, et al., 2020).

The spread of Covid-19 in 2020 and the consequent need to implement restrictive measures, as highlighted by National Geographic (2020) and the ESA (European Space Agency) (2020), emphasized that the reduction of vehicles in circulation and the reduction of the activity of factories have led to an improvement in air quality.

It is therefore necessary to change habits, choosing to share a new way of moving, this requires a multidisciplinary approach that involves citizens, car manufacturers, public administrations and politics.

It is, therefore, necessary to make cities smart by implementing strategies to optimize and innovate public services. A city, in fact, cannot be defined as a “Smart City” if it does not allow equal accessibility to everyone, including the disabled. With regard to sustainable and inclusive accessibility to mobility, several comparisons between the whole network and the network adapted to disabled people have been proposed to measure the equity/inequality of the network systems. According to (Bartzokas-Tsiompras, Paraskevopoulos, Sfakaki, & Photis, 2020), looking at fifteen cities in Europe, a disparity in accessibility persists between non-disabled and disabled individuals (in wheelchairs). In this direction, in addition to policies to promote active mobility, it is necessary to insert strategies to ensure equal accessibility (such as presence and width of sidewalks, sidewalk ramps, lifts, etc.) (Campisi, et al., 2020). This intelligent mobility, in addition to reducing congestion and pollution, is likely to improve traffic safety, inducing citizens to travel in a sustainable way (Garau, Masala, & Pinna, 2016) (Pinna, Masala, & Garau, 2017). Moreover, developing smarter and more sustainable mobility will allow you to:

- *Reduce air pollution:* Europe has set as a goal, by 2050, a 60% reduction in emissions from transport since transport sector consumes about one-third of total energy consumption and produces one-fifth of greenhouse gas emissions. To achieve the set goal, new technologies and the use of the most efficient systems must be encouraged (for example, hydrogen-powered trains, cars with electric motors, technological infrastructures, etc)
- *Reduce noise pollution:* transport generates excessive noise levels and roads, railways and airports are certainly among the main sources of disturbance. This pollution has consequences on the health and well-being of people (sleep disturbances, increased blood pressure, cardiovascular

diseases, etc) and regulations at national level indicate the exposure thresholds and the measures to be undertaken.

- *Reduce vehicular congestion*: by encouraging the use of shared and public transport to the detriment of private ones, in order to reduce congestion and travel times and to make cities more accessible to vulnerable users.
- *Reduce land use*: due to the growth of transport systems often irrespective of the landscape issues, it is necessary to optimize the collective built-up spaces.
- *Reduce costs and transport efficiency*: by creating innovative, integrated, efficient and connected transport, both individual and collective costs and times are reduced.

To make cities innovative, connected but at the same time sustainable, technology can be used to control and save energy as well as to optimize mobility and safety solutions. To do this, it is essential to make the transport service efficient by focusing on multimodality. Multimodal transport allows for the combined way different modes (at least two) of transport. Therefore, tailor-made offers must be developed including various ways, such as public transport, shared cars and bicycles, electric scooters, taxis and more, such as Mobility-As-A-Service (MAAS) systems that allow simple and safe access to the offers of mobility providers through an app, which becomes visible and bookable; allowing to maximize resources and time by combining the different available means.

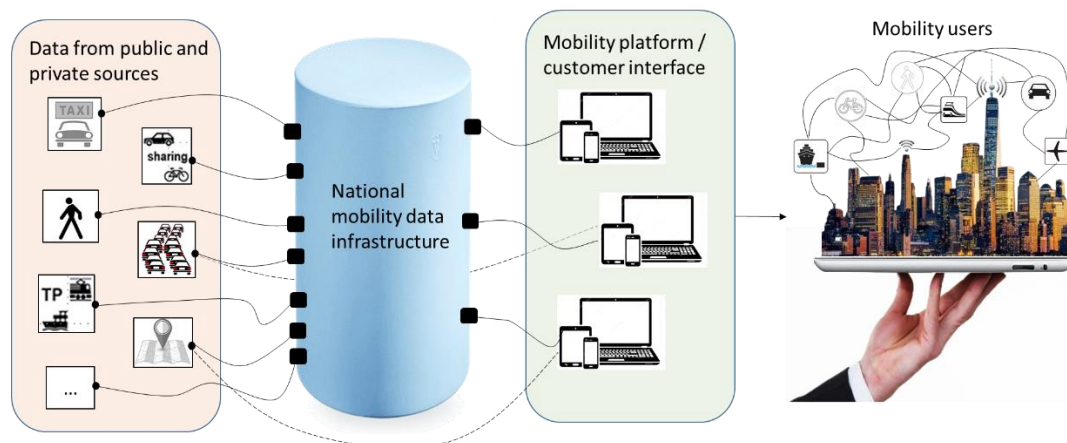


Figure I.0.5 Operation diagram of a multimodal service

Multimodality could become an existential experience against everyday stress, encouraging users to change their habits.

Creating integrated services, with a view to making cities smart, therefore means starting projects aimed at citizens to lead them to reflect on their mobility choices, encouraging awareness and convenience for changing behavior. In fact, more and more often targeted interventions are put in the cities; among the most frequent are mentioned:

- *the re-design of public transport* supply by means of the strengthening of the infra-structure and services both at local (urban) and national/international level.
- *the promotion of preferential lanes* intended exclusively for public transport (buses, trams, taxis) or emergency vehicles; this allows to avoid traffic congestion giving an advantage to those who use public transport instead of private transport.
- *the creation of cycling paths or pedestrian areas*, therefore areas dedicated exclusively to bicycles and pedestrians; giving the feeling of greater safety and protection, which encourages people to walk or pedal for short trips instead of using a car or motorbike.
- *road pricing (urban toll) and park pricing* to discourage or limit the access in urban areas to private vehicles (cars, motorcycles, scooters, etc.) in order to reduce traffic congestion, smog and encourage the use of public transport.
- *traffic blocking* i.e. a temporary and occasional public intervention to partially or totally limit vehicular traffic in urban areas.
- *the use of limited traffic areas (ZTL in Italy)* as a permanent blocking of traffic in the central or more congested areas of the city. The ban pushes people to use public transport or to replace their private vehicle with a low environmental impact vehicle (eg electric cars, gas cars, Euro 6-7, etc).
- *car-sharing or bike-sharing* i.e. forms of collective mobility based on the rental of a low environmental impact vehicle (electric car or bike) for a few hours or days, that are increasingly adopted in urban areas
- *car-pooling* i.e. another form of collective mobility which consists in the use of a private car by several people, often colleagues or acquaintances, who travel the same journey from home to work at the same times.

Despite the idea of moving towards multimodal transport, most European countries and cities have devoted most of resources in the construction and management of infrastructure for motor vehicles, neglecting those for active modes, namely walking and cycling. Among the many European projects implemented, the FLOW project (European Union, 2020) involving the implementation of strategies to promote

walking and the use of bicycles, both in large and small cities, on short and medium distance journeys is one of most noticeable.

However, despite the success of EU programs, the roads are still not completely safe, in fact, a report (2020) of the ETSC (European Transport Safety Council) highlights that in Europe from 2010 to 2018 the number of dead pedestrians was 21% of the total, 18% of cyclists and 8% of motorcyclists (bearing in mind that pedestrian deaths or injuries of vulnerable users are often not counted among road accidents because the police were not consulted). This suggests that in Europe there are on average more than 5180 deaths every year. Looking at the accident data, it seems that although there has been a slight reduction in fatal road accidents, there are no decreases in accidents involving vulnerable users.

Due to the intensity and speed of motorized traffic, cities are unsuitable for vulnerable users who are often forgotten. It is, consequently, necessary to reorganize the road network to promote the use of bicycles as a daily mode of transport for various reasons (home-work / study, recreation, sport and free time).

To promote the use of “active mobility” it is necessary to establish rules to reduce the high risk of injury to which cyclists and pedestrians are exposed. This implies the reorganization of the streets which become multifunctional spaces shared equally among all users.

People choose to travel on foot or by bicycle (European Union, 2009) based on subjective and objective factors. The former is linked to the sense of security, the feeling of comfort and social acceptance; while the latter ones are related to speed, topography, climate and safety (understood as the absence of obstacles).

Taking these factors into account, a cycle network or a pedestrian area can be designed, making it an integral part of urban mobility policies (Mobility plans and transport), which deal, among other aspects, to ensure that the journey takes place smoothly and therefore that the structure is:

- safe: the risk of injury due to interactions with other modes is reduced;
- direct: limiting the detours so that the travel time is reduced;
- continuous: so that the movements, between the different origins and destinations, do not have path interruptions (with good connections with other networks, mainly public transport stops and junctions);
- attractive or well integrated with the environment in which it is inserted;
- comfortable: allowing the cyclist to reduce physical effort and discomfort, so as to have a pleasant and relaxed travel experience.

In practice, it is not always possible to meet all these requirements, so there is the need to find the right balance based on the environment in which the designer is operating.

## **Road safety estimation and accident statistics**

The factor that mainly affects the choice of mode of transport is the perceived safety. To assess the safety levels of a road, reference is made to accidents that have occurred or near miss.

There are numerous measures for the prevention of road accidents created by the UN with the 2030 sustainable development agenda and at a national level with National Road Safety Plan. The common goal is to halve mortality and injury (in the decade 2010-2030), with particular reference to vulnerable road users. The result must be policies aimed at reducing the risk of hazardous events occurring. In recent years it has been highlighted that the risk is strongly connected to hazardous behavior on the part of users, but also partly depends on the failure to intervene in containing the hazards due to the geometry of the infrastructures and the failure to intervene with technological innovations. Moreover, the lack of maintenance determines, in many cases, the deviation of traffic on alternative routes that are often not suitable for supporting the flows; this generates inconvenience for users, lengthening travel times as well as creating opportunities for accidents.

Between 2010 and 2020, the average annual reduction in the number of road fatalities was 4.4% in the EU and 4.7% in Italy, variations that did not lead to the complete achievement of the European target (they should have reach about 15750 deaths by 2020); for this reason, the EU has set two new goals, namely halving road fatalities and the number of seriously injured by 2030 (compared to 2020 levels) (European Commission, 2019).

The figure below shows that since 2001 there has been a 64% reduction in the number of road deaths in the EU (European Transport Safety Council, 2021). It should be emphasized that the decrease in deaths and serious injuries observed in 2020 (the number of deaths on the road fell by 40% in April 2020 alone) is the consequence of travel restrictions, which have had a significant impact on traffic levels.

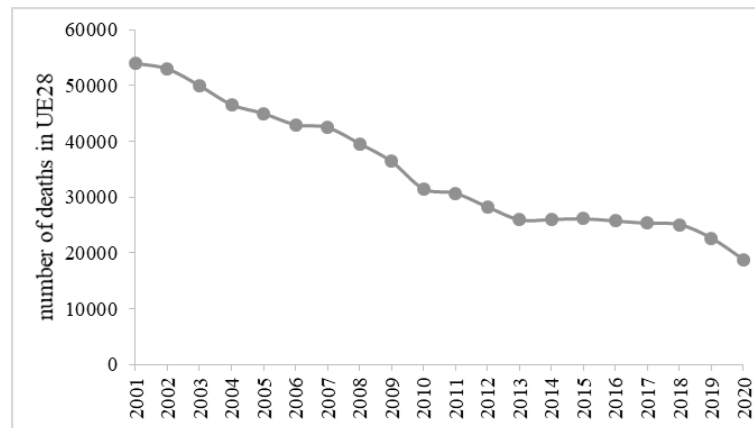


Figure I.0.6 Data of deaths in the EU (European Transport Safety Council, 2021)

This highlights that many countries have not well understood the concept of "vision zero"; that is an approach aimed at completely eliminating (not reducing) the victims of road accidents. It is an integrated approach to security in which technology must be refined, correct information must be disseminated, travel must be made efficient and infrastructures must be reorganized. There is a need to change the way people move and understand that road safety involves all road users, motorized and non-motorized. Deaths and injuries are mainly motorists because about 80% of the kilometers are traveled each year by car. Although, according to European Union statistics, around 30% of road fatalities are pedestrians and cyclists. The data for those who choose the bike or their legs to move around are dramatic across the EU, which is why the ETSC calls for a review of urban transport policies by applying a hierarchy for urban planning that privileges walking, cycling and public transport versus the use of private cars.

In Italy the situation is no better, just take a look at the Istat (Istituto nazionale di statistica) data of the last 20 years. (Istat is an Italian research institution that deals with censuses, every ten years (the last one dates back to 2011), of the population, services, industry and agriculture, and sample surveys on households and general economic surveys at a national level).

It can be noted that the number of deaths has certainly decreased over the years but an increase in injuries is observed.

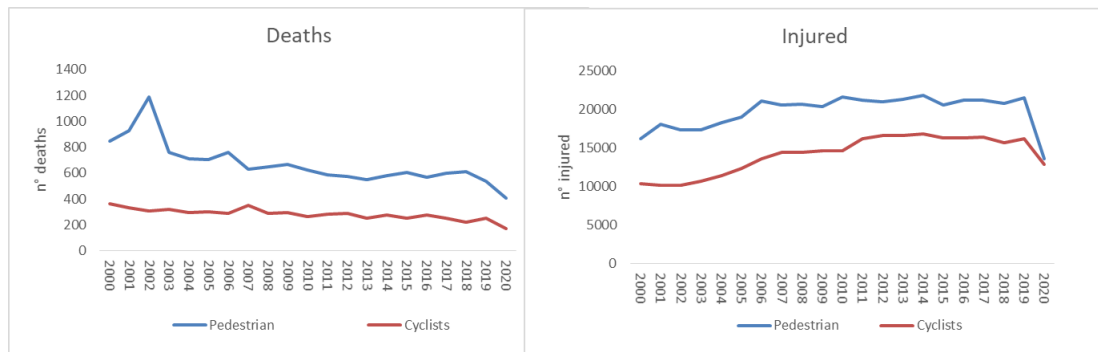


Figure I.0.7 Dead and injured 2000 to 2020 according to Istat

Istat 2019 data shows a reduction in car accidents but on the other hand an increase in accidents involving cyclists and pedestrians.

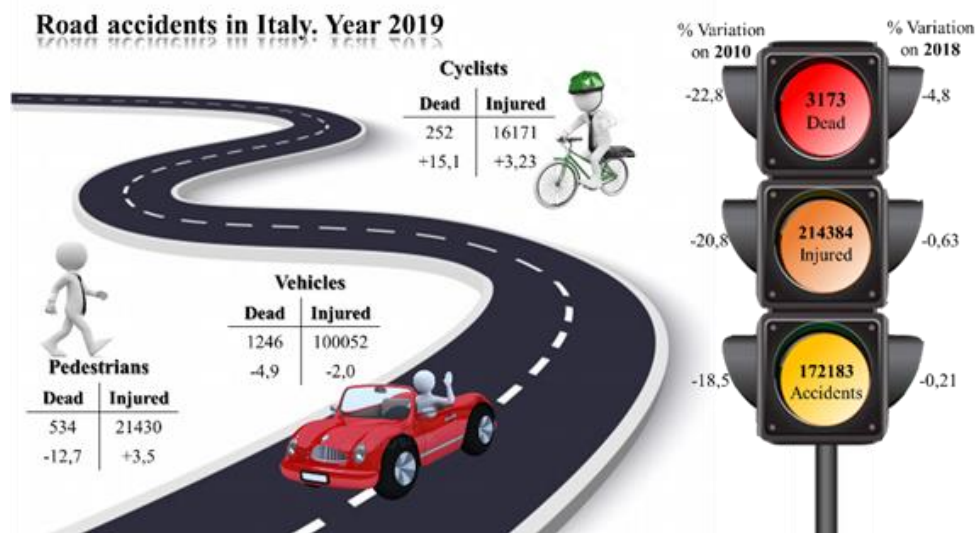


Figure I.0.8 Graphic representation of accidents by category in 2019 (source Istat)

The 2020 data show a significant decrease in accidents linked, as noted above, to the restrictions due to the Covid-19 emergency. It should also be noted that during 2020, also in part thanks to the various economic incentives of the Government (bike bonus and single-scooter bonus), the spread of micro-mobility began to be registered. The term micro-mobility refers to a set of vehicles and modes of travel used for short trips and for the transport of one or two people at the most. This group of vehicles includes bicycles, e-bikes, electric scooters, electric skateboards (monowheels and hoverboards), shared bicycles, and electric pedal assisted (pedelec) bicycles. Unfortunately, as there is a great deal of confusion at the legislative level that regulates the use of these means, there have been not a few infringements with consequent accidents.

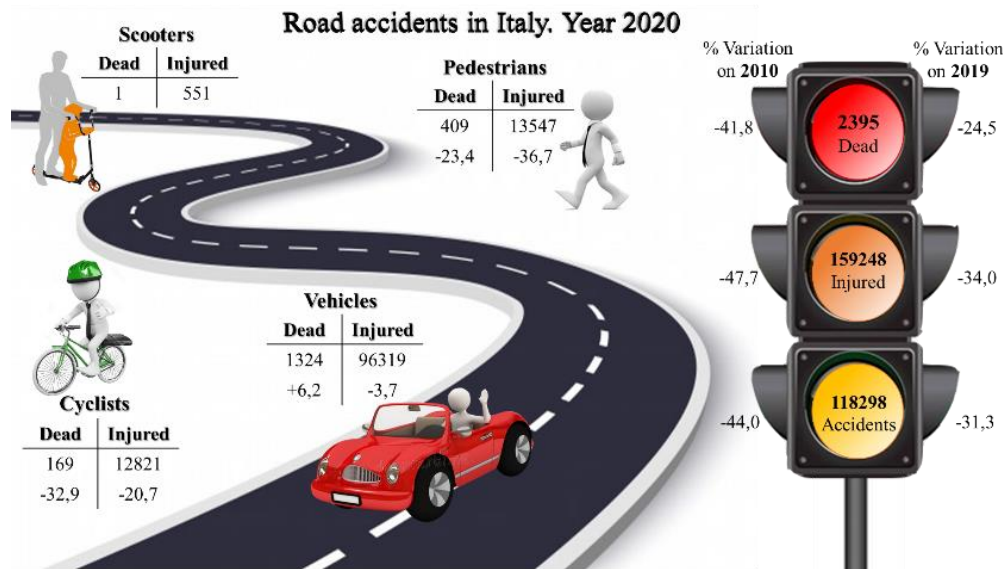


Figure I.0.9 Graphic representation of accidents by category in 2020 (source Istat)

As for 2021, Asaps (*Associazione sostenitori e amici polizia stradale/ Traffic police supporters and friends Association*) has published the data for the first three months. The picture is frightening, as many as 44 deceased cyclists were recorded, compared to 37 in 2019 (in total in that year there were 252 deaths among two-wheelers) and to 33 in 2018 (total for the year 219); while for pedestrians died there are 20, compared to 39 in 2019 (total for the year 534) and to 46 in 2018 (total for the year 612).

These data risk creating fears in users by pushing them to travel by private car. Therefore, to promote sustainable mobility it is necessary to create the conditions for them to feel safe. To do this, a risk-based procedure was developed that is primarily focused on vulnerable users. Starting from literature models, the various quantities were identified which made it possible to identify levels of "risk"; based on these, ad hoc measures can be implemented to make the urban environment more welcoming and safe.

Much effort has been made to reduce the frequency and severity of road accidents. Over the years it has been realized that the most efficient way to tackle the problem is to initiate a road safety management program. This requires multidisciplinary knowledge, in fact, it makes use of the experience of many basic sciences (medicine, social behavior) and many scientific disciplines (mathematics, physics, road engineering, safety, transport, education, psychology, sociology, ergonomics, medicine, law, urban planning). Taking into account all these aspects is complicated, but the technical literature proposes different models. In order to reconstruct the

reality, these start with the data of the accidents, the geometrical-operational characteristics of the road and the environmental conditions.

The different methods adopted are based on a “model” which is the abstract and simplified representation of reality. These models are more or less complicated based on the modeling assumptions, knowledge, needs and information possessed by the researcher and can change depending on the objective of the study (Hoogendoorn, 2003) (Helbing, Molnar, Farkas, & Bolay, 2001) (Hoogendoorn & Bovy, 2004).

The approaches used can be grouped into three macro families:

- statistical and mathematical methods;
- methods based on physical models;
- probabilistic methods.

## References

- Abdelwahab, H., & Abdel-Aty, M. 2001. Development of artificial neural network models to predict driver injury severity in traffic crashes at signalized intersections. *Transportation Research Record* 1746, pp. 6-13.
- Agency, E. S. 2020. La chiusura per fronteggiare il Coronavirus ha portato ad una riduzione dell'inquinamento in tutta Europa. Taken from [https://www.esa.int/Space\\_in\\_Member\\_States/Italy/La\\_chiusura\\_per\\_fronteggiare\\_il\\_Coronavirus\\_ha\\_portato\\_ad\\_una\\_riduzione\\_dell\\_inquinamento\\_in\\_tutta\\_Europa#:~:text=Agency-,La%20chiusura%20per%20fronteggiare%20il%20Coronavirus%20ha%20portato%20ad,dell'inqui](https://www.esa.int/Space_in_Member_States/Italy/La_chiusura_per_fronteggiare_il_Coronavirus_ha_portato_ad_una_riduzione_dell_inquinamento_in_tutta_Europa#:~:text=Agency-,La%20chiusura%20per%20fronteggiare%20il%20Coronavirus%20ha%20portato%20ad,dell'inqui)
- Alleanza Italiana per lo Sviluppo Sostenibile (ASviS). 2015. L'Agenda 2030 dell'Onu per lo sviluppo sostenibile. Taken from <https://asvis.it/1-agenda-2030-dell-onu-per-lo-sviluppo-sostenibile/>
- Bartzokas-Tsiompras, A., Paraskevopoulos, Y., Sfakaki, A., & Photis, Y. 2020. Addressing street network accessibility inequities for wheelchair users in fifteen European city centers. *Conference on Sustainable Urban Mobility* (p. 1022-1031). Springer, Cham.
- Cammarata, S. 1994. *Sistemi fuzzy: un'applicazione di successo dell'intelligenza artificiale*. Etaslibri.
- Campisi, T., Basbas, S., Tesoriere, G., Trouva, M., Papas, T., & Mrak, I. 2020. How to Create Walking Friendly Cities. A Multi-Criteria Analysis of the Central Open Market Area of Rijeka. *Sustainability*, 12(22), 9470.

- Commission, E. 2019. European Green Deal (COM/2019/640/final). Bruxelles.
- Council, E. T. 2020. How safe is walking and cycling in Europe? (PIN Flash 38).  
Taken from <https://etsc.eu/how-safe-is-walking-and-cycling-in-europe-pin-flash-38/>
- Council, W.B. 2020. Taken from <https://www.wbcsd.org/Programs/Cities-and-Mobility/Transforming-Mobility>
- European Commission. 2019. Commission Staff Working Document, EU Road Safety Policy Framework 2021-2030, Next steps towards “Vision Zero”. Taken from <https://bit.ly/3vgWTHt>
- European Transport Safety Council. 2021. Ranking EU progress on road safety: 15th Road Safety Performance Index Report.
- European Union. 2009. Cities for Bicycles, Cities of the Future. Taken from <https://www.ecf.com/sites/ecf.com/files/Future-cities-are-cycling-cities.pdf>
- European Union. 2020. Flow. Taken from <http://h2020-flow.eu/>
- Fioravanti, G., Frascetti, P., Lena, F., Perconti, W., Piervitali, E., & Pavan, V. 2020. Gli indicatori del clima in Italia nel 2019-anno XV. ISPRA – Istituto Superiore per la Protezione e la Ricerca Ambientale.
- Garau, C., Masala, F., & Pinna, F. 2016. Cagliari and smart urban mobility: Analysis and comparison. *Cities*, 56, 35–46, p. pp 35–46.
- Geographic, N. 2020. Coronavirus, le misure di contenimento hanno ridotto l'inquinamento. Taken from <https://www.nationalgeographic.it/ambiente/2020/04/coronavirus-le-misure-di-contenimento-hanno-ridotto-linquinamento-europa>
- Helbing, D., Molnar, P., Farkas, I., & Bolay, K. 2001. Self-organizing pedestrian movement. *Environment and Planning B: Planning and Design* 2001, Vol. 28, pp. 361 - 383.
- Hoodendoorn, S., & Bovy, P. 2004. Pedestrian route-choice and activity scheduling theory and models. *Transportation Research Part B*, Vol. 38, pp. 169–190.
- Hoogendoorn, S. 2003. Pedestrian Travel Behavior Modeling. Proceedings of the 10th International Conference on Travel Behavior Research. Lucerne.
- Manca, A., Benczur, P., & Giovannini, E. 2017. Building a scientific narrative towards a more resilient EU society.
- Nations, U. 2015. The 17 Goals. Taken from <https://sdgs.un.org/goals>
- Pinna, F., Masala, F., & Garau, C. 2017. Urban Policies and Mobility Trends in Italian Smart Cities. Sustainability.

- Sachs, J. 2012. From Millennium Development Goals to Sustainable Development Goals. Vol. 379. pp. 2206–2211 (doi: 10.1016/S0140-6736(12)60685-0).
- United Nations. 2015. The 17 Goals. Taken from <https://sdgs.un.org/goals>
- United Nations Organization (ONU). 2000. Millennium Declaration. Taken from [www.un.org/millennium/declaration/ares552e.htm](http://www.un.org/millennium/declaration/ares552e.htm)
- United Nations Organization (ONU). 2015. Millennium Development Goals Report 2015. United Nations, New York.
- UNSTATS. 2015. MDGs Progress Chart. United Nations, New York.
- World Health Organization (WHO). 2017. Report on the global tobacco epidemic, 2017: monitoring tobacco use and prevention policies.

# **CHAPTER 1. INTRODUCTION TO RISK ASSESSMENT IN ROAD SAFETY FOR VULNERABLE USERS**

## **1.1 Risk definition**

More and more often the news reports talk about the damage caused by natural phenomena. These are significant damage both to the natural and built environment with deaths and injuries, and to the long-term on communities as well as on the social aspects related to the reconstruction and restoration of the functionality of structures and infrastructures. This requires long recovery times for the return to "pre-disaster" conditions, therefore countries are moving towards a risk reduction policy with the aim of predicting the effects, on the most relevant territorial assets, to minimize the impact. This allows stakeholders (planners, public administrators, service managers, emergency departments, private investors, insurance companies, etc.) to take mitigation actions (D'Apuzzo, M. et al., 2019) ( D'Apuzzo, M. et al., 2020). Therefore risk analyzes are spreading; these were mainly created to activate forecasting and prevention measures in response to the damage generated by natural disasters, then they were extended to many other sectors. One of these is that relating to road safety.

However, it is necessary to clarify because in common language the terms "hazard" and "risk" are used as synonyms, even if from a technical point of view, they express different concepts. In fact, according to the legislation (UNI 11230, 2007), the hazard is the potential of a specific entity (machine, equipment, plant, substance, process, system, etc.) to cause damage. The hazard can, therefore, be defined as a "source of potential damage".

While, the risk depends on the interaction between the source of hazard and the person. Unlike the hazard that is characterized by its physical objectivity, the risk is linked to the hypothesis that a future event could cause damage.

The first risk assessment strategies were developed in the 1970s, when the international community began to emphasize the need to plan and prevent natural

phenomena that were becoming an obstacle to settlement development. Therefore, the effects of natural disasters began to be considered in humanitarian and social terms as well as economic and developmental ones, especially for those countries where urbanization involves areas subject to natural events (earthquakes, floods, tsunamis, fires, etc.). After years of research on the main natural hazards (phenomena) of meteorological, geological and geophysical origin in 1979, the conference of the United Nations Disaster Relief Office (UNDRO, 1979) defined risk as the predicted number of lives lost, injured, property damage and business disruption due to a particular natural phenomenon. Therefore, risk was defined as the product of a specific risk (i.e. the degree of expected loss due to a natural phenomenon, a function of both hazard and vulnerability) and elements at risk.

$$Risk = Hazard \cdot Consequences \quad 1.1$$

The UNDRO Committee also highlighted that in order to assess the potential loss due to a given natural hazard, the following must be taken into consideration:

- The randomness of natural hazards at a given site;
- The role of existing structures which have their intrinsic vulnerability;
- The importance of the elements (population, housing, economic activities, etc.) possibly affected, called “elements at risk”;
- The definition of the expected risk over a period of time.

So to emphasize both the concept of chance or possibility (for example, the risk of an accident) of potential losses, for a given cause, place and period, the risk can simply be expressed as the product of three integral components, namely hazard, vulnerability (of buildings, infrastructures and population) and exposure of these resources present in the study area. It is a probabilistic estimate that can be evaluated as:

$$R_0 = H \cdot V \cdot E \quad 1.2$$

Where:

$R_0$  is the risk referred to the assets displayed in the area of interest, expressed as far as possible in terms of probability or frequency of occurrence of predefined consequences;

$H$  expresses the hazard of the area of interest (as it increases, the risk increases); “A potentially damaging physical event, phenomenon and/or human activity, which may cause loss of life or injury, property damage, social and economic disruption or

environmental degradation. Hazards can be single, sequential or combined in their origin and effects " (UN/ISDR, 2004);

$E$  expresses the exposure in the area of interest (as it increases, the risk increases); is the measure of possible future losses that may arise from an activity or event or as reported by Kolluru et al.(1996) exposure is the process by which an organism comes into contact with a hazard;

$V$  expresses the vulnerability of the goods exposed (as it increases, the risk increases); "*The characteristics of a person or a group in terms of their capacity to anticipate, cope with, resist and recover from the impact of a natural or man-made disaster noting that vulnerability is made up of many political-institutional, economic and socio-cultural factors*" (IFRC, 1999) (Wolfensohn J. and D. Cherpitel, 2002).

This expression of risk is very broad both because it can refer to any type of hazard and because for a certain type of hazard there is no single risk assessment. It can be generalized by considering  $x$  the effects of natural phenomena on the site, whose distribution is the function  $\phi(x)$  which represents the probability of exceeding each value of  $x$  within the reference period. It is therefore possible to define the functions  $F(x) = 1 - \phi(x)$  or  $p(x) = dF/dx$  which respectively represent the probability that  $x$  is not exceeded or the probability density function. Since vulnerability represents the expected damage on an entity (structure or population) induced by a phenomenon of a given magnitude, it can be written as  $\alpha = \alpha(x)$ . To evaluate the probability of failure ( $df$ ) associated with the risk probability  $x$  between  $x$  and  $x+dx$  can be written as (Figure 1.1a):

$$df = p_H F_S dx \quad 1.3$$

Where:

$p_H(x)$  the probability density function;

$F_S$  the probability of exceeding.

Similarly, from Figure 1.1b, the probability of failure ( $df$ ) associated with the probability of the strength  $x$  ranging between  $x$  and  $x+dx$  is:

$$df = p_S \phi_H dx \quad 1.4$$

Where:

$p_S$  density function of distribution of the mechanical properties of the structure;

$\phi_H$  the probability of exceedance.

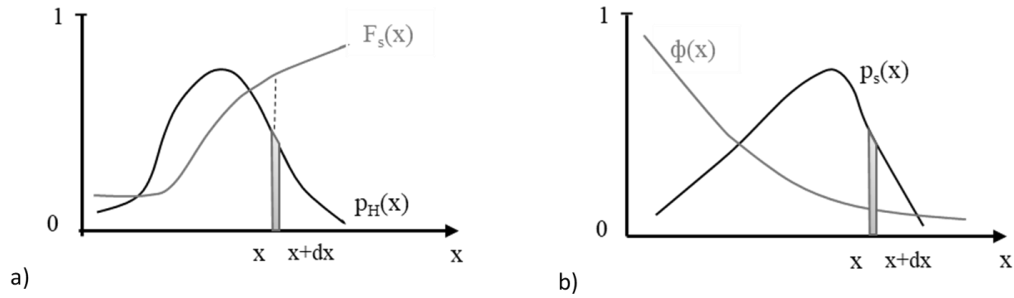


Figure 1.1 Functional forms of the hazard and structural strength probabilities: a) probability density function  $p_H(x)$  and probability of non-exceedance a level of structural strength  $F_S(x)$  for a given value of the magnitude  $x$ ; b) probability of exceedance  $\phi_H(x)$  and probability density function of a structural strength  $p_S(x)$  for a given value of the magnitude  $x$  (modified after (UNDRO, 1979)).

The elementary specific risk associated with the probability of the entity of the event between  $x$  and  $x + ds$  is:

$$\frac{dr}{(er)} = \alpha(x)F_S p_H dx = \alpha(x)\Phi_H p_S dx \quad 1.5$$

where (er) are the elements at risk (all the other parameters are described previously).

Considering the entire distribution of  $x$ , the specific risk is:

$$\frac{r}{er} = \int_0^{\infty} \alpha(x)F_S(x)p_H(x)dx = \int_0^{\infty} \alpha(x)p_S(x)\Phi_H(x)dx \quad 1.6$$

In the last expressions, the first two terms under the sign of integration depend only on the structures while the third only on the natural phenomenon. The first two terms, therefore, define vulnerability when considering the randomness of the properties of structures. This definition changes according to whether the hazard is introduced through its probability of exceedance or its probability density. Although the complete solution to the problem requires the randomness of the mechanical properties of the structures and their vulnerability, the original UNDRO procedure needs some simplifications. The first simplification consists in considering the randomness of the strength of the structures and their vulnerability is negligible compared to the variability of the hazard (Figure 1.2).

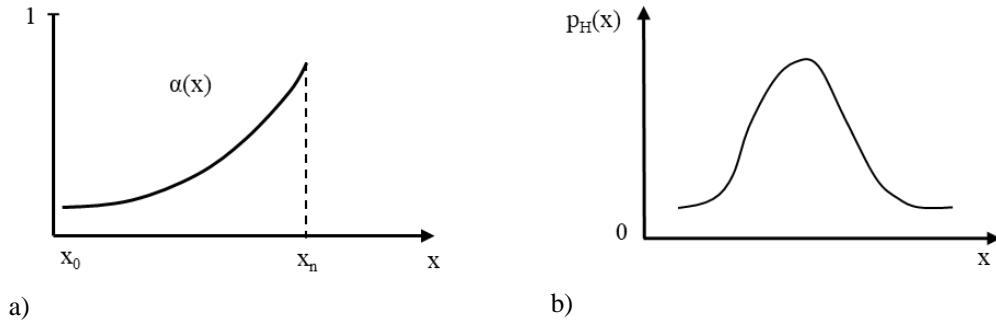


Figure 1.2 Sample vulnerability function  $\alpha(x)$  in the hypothesis of structural strength as hazard-independent variable; b) probability density function of the magnitude  $x p_H(x)$  (modified after (UNDRO, 1979)).

From the combination of the risk probability function and the vulnerability profile, the elementary specific risk is due respectively to the probability of the quantity  $x$  between  $x$  and  $x+dx$  and for the entire range of quantities is:

$$\frac{dr}{(er)} = \alpha(x)p_H dx \tag{1.7}$$

$$\frac{r}{er} = \int_0^\infty \alpha(x)p_H(x)dx \tag{1.8}$$

Considering the particular values of  $\alpha$  for  $x < x_0$  or  $x > x_1$

$$\frac{r}{er} = \int_0^\infty \alpha(x)p_H(x)dx = \int_{x_0}^{x_n} \alpha(x)p_H(x)dx + \Phi_H(x_1) \tag{1.9}$$

A further simplification is to replace the curve  $\alpha(x)$  as a step function (Figure 1.3).

It can be noted that in this case, the expression of the specific risk takes the form:

$$\frac{r}{er} = \sum_j \Delta_j \alpha \Phi_j \tag{1.10}$$

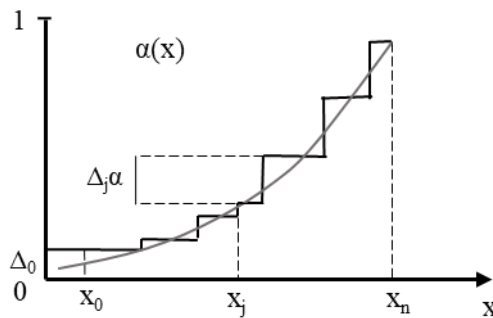


Figure 1.3 Simplification of vulnerability curve through step function (modified after (UNDRO, 1979)).

For a selected risk, the probability of exceeding  $\phi_j$  is generally tabulated, or it is assumed to be preliminarily characterized. This led the designers to take advantage of

this framework as they only needed to calculate the  $\Delta_j\alpha$  from the table of values of  $\alpha$  like the one displayed in Figure 1.3 and perform the summation above.

Following the UNDRR Conference, from 1 January 1990, the International Framework of Action for the International Decade for Natural Disaster Reduction (IDNDR) initiated the Yokohama strategy with the aim of reducing loss of life, damage to property, the social and economic hardships caused by "natural disasters", especially in developing countries. This strategy identified gaps related to governance, risk identification, assessment, monitoring and early warning, knowledge management and education, reduction of underlying risk factors, preparation for effective response and recovery. Starting from these shortcomings, the Hyogo action was then launched (2005-2015) aimed at making countries aware of their primary role in the prevention and reduction of the risk of disasters. This has pushed them towards international cooperation policies and the development of regional strategies with the creation of global and regional platforms for disasters. While in the past the protection of social and economic development from external shocks was considered, now the goal is growth and development planning to manage risks holistically; which means the establishment of multidisciplinary approaches to promote sustainable economic and social growth, protect environmental health conditions and strengthen resilience (i.e. take proactive behaviours, ready to survive disasters and maintain economic competitiveness) and stability. This gave rise to the Sendai Framework 2015-2030 plan (UN General Assembly, 2015) which is aimed at strengthening risk governance by developing risk prevention, mitigation and management activities, in order to reduce the risk of catastrophes and loss of life, human resources, livelihoods and health, and the economic, physical, social, cultural and environmental assets of people, businesses, communities and countries.

### **1.1.1 Risk analysis**

Therefore, starting from a mainly geotechnical risk definition, risk assessment processes (or risk analysis) are being tested in various sectors.

The risk assessment consists of a set of activities that make it possible to identify and quantify the risk, to then put in place the appropriate prevention and protection measures, to activate all those activities measures of a technical, organizational and procedural nature that make up the so-called process of "risk treatment" and more generally "risk management".

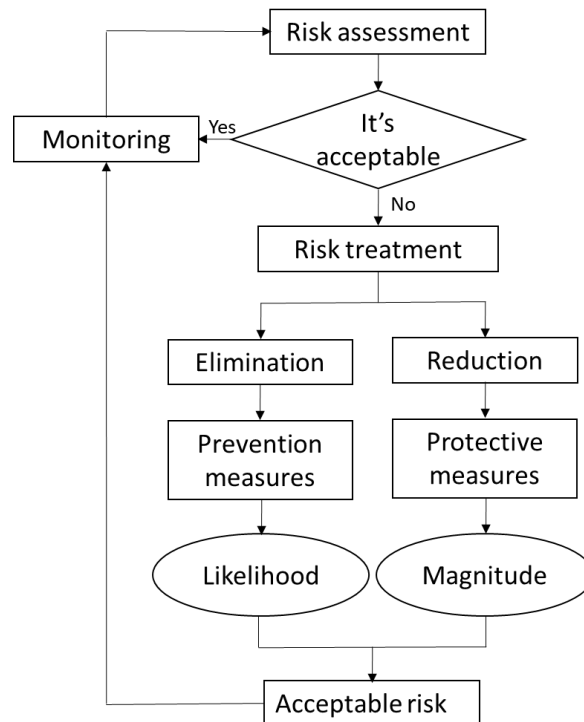


Figure 1.4 Flow chart adapted from (D.Lgs n°81, 2008).

In general, the process starts with the identification of risk factors and then estimates the identified risks. To do this, probabilistic approaches can be used that evaluate both the probability of occurrence ( $P_r$ ) and the magnitude of the damage ( $M$ ).

These approaches can be grouped into two macro-categories:

- quantitative or semi-quantitative approach;
- qualitative approach.

The first is based on the use of mathematical models, which use inferential statistical methods; it is used in specific contexts, where the analysis of safety standards must be very precise and accurate. Quantitative analyses provide a more objective understanding; however, their effectiveness is fundamentally based on the quality of the information available, which is the number and accuracy of the data, which represent various possible situations.

Whenever possible, a quantitative approach should be preferred to be more objective and examine the system in more detail, but supplementation with qualitative analysis should be considered. An appropriate combination to sum the advantage of both approaches becomes crucial when not all factors can be parameterized.

While the qualitative approach is also called "subjective" as it is based on the "expert judgment" of the risk analyst, whose level of competence and the quality of

the data acquired in the preliminary phase must be reliable. Qualitative methods offer analysis without detailed information, are performed with intuitive and subjective processes and can lead to different results/conclusions depending on who uses them. Although suspected of leading to subjective conclusions, they offer the possibility of considering factors that are difficult to quantify, such as those related to human behavior, and sometimes lead to an adequate risk assessment. There are several theories that allow you to transform qualitative into quantitative assessment (e.g., probability of imprecise interval, possibility and theories of evidence), an overview is provided by Tesfamariam and Goda (2013).

In qualitative estimation, the definition of scales is used, in which both the probability and magnitude of graduation are explicitly defined.

*Table 1.1 Qualitative estimation scale relationship between probability and damage.*

<b>Likelihood</b>	<b>Magnitude</b>
Very low	Negligible
Medium low	Moderate
Medium high	Remarkable
High	Huge

Based on this estimate, the analyst identifies three classes of risk: HIGH RISK, MEDIUM RISK, LOW RISK which determine different levels and priorities of intervention.

Table 1.2 Levels and Priorities of intervention definitions.

Likelihood	Magnitude	Risk	Intervention
High	Huge	High	The measures are urgent. The intervention plan goes beyond cost / benefit assessments.
High	Remarkable		
Medium high	Huge		
High	Moderate	Medium	Plan and apply prevention and protection measures; these must be checked to assess the effectiveness of the risk reduction process.
High	Negligible		
Medium high	Remarkable		
Medium high	Moderate		
Medium high	Negligible		
Medium low	Huge		
Medium low	Remarkable		
Medium low	Moderate		
Very low	Huge	Low	No interventions are necessary but it is necessary to continue to monitor by evaluating possible future improvements.
Very low	Remarkable		
Medium low	Negligible		
Very low	Moderate		
Very low	Negligible		

Once the probability and magnitude have been estimated, graphical representations have used that highlight the assessment carried out for each risk. Among the most used is the "risk matrix" which is obtained by plotting in a Cartesian graph, the probability scale in the ordinate and the magnitude scale in the abscissa.

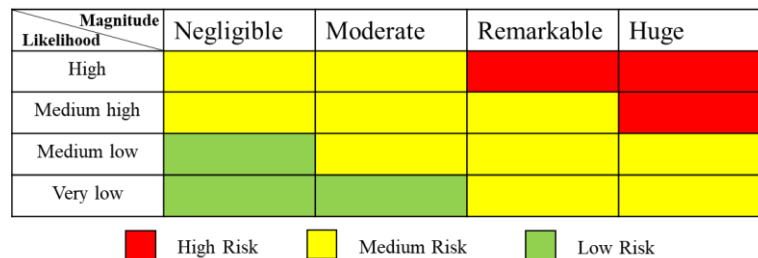


Figure 1.5 Risk matrix

The next step is the "risk weighting" phase which serves to determine whether the risk is acceptable and to what extent. That is, it is necessary to establish for each risk its limit of acceptability, beyond which it must be reduced with prevention and protection measures. The acceptability of the risk depends on several factors, including the phenomenon (whether or not controllable), the type and nature of the consequences, the short and long-term effects, the benefits obtained, the preparedness for natural hazards and the influence of individual and total risk. The definition of acceptability limits depends on legal constraints, rather than on technical standards or improvement practices. Therefore it is required that, in order to satisfy the safety conditions, the measured risk is to a lesser extent equal to the acceptable one.

Therefore, once the pre-mitigation risk  $R_0$  has been assessed, a benefit-cost analysis must be carried out to assess the suitability of the mitigation. In general terms, it can include risk reduction (active mitigation), vulnerability reduction (passive mitigation) or both options (active and passive mitigation). Regardless of the type, assuming a mitigation cost equal to  $U_d$ , the residual risk  $R'_d$  can be calculated:

$$R'_d = H' * V' * E' + U_d \quad 1.11$$

Where:  $H'$ ,  $V'$  and  $E'$  represent the new terms of Hazard, Vulnerability and Exposure respectively after mitigation. Starting from the same risk level  $R_0$ , there are two different scenarios:

- $R'_d < R_0$  there is a convenient situation that justifies the adoption of countermeasures;
- $R'_d > R_0$  a situation of non-economic convenience emerges. While effective countermeasures reduce hazard or vulnerability, their cost has resulted in a residual risk greater than pre-mitigation.

At the end of this phase, a risk map is obtained which highlights the unacceptable risks that must be reduced by adopting measures that will be programmed and planned with a prioritization process. The general criterion is based on the entity of the risk, i.e. the higher the estimated risk level, the higher the priority of intervention.

So the priority is divided into three categories:

- High Priority: urgent interventions to be implemented in the short term, for unacceptable risk situations according to previous regulations.
- Medium Priority: interventions to be implemented in the medium term, for risk situations to be reduced to acceptable values within the terms set by the regulations.
- Low Priority: interventions to be implemented in the long term for situations of acceptable risk, but aimed at the continuous improvement of safety (further reduction of the risk).

The last phase of risk management is the monitoring or the periodic process of control and measurement of the risk parameters, review and weighting of new and/or modified risks following the changes made to the environments.

## 1.2 Road safety risk

The risk arising from the evaluation of the protection and prevention measures to be adopted in the event of natural disasters can actually be applied in various fields. Precisely from the understanding and application of risk estimation techniques it is possible to evaluate road safety. The main task in the road safety audit is to identify the elements of hazard that could cause death or injury. Therefore road risk is usually implicitly linked to accidents (the severity and frequency of which must be defined).

These, in fact, represent a problem of absolute priority for public health since in addition to the loss of human life they generate enormous social and human costs, to which are added high economic costs, which make the issue of road safety a topic of enormous importance for the prevention departments and health systems of all countries. There is talk of a social scourge that causes almost 10 deaths and about 700 people with injuries every day.

The causes can be attributed to numerous risk factors:

- related to the person or health conditions, age, the intake of compromising drugs, attention, balance and reflexes.
- lifestyles that involve the consumption of alcohol and psycho-altering substances, and incorrect driving behaviour (use of cell phones, inattention, excessive speed, failure to use protection systems).
- safety of roads and vehicles.
- social: the poor socio-economic conditions have less access to training and information resources on prevention measures and more generally to the acquisition of a culture of safety on the roads.

To obtain a good reduction in the number and severity of road accidents, a program of prevention interventions is required that considers the multiple factors that underlie a certain type of accident and that simultaneously weigh on the risk. Below is an outline of the macro-objectives aimed at preventing road accidents and reducing their severity.

*Table 1.3 Macro-objectives aimed at preventing road accidents and reducing their severity.*

<b>Risk factors</b>	<b>Targets</b>	<b>Strategies</b>
Behaviour at risk (taking drugs that alter the psycho-physical state, harmful consumption of alcohol and psychotropic substances, excessive speed, failure to use safety devices - belts, child seats, helmet)	Reduce the number of traffic fatalities	Promotion of healthy lifestyles among the population with particular attention to the weakest and most disadvantaged groups  Information/communication on the risk of a road accident related to risky behaviours  Promotion of intersectoral policies aimed at improving the safety of roads and vehicles, thus integrating interventions that affect behavior with those of improving the environment  Promotion of sustainable and safe mobility
	Reduce the number of hospitalizations due to road accidents	
	Increase the subjects with correct driving behaviours	
Road and vehicle safety		
Social factors (economic conditions, work organization)		

Globally, the World Health Organization (WHO) through the World report on road traffic injury prevention (Peden M, 2004) encourages countries to plan a multisectoral strategy for road safety, which takes into consideration the needs of each one by implementing specific intervention projects.

In Europe, therefore, the European Commission has promoted a road safety program which identifies some areas of intervention such as: encouraging road users to behave more responsibly, making vehicles safer thanks to technological innovations, improving road infrastructures through information and communication technologies, collect and analyse data relating to physical injuries due to road accidents.

In Italy, according to Istat estimates, since 2007 there has been an average reduction in accidents with injured people of about 3% every year (ISTAT, 2018). This reduction is explained by the fact that users have begun to use alternative means of transport to private vehicles.

It has been understood that, in order to reduce the risk of an accident and know the result that can be obtained in terms of safety, it is necessary to go beyond simple

compliance with the Highway Code or awareness of potential damage. It is essential to focus on techniques and tools for forecasting events on the road. Therefore, by systematically analyzing the information of "near miss" accident situations, it is possible to implement the related corrective actions.

Some researchers who have dealt with the evaluation of road safety (Hadden W., 1980; Koornstra M.J., 1992) have defined the risk as:

$$\text{Risk} = \text{Exposure} * \text{Hazard} * \text{Vulnerability} \quad 1.12$$

Where:

*Exposure*: quantifies the exposure of road users to potential road hazards;

*Hazard*: quantifies the possibility that a vehicle or user is involved in a collision;

*Vulnerability*: quantifies the severity level resulting from potential collisions.

It can therefore be observed that, with respect to the risk defined previously for natural phenomena, there is an inversion of the terms, but the assessment procedure remains the same.

Basing on this approach a conceptual framework has been proposed to evaluate the road safety risk for vulnerable user, namely pedestrian. The risk thus defined is therefore a function of multiple variables whose correlations are outlined in the following flow chart (Figure 1.6).

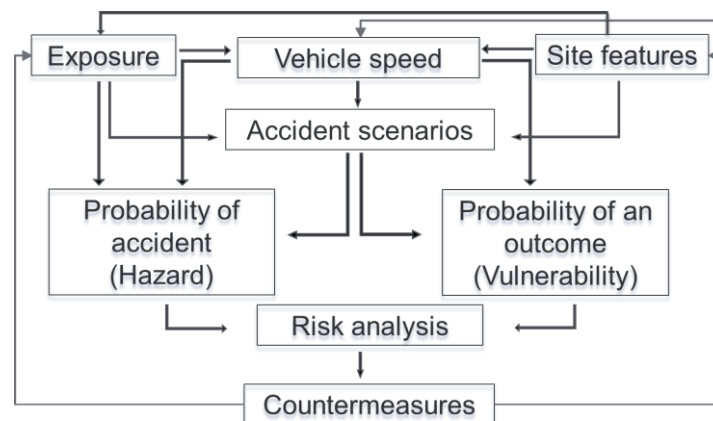


Figure 1.6 Summary scheme of the procedure.

Therefore, once the global risk has been quantified, it is possible to arrange interventions that will improve exposure, vehicle speed and site conditions.

In order to being assessing the risk of having an accident in the study area, it is

necessary to know the history of accidents and their characteristics, in order to bring them back to a typical scenario (Figure 1.8, Figure 1.9).



Figure 1.7 Possible accident scenarios

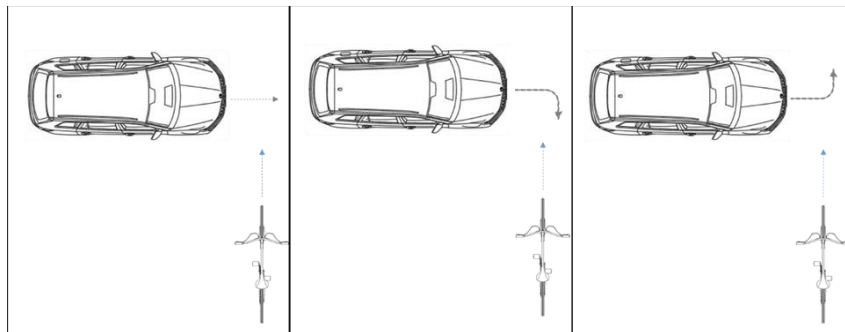


Figure 1.8 illustration of typical cases of auto accidents with bicycle- vehicle.

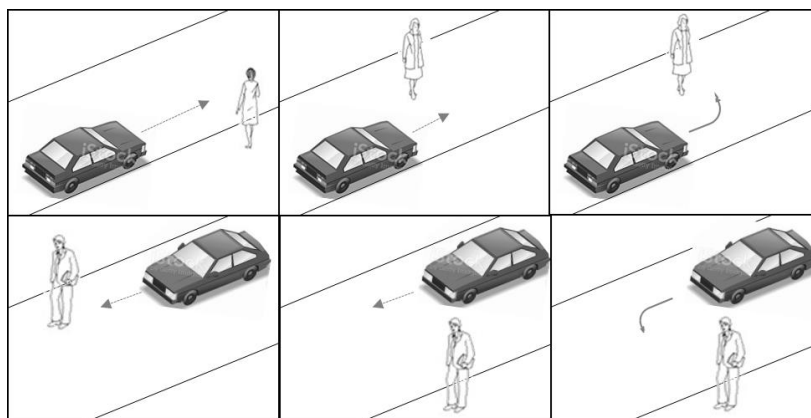


Figure 1.9 Possible pedestrian-vehicle impact configuration

Once the accident scene has been identified, the three key parameters of the risk begin to be assessed. In this chapter the parameters are only partially described, please

refer to the following chapters for a detailed analysis.

### 1.2.1 Exposure

To identify the factors that best predict where and when accidents are likely to occur, exposure needs to be assessed. This is understood as the assessment of potential arrests under sudden conditions. When it comes to exposure, both vehicular and pedestrian flows are involved. The first requires knowledge of the traffic in transit on the section of the road network to be analysed; this can be obtained from survey-based models or from simplified or forecast models. While for the estimation of cycle-pedestrian flows, there are no consolidated models, therefore direct (based on socio-economic and demographic variables) or forecast models (configurational or four-stage, similar to vehicular ones) are used.

#### Vehicular flows exposure

One of the factors that influence the exposure linked to vehicular flows is the speed held by the vehicles, which in turn is a function of both the characteristics of the site and the flows themselves.



Figure 1.10 Vehicular flow in urban areas.



Figure 1.11 Vehicular flow in rural areas.

Many studies link road safety to speed, but the relationships between risk (intended for example as the number of deaths on the road per distance travelled) and speed are almost absent.

The underlying problem is the lack of data collected or their poor quality, i.e. in the databases or in the reports of the law enforcement agencies there is an underestimation of the reports of accidents according to the severity, the number of victims, the number of vehicles involved, location, etc. This indicates that the relationship between speed and risk of collision is based on the number of collisions observed with serious injuries and in strategic locations, but little or nothing is known about accidents with minor injuries or localized in little-known areas, so the problem is underestimated. To overcome the problem of localization relating to areas that are neither urban nor rural, an alternative method could be to consider the real speeds recorded on a road section

by extrapolating them from the black boxes mounted on cars (the Floating Car Data, FCD) (D'Apuzzo M. et al.,2021). Once these data have been obtained, it is possible to evaluate the speeds also in areas other than urban or rural, or for transition areas.

This area represents the space of passage between a rural to an urban area in which, however, the user is still unable to realize the passage and therefore may not adopt a suitable speed. Formally, the transition between the rural and the urban environment is highlighted by warning signs that are displayed at the entrance to urban areas. Often these signs are associated with specific urban speed limits. However, it must be recognized that "official" administrative boundaries do not always express the real boundary between the urban environment and the surrounding areas.

Therefore it is possible to apply a generalized predictive model that starts from the re-calibration and readjustment of the literature models.

### **Pedestrian and cycling flow**

The estimation of the exposure of pedestrian flows can be approached starting from the use of configurational methodological tools (D'Apuzzo M. et al., 2020) which will then be enriched with “demand-driven” models (four-stage) which will also allow obtaining estimates of the cycle flow.



*Figure 1.12 Pedestrian flow*



*Figure 1.13 Cycle flow*

The configurational analysis considers only the connectivity of the network, so the more this is connected, the greater the connectivity of the sections. This exemplified approach has been enriched by integrating the analysis with behavioral models deriving from the transport analysis. The results of the hybrid approach obtained can then be correlated to the pedestrians observed on the network in order to understand the goodness of the estimate.

In order to improve the estimation of pedestrian flows and to evaluate cycling flows, the hybrid configurational model can be enriched using the four-stage model (similar to vehicular) starting from literature models. This allows to obtain an estimate of the flows and distribute them on the network so as to be able to understand where it is necessary to intervene to redevelop the area.

## 1.2.2 Hazard

Whenever the user enters a road, he is exposed to accept the hazard and therefore the risk of being injured. In order to evaluate the hazard it is necessary to understand if the user correctly perceives the environment crossed, this requires an analysis of the site.

So first of all, it must be understood in what administrative environment you are, then let's talk about urban or rural context. The urban area is that set of buildings, delimited along the access roads by the appropriate start and end signs (Ministero delle infrastrutture e dei trasporti, 1992). In which the set of buildings includes a continuous grouping, albeit interspersed with streets, squares, gardens or the like, consisting of no less than twenty-five buildings and areas of public use with vehicular or pedestrian accesses on the street. Anything that does not fit this definition is rural. It should be emphasized that the boundaries between the two areas are never clearly defined; however, formally, in most Western countries, urban limits or "administrative boundaries" are identified with vertical entry warning signs usually associated with speed limits.



Figure 1.14 Street in urban area



Figure 1.15 Street in rural area



Figure 1.16 Urban border



Figure 1.17 Rural border

Depending on the context, there is a greater chance of coming into conflict with other users, therefore it is necessary to take into account the presence of local attractions, such as schools, hospitals, shopping centers or any other activity that may

generate greater crowding.

In addition to other users, further sources of hazard are linked to the presence of obstacles on the route which are often not correctly displayed due to poor visibility conditions. Visibility is defined as the minimum stopping distance, this depends on many factors such as speed, the conditions of the road surface (the type of road surface, maintenance status, etc.), the condition and pressure of the tires, the characteristics and condition of the vehicle's braking system, the weather conditions as well as the geometric characteristics of the site (considering the road as the sum of straights and curves, number of lanes, longitudinal and trans-verse slope, etc.).

### **1.2.3 Vulnerability**

To assess the risk, vulnerability remains to be defined. This is the probability, conditioned by the type of accident, that a vulnerable user suffers damage (injured or dead) or that the driver suffers damage (uninjured, injured or deceased).

In addition to a security point of view, vulnerability is seen as a problem of reduced accessibility that occurs for various reasons. In general, accessibility is understood as "ease of access", or the opportunity provided by the transport system for users to carry out an activity (Jones S., 1981). Improving accessibility means increasing the number of routes or the quantity of services considering low costs.

Estimating vulnerability means studying all those events, of a more or less sudden and/or unpredictable nature, which cause circulation problems. These events depend on adverse weather conditions, rather than physical breakdowns or road accidents, or planned road works, etc. Depending on the event and the category, there is a variation in terms of frequency, predictability, geographical extension, etc.

To achieve a reduction in vulnerability it is necessary to limit the risks involved in various incidents; this implies the need to identify a spectrum of accidents, collect data on the probabilities and consequences of these, having done this it will be possible to establish experiments to identify acceptability values, as well as investigate and evaluate the effects of possible mitigation measures and strategies for improvement.

Numerous relationships are reported in the literature that considers the links between stress characteristics, kinematic or mechanical magnitudes of the impact of the occupants, but there are still few of them regarding vulnerable users. The basic problem is that the existing ones are based on simulations with corpses or with limited data-sets in terms of location, severity and number of accidents, necessary for the calibration and validation of the models.

Hence the need to create a virtual laboratory that through multibody numerical

simulations, as the position (front, side), age, weight and height of the pedestrian, vehicle fronts and travel speed vary, allows obtaining objective kinematic parameters (acceleration, speed, etc.) or mechanical (moments, shear, normal stresses, etc.) with which to enrich the vulnerability functions.

In the preliminary phase, studies are being carried out on injuries on parts of the body with a high probability of death, using the scale based on damage, disability and social cost; in this, the long-term consequences and the influence that the injuries have on the patient's quality of life are assessed. Damage criteria were then used to estimate the severity of damage to the head, chest and spinal cord. Then the data obtained from our model in terms of ISS were compared with those obtained from vulnerability models present in the literature to verify the veracity of the results.

It has been highlighted that in collisions between vehicle and pedestrian there is different kinematics according to the impact speed, the pedestrian position, the different height and length of the bumper and the angle of inclination of the bonnet; this means that the pedestrian impacts the various regions of the human body (eg head and thorax) in a different way also based on his build.

The use of numerical simulation allows taking into account numerous variables, compared to canonical vulnerability models, which allows for more realistic outcomes.

### **1.3 Conclusion**

Despite the large number of deaths and injuries due to road accidents, there is still no clear regulation according to which the safety assessment for vulnerable users is reported. The goal of this study is to identify a procedure for estimating the main risk factors starting from microscopic analyzes. The results of these analyzes can then be integrated at a macroscopic level to define and predict safety performance as well as predict the probability of collision.

Starting from the traffic and cycling-pedestrian data, from the accident data and from the speed estimates, it is possible to identify blackspots i.e those points or section of the road network that present anomalous concentrations of accidents. Once the risk of each road section has been identified, it is necessary, before implementing the proposed interventions, to evaluate the benefits that these would bring and the respective costs. Until now, road safety analysts have relied on personal experience in order to make reliable forecasts, thus working subjectively; to avoid this, analysis methodologies have been developed that take into account the correlations between “cause” (man-road-environment) and “effect” (occurrence of the accident). These

methodologies, typical of the engineering field, try to identify links of an empirical nature between the occurrence of the generic accident and the multiplicity of factors that make up the road environment, to the point of proposing mathematical models for forecasting purposes. In the Italian context, such models do not yet exist, so it is intended to apply macroscopic models calibrated in the international scientific literature (cf. Highway Safety Manual recently released in United States) to transpose them to Italian context and calibrate corresponding Safety Performance Functions (SPFs). These latter mathematical tools, based on statistical analysis, evaluate the impact in terms of the number of accidents, as a function of the characteristics of the site and of the exposure. SPFs, refer to basic conditions but can be applied to different study conditions with the use of accident modification factors (Crash Modification Factor - CMF) that take into account specific local site-conditions.

Once the procedure will be developed and applied, it will be possible to evaluate, depending on the characteristics of the site and the type of risks present in the area, the countermeasures to be adopted to increase safety.

## References

D.Lgs n°81. 2008. modulo B8.

D'Apuzzo M., Evangelisti A., Modoni G., Spacagna R.L., Paoletta L., Santilli D. & Nicolosi V. 2020. Simplified approach for liquefaction risk assessment of transportation systems: preliminary outcomes. *Computational Science and Its Applications – ICCSA 2020 VII* (p. pp.645-657). Cagliari, Italy. Springer. [https://link.springer.com/chapter/10.1007/978-3-030-58820-5\\_10](https://link.springer.com/chapter/10.1007/978-3-030-58820-5_10)

D'Apuzzo M., Evangelisti A., Santilli D., Rasulo A., Zullo M. & Nicolosi V. 2019. A Simplified Approach for the Prioritization of Bridge Stock Seismic Retrofitting Conference: Proceedings of the 29th European Safety and Reliability Conference (ESREL), September 22 - 26, 2019, DOI: 10.3850/978-981-11-2724-3\_0592-cd ISBN: 978-981-11-2724-3.

D'Apuzzo M., Santilli D., Evangelisti A., Fusco G., Nicolosi V., Perneti M., Isaenko N. 2021 Traffic Injury Prevention. Towards the development of a hybrid approach to speed estimation in urban and rural areas. Taylor & Francis. DOI:10.1080/15389588.2021.1935904

D'Apuzzo M., Santilli D., Evangelisti A., Pelagalli V., Montanaro O. & Nicolosi V. 2020. An exploratory step to evaluate the pedestrian exposure in urban environment. *Computational Science and Its Applications – ICCSA 2020 VII*

- (p. pp.645-657). Cagliari, Italy. Springer. DOI:10.1007/978-3-030-58820-5\_47. ISBN:978-3-030-58819-9  
[https://link.springer.com/chapter/10.1007/978-3-030-58820-5\\_47](https://link.springer.com/chapter/10.1007/978-3-030-58820-5_47)
- Hadden W. 1980. Advances in the Epidemiology of Injuries as a Basis for Public Policy. Public Health Reports, Vol. 95, No. 5, pp. 411–421.
- IFRC.1999. Vulnerability and Capacity Assessment. An International Federation Guide. Geneva: Source: <http://www.proventionconsortium.org/files/vca.pdf>.
- ISTAT. 2018. Dati ISTAT. Taken from <http://dati.istat.it>
- Jones S. 1981. Accessibility Measures: A Literature Review. Rapporto TRRL 967. Crowthorne, Berkshire.: Transport and Road Research Laboratory,.
- Kolluru R.B.S.1996. Risk assessment and management handbook. New York: McGraw-Hill.
- Koornstra M.J. 1992. The Evolution of Road Safety and Mobility. IATSS Research, Vol. 16, No. 2, pp.129–148.
- Ministero delle infrastrutture e dei trasporti. (1992). Art. 3. Definizioni stradali e di traffico. Nuovo codice della strada. D. lgs 30 aprile 1992 n. 285.
- Peden M., Scurfield R., Sleet D. & al.2004. World report on road traffic injury prevention. Geneva: World Health Organization.
- Tesfamariam S. and Goda K. 2013. Seismic risk analysis and management of civil infrastructure systems: an overview. In Handbook of seismic risk analysis and management of civil infrastructure systems. S. Tesfamariam and K. Goda editors, Woodhead Publishing Limited, pp.141-174.
- UN General Assembly. 2015. The Sendai Framework for Disaster Risk Reduction 2015–2030. Available online at [www.unisdr.org/we/inform/publications/43291](http://www.unisdr.org/we/inform/publications/43291).
- UN/ISDR. 2004. Glossary. Basic Terms of Disaster Risk Reduction. Source <http://www.unisdr.org/unisdr/eng/library/lib-terminology-eng%20home.htm> <viewed2004>.
- UNDRO. 1979. “Natural disasters and vulnerability analysis”. Report of expert group meeting.
- UNI11230. 2007. Gestione del rischio: Vocabolario.
- Wolfensohn J. and Cherpitel D.2002. Why we need to do what we are doing. Washington DC: Source: (<http://www.proventionconsortium.org/articles/whyweneed.htm>).

# CHAPTER 2. VEHICULAR FLOWS

## EXPOSURE

To analyze or plan interventions for the safety of transport systems, it is necessary to estimate the demand of users, to know the variations and exposure. To estimate the current demand, it is possible to carry out surveys on a sample of users and from these, using the techniques of inferential statistics, direct estimates of the demand are obtained. While models are used to estimate demand (current or future). In the literature, there are several models with different complexities depending on the examined area and the resources available for the estimation. These models can generally be divided into: deterministic or stochastic, static or dynamic, macroscopic (aggregate) or microscopic (disaggregated), analytical models and simulation models. The combination of transport demand forecasting models at the macro level (e.g., regional or national), are typically based on variants of four-stage planning models, with microscopic or mesoscopic traffic simulation approaches.

The use of a single variable or multiple variables in the model specification results in univariate and multivariate forecasting models, respectively.

So the common element is that they all allow to define the number of trips made by an area, the destination of these trips, the travel modes used and the chosen path.

After evaluating the flows and their variations in time, by imposing the characteristics of the infrastructure, it is possible to estimate the travel speed.

There has been a remarkable debate on the relationship between road safety and vehicle speed in the last seventy years and a huge amount of studies has been carried out to investigate intimate connections between accidents and vehicle speed (Elvik et al., 2009). Speed-accident relationship developed by several authors have been often used as a scientific basis to implement speed limit policies, however, to a more careful examination, the connection between speed and safety is not obvious as it can appear, especially if the relationship between average flow speed and accident risk is concerned (Hauer, 2009). An updated meta-analysis of the scientific studies on this issue confirmed even a stronger relationship, in terms of exponential or power model, between road accidents and the traffic speed (Elvik et al., 2019).

The objective of this research is the development of a generalized model to estimate the speed sustained by vehicles in urban, rural areas and in the transition zone between them, with the final aim of providing a tool that can simulate travel speed in a more realistic manner. The data used in the analysis have been derived from Floating Car Data (FCD) that allow to know, for each probe vehicle, speed and position at a specific time with high sampling frequency thus reconstructing the main characteristics of traffic on a road network such as data on travel time, speed, route. The filtered speed data were compared with the estimated speed obtained with the use of models already present in the literature and conveniently selected for the different contexts analyzed.

In particular, the model has been developed in order to describe the speeds adopted by users in the transition areas.

As a matter of fact, although not foreseen in Italian Highway Design Standards, these peculiar road sections are very common in the Italian road network environment since they represent the results of a stratification of urban and transportation planning that has been often regulated in a confused and disorganized manner in the past seventy years.

Following the above-mentioned premises, a calibration of the used models was carried out, with the aim to provide an adequate tool for estimating the speeds in each context area.

## 2.1 Literature review

The present study considers the factors influencing the speed of drivers, both in free flow and congested conditions on urban and rural and suburban roads. As previously mentioned, speed prediction has always been considered as the “Holy Grail” of the research in road safety as it affects most of methodologies currently adopted in highway design. On the other hand, it has to be reminded that vehicle speed is of paramount importance for the evaluation of road network performance, as it affects travel time. Following these premises, past research has tackled the problem under two main point of view:

1. “Spot” speed in free flow conditions, on which *Time Mean Speed (TMS)* can be evaluated by means of simple arithmetic mean of the instantaneous speed derived from cross-sectional measurements within a defined observation time;

$$V_t = \frac{1}{n} \sum_{i=1}^n V_i \quad 2.1$$

Where:

$V_t$  = time mean speed;

$V_i$ = spot speed of  $i^{\text{th}}$  vehicle

$n$ = the number of observations

2. “Running” speed under traffic, which is based on *Space Mean Speed (SMS)* concept;

$$V_s = \frac{n}{\sum_{i=1}^n \frac{1}{V_i}} \quad 2.2$$

Where:

$V_s$ = space mean speed;

$V_i$ = spot speed of  $i^{\text{th}}$  vehicle

$n$ = the number of observations

The rationale to understand these two fundamental approaches is based on the difference between the time mean speed and the space mean speed where the former comes from cross-sectional speed measurements, and it can be defined as the simple arithmetic mean of the instantaneous speed of vehicles traversing a specific line within a defined observation period whereas the latter is derived from measurements carried out on a specific road section and, among the several definitions available, it can be evaluated as the ratio between the examined road section length and the average travel time (Ajay et al., 2001).

If the speed of the vehicles is constant (plausible assumption if the length of the road section is sufficiently short) the space mean speed can be evaluated as the harmonic mean of spot speeds. As a matter of fact, since harmonic and arithmetic averages are evaluated on the same dataset, it is possible to mathematically demonstrate that the space and time mean speeds are analytically related and then it is possible to estimate the time mean speed starting from the space mean speed, exploiting a mathematical correlation (being such quantities linked by corresponding standard deviations) (Wardrop, 1952). The estimated space mean speed values have been converted in equivalent mean time values by making use of the following experimental relationship as a function of Average Travel Speed, ATS, reported in HCM2000 (Wachs et al., 2000):

$$V_{mt} = \frac{3.042 + ATS}{1.026} \quad 2.3$$

To determine the allocation of new resources or to improve the transport system, and therefore the quality of service provided to drivers, speed prediction models are used according to the two different traffic scenarios previously mentioned.

It is believed that free-flow conditions are more often reached in the rural environment and, therefore, most TMS prediction models are based on road alignment

characteristics. First studies explored the influence of horizontal curves on speed and early relationships based on vehicle cornering stability and skidding have been proposed (Hassan et al., 2011) (AASHTO, 2004).

Later on, experimental statistical distributions of spot speeds have been derived and the concept of operating speed, V85, has been introduced, which is defined as the speed below which 85% of the drivers (cars only) travel on a particular element of the road layout. Furthermore, additional independent variables such as posted speeds, cross-section features have been proposed (Hassan et al., 2011).

As far as the conditions under traffic are concerned, pioneering works by B.D. Greenshields (1935) shed light on relationships between SMS, flow rate, and vehicle density that were further used as a basis for the evaluation of Level of Service (LoS) of road infrastructures (Wachs et al., 2000), on the one hand, and for the development of road link cost functions (Cascetta, 2009) (Pinna et al., 2018), on the other.

### **2.1.1 Free flow conditions (or isolated vehicle)**

Relationships between road alignment characteristics and speed chosen by drivers have been the subject of a huge amount of research in road safety for the past eighty years, and exhaustive critical analysis is beyond the scope of the present paper. Nevertheless, it is worth to be highlighted that, as previously stated, the main interest has focused on spot speed collected in a rural environment, especially on two-lane rural highways. First attempts have acknowledged that horizontal curves are the most significant road geometric elements able to affect the speed actuated by drivers and therefore early relationships have been proposed based on physical principles related to vehicle cornering stability against skidding that are still used in several Road Geometric Standards worldwide (Hassan et al., 2011) (AASHTO, 2004).

Later on, experimental distributions of spot speed have been derived and the concept of operating speed has been subsequently introduced, since it has been considered in the literature as a speed descriptor more representative of the effective behaviour of the road user.

Conventionally, the operating speed is defined as the speed below which 85% of the drivers (cars only) travel on a particular element of the road layout under conditions of free flow, dry road, daylight and good weather conditions, it is universally termed as V85 and its use is fundamental in the evaluation of highway design consistency.

It has been recognised that driver speed choice on two-lane rural highways is highly correlated to the geometric road features such as the Radius of circular curves, the

Curvature Change Rate (CCR), the speed on preceding/subsequent tangents and of road section layout characteristic, the “environmental speed” and speed rules.

In detail, some models in the literature investigate the relationship between operating speed and imposed speed limit (Dixon et al., 1999) (Ali et al., 2007), other relationships see the characteristics of the road section as independent variables (Tarris et al., 1996) (Capaldo et al., 1998) (IAPSIS, 2001) (Bakaba, 2003) (Poe and Mason, 2000) and other models still highlight that the operating speed and the recorded velocity are correlated (Fitzpatrick et al., 2003). Further models link the project speed with the 85th percentile operating speed (Fitzpatrick et al., 1997) (Wang et al., 2006). In the following Table 2.1, a synoptic figure of the relevant prediction models is reported.

Table 2.1 Review of spot speed prediction models (taken from D'Apuzzo, Santilli, et al., 2021)

Author(s) (Year)	Dependent variables	Independent variables	R <sup>2</sup>	Area
Tarris et al. (1996)	V85	DC = degree of curve (degrees)	0.63	U
Fitzpatrick et al. (1997)	V85	R = curve radius AD = approach access density (Number of access points per km)	0.71 0.83	S
Capaldo and Grossi (1998)	V85	CCR= curvature change rate i=longitudinal slope (%);	-	R
Lamm et al. (1999)	V85	CCR= curvature change rate	0.73 0.80 0.81	R
Poe and Mason (2000)	Va	DEGCVR = degree of curvature LANWIDN = lane width [m]; HZRT5N = (roadside hazard rating) indicates the risk of an accident on a single two-lane roadway	-	U
IASPIS project (2001)	V85	CCR= curvature change rate	-	
Fitzpatrick et al. (2003)	V85	PSL = posted speed limit (mph), AD = access density (pts/mi)	0.90 0.92	U-R
Figueroa and Tarko (2004)	Vp	PSL = posted speed; RUR = segment is in a rural area; SD = sight distance (ft); INTD = intersection density; DRWD = driveway density ECLR = distance from edge of traveled way to roadside obstruction (ft); ICLR = distance from internal edge of traveled way to inside edge of opposing traveled way or median barrier face (ft); RAIL = guardrail TWLTL = two-way left-turn median lane is present. Zp = standardized normal variable corresponding to a selected percentile speed.	0.86	U-S
Wang et al. (2006)	V85	lane.num = number of lanes; roadside = density of trees; driveway = density of driveways; intersection = density of T-intersections.		U

Author(s) (Year)	Dependent variables	Independent variables	R <sup>2</sup>	Area
Ali et al. (2007)	FFSmean V 85	PS = posted speed	0.76 0.77	U
Cafiso et al. (2007)	V 85	$\gamma_i$ = deflection angle of the geometric element; CCRsect = section curvature change rate; W = width of the paved cross section (lanes and shoulders) (m)	-	
Nie et al. (2007)	V 85	LAT = length of approach tangent (m); CCR = curvature change rate; LDT = length of departure tangent (m); R = radius of curve (m); DFC = curve deflection angle (degrees).	0.698 -0.99	U-S
Marchionna and Perco, (2008) cited in Hassan et al.(2011)	Vd	CCR= curvature change rate	0.77	R
Federal Highway Administration(2008)	V 85	R = radius of curvature (m) G = grade (%)	-	R

Where:

V 85= 85th percentile speed for safety;

Va = average speed;

FFSmean = average free flow rate over time;

Vp=estimated operating speed for a selected percentile value;

Vd= desired speed (the maximum speed attained by drivers on long (independent) tangents of the homogeneous road section).

### 2.1.2 Conditions under traffic

The study of the influence of the traffic flow on space mean speed originated in the 1930s with the pioneer Bruce D. Greenshields (1935) and then developed after the Second World War, with the huge increase in cars and the expansion of the road system, until reaching in our day (Kuhne, 2008).

Since the efforts have been mainly devoted in deriving road link cost functions that are relevant in the development of transportation system supply and travel demand models, several independent variables other than flow itself have been proposed regarding the road link characteristics and in a more generalized manner in the road environment in which road users move. Indeed, the generalized transport cost associated with a road trip can be evaluated by summing all the costs born by travelling along the different road link in which the trip can be decomposed. For each road link the generalized transport cost is a function of the travel time along the road section (that, in turn, is related to the running speed), of the waiting time (e.g., at the final junction, at the toll, etc.) and of the monetary cost (Carteni and Punzo, 2007) (Wardrop, 1952).

On the other hand, it has to be reminded that Level of Service Evaluation procedures in uninterrupted flow conditions are based on Space Mean Speed (namely Average Travel Speed) versus flow relationships and therefore even in a rural environment and for different kind of road layout prediction models under traffic have been developed (Hassan et al., 2011).

Several models have been proposed in order to estimate the space mean speed (in terms of running speed or average travel speed) according to the characteristics of the study area and the flows and some of the most recent and relevant ones are reported in the following Table 2.2.

Table 2.2 Review of running speed/average travel speed prediction models (taken from D'Apuzzo, Santilli, et al., 2021)

Author(s) (Year)	Dependent variables	Independent variables	R <sup>2</sup>	Area
Karlgren (2001)* cited in Aronsson(2006)	V <sub>a</sub>	Flow= vehicle flow per hour in the studied direction CW= average carriageway width C=number of crossing pedestrians and cyclists	0,69	U
Arosson K. F.M. (2006)	V <sub>obs</sub>	Flow = Observed average traffic flow Ped = Average Number of crossing pedestrians and cyclists Lanes = Number of lanes BicSep = Separated bicycle lane Park = Roadside parking permitted Bus = Roadside bus stop	-	U
Carteni, A., & Punzo, V. (2007)	V <sub>a</sub>	L <sub>ua</sub> = the useful width; P <sub>a</sub> = the nonnegative slope ; T <sub>a</sub> = tortuosity D <sub>a</sub> = an index of disturbance S <sub>a</sub> = the percentage of length of a occupied by parking; P <sub>va</sub> = a dummy variable Flow= vehicle flow per hour in the studied direction.	-	U
Wachs et al. (2000)	ATS	FFS = Free Flow Speed %NP =% of No passing section on the overall road sections HFR= Hourly Flow Rate FHV =Fraction of Heavy Vehicles FRV = Fraction of Recreational Vehicles G = Road Grade Factor	-	R
Zedda M. & Pinna F. (2018)	V <sub>a</sub>	F = flow C = presence of crosswalk TL = length of tangent between two intersections O = type of left-lateral obstacle LW = lane widths M = type of median	0.81 0.84	U

Where  
V<sub>i</sub>=speed of travel of the arc i;  
V<sub>a</sub>= average speed;  
ATS= average travel speed;  
V<sub>obs</sub>= observed space mean speed.

It has to be underlined that almost all the prediction models proposed are empirical and therefore, they have been derived by a statistical analysis of experimental data. This implies some important constraints regarding (Hassan et al., 2011):

- statistical significance, insofar most of them have been developed on an insufficient amount of test sites or following a poor experimental design;
- model transferability, since results obtained following an experimental campaign carried out on a specific country/state cannot be consistent with those derived from another country/state.

As far as the former issue is concerned, the recent availability of Floating Car Data (FCD) in Italy has widened the landscape of the possibilities in collecting traffic information.

## **2.2 Driver behaviour in transition urban-rural area**

In road design, there is a clear distinction between urban and rural area, and this implies different criteria and procedures to be adopted in the International Design Standards. Formally, the transition between the rural and the urban environment is highlighted by means of warning signals that are exposed at the entrance of urban areas. Often these signals are coupled with specific urban speed limits.

However, it has to be acknowledged that “official” administrative limits not always express the real boundary between the urban environment and its surrounding areas. The problem can also be ascribed to the fact that urban development worldwide has historically followed an irregular and somehow uncontrolled spatial pattern with a gradual urban density decreasing when leaving the urban centre irrespective of the presence of warning signs. This can also be due to the fact that urban limits are often defined by local municipalities according to an approach that is, sometimes, inconsistent with road network planning criteria. Furthermore, while in town planning the suburban area is somehow a more consolidated concept, in road design there is still a lack of knowledge and of Standards to deal with these critical areas (AASHTO, 2004).

Given these premises, there is a need to investigate driver behaviour in these areas, provided that extensive speed data are made available.

Most of the reviewed models are empirical and this implies some important constraints regarding (Hassan et al., 2011): model transferability (the results are site-

dependent) and statistical significance (low sample size).

On the other side, since the 2000s, massive use of combined GPS car tracking on-board units, formerly known as “Black Boxes” (BB), have been increasingly spreading in Europe. Kinematic and position vehicle data, namely Floating Car Data (FCD), are remotely acquired, allowing for profiling road user behaviour.

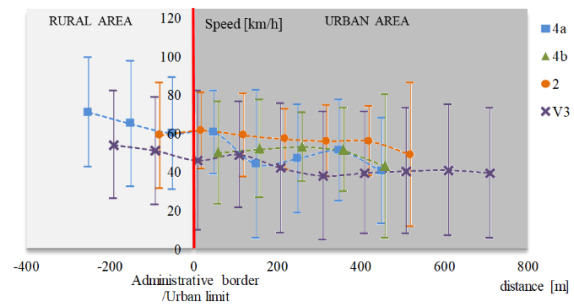
Given the usual traffic speed values experienced in rural (50-100 Km/h) and urban (20-60 Km/h) areas, with such low sampling frequency, a single spot speed value is acquired each 0,5 Km and each 1 Km, on average, in urban and rural areas respectively. This makes this data practically useless, as far as the reconstruction of a single vehicle speed profile is concerned.

However, the huge amount of FCD nowadays available allows, on the contrary, to evaluate the spatial variation of spot speeds along the road alignment with a very high density. In this connection, speed data derived from FCD have been averaged on 100 m long sections and have been evaluated and positioned with respect to the urban/rural administrative border. In such a way, it became possible to derive a speed profile as a function of travelled distance in terms of average values.

In the following figure (Figure 2.1 a) a typical outcome of this analysis procedure is presented within a Geographic Information System (GIS) environment, whereas in the Figure 2.1b speed profiles for some of the investigated sites, have been conveniently reported.



a)



b)

Figure 2.1 a) Spot speed values derived from the georeferenced FCD along a selected road alignment presented in a GIS platform. b) diagram describing the speed data, aggregated on a 100 m long section basis and depicted as a function of travelled distance from the administrative urban/rural border with corresponding confidence levels thresholds.

The large dataset of speed and position of vehicles has been recently used to seek the opportunity of calibrating and validating data-driven short-term traffic prediction methods in urban areas also by means of a machine learning approach able to catch the time-space correlation underlying the stochastic process of traffic dynamics and to

provide very short-term prediction within traffic control systems (Fusco et al., 2015) (Fusco et al., 2016), although a better accuracy can be obtained by a mixed “regime based” approach (Fusco et al., 2017).

However, it has to be underlined that the geometrical and functional road characteristics are implicitly embedded in the machine learning model architecture, so that the speed prediction models based on soft computing techniques appear as “black box” with respect to the road characteristics. It follows that they cannot help engineers in the safety design/retrofitting stage because of the lack of an explicit relationship with the physical influencing factors such as the road or site layout.

On the other hand, the huge amount of FCD data made recently available lays the foundations for the development of more refined speed forecasting models.

In this connection, the objective of this research is to propose a methodology aimed at developing a generalised model for estimating more realistic vehicle speed values in urban, rural, and transition areas. Such speed prediction models can represent a useful tool in the design of engineered road safety countermeasures due to the aforementioned strong connection between traffic speed and road accidents.

With the aim to reconstruct the main characteristics of traffic on a road network, the FCDs, which, for each probe vehicle, provide speed and position with high spatial sampling and acceptable sampling frequency, have been used. The methodology of data analysis and the obtained preliminary results are detailed in the followings.

### **2.3 Proposed method for the speed evaluation**

The basic idea is that road user travelling from a rural area cannot immediately realise that is entering in an urban area with different speed rules since the presence of a “blurred” road environment (Girling et al., 1994) and poor or absent road sign may affect his speed choice. Therefore, he makes some time (and thus some travelled distance) in order to adapt the speed to the different environment. In this preliminary study, a “mirrored” road user behaviour is assumed when he is leaving an urban area. Although the transition between the rural and urban environment is not always clear to the driver and some other factors such as road layout and building density close to the street may affect driver speed, some significant evidence of the postulated behaviour has been provided by analysing the spatial distribution of vehicle speed derived by FCD.

Following these premises, the time mean speed on specific road cross-section falling in this “transition” area can be evaluated as a linear combination of urban and rural spot speed estimates following a linearly decreasing trend.

Furthermore, the methodology that has been proposed in order to evaluate the vehicle speed in transition areas is based on the following constraints and assumptions:

- the model applies only for two-lane rural/urban roads;
- time mean speed (only for passenger cars) chosen as dependent speed descriptor;
- well-known travel speed and road link cost function have been used to evaluate space mean speed for rural and urban areas; in detail, for the urban area, the formulation proposed by Cartenì and Punzo (2007) has been selected; instead, for the rural area the Highway Capacity Manual 2000 (Wachs et al., 2000)
- provided that the length of the examined road section is relatively small, time mean speed and space mean speed can be derived from the same speed dataset as the arithmetic and the harmonic mean respectively; therefore, there is a theoretical relationship (that has also been experimentally validated (Wachs et al., 2000)) that can be exploited to express time mean speed,  $V_{tm}$ , as a function of the space mean speed or Average Travel Speed, ATS;
- a buffer area of an overall 1 km long centred in the examined road cross-section has been considered for space mean speed evaluation, to take into account the road environment (road layout, width, adjacent parking activities and land use, number of accesses, etc.) as a relevant independent variable affecting driver’s speed (Cartenì and Punzo, 2007) (Wachs et al., 2000) (Hassan et al., 2011) (Wardrop, 1952);
- since traffic flow cannot be directly inferred from FCD, flow values collected on an hourly basis at the nearest traffic census station have been considered.

Based on these premises, the proposed prediction methodology has been developed according to the following procedure:

1. the road cross-section (station point) on which time-space mean speed is to be evaluated, is selected and pertaining area type (rural or urban) is identified;
2. the closest administrative border between rural and urban area is detected and its distance,  $d$ , from the selected road cross-section is evaluated;
3. FCD are extracted on a 1 km long road section centred in the selected station point and conveniently analysed and filtered in order to expunge not relevant data;

4. FCD are aggregated on an hourly basis and the highest value usually reached in the off-peak period is selected, in order to obtain the experimental free-flow speed for each selected test site;
5. experimental free-flow speeds are converted into equivalent time mean speeds;
6. road section characteristics are collected on a 1 km long road section centred in the selected station point and average values are derived;
7. space mean speed for the rural and urban areas are evaluated in free-flow conditions according to the aforementioned well-known prediction models reported in Eqs. (2.42.3)
8. estimated free-flow speeds are converted into equivalent time mean speeds by means of Eq. (2.5);
9. the time mean speed estimate for transition area is evaluated as a linear combination of previously estimated rural and urban speed values according to a transition length,  $L^*$ , that is derived by means of least square optimisation procedure based on the comparison with experimental data derived from FCD for all the examined tests.

Once that the calibration of the transition free-flow speed prediction model has been completed, a subsequent calibration of the model under traffic can be undertaken:

10. experimental and estimated speed values are converted into equivalent time mean speeds;
11. a comparison between the experimental speeds under traffic derived from FCD data and the estimates provided by the generalised transition model is carried out;
12. if the scattering is high, thus providing the evidence for a low correlation between the two datasets, a refined calibration for each test site is carried out;
13. the calibration is obtained by means of least square optimisation procedure based on the comparison with experimental data derived from FCD for each test site by varying the value of the coefficient multiplying the flow term, namely  $K_{urb}$  and  $K_{rur}$ , for the urban and in the rural prediction model, respectively;
14. the statistical regression is tested in order to express the  $K_{urb}$  or  $K_{rur}$  value as a function of road characteristics related to independent parameters pertaining to each selected test site.

The flow chart describing the overall procedure is depicted in Figure 2.2.

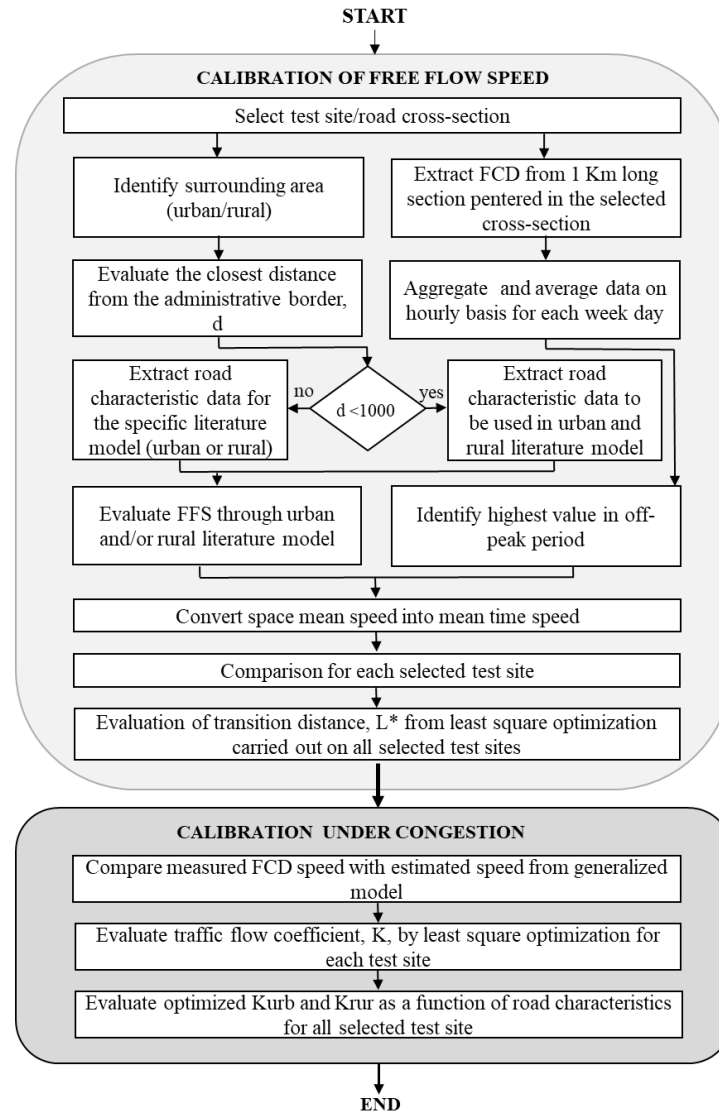


Figure 2.2 Flowchart of the proposed methodology to develop generalised speed prediction models for two way single carriageway road layouts in urban, rural and “transition” area

## 2.4 Results

FCD used in the research, although conveniently “masked” in order to minimize road user’s privacy issues, collect several interesting information on vehicle trip with a sampling frequency of one sample per second. Each record contains the following data: ID number of vehicle, and black box, type of vehicle, spot speed and corresponding direction, signal quality (depending on the number of visible satellites), geographical coordinates, recording time. Obviously, not all the records are significant for the study and therefore a post-processing of data needs to be carried out.

FCD data have been collected on different candidate sites Italian road sections located in rural and urban areas in central Italy. An overall amount of eleven test sites has been selected pertaining urban, transition and rural areas, in central Italy. Criteria for selection of the test sites were based on different traffic volumes and on mutual distance higher than 10 km in order to obtain uncorrelated speed and traffic patterns for each selected site. An overall amount of 111410 FCD records has been examined and subsequently imported on GIS software and following a filtering process, data have been aggregated on an hourly basis and averaged according to the specific weekday.

### 2.4.1 Speed analysis in free-flow conditions

Since free-flow conditions cannot be directly inferred by FCD, isolated vehicle speeds have been derived from off-peak period traffic scenarios for each selected test site. Surprisingly, the maximum hourly averaged daily speeds were found similar to the maximum averaged speeds in the night period (between 10.00 pm and 6.00 am on weekdays) for each examined site.

#### Urban area

For the urban area, reference is made to the formulation proposed by Cartenì and Punzo (2007) since it has been developed from a significant amount of experimental data that has been also complemented by results provided by numerical simulations carried out by means of a traffic microsimulation approach (Cartenì and Punzo, 2007).

$$V_i = 29.9 + 3.6Lu_i - 0.6S_i - 13.9W_i - 10.8H_i - 6.4I_i + 4.7X_i - 1.0 \cdot E - 04 \frac{(\frac{f_i}{Lu_i})^2}{1+W_i+H_i+I_i} \quad 2.4$$

Where:

$V_i$  = mean travel speed of the  $i$ -th (1 km long) road section test site in km / h;

$L_{ui}$  = average useful width of the  $i$ -th (1 km long) road cross-section test site in m;

$S_i$  = average slope in % of the  $i$ -th (1 km long) road section test site in m; , not negative;

$W_i$  = dimensionless tortuosity of the  $i$ -th (1 km long) road section test site [0,1];

$H_i$  = index of the disturbance caused to traffic by external factors (lateral entries, irregular stops, pedestrian crossings, etc.) in values included in the interval [0,1]

$I_i$  = fraction of the road section which has side parking;

$X_i$  = a dummy variable equal to 1 if the  $i$ -th road section is paved, 0 otherwise;

$f_i$  = flow on the  $i$ -th (1 km long) road section test site, expressed in terms of equivalent passenger car per hour (two-way flow).

The model parameters have been evaluated according to the following rules:

- the useful width of the 1 km long road section is equal to the width of the entire carriageway because isolated vehicles tend to use the whole available carriageway;
- the tortuosity and other site characteristics were evaluated with reference to a 1 km long road section; in detail, the disturbance index is defined as the average of the various indices that consider unauthorised access, intersections and stops.

The estimated space mean speed values have been converted in equivalent mean time values by making use of the following experimental relationship reported in the Eq.2.3

The data obtained are conveniently reported in the Table 2.3.

*Table 2.3 Input data for the assessment of free-flow time mean speed in urban areas*

	$L_u$	S	W	H	I	$X_i$	$f_i$	$V_a$	$V_{mt}$	$V_{measured}$
1	10,5	0	0	0,7	0,001	1	0	64,83	66,16	82,619
2	8,3	0	0	0	0,0002	1	0	64,48	65,81	71,000
3	10,1	0	0	0,4	0	1	0	66,64	67,92	92,000
4a	9,1	0,09	0	0,1	0	1	0	66,23	67,51	84,333
4b	9,1	0,13	0,026	0,8333	0,031	1	0	57,72	59,22	57,286
5	9,5	0,007	0	0,4	0,005	1	0	64,44	65,78	69,778
6	9,9	0,027	0	0,7	0,007	1	0	62,62	64	57,555
7a	12,82	0,181	0,0731	0,2333	0	1	0	77,11	78,12	81,963
7b	11,5	0,267	0,0207	0,2333	0	1	0	73,03	74,15	75,518
8	10	0,04	0,0387	0,5333	0,005	1	0	64,25	65,58	66,112
9	9,7	0,033	0	0,4	0,001	1	0	65,17	66,49	57,823

### Rural area

The average rural speed is calculated with reference to the Highway Capacity Manual 2000 (Wachs et al., 2000). The expression used to evaluate the Average travel speed is reported below:

$$ATS = FFS - 0,0125 \cdot V_p \quad 2.5$$

$$FFS = BFFS - fls - fa \quad 2.6$$

Where:

ATS = Average Travel Speed [km/h];

FFS = Free-Flow-Speed [km/h];

BFFS = 100 km/h Base Free-Flow-Speed [km/h];

fls = coefficient that considers the width of the lanes and of the docks;

fa = coefficient that considers the presence of accesses;

$f_{np}$  = coefficient that considers overtaking prevented

$V_p$  = Bidirectional flow rate.

Similarly to what has been carried out in the urban model, the parameters of the rural model have been evaluated and free flow conditions in terms of space mean speed estimates and the equivalent converted time mean speed values through Eq. 2.3 have been derived. All the relevant data have been conveniently reported for each test site (inserting  $v_p$  and  $f_{np}$  equal to 0) in the Table 2.4.

Table 2.4 Input data for the assessment of free-flow time mean speed in rural areas

	BFFS	fls	fa	Q	$f_{np}$	ambit	border distance u/r	ATS	$V_{mt}$	$V_{measured}$
1	100	6,8	15	0	0	e	-4900	78,2	79,18	82,62
2	100	6,8	3	0	0	u	500	90,2	90,88	71
3	110	4,2	14	0	0	u	20	91,8	92,44	92
4a	100	0,7	5	0	0	u	650	94,3	94,88	84,33
4b	95	0,7	26	0	0	u	300	68,3	69,53	57,29
5	100	7,5	32	0	0	u	1000	60,5	61,93	69,78
6	100	0	34	0	0	u	1900	66	67,29	57,56
7a	93	6,8	5	0	0	e	-2800	81,2	82,11	81,96
7b	91	6,8	6	0	0	u	900	78,2	79,18	75,52
8	95	4,2	18	0	0	e	-500	72,8	73,92	66,11
9	100	6,8	28	0	0	u	1200	65,2	66,51	57,82

### Transition length concept

The basic idea is that road user traveling from a rural area cannot immediately realize that is entering in a urban area with different speed rules since the presence of an suburban road environment, on one hand, and poor or absent road sign may affect his speed choice. Therefore, he makes some time (and thus some travelled distance) in order to adapt speed to the different environment. In this preliminary study is also assumed a “mirrored” road user behavior when he is leaving an urban area.

Following these premises, the time mean speed on specific road cross-section falling in the suburban area can be evaluated as a linear combination of urban a rural spot speed estimates following a linear decreasing trend depicted in the Figure 2.3, it the position of the station point is known against the nearest administrative border and the transition length defining the extension of the suburban area is known.

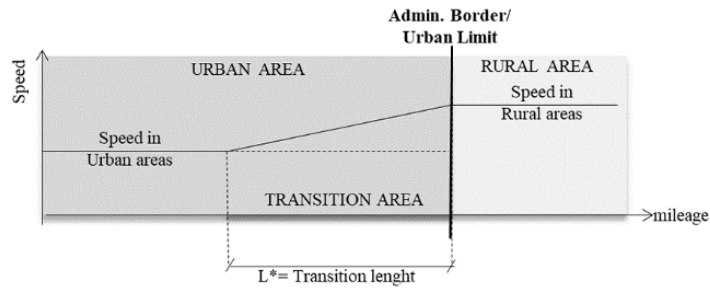


Figure 2.3 The transition length concept.

Once the speed values in the transition area were evaluated, as described above, a least square minimisation was used to derive the value of the transition length yielding an optimal value of 704.01 m. This transition length value has been, therefore derived from the overall amount of examined sites.

### 2.4.2 Speed analysis under traffic

The next step was to analyse the speed under congested conditions. Data relating to working days, pre-holidays and holidays aggregated with reference to period from 6:00 am to 10:00 pm. Speed data were aggregated on hourly basis and averaged according to the specific weekday. The data of the vehicular flow considered for the study were obtained from the traffic census program carried out by Lazio Regional Highway Agency in 2011.

Urban, Rural and combined transition area models that have been previously calibrated in free-flow conditions, have been employed by taking into account flow-related term according to the Eqs.(2.4-2.5). Preliminary results showed somehow higher dispersion with a Pearson Coefficient equal to 0.4056.

For this reason, for each test site, a least-square optimisation has been performed by re-arranging both models in the following forms:

$$V = 29.9 + 3.6Lu - 0.6S - 13.9W - 10.8H - 6.4I + 4.7X - \mathbf{K}_{urb} \cdot f \quad 2.7$$

$$ATS = BFFS - fls - fa - \mathbf{K}_{rur} \cdot Q \quad 2.8$$

From the optimisation, an effective improvement in the accuracy of the speed estimation has been reached. In particular, the dispersion has been reduced and the Pearson coefficient has been improved, from 0.4056 to 0.9127.

In order to obtain a generalised prediction model, statistical dependency of  $\mathbf{K}_{urb}$  and  $\mathbf{K}_{rur}$  on the road section characteristics, namely the aforementioned average useful road width (Lu), has been investigated and the result, from Ordinary Least-Square (OLS) models, have been summarised in Figure 2.4.

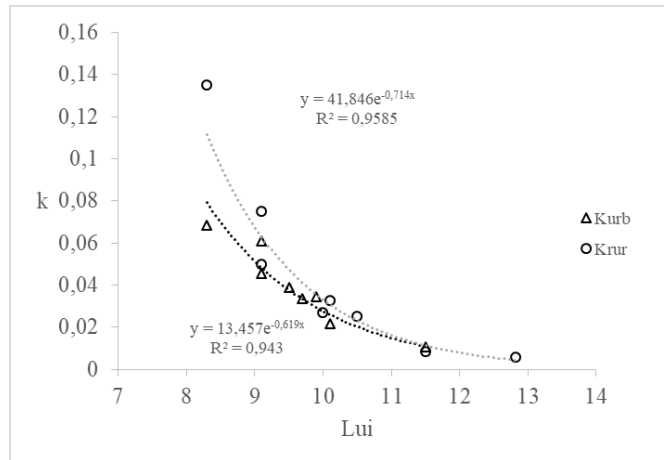


Figure 2.4 OLS relationships obtained for  $K_{urb}$  and  $K_{rur}$  as a function of average useful road width of the road cross-section,  $Lu$ .

As observed in Figure 2.4, the correlation coefficient for urban sites exhibits a fairly lower value than for rural ones, probably due to the average useful road width as the only explanatory variable in speed-flow gradient in the urban area. However, the reduced amount of examined sites did not statistically allow to seek for a multivariate relationship. Thus, the final re-arranged generalised time mean speed prediction models can be expressed in the following form:

$$MSS_{urb} = 29.9 + 3.6Lu - 0.6S - 13.9W - 10.8H - 6.4I + 4.7X - (13.457e^{-0.619 \cdot Lu}) \cdot f \quad 2.9$$

$$MSS_{rur} = FFS - (41.846 e^{-0.714 \cdot Lu}) \cdot Q \quad 2.10$$

$$MSS_{trans} = [(MSS_{rur} - MSS_{rur} + MSS_{urb}) \cdot d] / L^* \quad 2.11$$

Where,  $MSS_{urb}$ ,  $MSS_{rur}$ ,  $MSS_{trans}$  are the Space mean speed in urban, rural and transition area in Km/h, respectively,  $d$  is the distance from the rural/urban administrative border and  $L^*$  is the calibrated transition length (other variables have been defined in the previous section).

Comparison between experimental data from FCD and speed estimates by Eqs. (2.9-2.11) is reported in Figure 2.5b, thus showing a fairly good fitting and a satisfying Pearson Correlation Coefficient equal to 0.89. For the sake of clarity, the former dispersion with optimised flow-related coefficients has also been reported (Figure 2.5a).

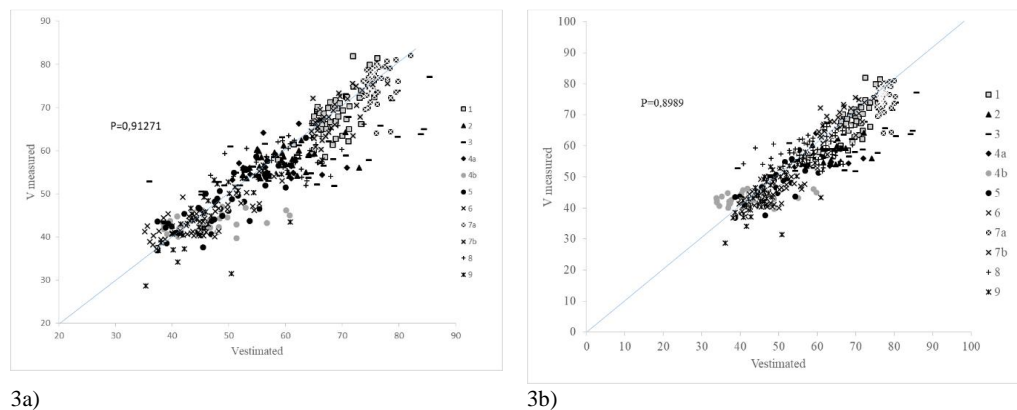


Figure 2.5 Comparison between the observed and estimated Time speed under congestion with optimized coefficients (a) and through the generalized calibrated model (b).

## 2.5 Statistics

After the model was developed, the problem arose of evaluating the possible correlations between the speeds (or the relative standard deviations) obtained from the FCDs and those estimated with the site characteristics. To do this, statistical studies were used. Statistics is often defined as the discipline that has the purpose of studying a phenomenon and highlighting its essential aspects, possibly going back to the laws that regulate it. This investigates collective phenomena, collecting information related to them and then translating them into a numerical model that can be easily analyzed. The first problem that arises in a statistical survey is the character, or rather the aspect, of the phenomenon to be investigated. The second problem is to precisely identify the population, which is the set of data to be investigated. As the last step, the analysis are carried out using the data obtained.

Statistics can be divided into two categories: descriptive and inferential (Zedda, 2015). Descriptive statistics aims to describe the basic characteristics of the data collected in a study; while the inferential one uses a model to understand a phenomenon and provide any future predictions.

### 2.5.1 Descriptive statistics

In this work, descriptive statistics were used to describe and synthesize the sample information of a numerical phenomenon of interest. This focuses on three main aspects, each represented with summary indices (arithmetic mean, percentiles, median, etc). These express, with a single value, a specific characteristic of the data distribution:

- *the central trend or position* represented with the mean, the median, the mode and the percentiles;
- *the variability or dispersion* represented with variance, standard deviation or standard deviation, range of variation;
- *the shape of the distribution* or the possible presence of asymmetries

The tools made available by descriptive statistics can be both graphical and numerical. The former allows to an investigation of the phenomenon in a visual way allowing to identify the function that expresses the trend of the phenomenon under study and therefore the most appropriate mathematical model (Muschitiello, 2011).

While the numerical organization allows you to extract the most important information.

However, the model is not able to represent the phenomenon with extreme accuracy but tends to simplify it. To understand the effects that independent variables have on the dependent variable and to predict the value of the dependent variable through a combination of independent variables, the multivariate regression technique is used.

Once the model has been created, it is necessary to make sure that the observed data are well described, then the goodness of fit of the model is evaluated using correlation coefficient ( $R^2$ ) and Pearson coefficient (P).

### **2.5.2 Analysis tools**

For the statistical study, for data processing and model verification, two calculation tools were used.

The first was used to perform multivariate regression, statistical analysis of the variables and coefficients of the models. Then the regression model and its synthetic statistical parameters were identified, the goodness of regression and the probability of false rejection of the coefficients introduced in the model were verified.

While the second tool provided statistical information on a population of data. Then the distribution of the data was identified and its adaptability with respect to probability functions of existing statistical models was assessed, through statistical tests (Kolmogorov-Smirnov, Anderson-Darling, Chi-Square test ).

#### **Statistical analysis**

For both the isolated vehicle and the traffic conditions, statistical analyzes were performed to identify possible correlations between the variables characterizing the sites analyzed. The goal of this analysis is to identify a regression model of the

experimental points characterized by a simple structure and with the least number of coefficients. The quantities considered are the following:

- Average measured speeds obtained from FCD data;
- Speeds estimated by the model;
- Standard deviation values obtained by reprocessing from FCD data;
- Useful width of the arc (Lu);
- Tortuosity (W);
- Number of accesses;
- Number of pedestrian crossings;
- Percentage of illegal parking;
- Presence of buildings in percentage;
- Vehicular range.

By way of example, the correlation diagrams between the standard deviation and the different site characteristics for the isolated vehicle are shown below.

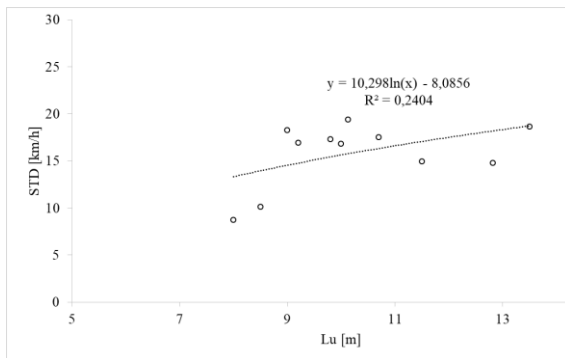


Figure 2.6 STD - Lu correlation

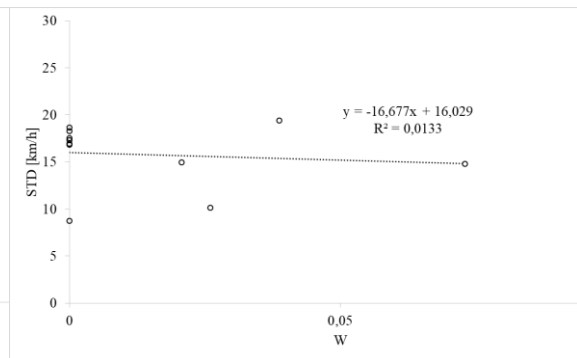


Figure 2.7 STD – W correlation

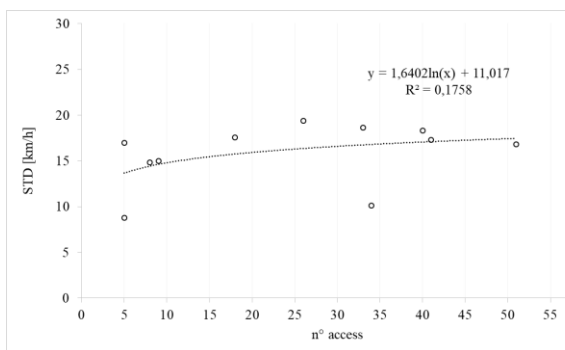


Figure 2.8 STD correlation - n. accesses

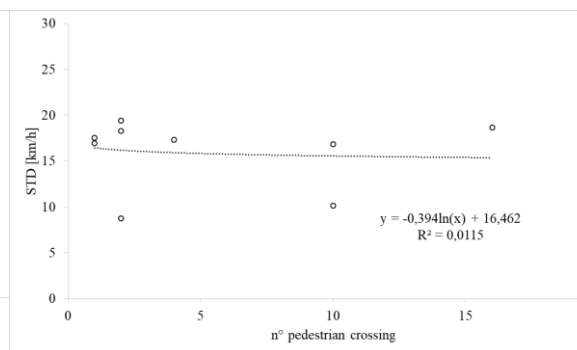


Figure 2.9 STD correlation - n. crossing

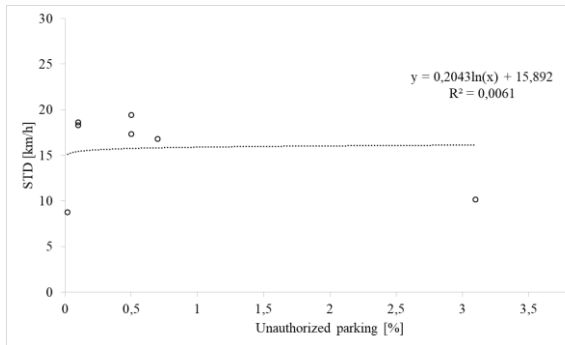


Figure 2.10 STD correlation -% illegal parking

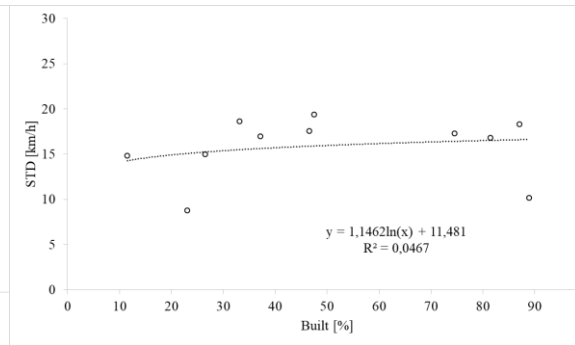


Figure 2.11 STD correlation -% occupied by buildings

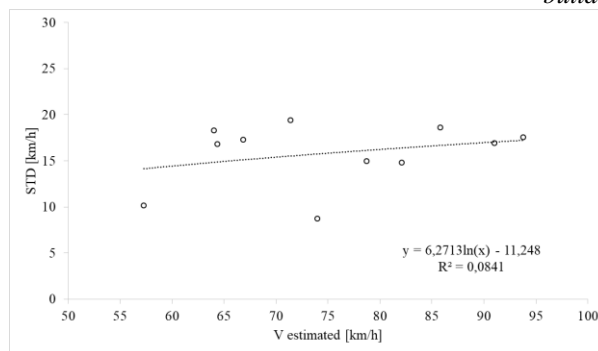


Figure 2.12 STD correlation - Vs

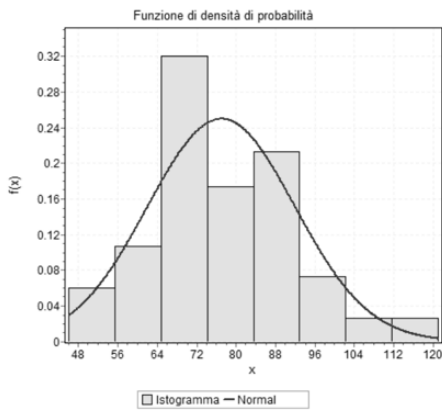
The standard deviation was chosen as it represents a synthetic parameter of fundamental importance; in fact, in the analyzes carried out, it provides an estimate of the dispersion of the speeds adopted by the drivers with respect to the average speed value. According to sector studies, a high value of this parameter indicates an excessive variability of the speeds in the road section analyzed and therefore a greater interaction between vehicles; the increase in interactions can translate into a higher frequency of accidents. The expected behavior is the decrease in the dispersion of speed as the flow of traffic increases, given the decrease in the quality of traffic.

In the analyzes, no regression models were identified that corresponded to the parameters initially estimated, in fact for no correlation a significant value of the determination coefficient was obtained (neither for the isolated vehicle nor with traffic).

Therefore it can be said that the standard deviation is invariant with respect to the variables characterizing the site. In fact, it assumes a variable value in a range of 5 km/h, between the value of 15 km/h and 20 km/h. The average standard deviation value over all the sites is equal to 15.79 km/h.

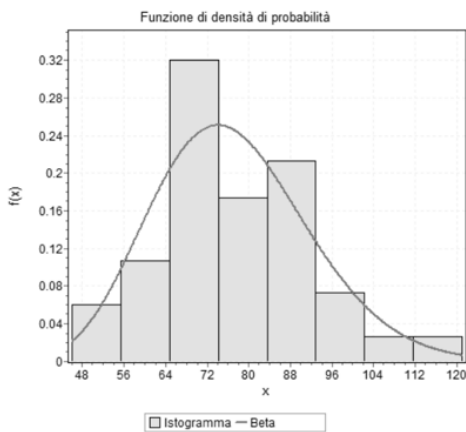
### Site 7b

Table 2.5 Results Normal model - site 7b.



Normal [#44]					
Kolmogorov-Smirnov					
Dimensione del campione	150				
Statistica	0.08497				
Valore P	0.21633				
Rango	30				
$\alpha$	0.2	0.1	0.05	0.02	0.01
Valore critico	0.08761	0.09986	0.11088	0.12394	0.13301
Respingi?	No	No	No	No	No
Anderson-Darling					
Dimensione del campione	150				
Statistica	0.73189				
Rango	27				
$\alpha$	0.2	0.1	0.05	0.02	0.01
Valore critico	1.3749	1.9286	2.5018	3.2892	3.9074
Respingi?	No	No	No	No	No
Chi-quadrato					
Gradi di libertà	7				
Statistica	9.8951				
Valore P	0.1946				
Rango	25				
$\alpha$	0.2	0.1	0.05	0.02	0.01
Valore critico	9.8032	12.017	14.067	16.622	18.475
Respingi?	Si	No	No	No	No
Normal	$\sigma=14.975 \quad \mu=76.987$				

Table 2.6 Results model Beta- site 7b.



Beta [#1]					
Kolmogorov-Smirnov					
Dimensione del campione	150				
Statistica	0.06111				
Valore P	0.60769				
Rango	9				
$\alpha$	0.2	0.1	0.05	0.02	0.01
Valore critico	0.08761	0.09986	0.11088	0.12394	0.13301
Respingi?	No	No	No	No	No
Anderson-Darling					
Dimensione del campione	150				
Statistica	0.4586				
Rango	13				
$\alpha$	0.2	0.1	0.05	0.02	0.01
Valore critico	1.3749	1.9286	2.5018	3.2892	3.9074
Respingi?	No	No	No	No	No
Chi-quadrato					
Gradi di libertà	7				
Statistica	6.3026				
Valore P	0.50489				
Rango	8				
$\alpha$	0.2	0.1	0.05	0.02	0.01
Valore critico	9.8032	12.017	14.067	16.622	18.475
Respingi?	No	No	No	No	No
Beta	$\alpha_1=11.405 \quad \alpha_2=40.564$ $a=19.386 \quad b=281.85$				

Again for both conditions (isolated vehicle and flow condition), the speed obtained by the FCDs was compared with the frequency with which the speed values are repeated. It is therefore possible to define a probability density function of the observed data which is compared with probability density functions of known statistical models. This comparison is done through three statistical tests: Kolmogorov-Smirnov, Anderson-Darling, Chi-square.

The statistical study was conducted for each site but only some results in the isolated vehicle condition are reported below.

For the different sites (as also highlighted in site 7b), the adaptability of the data population to both the Normal statistical model and the Beta model is observed.

### 2.5.3 Removals of outliers

In the previous paragraphs, the absence of regression models and relationships that can explain the correlation between standard deviation STD, flow rate Q and Velocity estimated by the Vms model was ascertained. Then an average standard deviation value was evaluated for each site and to eliminate the aberrant points with respect to the confidence band. The confidence band, for each site, was evaluated as the area of the graph that extends from the mean value of standard deviation and more or less twice the standard deviation. The diagrams obtained for some sites and the diagram containing the experimental data of all the sites are shown below.

Table 2.7 Standard deviation and flow rate data for the site 1

Site 1		Weekdays		Pre-holidays		Holidays	
		STD [km/h]	Q [n. veic.]	STD [km/h]	Q [n. veic.]	STD [km/h]	Q [n. veic.]
Non-isolated vehicle	06:00 - 06:59	16,90	62	14,49	89	11,76	40
	07:00 - 07:59		147	16,32	148		52
	08:00 - 08:59	17,11	175	14,26	206	13,25	93
	09:00 - 09:59	14,75	185	15,90	215	14,13	120
	10:00 - 10:59	15,21	212	13,51	211	15,96	164
	11:00 - 11:59	13,83	250	15,67	238	11,77	210
	12:00 - 12:59	14,01	278	16,33	259	10,92	290
	13:00 - 13:59	14,64	276	13,94	277	14,79	249
	14:00 - 14:59	15,76	270	12,49	231	13,99	165
	15:00 - 15:59	14,50	289	15,26	263	14,94	222
	16:00 - 16:59	14,44	294		246	13,67	296
	17:00 - 17:59	14,95	261	13,18	201	12,43	419
	18:00 - 18:59	14,55	231	13,36	187	11,59	363
	19:00 - 19:59	13,98	173	13,78	171	17,27	255
20:00 - 20:59	16,05	125	17,22	197	15,01	162	
21:00 - 21:59	17,40	71	10,96	120	13,59	78	
Coeff. variation	0,08		0,12		0,13		
Average STDs	15,20		14,45		13,67		

Average all STDs	14,44
STD	1,65

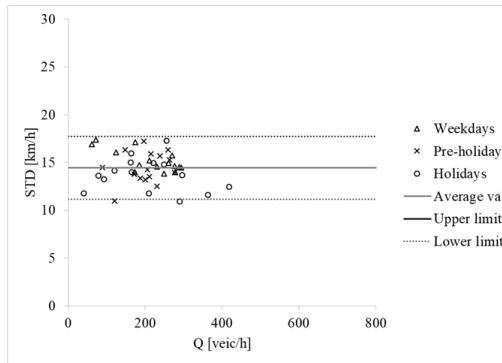


Figure 2.13 Standard deviation correlation with flow rate and relative confidence band.

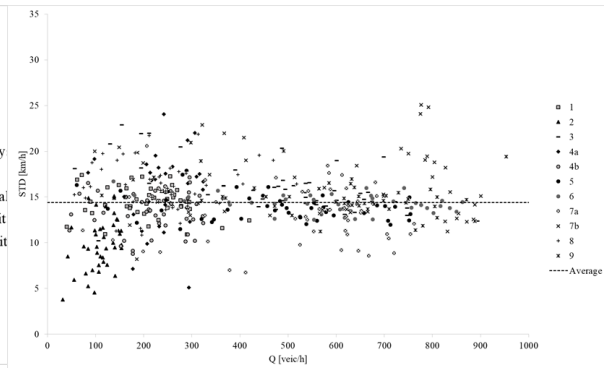


Figure 2.14 Standard deviation correlation with range for all sites.

With the elimination of the outliers, for each site an average value of standard deviation STD was evaluated which are reported below:

site 1	→ $STD = 14.44 \text{ km/h}$ ;
site 2	→ $STD = 9.87 \text{ km/h}$ ;
site 3	→ $STD = 16.04 \text{ km/h}$ ;
site 4a	→ $STD = 15.40 \text{ km/h}$ ;
site 4b	→ $STD = 13.41 \text{ km/h}$ ;
site 5	→ $STD = 13.95 \text{ km/h}$ ;
site 6	→ $STD = 14.30 \text{ km/h}$ ;
site 7a	→ $STD = 12.88 \text{ km/h}$ ;
site 7b	→ $STD = 16.49 \text{ km/h}$ ;
site 8	→ $STD = 16.26 \text{ km/h}$ ;
site 9	→ $STD = 15.05 \text{ km/h}$ .

The variation in STD is between a minimum value of 9.87 km/h and 16.49. The lowest value found is that relating to site 2 due to the low number of FCD data available for the site. It can be seen that the range of variation is very low between all sites. Subsequently, considering the data of the sites as a whole, an average STD value of 14.40 km/h was reached.

The mean STD values obtained for each site were correlated with the following parameters:

- Useful arc width  $L_u$ ;
- Tortuosity  $W$ ;
- Number of accesses;
- Number of pedestrian crossings;
- Percentage of illegal parking;
- Presence of buildings in percentage.

The correlation diagrams between the various parameters are shown below.

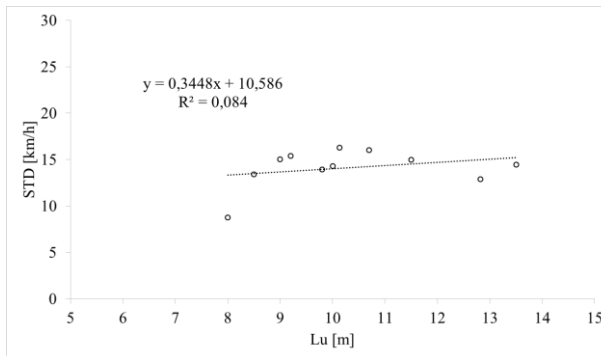


Figure 2.15 Correlation between standard deviation and useful arc width.

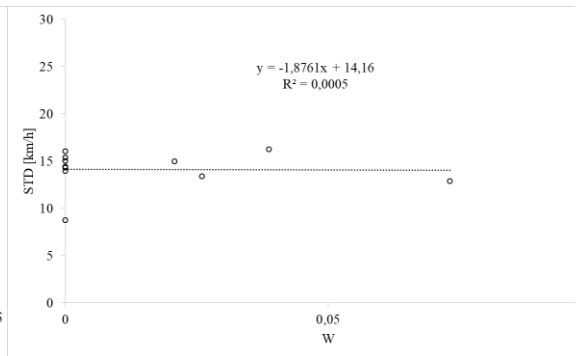


Figure 2.16 Correlation between standard deviation and tortuosity.

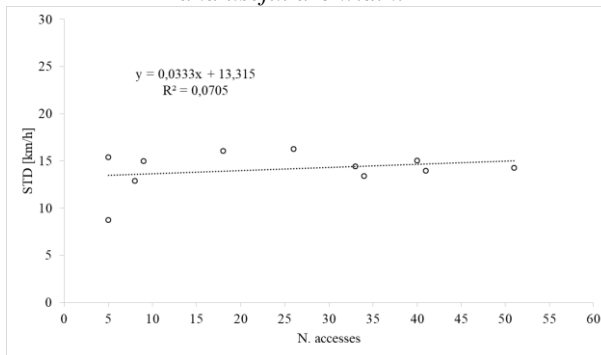


Figure 2.17 Correlation between standard deviation and n. accesses.

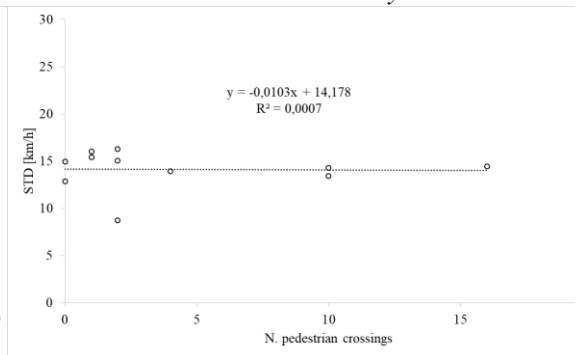


Figure 2.18 Correlation between standard deviation and n. crossings.

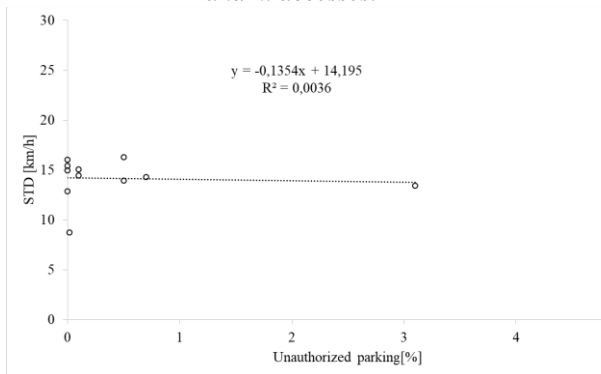


Figure 2.19 Correlation between standard deviation and percentage of unauthorized parking.

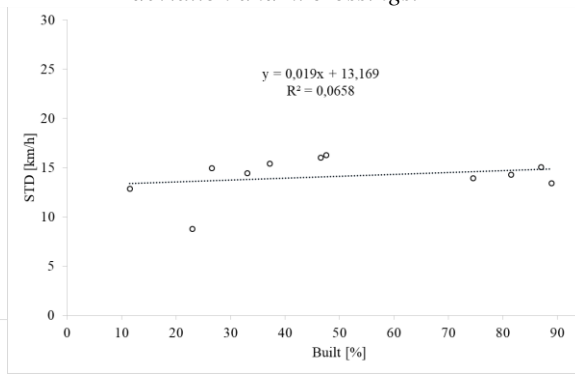


Figure 2.20 Correlation between standard deviation and built-up percentage.

For none of the correlations investigated a regression function was identified that would allow explaining the experimental points.

### 2.5.4 Influence of buildings and site factors on traffic

The FCD data were reworked to assess the influence of the building, regardless of the administrative area of the sites analyzed and other site characteristics. The goal is to identify common and valid aspects, in general for each site, reaching a greater level of detail by increasing the number of experimental points.

The road sections were divided into sections of 100 or 200 m, depending on the number of FCD data available.



Figure 2.21 Representation of FCD data at site 5 (source: QGIS)

Below is a summary table of the sections and the number of sections analyzed as a function of the length and number of FCD data available per site.

Table 2.8 Number of sections per site as a function of the length and number of FCD data.

Site	Route width (m)	n°sections	length of the sections
1	1400	14	100
2	1000	5	200
3	1400	14	100
4a	1200	6	200
4b	1200	6	200
5	1700	17	100
6	3600	36	100
7a	1000	10	100
7b	1000	10	100
8	1000	10	100
9	1000	10	100

With the use of QGIS and the contribution of Google Earth, the following characteristics have been identified for each trunk:

- Speed limit;

- Tortuosity;
- Lane width;
- Width of the docks;
- Number of accesses;
- Number of pedestrian crossings;
- Percentage of buildings on the sides of the carriageway;
- Percentage of illegal parking;
- Regular parking percentage;
- Average speed per hour for the condition of the vehicle under traffic;
- Hourly standard deviation for the condition of the vehicle under traffic;
- Average speed for isolated vehicle condition;
- Standard deviation for the isolated vehicle condition.

As an example of the analyzes carried out, the summary table of the data collected for the site 5 is shown.

*Table 2.9 Site 5 data (source: QGIS, Google Earth)*

Section	Speed	W	Lane	Platform	Lu	N.	N.ped.
	limit[km/h]		width[m]	width[m]			
1	50	0,100	6,8	0,6	7,4	1	0
2	50	0,100	6,75	0,64	7,39	2	0
3	50	0,000	6,65	0,71	7,36	4	0
4	50	0,000	6,63	0,9	7,53	1	0
5	50	0,000	6,62	0,66	7,28	1	0
6	50	0,078	8,1	0,7	8,8	3	0
7	50	0,156	8,66	2,25	10,91	5	1
8	50	0,078	8,16	3,45	11,61	6	1
9	50	0,000	6,9	3,42	10,32	6	2
10	50	0,000	7,4	1,5	8,9	7	1
11	50	0,017	7,66	1,33	8,99	8	0
12	50	0,017	7,72	1,6	9,32	7	1
13	50	0,000	7,45	1,3	8,75	3	1
14	50	0,039	7,98	1,53	9,51	2	0
15	50	0,031	7,53	1,55	9,08	3	0
16	50	0,061	7,23	1,37	8,6	5	0
17	50	0,000	7,72	1,32	9,04	4	0

Greater attention was paid to the presence of buildings: for each site, the presence of buildings was calculated as a percentage, according to the length occupied on the sides of the carriageway by commercial activities, industrial plants and private homes. The data obtained, relating to the presence of buildings in percentage on the right and left side of the carriageway, were combined in order to obtain a single synthetic parameter for the section under analysis. The calculated parameters are:

- Arithmetic average;
- Minimum built;
- Maximum built;
- Harmonic mean;

- Geometric mean.

As an example, the summary table of the data obtained for the site 5 is shown below.

*Table 2.10 Parameters according to the buildings for the site 5.*

Section	Arithmetic average	Maximum built	Minimum built	Harmonic mean	Geometric mean
1	0,500	0,500	0,500	0,500	0,500
2	14,600	18,800	10,400	13,392	13,983
3	7,850	14,700	1,000	1,873	3,834
4	7,700	14,900	0,500	0,968	2,729
5	11,500	22,500	0,500	0,978	3,354
6	43,230	58,160	28,300	38,074	40,570
7	62,670	70,630	54,710	61,659	62,162
8	64,000	100,000	28,000	43,750	52,915
9	80,250	100,000	60,500	75,389	77,782
10	38,400	44,300	32,500	37,493	37,944
11	59,320	100,000	18,640	31,423	43,174
12	30,800	50,600	11,000	18,071	23,592
13	12,900	25,300	0,500	0,981	3,557
14	0,500	0,500	0,500	0,500	0,500
15	0,500	0,500	0,500	0,500	0,500
16	20,100	39,700	0,500	0,988	4,455
17	0,500	0,500	0,500	0,500	0,500

### Statistical analysis

As previously done, the data collected from the analyzes were correlated as a function of the measured velocity and the standard deviation. This correlation was carried out individually for each site and subsequently for all sites, without disregarding the hypothesis of isolated vehicle and non-isolated vehicles.

For both conditions (isolated vehicle and presence of traffic) the correlations between average speed measured and tortuosity/arithmic average built-in percentage/minimum and maximum built-in percentage/harmonic and geometric average built-in percentage/site limit speed/useful width.

For each of them, regression models were evaluated that would allow explaining the experimental points obtained.

Also in these analyzes carried out by subdivision of the sections into sections of 100 and 200 m, the standard deviation assumes the same behavior found in the analyzes carried out on the complete sections. By calculating an average of the STD for the 134 experimental points available, a standard deviation of 15.67 km/h is obtained, a value in line with what was obtained in the previous analyzes.

## 2.6 Conclusion

Speed evaluation represents a critical task in highway and transportation

engineering since it affects road safety and network performance. The objective of the present study is to demonstrate that the statistical prediction models can effectively exploit the huge amount of FCD made available nowadays in order to deliver more comprehensive and generalised speed prediction tools, provided that a sound calibration procedure and an effective criticism on speed evaluation criteria and existing models are taken into account. The validity of the proposed methodology has been tested against several sites with a typical two-way single carriageway urban and rural, road layout that is, by far, the most diffused worldwide. Following an analysis of FCD data, the presented approach also allowed to satisfactorily “capture” the main essence of driver behaviour in the transition area between rural and urban environment, the area that remains, in fact, very “tricky” to be identified and treated by road engineers. One may argue that the postulated linear behaviour is not always found in reality but, due to the low sampling frequency of FCD so far available (1-2 sample per minute, on average), it was not possible to model more complex behaviour.

In addition, it has to be acknowledged that, the good agreement between the estimated and measured speed data is somehow worse for some of the calibration sites if their performance is individually evaluated, suggesting that some roadway influencing factors deserve a deeper analysis and urban density can play a significant contribution in drivers’ behaviour. Nevertheless, the overall prediction performance seems promising, especially if the reduced sample investigated is considered.

In addition, the presented prediction framework appears to be an effective candidate tool to improve road safety. For sake of clarity, if the well-known fourth and square power-law relationships between fatal and injured accidents, respectively, and vehicle speed are recalled (Elvik et al. 2009) (Elvik et al. 2019), a 5% decrease of vehicle speed that can be obtained by reducing the average useful road width,  $L_u$ , or by increasing the site dimensionless tortuosity,  $W$ , (or by a combined approach on both terms) according to the Eqs.(2.7-2.8), can virtually yield to a nearly 20% of decrease of fatal accident and a 10% decrease of injured accidents.

If the speed, in fact, provides an indication of the conduct of the drivers and the possible severity of the damage following an accident, the standard deviation of the speeds allows to define of the dispersion of the same values with respect to the average value. According to sector studies, the standard deviation is indicative of the probability of an accident occurring: as the dispersion increases, the probability of interaction between vehicles and of an accident increases. The analyzes carried out in this sense led to the definition of an almost invariant standard deviation value for each site (included in a range between 13 km/h and 15 km/h).

Statistical studies were conducted on the data samples for each site, in isolated vehicle conditions, and likelihood tests to identify the distribution of data according to statistical models, mainly identifying the Normal and Beta model, fundamental for evaluating the behavior of drivers according to simplified statistical schemes.

Possible correlations between the various factors that influence the traffic flow were investigated, identifying the presence of buildings and the number of accesses as possible independent variables for the development of future forecasting models, recommending a more detailed analysis of the buildings through a volumetric relief.

However, it has to be underlined that further investigations and analyses are needed in order to:

- increase the statistical significance for calibration and validation by collecting and analysing a greater number of test sites;
- evaluate and predict the dispersion characteristics of speed distribution by collecting a higher amount of FCD per site;
- investigate the influence of factors other than those related to roadway layout and urban limits that may affect the driver's behaviour in transition areas.

Nevertheless, preliminary results appear fairly encouraging, in fact, the higher information content provided by FCD, if it is combined with a careful examination of road section characteristics, can provide useful engineering tools that can be employed in road safety design and retrofitting.

## References

- AASHTO. 2004. A Policy on Geometric Design of Highways and Streets. Paper presented at: 5th ed. American Association of State Highway and Transportation Officials; Washington DC, USA.
- Ajay KR, Messer CJ, Gartner N. 2001. Traffic flow theory revised report. Organised by the Committee on Traffic Flow Theory and Characteristics (AHB45).
- Ali AT, Flannery A, Venigalla MM. 2007. Prediction models for free flow speed on urban streets. Paper presented at: Transportation Research Record 86th Annual Meeting, United States. 2007 January 21-25; Washington DC (USA).
- Aronsson K.F.M. 2006. Speed characteristics of urban streets based on driver behaviour studies and simulation. Doctoral Thesis in Infrastructure. Stockholm (Sweden): Royal Institute of Technology.
- Bakaba J.M. 2003. Ableitung vereinfachter Modellansätze zur Geschwindigkeitsprognose auf Ausserortsstrassen auf der Grundlage der

- verfuegbaren Variablen aus der Strassendatenbank. Ph.D. Dissertation. Dresden (Germany): Technical University of Dresden.
- Cafiso S, Di Graziano A, Di Silvestro G, La Cava G. 2007. Safety Performance Indicators for Local Rural Roads: A Comprehensive Procedure from Low-Cost Data Survey to Accident Prediction Model. *Transp Res (E-C151)*.
- Capaldo FS, Grossi R, Tocchetti A. 1998. Procedure e tecniche per la valutazione della sicurezza stradale. Paper presented at: 54° Conferenza del Traffico e della Circolazione,ACI; Riva del Garda (Italy).
- Cartenì A, Punzo V. 2007. Travel time cost functions for urban roads: a case study in Italy. Paper presented at:Urban transport XIII: urban transport and the environment in the 21st century. Wessex Institute of Technology. August 2007; Coimbra, Portugal.
- Cascetta E. 2009. *Transportation Systems Analysis. Models and Applications*. Second Edition, Berlin (Germany): Springer. DOI:10.1007/978-0-387-75857-2.
- D'Apuzzo M., Santilli D., Evangelisti A., Fusco G., Nicolosi V., Perneti M., Isaenko N. 2021 Traffic Injury Prevention. Towards the development of a hybrid approach to speed estimation in urban and rural areas. Taylor & Francis. DOI:10.1080/15389588.2021.1935904
- Dixon KK, Wu CH, Sarasua W, Daniels J. 1999. Posted and Free-Flow Speeds for Rural Multilane Highways in Georgia. *J. Transp Eng*; 125(6):487–494.
- Elvik R, Høy A, Vaa T, Sørensen M. 2009. Factors Contributing to Road Accidents. *The Handbook of Road Safety Measures*. Oxford (UK): Emerald Group Publishing Limited. DOI:10.1108/9781848552517-003.
- Figuroa A, Tarko A. 2004.Reconciling Speed Limits with Design Speeds. Cited in Report No. FHWA/IN/JTRP- 2004/26, Purdue University, West Lafayette, Ind.
- Fitzpatrick K, Carlson P, Brewer M, Wooldridge M, Miaou S. 2003.Design Speed, Operating Speed, and Posted Speed Practices. NCHRP Report 504. Washington DC (USA): Transportation Research Board of the National Academies.
- Fitzpatrick K, Shamburger C, Krammes R, Fambro D. 1997. Operating Speeds on Suburban Arterial Curves. *Transp Res Rec*.1579: 89–96.
- Fusco G, Comelli L, Colombaroni C, Isaenko N. 2015. Short-term traffic predictions on large urban traffic networks: Applications of network-based machine learning models and dynamic traffic assignment models. Paper presented at: Models and Technologies for Intelligent Transportation Systems (MT-ITS); 2015 June 3-5; Budapest, Hungary. doi: 10.1109/MTITS.2015.7223242.

- Fusco G, Colombaroni C, Isaenko N. 2016. Short-term speed predictions exploiting big data on large urban road networks. *Transp Res (Part C)*. Elsevier.73:183-201. doi:10.1016/j.trc.2016.10.019.
- Fusco G, Colombaroni C, Isaenko N. 2017. Traffic dynamics estimation by using raw floating car data. Paper presented at: 5th IEEE International Conference on Models and Technologies for Intelligent Transportation Systems (MT-ITS); 2017 June26-28; Naples, Italy.
- Girling C L, Helphand K I. 1994. *Yard street park, The design of suburban open space*. John Wiley & Sons. ISBN-13: 978-0471178446.
- Hassan Y, Sarasua W, Daniels J.2011. *Modeling Operating Speed, Synthesis Report Transportation Research Circular Number E-C151*. Transportation Research Board 500 Fifth Street, NW Washington, DC; 2001. www.TRB.org.
- Hauer E. 2009. *Speed and Safety*. *Transp Res Board*. 2103: 10–17. DOI:10.3141/2103-02.
- IASPIS. 2001. *Progetto.Rapporto conclusivo*. Firenze (Italy).
- Karlgren J. 2001. *Bilars hastighet längs gator med gupp: metod för framställning av hastighetsprofiler och analys av hastighetsförlopp*. Chalmers Tekniska. Högskola, Sweden.
- Lamm R, Psarianos B, Mailaender T. 1999. *Highway Design and Traffic Safety Engineering Handbook*. New York (USA): McGraw Hill.
- Lum H, Reagan JA. 2008. *Interactive Highway Safety Design Model*. Washington DC (USA): Federal Highway Administration.
- Marchionna A, Perco P. 2008. *Operating Speed Profile Prediction Model for Two-Lane Rural Roads in the Italian Context*. *J Adv Transp Stud*. (14): 57-68. ISSN: 1824-5463.
- Muschitiello, C. 2012. *Lecture notes Elements of Statistics, Vol. 1, pp. 17-18*.
- Nie B, Hassan Y. 2007. *Modeling Driver Speed Behavior on Horizontal Curves of Different Road*. *Transp Res (E-C151)*.
- Pinna M, Zedda F. 2018. *Prediction Models for Space Mean Speed on Urban Roads*. Paper presented at: *Proceedings of International Conference on Computational Intelligence and Data Engineering*; Vijayawada, India. [https://doi.org/10.1007/978-981-10-6319-0\\_2](https://doi.org/10.1007/978-981-10-6319-0_2).
- Poe CM, Mason JM. 2000. *Analyzing influence of geometric design on operating speeds along low-speed urban streets: mixed-model approach*. *Transp Res Rec: J Transp Res Board*. 1737:18-25. <https://doi.org/10.3141/1737-03>.

- Tarris JP, Poe CM, Mason JM, Goulias KG. 1996. Predicting operating speeds on low-speed urban streets: regression and panel analysis approaches. *Transp Res Rec: J Transp Res Board.* 1523:46-54. <https://doi.org/10.1177/0361198196152300106>
- Wachs M, Skinner RE, Samuels JM. 2000. *Highway Capacity Manual. HCM 2000.* Washington DC(USA): Transportation Research Board. ISBN 0-309-06681-6.
- Wang J, Dixon KK, Li H, Hunter MP. 2006. Operating Speed Model for Low-speed Urban Tangent Sections based on In-vehicle Global Positioning Systems. *Transp Res Rec: J Transp Res Board.* 1961. <https://doi.org/10.1177/0361198106196100104>
- Zedda, M. 2015. *Accidentality in the urban environment: study of driving behavior in relation to the geometric characteristics of the road infrastructure.* Cagliari.

# CHAPTER 3. PEDESTRIAN FLOWS

## EXPOSURE

Since the new millennium, the problems generated by natural disasters, attributable to increasing levels of pollution, have pushed nations to seek solutions. In order to reduce environmental pollution (noise and air) linked to road traffic, the researchers are moving towards alternative mobility also known as sustainable mobility. For this reason, policies are being developed that push the population to use different modes of travel to the motor vehicle, favoring multimodal transport alternatives. These involve the combination of the use of public transport, cycle and pedestrian routes, as well as sharing services (where available). Regardless of the type of transport, the pedestrian component turns out to be relevant in cities though the infrastructure is not adequately designed to accommodate it and conflicts arise with the traffic components, which must be managed. To design the road infrastructure wisely, it is therefore necessary to assess the risk exposure. Exposure is distinct from risk, which is understood as the probability of a dangerous event occurring. Clearly, the exposure and the risk are correlated; in fact, a high exposure, due for example to high pedestrian volumes in a busy intersection, could involve a reduced risk if this is well designed. In reverse, a low exposure (fewer pedestrians crossing a busy and dangerous intersection) can involve high risk and therefore a greater probability of a deleterious event occurring. When applied to pedestrian safety, exposure is defined as the ratio of pedestrian accidents to pedestrian volume.

In particular, pedestrian exposure is defined as the percentage of pedestrians in contact with potentially harmful vehicular traffic (Raford & Ragland, 2003). In practice, this can be defined as the annual number of vehicle-pedestrian collisions divided by the estimated annual pedestrian volume at a given intersection (Leden, 2002) (Jacobsen, 2003).

Before evaluating the exposure, it is, therefore, necessary to define the geographical area on which to perform the study. Usually, the study area can be broken down into facility-specific and area wide. The first category considers a point (where traffic flows intersect, merge or diverge) or a segment (part of the road or carriageway between two

points, where traffic volumes and characteristics remain unchanged). While the second analyzes the network (a medium-sized geographical area in which there are interconnected transport structures) or the region (large geographical area that includes all transport structures within a defined political boundary).

Depending on the geographic scale chosen, the exposure, to be used in the risk calculation, can be measured in a different way.

*Table 3.1 The most popular exposure measures*

Classes	Distance traveled	Time traveled	Volume/Count	Trips made	Population
<b>Measures</b>	Pedestrian miles traveled (PMT) or bicycle miles traveled (BMT)	The hours traveled by pedestrians or cyclists	The volume or count of pedestrians or cyclists for a specified time period and geographic scale	The cumulative number of trips made by all users of the analysis area. Trips are usually estimated with counts or acquired using GPS	The number of people (or percentage of the population) who walk or cycle
<b>Limitation</b>	It does not allow to compare the risk between different modes because it does not consider the short distances traveled by pedestrians and cyclists.	The surveys often underestimate the number of journeys on foot or by bicycle and travel times are overestimated	Do not take into account distance or travel time, but only the number of vulnerable users	A large number of data is required	Do not consider tourist travel

In this chapter, the consolidated methods present in the literature for the estimation of traffic and pedestrian flows were first presented. Two proposed procedures were reported below, which could be merged to obtain realistic estimates of flows. The first method proposed uses a configurational model to estimate pedestrian flows (by running simulations with the Space Syntax). Since numerous researches have shown that pedestrian activity is linked to network connectivity, but at the same time it is influenced by other variables such as population, land use, purpose of travel, means of connection, etc. The configurational model has been improved by incorporating numerical evaluations related to the different attractors present in the area. The data obtained from the model were then compared with those collected in the area using the mobile observer technique.

The second method is based on a demand-driven approach, very similar to the four-stage model, which starts from statistical data (collected with interviews or from national databases) in order to reconstruct the movements for the different modes of transport and in different time slots.

Both methods make it possible to estimate the extent of flows and to represent their distribution on the road network.

## 3.1 Counting and estimating technologies for non-motorized travel: state of the art

For the reconstruction of the mobility of a site, it is necessary to consider the relationships between the urban structure and the pedestrian flows. The latter are interchange movements having origin and destination in the different areas of the area and are linked to the demand for mobility understood as the number of people who, based on choices, move in an interval of time to use service goods differently located on the territory. In order to predict the estimate of pedestrian flows, data obtained from the pedestrian count are used. These are acquired by:

- *Direct measurement*: many cities collect data by counting vulnerable users. However, these counts are collected in a very limited number of sections and often in locations where there are larger volumes of people. These measurements are commonly used to estimate exposure when the coverage of the analyzed facility is limited; this is because the collection of counting data for all facilities within a large network or region is prohibitive in terms of costs. Besides the fact that in some cases, it is a challenge to get a representative number of pedestrians and cyclists due to the seasonal variation with walking or cycling modes.
- *Forecasting models*: because the counts are collected in a limited number of locations, various methods of estimation and modelling are often used; this allows to obtain count estimates for all locations within a city or other defined area. In many cases, the direct count sample is used in the development and calibration of these estimation models.

### 3.1.1 Direct measurement

Much progress has been made in the past decade for the direct measurement of vulnerable users. The techniques used for the counting of the non-motorized volume are sometimes different from those established for the motorized; this is because it must be taken into account that non-motorized traffic is characterized by a greater sensitivity to environmental conditions (precipitation, temperature, darkness, etc.) and does not follow regular patterns as it is not confined to fixed lanes (vulnerable users can travel outside designated footbridges and cycle paths, take unmarked shortcuts or stop unexpectedly). Below is a synoptic table of the possible techniques used for the survey of non-motorized travel.

Table 3.2 Techniques used for the survey of non-motorized travel

Technology	Bicycle/Pedestrian	Overall Cost	Count Duration	User Volume	Strengths	Weaknesses	Installation Considerations
Manual field-based counting	B/P	\$\$\$\$	≤4 hours	≤600/hour	Flexible and mobile	short-term	Trained to classify users; positioned to view easily; short-term only
Manual video counting	B/P	\$\$\$\$	longer counts available	≥600/hour	flexible; no field-base work required	short-term;	Installed high enough; clearly recorded; require site visits
Piezoelectric strips	B	\$\$\$	Long-term	N/A	capture speed	not in mixed-flow traffic; specialized installation	Require pavement cuts; data logger stored in a nearby utility box; avoid intersections
Automated video counting	B/P	\$\$\$	≤48 hours	≥600/hour	minimal labor	short-term; outdoor processing	Installed high enough; avoid vibration; require vendor processing
Pressure and acoustic pads	B/P	\$\$\$	Long-term; short-term (pressure pads)	N/A	can be in-ground	user direct pass required; only for pedestrians; unpaved trails used	Require users to pass directly above the sensor; commonly used on unpaved trails
Radiobeam	B/P	\$\$	Short-duration and long-term	≤200/hour	movable; easy; hidden in post	mounting device required; limited monitoring distance	Placed on both sides of the corridor/existing infrastructure; pointing toward a fixed object; avoid bus stops/street corners/metals/electronic signals
Inductive loop detectors	B	\$	Short-duration (<6 months) and long-term	≤600/hour	used for on-road bicycle facilities	not possible to cover entire facility	Require pavement saw-cutting; data logger stored in an adjacent utility box; avoid electromagnetic interference
Passive infrared	P	\$	Short-duration and long-term	≤600/hour	small, portable and easy; may be combined with other technology	may be affected by extreme temperatures	Placed on one side of the corridor/existing infrastructure; pointing toward a fixed corners/reflection from foliage/windows
Pneumatic tubes	B	\$	Short-duration and long-term	≤200/hour	portable; capture speed/direction	vulnerable to snowplowing	Installed across the paved surface; avoid street sweeping; secure using tape/metal
Active infrared	P	\$	Short-duration and long-term	≥600/hour	movable; may be combined with other technology; precise	mounting device required	The receiver and transmitter should be installed facing each other on each side; avoid bus stops/street corners
Laser scanners	B/P	N/A	Short-term	N/A	N/A	N/A	Primarily indoors; electrical power supply required; horizontal scanners require locations with no obstruction; vertical mounted overhead

Where N/A=not applicable; \$=Low; \$\$=Medium; \$\$\$=High; \$\$\$\$=Very High. The table contents retrieved from: NCHRP REPORT 797 Guidebook on Pedestrian and Bicycle Volume Data Collection (Rus et al., 2014)

The monitoring techniques (Federal Highway Administration (FHWA), 2016) most used for identifying pedestrian flows can be grouped into two macro-types: manual and automatic detection.

The manual survey consists of the acquisition of data based on the direct survey of an operator. These provide a wide range of data (e.g. age, gender, physical handicap and pedestrian behavior) (Robertson, Hummer, & Nelson, 1994), they are quick to set up and run (Roess, Prassas, McShane, & William, 2004) but they require a great deal of effort by qualified personnel to collect the data; therefore these are unattainable for long periods of observation given the high economic costs (Greene-Roesel, Diogenes, Ragland, & Lindau, 2008). This technique requires a fixed observer at different points and at pre-established times; this man observes and manually counts the number of pedestrians by filling in suitably prepared forms in advance.

The weaknesses deriving from the human condition, in manual surveying, combined with the need to collect data continuously, with high precision and in short periods of time, has led the research to develop techniques and tools capable of achieving these objectives. Therefore, the automatic survey was introduced to meet these needs. To detect non-motorized traffic, various methods have been developed that require instruments with high precision and sensitivity; as well as being able to record and store video/audio and position data by interacting with other computer systems. The automatic survey method was initially created for indoor use, and consequently finds its maximum development in this area, but with the necessary precautions, it can also be a useful procedure in outdoor environments with countless advantages to support the operator.

The most popular automatic methods include:

- *carpets with pressure sensors* which send an impulse to the counter when they are crossed and processes the data in real time;

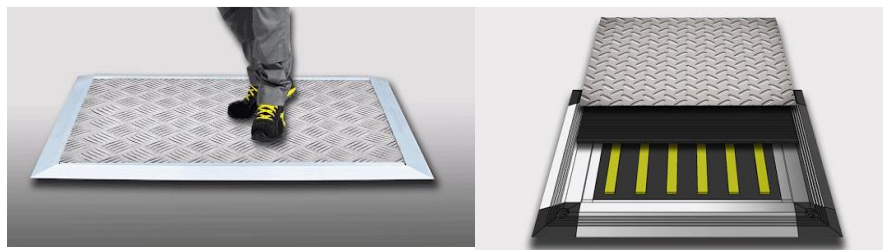


Figure 3.1 Carpets with pressure sensors (taken from Google Images)

- *infrared sensors* that allow to identify pedestrians from the body heat emitted. If the temperature exceeds a certain threshold, the counter is

activated (Federal Highway Administration, 2013). They are not very common as they may not distinguish between one or more pedestrians traveling in the immediate vicinity, and therefore generally underestimate the pedestrian volumes (Bu, Greene-Roesel, Diogenes, & Ragland, 2007).

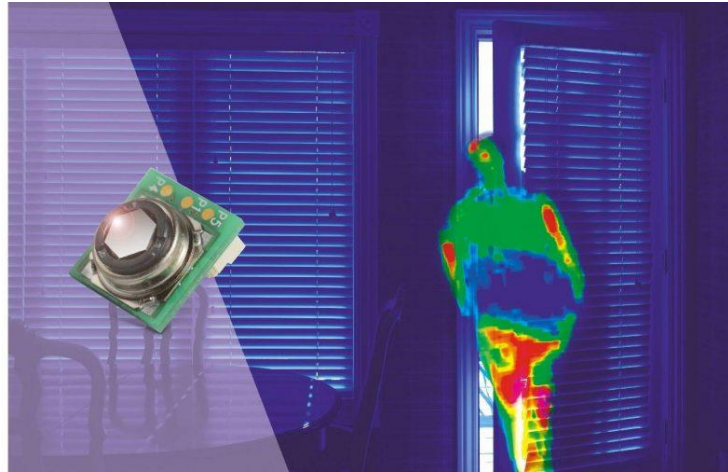


Figure 3.2 Infrared sensor (taken from Google Images)

- *pneumatic tubes* are rubber tubes that if crossed send a pulse of air passes to the detector and then record the count. These systems are also used to evaluate the speed and directionality of flows (Hyde-Wright, Graham, & Nordback, 2014) (Hjelkrem & T., 2009). Pneumatic hoses are used on surfaces in areas where temperatures remain above freezing because the hoses may not maintain their properties in cold climatic conditions and can deteriorate.
- *Inductive Loop Detectors* these are cables installed under the surface of the flooring (incorporated) or above the flooring (temporary) crossed by electric current; the wires that form the coils generate a magnetic field. When they have crossed the magnetic field changes and the measurement is obtained. These systems are mainly used for the survey of bicycles but are subject to an underestimation of the flows given the difficulty of detecting several vehicles at the same time (Nordback & Janson, 2010) (Nordback & Koonce, 2014).
- *Laser scanners* emit laser pulses in different directions and analyze the reflections of the pulses to determine the characteristics of the device's surroundings, including the presence of pedestrians or cyclists who cannot be distinguished. Usually, this technology is used for short-term counting and in closed areas without obstacles.

- *Magnetometers* are devices sensitive to ferrous objects and for this reason, they are often used to detect the presence of bicycles; when these pass through them, they change the magnetic field and the passage is recorded. The limitation in the use of these devices is that they can be applied in a limited area.
- *detection with video images*: is a monitoring system that is based on the use of cameras to continuously detect pedestrian traffic, in order to have a spatial-temporal representation of the pedestrian flow with a very high set of information. However, the processing of such video images is far from simple and immediate, since the images must be processed with rigorous methodologies in order to allow the interpretation of the contents. This method can also be a valid help in the manual field with an operator who collects the data; in an automated system, on the other hand, specific software accelerates the work and increases its accuracy (Dobler, Vani, & Dam, 2019);



Figure 3.3 Video surveillance cameras (taken from Google Images)

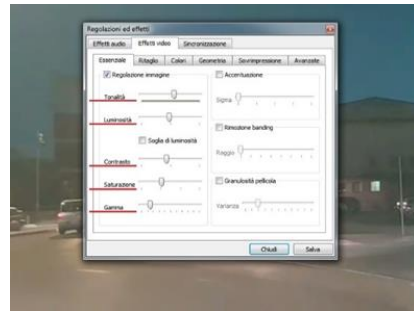


Figure 3.4 Software to process and process video images (taken from Google Images)



Figures 3.5 software that recognizes and counts the movements of objects from a video (taken from Google Images)



Figures 3.6 facial recognition software (taken from Google Images)

- *real-time detection*: a precise and constantly evolving method. This is essentially linked to the possibility of detecting a person at a certain time and position, thanks to any device with an active internet or GPS or Bluetooth connection. (Traunmueller, Johnson, Malik, & Kontokosta, 2018)

(Abedi, Bhaskar, & Chung, 2013) (Kurkcu & Ozbay, 2017) (Bongiorno, Santucci, Kon, P., & Ratti, 2019). An example can be the ability of the Google maps app to identify people who are on a certain route through the GPS of smartphones; depending on the speed and density data, this identifies and superimposes a range of colors on the pre-established itinerary, which indicate whether or not there are delays (Ziye, 2011).



Figure 3.7 Instant tracking with GPS

### 3.1.2 Forecasting models

As previously mentioned, if the counting data is not available on the entire network, it is possible to extend the study to the entire network using forecast models. A wide range of theories have been used for this, such as: tail models (Hoogendoorn & Bovy, 2004), transition matrix model (Helbing, Molnár, Farkas, & Bolay, 2001) (Kurose & Satoshi, 1995), stochastic model (Ashford, O'Leary, & McGinity, 1976), path choice model (Hoogendoorn SP, 2004). They are all, at least in part, similar to each other and are used to describe the behavior of pedestrians in critical situations. Volume estimation models are used to take into account the unpredictability of pedestrian behavior. So these are mathematical models that combine existing data with key assumptions to estimate volumes. They are typically used when data is not available or to estimate future conditions by changing variables in the model.

The most relevant models include:

1. *Sketch Sketch plan models or Direct Demand Models*: they are used as a planning guide as they attempt to approximate pedestrian demand based on simple rules of thumb (Federal Highway Administration, 1999). Pedestrian volumes are predicted through the use of counts and regression analyzes as a function of land uses (such as the surface of offices or commercial spaces) and/or travel generation indicators (parking capacity, transit volumes,

movements of traffic, etc.)(1,000 Friends of Oregon, 1993) (Systematics, 1994) (Rossi, Lawton, & Kim, 1993) (Navin & Wheeler, 1969) (Pushkarev & Zupan, 1971). The advantage of these models is that they require minimal data collection and no knowledge in mathematical simulation or computer modeling. They are able to offer quick pedestrian volume estimates but are only effective at the aggregate level. The downside is that they are unable to assign realistic pedestrian volumes to specific streets or intersections and do not take into account the type of dynamic pedestrian behavior. These models have been applied in large urban environments where neither high precision nor detailed estimates are required(1,000 Friends of Oregon, 1993) (Rossi, Lawton, & Kim, 1993);

2. *Regional travel demand models*: These models estimate existing and future travel demand from numerous input data, such as transport network, demographic characteristics and travel behavior. These are travel-based models (Sener, Ferdous, Bhat, & Reeder, 2009). Traditionally they are known as four-stage models because to estimate the pedestrian/cycle volume it uses four sub-models: trip generation, trip distribution, choice of travel mode and trip assignment (Clifton, Singleton, Muhs, Schneider, & Lagerwey, 2013). They are usually used in traffic analysis zones (TAZ, i.e. geographical census areas). Due to their coarse level of spatial analysis framework, such travel-based models are limited in estimating non-motorized travel; therefore models were developed that consider individuals rather than travel by reducing the geographical scale of analysis (parcels instead of TAZ) (Southern California Association of Governments (SCAG), 2016). These simulate the decisions of an individual participating in an activity. They are certainly realistic models even if they do not capture recreational travel (Kuzmyak J. R., Walters, Bradley, & Kockelman, 2014); but complex to apply because they require time, financial resources and qualified personnel.
3. *Demand driven models*: they are conceptually similar to regional models, but use smaller geographical areas instead of TAZ and consider origin-destination / choice of route. These models resemble traditional models of vehicular travel demand in many respects (Hoodgendoorn & Bovy, 2004) (McNally, 2000); in fact, to estimate the pedestrian volume, it uses four sub-models (travel generation, travel distribution, choice of travel mode and travel assignment). These approaches are based on the utility maximization theory, i.e. that all pedestrian actions are performed for a reason and therefore have

utility with respect to a set goal. The disadvantage is linked to the fact that in the choice of the route a defined number of routes is considered (Hamacher & Tjandra, 2001) (Hoodgendoorn & Bovy, 2004) with few possible deviations. Ultimately it can be said that these models offer complex descriptions of the built environment and the pedestrian behavior within it. But they require a large volume of data, a high level of specialized technical skills, and take time to set up, calibrate and review.

4. *Simulation-based traffic models*: they use mathematical models and computerized systems to simulate and reconstruct movements. They mainly use the outputs of the Regional Travel Demand Model (TDM) as inputs into their algorithm for determining detailed activity levels (Abdelghany, Abdelghany, Mahmassani, & Al-Zharani, 2012). These can be divided into:
  - *Microsimulation models* in which the behavior of the single individual represented is reconstructed through his speed and interaction with other pedestrians following predefined rules of behavior. Such models offer highly realistic simulations of small areas such as single streets or intersections and enclosed spaces such as transit centers, airports and shopping malls. This allows researchers to create large-scale forecasts of demand and travel volumes at a given point (Schadschneider, 2002) (Lovas, 1994) (Timms, 1992) (Annesley, Dix, Beswick, & Buchanan, 1989). The most popular models are cellular automata (Blue & Adler, 1999) (Blue & Adler, 2000) and agent-based models (Batty, 2001) (Schadschneider, Kirchner, & Nishinari, 2002). These models allow to have a high level of detail, but on the other hand, they require a good understanding of mathematics as well as computer skills.
  - *Macroscopic models* aggregate pedestrian movements into flow or density and average speed. These are made up of partial differential equations deriving from fluid dynamics and which take into account the conservation of mass and possibly an equilibrium equation of the moment (Hughes, 2002). Approaches such as cellular automata and intelligent agents are used for macro simulations (Burstedde, Klauck, Schadschneider, & Zittartz, 2001) (Wang & Chen, 2009). As for micro-simulation models, realistic detailed reconstructions of reality are obtained but a great computational burden is required.
5. *Land use models (seamless pedestrian)* are regression models used to explain "the levels of demand recorded in the counts as a function of the measured

characteristics of the adjacent environment" (Kuzmyak, Walters, Bradley, & Kockelman, 2014); indeed, they represent travel behavior based on the characteristics of an area (e.g. population density, employment density, household income, type of facility) and land use (schools, transit stops, parks, beaches, shops) and civic facilities (libraries, post offices and government buildings). These models provide estimates of overall travel in an area based on demographics, individual/family data travel, and/or survey data. They are simple to use as they take advantage of readily available data and methods (Jones et al., 2010). Their weakness is that they are limited in terms of acquisition of behavioral structure and are not transferable due to the relatively small sample size and characteristics upon which the models are built.

6. *Configurational models* allow to understand how the environment and the built environment can influence the dynamics of pedestrian movement. These are more detailed than sketch plan models and can estimate volumes for street segments and intersections over an entire city or neighborhood. Although the models present varying techniques as a function of the amount of walking trips in a study area and the various algorithms for choosing the route. Most use a gravity model (McNally, 2000) (Olson & Spring, 1997) (Teklenburg, Timmermans & van Wageningen, 1993). Since they are less complex than the others, they are also less expensive from a computational point of view; this allows for quick and easy modeling with different scenarios. This category includes the Space Syntax which uses a graphic "proximity" algorithm to estimate the movement potentials of pedestrians.

In this work, a correct configurational model was used to estimate the pedestrian flows (by carrying out the simulations with the Space Syntax); this can be further improved with a demand driven model, mainly used for estimating cycle flows.

Given that in Italy, as well as many other states, the data of the collision vehicles-vulnerable users are collected through the reports of the police; there are limitations due to both the loss of data related to:

- ✓ collisions with minor damage;
- ✓ inaccuracy of localization of collisions and fatal accidents;
- ✓ lack of exposure data.

To calibrate a model it is instead necessary to have pedestrian or cycle counts. The configurational approach allows, starting from counts on a limited number of streets, to estimate the flows over the entire city. However, the data obtained from the

calculations are often misleading; in fact, numerous studies have shown that pedestrian activity is indeed linked to the connectivity of the network but at the same time is influenced by other variables such as population, land use, the purpose of the trip, the means of connection, etc. (Cervero & Radisch, 1995) (Landis, Ottenberg, & Vattikuti, 1999) (Kitamura, Mokhtarian, & Laidet).

The configurational analysis, therefore, allows to estimate the crowding not related to the emission, to the matrix or to the modal choice (it does not reflect a structure based on supply and demand) but can only be ascribed to the configuration of the network. This is the result of the history of urban evolution in which city centers are made up of densely meshed road networks and therefore are very connected. This approach presents acceptable results because cycle and pedestrian movement is a granular and less discrete phenomenon than the transport model (in which zoning is performed, defined the movements that occur at certain times of the day, etc.); therefore a continuous model have many uncertainties, which however a transport model would not be able to grasp.

At the transport level, this is open to criticism since a movement is made for a reason, to satisfy needs and in a different way; therefore the configurational analysis must be integrated with a demand driven approach. This model makes it possible to improve the estimates of pedestrian flows as well as estimate cycling flows. Therefore, starting from a four-stage model, it is possible to estimate the flow channeled on each section of the network in order to make a ranking/gradation in terms of propensity to host cycling or pedestrian flows and therefore to make useful hypotheses for the design (being a relative knowledge of the flows on each stretch, the network can be dimensioned or upgraded).

### **3.2 Pedestrian flow estimation: configurational approach**

As previously stated, the gravitational approach is based on the use of the Space Syntax, that is a series of theories and techniques for the analysis of the spatial configuration of road networks and buildings, and of the interactions that coexist with each other. It was conceived by Bill Hillier, Professor of the Bartlett School of Architecture, University College London (UCL), in the late 1970s. The Space Syntax was created to help urban planners simulate the likely social effects (understood as human behavior and activity development) generated by their projects. According to Hillier (Hillier & Iida, 2005) pedestrian movements are influenced by the configuration

of the network. The configurational approach assumes that urban space, as it is structured, influences both settlement processes and movement, on roads and spaces, linked to the presence of settlement activities.

All movements estimated by the Space Syntax are defined by Hillier as natural movements (Hillier, Penn, Hanson, Grajewski, & Xu, 1993). The latter are the relationship between the configuration of the network and any other element of the road system. In many cases, the displacements are not generated only by the configuration of the network but can also be influenced by other attractors.

The Space Syntax is based on the axial analysis technique with which the two-dimensional urban space is reduced into a one-dimensional system. This technique starts from the hypothesis that the urban space is made up of a series of linear segments with which the grid is discretized and that the observer moves in it according to the visual perception, preferring linear paths not linked to the visual variations.

The results of the axial analysis present indices that allow to describe the configurational consistency of the elements, among these the most used are:

- The global choice index (choice) represents the flow present through a space (a high value is obtained when there are short paths that connect more spaces);
- The connectivity index, understood as a local variable, indicates the number of elements directly connected to a space;
- The integration index is a global measure of accessibility, that is the minimum number of steps of a graph necessary to reach a point starting from another. This parameter can be evaluated both locally (with topological radius 3 or metric 400m (Jiang, Claramunt, & Klarqvist, 2013) (di Pinto, V., 2013)) which turns out to be the best predictor of small-scale movements (because pedestrian trips tend to be shorter and see the road grid in a relatively localized way); or there is the global integration (with topological radius n) which predicts movements on large scale (including vehicle movements, because people on longer journeys will tend to read the grid in a more globalized way) (Hillier, 1996, 2007).

This index presents several mathematical formulations (Jiang & Claramunt, 2002) (Ostwald, 2011) (Xu, et al., 2020) (Volchenkov & Blanchard, 2008), the most immediate seems to be the one reported by Raford and Regland (2005)

$$INT = \frac{2(MD - 1)}{K - 2} \quad 3.1$$

Where:

- ❖ MD is the Mean Depth of the entire system; the Mean Depth is calculated by the equation:

$$MD = \frac{L}{(n-1)} \quad 3.2$$

where L is the Total Depth (that is the sum of all possible sections, given a starting point, to be traveled to reach a point of the network) and n is total number of sections in the network;

- ❖ K the number of nodes in the network.

The global variables are those that correlate each axial line with respect to all the other lines of the system, while the local ones measure accessibility up to a radius of 300 m.

The type of analysis that best takes into account the geometric, topological and angular characteristics of the network and that produces the best results in terms of forecasting traffic flows is the Angular Segment Analysis with Metric Radius; i.e. an analysis, carried out on a network consisting of segments, based on the calculation of the angular depth of each section in relation to the other sections of the network, setting a buffer with a finite metric radius within which to evaluate these connections between the sections (Al\_Sayed, 2018).

The angular depth is the "distance" that separates a pair of trunks, where this is understood as the sum of the angular variations of the sections, from the origin to the destination of the path (Al\_Sayed, 2018). The angular variation represents the "cost" of the move. According to Hillier (2005), in fact, the ability of the road user to plan the most convenient route from point A to point B is linked to the perception that he has of the distance to travel, which is unconsciously evaluated not necessarily with respect to the metric length of the journey, but in largely on the basis of its tortuosity, expressed precisely as a total angular variation. The user is willing to go further, "spending less" in terms of tortuosity.

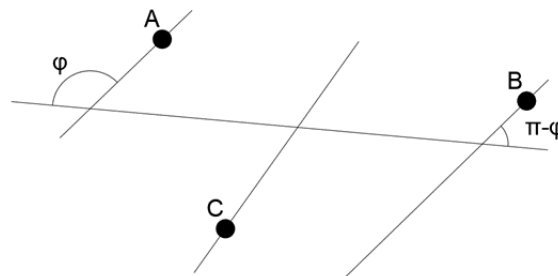


Figure 3.8 Angular variation between the sections of the network

All this is evaluated within a buffer with variable metric radius depending on the purpose of the analysis. For the evaluation of pedestrian flows in an urban center, a radius of 400 m is usually assumed, corresponding to a journey of about 5 minutes on foot. With this restriction, the system will calculate the angular turns of all legs within 400 meters of the current leg; those beyond this radius will not be calculated. The system will only identify local relationships between elements within 400 meters of each of the segments. Higher radii place a larger restriction on the analysis, up to radius  $n$ , i.e. no spatial restriction: all sections of the network are considered. The choice of the radius  $n$  is more suited to the analysis of vehicular flows (Al\_Sayed, 2018).

The analysis thus conceived returns, among the many configurational parameters of the network, those of Integration (INT) and Choice (CH), which contain an intrinsic meaning relating to the probability of each trait to be chosen or not in the various possible paths from an Origin to a Destination. Integration is a good indicator of how each of the segments can be a highly desired destination by users; Choice indicates the probability that each segment can be chosen by pedestrians as the shortest path.

Integration was correlated with pedestrian flows, in different contexts (Hiller, Penn, Hanson, Grajewski, & Xu, 1993) (Lerman, Rofè, & Omer, 2014) (Dai & Yu, 2013), obtaining low correlation coefficients varying between 0.2 and 0.4; therefore it was proposed to use a hybrid approach that would allow to obtain better forecasts.

### 3.2.1 Description of the procedure

The analysis conducted in this study can be divided into two phases.

In the first, the road-pedestrian network was reconstructed, creating the spatial relationship of contiguity between the census sections and the stretches of the road system. The resident population values (obtained from ISTAT as described below) in the census sections were attributed as an average to the sections of the network through the proximity approach. This approach correlates the characteristics of each of the network centroids with the surrounding ones, according to a succession of buffers with increasing radius ( $j_{th}$ ). The buffer radii range from 100 to 1600 meters, chosen on the basis of an impedance function (Kuzmyak, Walters, Bradley, & Kockelman, 2014). It describes the propensity to move ( $k$ ) of pedestrians as the distance to be covered varies.

The impedance function is shown below, with a table of  $k$  factor values as a function of the distance values assumed by the buffers.

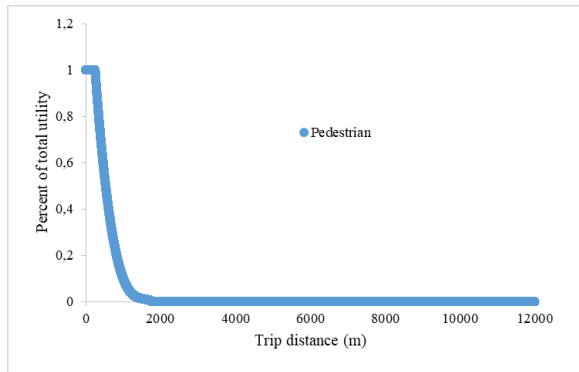


Table 3.3 Values of  $k$  as a function of distance  $d$

Distance (m)	$k$
0	1
100	1
300	1
600	0.4
800	0.2
1000	0.1
1300	0.03
1600	0.01

Figure 3.9 Impedance function for pedestrian movement.

It should be noted how the propensity to move remains unchanged at 100% from 0 to 300 m, and then gradually decreases until it becomes practically zero once approximately 1600 m is reached.

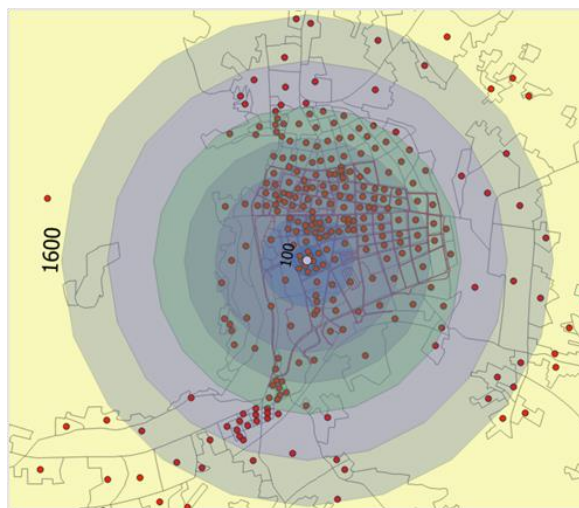


Figure 3.10 Succession of buffers from the network centroid up to 1600 m away (taken from Qgis).

To obtain a coefficient that expresses the ability of each stretch to attract pedestrian movements, it is necessary to multiply the average population values  $M$  of each circular crown by the respective value of  $k$ ; then add them and obtain a single  $P_{prox}$  weight (proximity weight). If the values of  $k$  of the previous table were considered, the populations of each circular crown would be multiplied by the upper extremes of the values assumed by  $k$  in that spatial interval. For a more even and uniform distribution, the average value ( $k_M$ ) that  $k$  assumes in each circular crown is taken instead.

Buffer	M.	<del>km</del>
0-100	M100m	1
100-300	M300m	1
300-600	M600m	0.7
600-800	M800m	0.3
800-1000	M1000m	0.15
1000-1300	M1300m	0.065
1300-1600	M1600m	0.02

$$P_{prox,i} = \sum_{j=100m}^{1600m} k_{Mj} M_{ij}$$

Figure 3.11 Table of mean  $k$  values for each circular crown

For each network centroid, a  $P_{prox}$  weight is obtained; this is evaluated at an increasing distance from the single centroid, taking into account the actual propensity of users to move as their distance from it increases. The aim was to define a weight factor, understood as the attractiveness of pedestrian flows as a function of the average of the population residing within the circular ring.

In the second phase, the weights used in the analysis with the Space Syntax were compared with the counts on the network, looking for a correlation between the values. The results of the weighted analyzes were compared with those of the unweighted analysis.

### Construction of the network and collection of variables

In order to calibrate the forecast model of pedestrian flows, it is necessary to start from the collection and processing of data on the central area of the city of Cassino (FR).

This is a town of 36497 inhabitants in the Province of Frosinone in the Lazio region (Italy). It stands at the foot of the Montecassino hill, in the shadow of the famous Benedictine abbey. The city is the second most populous in the entire province. The choice to use Cassino as a case study for the layout of its network is linked to: relatively small size, easy accessibility, presence of transport infrastructures (railway station, bus services, bike sharing service, etc.), aptitude for walkability (mainly flat territory, etc.). Furthermore, the presence of schools, universities, restaurants, shops, public and private offices, etc. guarantees a regular movement of people for ordinary daily activities.



Figure 3.12 In red the position of the municipality of Cassino in the province of Frosinone (Source: [https://it.wikipedia.org/wiki/Cassino#/media/File:Map\\_of\\_city\\_of\\_Cassino\\_\(province\\_of\\_Frosinone,\\_region\\_Lazio,\\_Italia\)](https://it.wikipedia.org/wiki/Cassino#/media/File:Map_of_city_of_Cassino_(province_of_Frosinone,_region_Lazio,_Italia)))



Figure 3.13 Aerial photography Cassino center, study area

The study was conducted only in the downtown area.



Figure 3.14 Portion of the Cassino center affected by the study.

The procedure can be outlined as shown in the following flow chart.

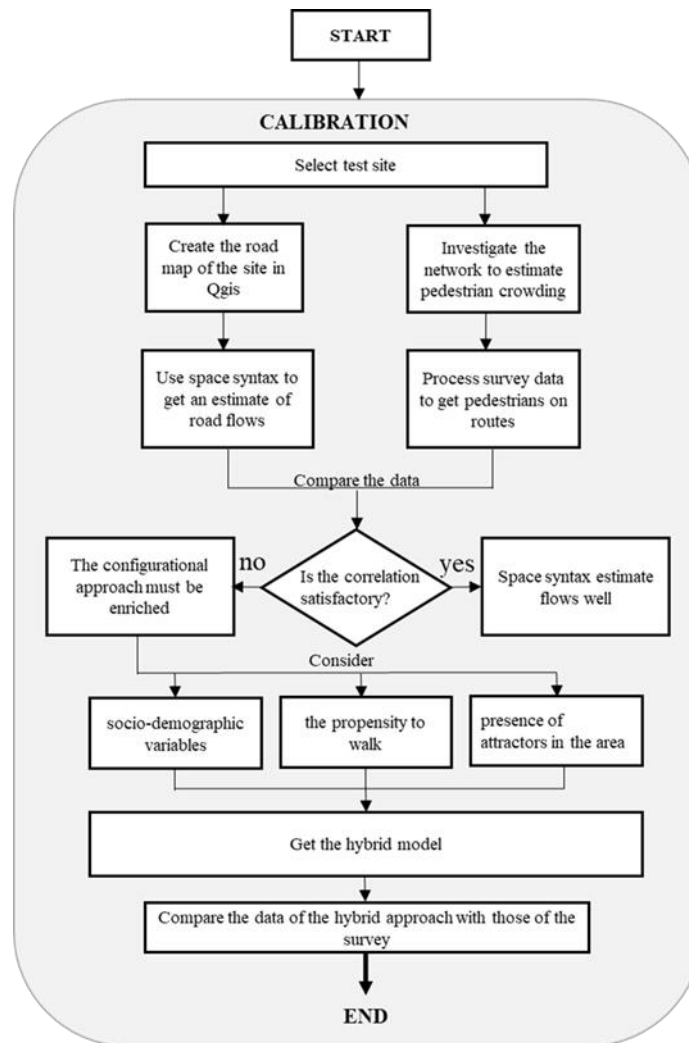


Figure 3.15 Flow chart of the proposed methodology.

Before proceeding with the definition and application of the procedure, the data must be collected, thus starting with data on the census and socio-demographic sections of the area. Subsequently, the road network is reconstructed and, with the help of the Field Calculator tool of the QGIS, the aggregation between the two layers Sections and Network is carried out.

#### Socio-demographic data

The data necessary for the analysis were obtained from the Istat website. The surveys obtained are made available to citizens on the Istat web archive (ISTAT). In this work, the data relating to the resident population in the Lazio Region and in particular in the Municipality of Cassino were extrapolated. This and other information is provided by Istat in relation to the various census sections in which the national territory is discretized.

The census section is the minimum unit of aggregation of census data in the municipal area. According to the Istat definition (2015), it consists of a single body delimited by a closed broken line. By adding together the census sections, it is possible to reconstruct the geographical and administrative entities of a higher level (inhabited localities, sub-municipal areas, constituencies and others).

Geometria	Valore
▼ R12_11_WGS84	
▼ Titolo	12
> (Derivato)	
> (Azioni)	
COD_REG	12.000000000000
COD_ISTAT	12060019.000000000000
PRO_COM	60019.000000000000
SEZ2011	600190000001
SEZ	1.000000000000
COD_STAGNO	0.000000000000
COD_FILME	0.000000000000
COD_LAGO	0.000000000000
COD_LAGUNA	0.000000000000
COD_VAL_P	0.000000000000
COD_ZONA_C	0.000000000000
COD_IS_AMM	0.000000000000
COD_IS_LAC	0.000000000000
COD_IS_MAR	0.000000000000
COD_AREA_S	0.000000000000
COD_MONT_D	0.000000000000
LOC2011	6001926723.000000000000
COD_LOC	26723.000000000000
TIPO_LOC	2.000000000000
COM_ASC	0.000000000000
COD_ASC	0
ACE	0
Shape_Leng	430.81916619800
Shape_Area	8225.95793667000

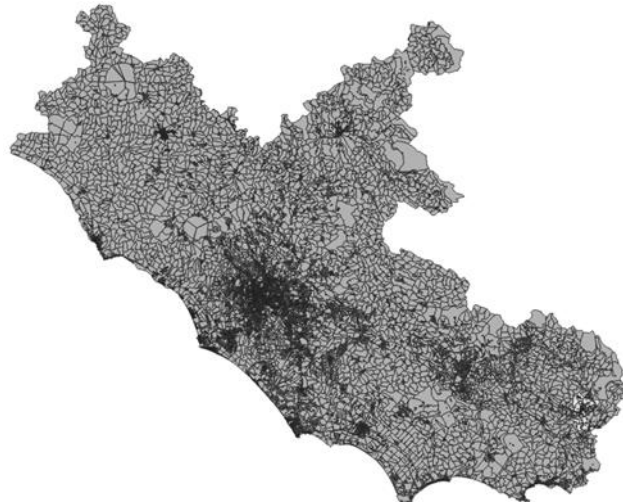


Figure 3.16 Attributes of Section 1 of the Municipality of Cassino

Figures 3.17 Lazio Region divided into its census sections. The sections of the Municipality of Cassino are selected in yellow

From the online archive of Istat data it was, therefore, possible to find the necessary statistical data, downloaded in the form of shapefiles so that these can be opened by the QGIS software and Excel spreadsheets from which to extrapolate data on the population.

The shapefile R12\_11\_WGS84.shx downloaded from the “Territorial bases” table of the Istat archive allows you to view the entire Lazio Region in GIS with the census sections that represent its geometries.



Figure 3.18 Census sections constituting the municipal territory of Cassino

Each geometry is identified by an identification code of the Region, Province, Municipality and of the section itself, with geometric data on the area and the perimeter of the section. By applying a filter in the visualization of the layer of the census sections on QGIS, it is possible to show only the sections belonging to the Municipality of Cassino (identified by the progressive code PRO\_COM = 60019). The municipal territory is discretized into 689 census sections.

The Excel spreadsheet containing, for each census section of the Lazio Region, and therefore of Cassino, the socio-demographic data of the area, including data on the total resident population or organized by gender, age and more, as well as the number and type of buildings present. It is possible to insert this data inside the shapefile in QGIS by performing a Join operation.

In this way, a QGIS layer is obtained consisting of the various census sections of the Municipality of Cassino; each of which preserves data on its geometry and geographical location, in addition to the socio-demographic information that characterizes it. It is possible to identify the areas of the Municipality with the greatest demographic density and on which there are residential and commercial buildings in the greatest number.

Geometria	Valore
▼ R12_11_WGS84	
▼ Titolo	12
> (Derivato)	
> (Azioni)	
COD_REG	12.000000000000
COD_ISTAT	12060019.000000000000
PRO_COM	60019.000000000000
SEZ2011	600190000001
SEZ	1.000000000000
COD_STAGNO	0.000000000000
COD_FLUME	0.000000000000
COD_LAGO	0.000000000000
COD_LAGUNA	0.000000000000
COD_VAL_P	0.000000000000
COD_ZONA_C	0.000000000000
COD_IS_AMM	0.000000000000
COD_IS_LAC	0.000000000000
COD_IS_MAR	0.000000000000
COD_AREA_S	0.000000000000
COD_MONT_D	0.000000000000
LOC2011	6001926723.000000000000
COD_LOG	26723.000000000000
TIPO_LOG	2.000000000000
COM_ASC	0.000000000000
COD_ASC	0
ACE	0
Shape_Leng	430.81916619800
Shape_Area	8225.95793667000
orig_ooc_fid	31688
_P1	31
_E3	2
E4	0

Figure 3.19 Addition of the fields "\_P1" (Resident Population), "\_E3" (Residential Buildings), "\_E4" (Commercial Buildings)

It should be noted that some of the census sections represented in the shapefile are not indicated in the Excel file since for these there are no socio-demographic data to be analyzed. Attempts have been made to find this information elsewhere, without success. Later it was noted that this lack of data is due in most cases to the fact that the

census sections in question are placed in correspondence with school complexes, administrative offices, etc.

However, these analyzes are strictly related to the geometric and topological characteristics of the network, which could distort the results if the singularities present in the analysis area were not taken into account. To overcome this problem, using the Depthmap UCL software, it is possible to carry out these analyzes by attributing weight to the calculation of the configurational characteristics, consisting of any peculiarity of the network, which acts as a multiplication factor of the values obtained without weight. The most used method is to attribute the weight based on the length of each segment. Mainly because longer road segments are likely to be characterized by a greater number of entrances on both sides, consequently leading to higher rates of movement. This is especially true for pedestrian movement and for analyzes with small metric radii.

The idea behind this study is, instead, to use as weights quantities such as the population or the number of commercial and residential buildings that insist on each section. This derives from the consideration that, although an area of the road network can be geometrically and topologically "attractive" (well connected and integrated) it will be affected by quantitatively different pedestrian flows depending on the resident population and depending on whether or not they are present in the area of elements with a strong attractive capacity such as large residential and/or commercial complexes.

The analyzes thus carried out with the Depthmap UCL software return different thematic representations of the road network, with the sections that differ from each other based on the value assumed for a given quantity calculated by the analysis.

### **Construction of the network and the criticalities encountered**

There have been numerous implementation criticalities which are analyzed below.

#### *1. Construction of the pedestrian network*

In order to carry out an analysis as realistic as possible, it was necessary to reproduce the actual choice of the pedestrian in the best possible way, for this reason it was necessary to represent each street following the progressive.

For each street, the segments corresponding to the two sidewalks, which can be crossed in both directions, joined by pedestrian crossings where present, have been traced.

Since such a setup network was not available, it was necessary to "draw" it directly on the QGIS, taking as reference the streets shown on the Open Street Map. On the QGIS the map was then inserted as a background on which the pedestrian network was

traced as a linear layer, consisting of only broken sections. This is because the forecast analysis of the Space Syntax Toolkit requires a graph consisting of independent segments.



*Figure 3.20 Use of Open Street Map in the construction of the pedestrian network (taken from Qgis)*

Since the level of detail of Open Street Map, as well as of Google Maps or other similar base-maps, does not allow pedestrian crossings to be displayed, a connection with Google Satellite was created to design them (Geogeek.xyz, 2018). In some cases, the resolution was not sufficient to correctly display the roads and crossings. Google Earth was then used.



*Figure 3.21 Use of Google Satellite in the construction of the pedestrian network (taken from Qgis)*

The greatest criticality regarding the tracing of the pedestrian network occurred in some areas of the center of Cassino where the lack of pedestrian crossings is highlighted. Therefore, following the actual road layout, “islands” were formed, or portions of the network disconnected from the rest of the graph.

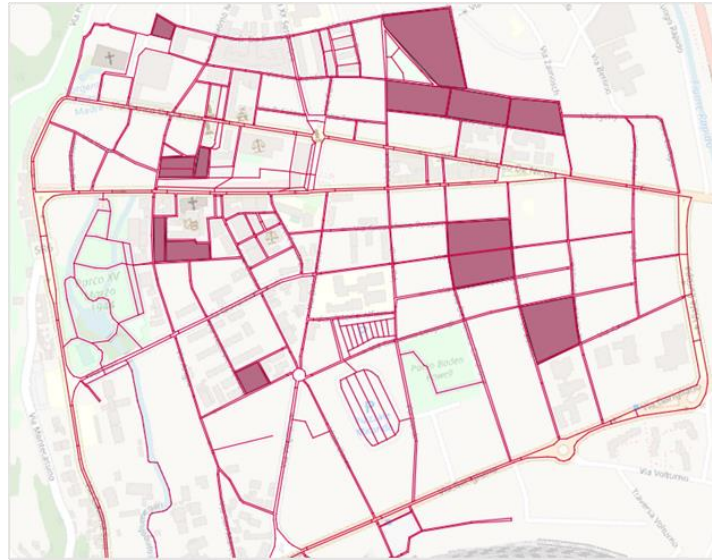


Figure 3.22 Isolated areas of the center as they do not have pedestrian crossings (taken from Qgis)

In such areas, if pedestrians followed the highway code to the letter, they would be trapped in a dead-end maze. Realistically, this never happens, in fact, in such cases the pedestrian is forced to cross the street without a pedestrian crossing, with obvious risks to his safety.

Taking note of this lack and in order to ensure the success of the forecast analysis, some pedestrian crossings where the real road network was lacking have been added arbitrarily in this work, in order to eliminate the analytical error due to the formation of these islands. This was done wisely, avoiding not adding too much, otherwise there would be a risk of compromising the reliability of the analysis.

It is necessary to specify that the satellite images used to verify the presence of pedestrian crossings date back in some cases to the years 2018-2019, in other cases to previous years. So it could happen that missing pedestrian crossings may have been integrated in some of these areas.

## 2. QGIS field calculator

In order to assign the resident population to each section of the network, it was necessary to use the Field Calculator tool.

Although many have dealt with these issues using this tool, no one specifically refers to the case presented in this work.

To the theoretical strategies developed for carrying out the analyzes, it was necessary to find a way to approach their actual possibility of realization on the GIS software.

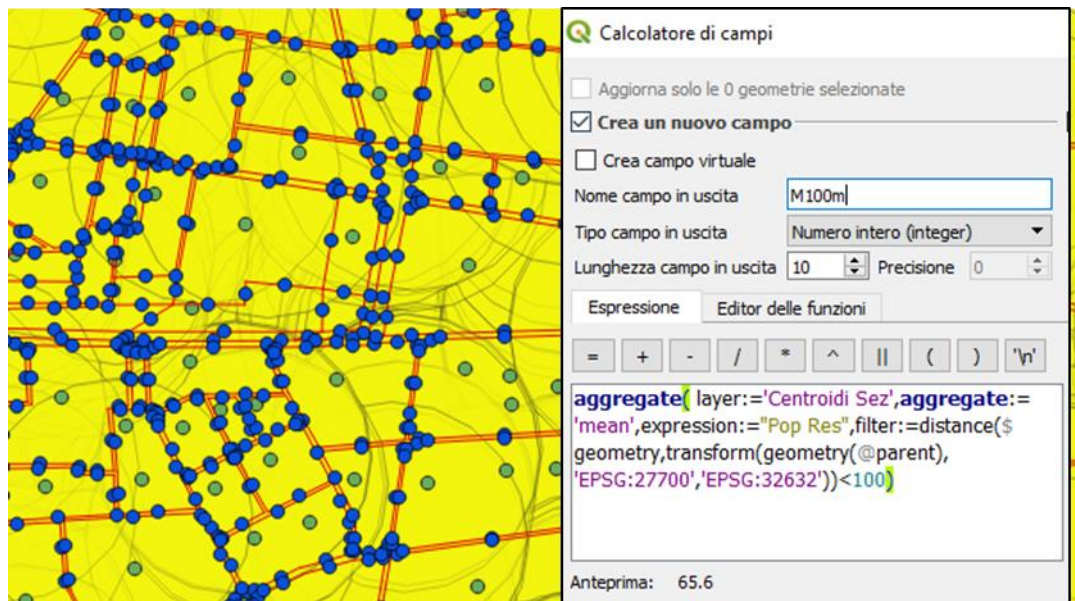


Figure 3.23 Calculation of a field in the “network centroid” layer, containing as values the average of the resident population of the centroids of the sections within 100 m of each centroid of the network. There are terms of transformation of the Reference Systems (SR)

Outlining the problem: the centroids, buffer and other algorithms functions were used, and through the query/aggregation functions between different layers it was finally possible to solve the problems arising from the software approach.

### 3. Space Syntax

Once the network was defined, the Space Syntax model was calibrated, attributing, to each section, a weight linked to the resident population in the various census sections. The calculation of this weight was defined with the implementation of the gravitational weight. Therefore, each stretch of the network and each census section have been simplified by considering their respective centroids (preserving the information contained in the geometry from which they come).

To obtain the centroids of the census sections just select the layer of the sections (which will necessarily be a polygonal layer), and then select the Centroids algorithm in the Processing Tools. A dialog box opens in which you select the layer to use (eg Cassino Census Sections) and locate the folder in which to save the file in shp format.

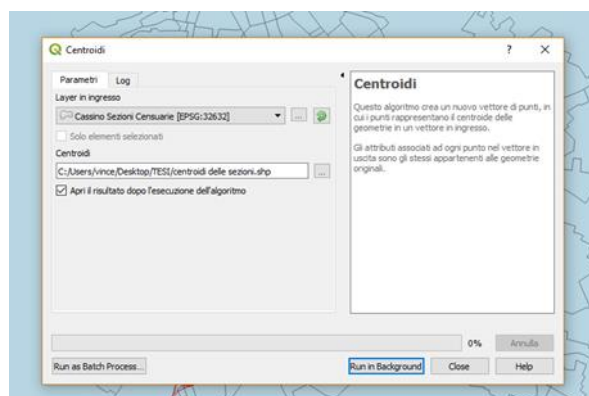


Figure 3.24 Creations of the centroids of the census sections.

Alternatively, you can avoid saving the file, thus obtaining a virtual layer that can be saved later if necessary.

The centroids of the sections of the pedestrian network are then created using the Centroids algorithm, or the Points along the line algorithm, setting the creation of the centroids at the 0.5 interval of the geometry, that is, in the midpoint of the sections.

Two new layers are obtained, one with the centroids of the census sections and the other with the centroids of the pedestrian sections. In both cases, each centroid contains in its attributes the same fields and data as the geometry from which it comes (section or feature).

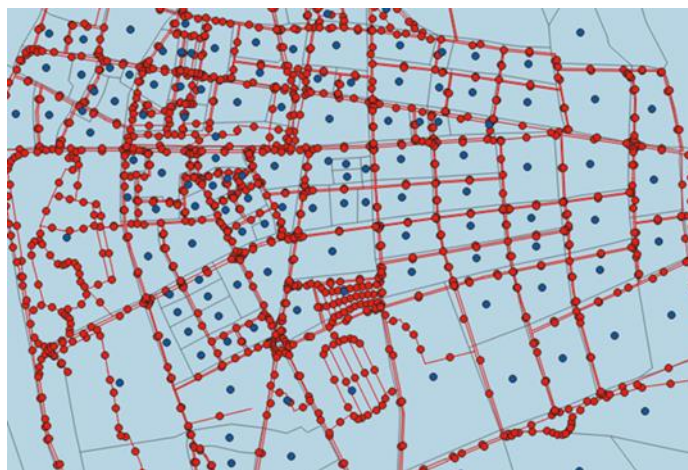


Figure 3.25 Centroids of the census sections (in blue) and of the sections of the network (in red) (taken from Qgis)

It should be noted that some sections, and therefore also the corresponding centroids, do not have resident population values as they are sections characterized by the presence of school complexes or administrative offices. Giving it a population

value of NULL or zero would compromise the analysis, so it was decided to remove these centroids.

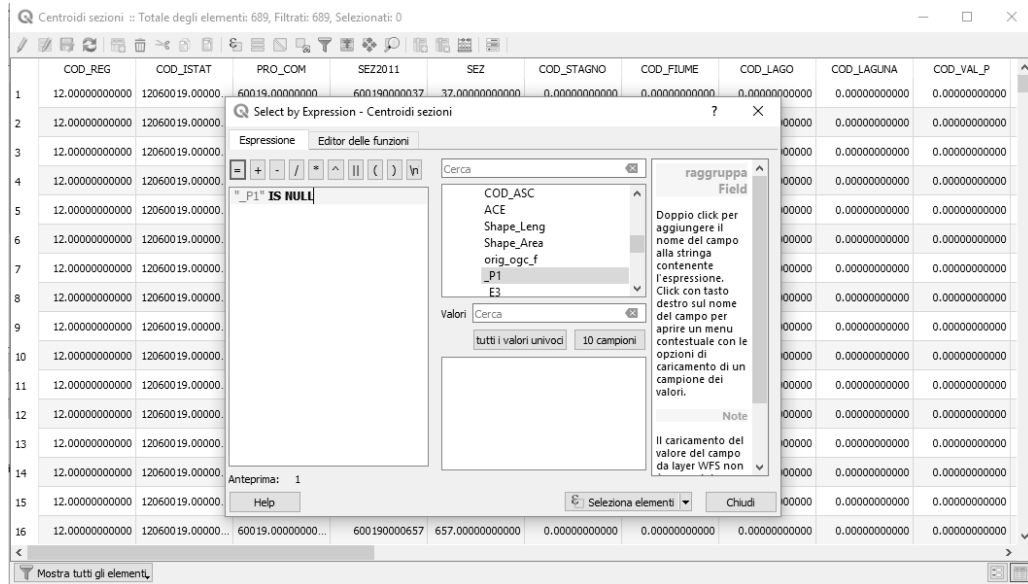


Figure 3.26 Removal of geometries without information on the resident population (*\_P1*) (taken from Qgis)

Once the population information has been transferred from the section centroids to the network centroids, the respective values of the proximity weights (Pprox) are associated to the sections of the network and then the forecast analysis is started.

One of the ways of carrying out this data transposition is through the Join function of QGIS. This function allows to introduce an excel or csv file into the project as a layer and join its columns to the attributes of a pre-existing layer, thus creating new fields.

Then inserting an excel file containing the new Pprox field, these values are introduced in the layer on each section of the pedestrian network.

You can then move on to the forecast analysis phase by finally using the Space Syntax Toolkit (SST). It is good to reiterate that for this phase of the project it is necessary to use version 2.18.24 of the QGIS software, this being one of the last for which it is possible to use the SST application.

For the use of the Space Syntax model, the analysis of theoretical principles and practical applications was performed, which are also very different from the case in question. The consultation of articles, publications and manuals drawn up by the creators of the model themselves has made it possible to unravel, not without difficulty, in the approach to this tool. In particular, for the possibility of introducing the population weight and for identifying the right configurational parameters on

which to focus, it was essential to know the practical applications carried out by scholars in different parts of the world.(Hillier & Iida, 2005) (Cutini, 1999).

### 3.2.2 Pedestrian survey

Before proceeding with the simulations with the software, counts were carried out on some of the main road sections or in any case characterized by the presence of attractors.

In order to determine the flows, one must:

- define a catchment area according to the urban environment taken into consideration,
- carry out research on the attractive capacities inherent to the travel request,
- determine hypothetical time slots and critical days.

These elements involve a high degree of complexity as they are linked, directly or indirectly, to the unpredictability and variability of human behavior. (Ministry of Infrastructure and Transport) (Armor, 1999).

In recent decades, surveys on pedestrian flows for internal spaces (private, public and commercial) have spread widely; consequently, many research theories have been developed for these fields and studies have been undertaken in order to make this knowledge suitable for external environments. As mentioned in Paragraph 3.1.1, there are numerous relevant techniques. Before starting, the pros and cons of the procedures were evaluated, highlighting that the fixed observer technique would certainly allow obtaining a better overview of a site but there is a final figure that will be averaged over the observation time window (hourly, daily, monthly or seasonal). Therefore it was decided to use an innovative technique in this field, given the time and economic means available: the technique of the mobile observer. This technique is consolidated and widespread for the survey of motorized traffic but it seems that so far no one has ever adopted it in this field.

This technique provides that its survey is conducted by a monitoring vehicle, equipped with video recording devices, which moves along the route to be examined.

This technique has the advantage of being able to acquire data over an entire network, albeit for a shorter period of time. This makes the data unstable at a statistical level therefore it is necessary to repeat the survey several times in order to stabilize it..

To determine the route, the attraction areas were taken into account in order to detect the pedestrian flows in, out and crossing.

These areas have been identified starting from the Istat basket of the year 2019 which highlights the needs of the inhabitants. This makes it possible to identify basic

service categories that may be of interest to the population, taking into account the habits of families and the socio-economic fabric of society (ISTAT, 2019).



Figure 3.27 ISTAT basket year 2019 (Source:

<https://www.istat.it/it/files/2019/02/infograficaPaniere.pdf> - 19/8/2019)

Considering home-work-study trips, the following are considered as attractive points:

- Education: schools of all levels, private or public.
- Healthcare: medical clinics, analysis centers, clinics for the elderly, pharmacies and medical facilities of any kind.
- Transport: railway station, the main bus stops of the urban and extra-urban lines, large non-paid car parks,
- Services: commercial, tourist, recreational, hospitality and catering.
- Corporate, postal, municipal and judicial offices.
- Green areas: Parks and gardens.
- Areas of cultural interest: museums and archaeological sites.
- Market areas.
- Pedestrian areas.

Taking these preliminary considerations into account, two itineraries have been defined (one for a weekday and one for a day before a holiday), both having the same starting and ending point, identified with the roundabout near the Roman amphitheater area.



Figure 3.28 Bing Maps Aerial view; on the left, circled in red, the position of the roundabout in the Roman amphitheater area of Cassino and on the right enlarged in detail. (Source: <https://www.arcgis.com/home/webmap/viewer.html?webmap=4628bbe4f10b4a81b41b520ba5cae20>)



Figure 3.29 Google street view, roundabout in the Roman amphitheater area of Cassino, first exit viale Bonomi; second via G. Di Biasio.

The routes, therefore, are composed of a series of road sections that are created between the main streets of the area, referring to the stops, to giving way (including roundabouts) and to traffic light systems. These constraints in the path are considered as nodes having distinctive and progressive numbers and determining the beginning and the end of each section.

Table 3.4 Tables of road sections existing on streets and squares of the survey route.

WEEKDAY ROUTE		PRE-HOLIDAY ROUTE	
PIAZZA WAY	ROAD SECTION	PIAZZA WAY	ROAD SECTION
VIALE BONOMI	0--1	VIALE BONOMI	0--1
VIALE BONOMI + VIA GARIGLIANO	1--2	VIALE BONOMI + VIA GARIGLIANO	1--2
VIA GARIGLIANO	2--3	VIA GARIGLIANO	2--3
VIALE EUROPA	3--4; 30--3	VIALE EUROPA	3--4; 30--3
VIA E. DE NICOLA	4--5	VIA E. DE NICOLA	4--5
VIA E. DE NICOLA	5--6	VIA E. DE NICOLA	5--6; 31--6
VIA E. DE NICOLA	6--7	VIA E. DE NICOLA	6--7
VIA E. DE NICOLA	7--8	VIA E. DE NICOLA	7--8
VIA E. DE NICOLA + VIA R. DA S. GERMANO	8--9	VIA E. DE NICOLA + VIA R. DA S. GERMANO	8--9
COURSE OF THE REPUBLIC	9--10	COURSE OF THE REPUBLIC	9--10
COURSE OF THE REPUBLIC	10--11	COURSE OF THE REPUBLIC	10--11
VERDI STREET	11--12	VERDI STREET	11--12
COURSE OF THE REPUBLIC	11--26	COURSE OF THE REPUBLIC	11--31
VIA VIRGLIO	13--14	VIA VIRGLIO	13--14
VIALE DANTE NORD	14--34--15	VIALE DANTE NORD	34--14
VIA D'ANNUNZIO	16--14	VIA D'ANNUNZIO	16--14
VIALE DANTE SUD	14--1	VIALE DANTE SUD	14--1
VIA G. DI BIASIO	0--9	VIA G. DI BIASIO	0--9
VIA CONDOTTI	17--18	VIA CONDOTTI	17--18
VIA VARRONE (PART)	18--19	VIA VARRONE (PART)	18--19
VIA TOSTI	19--20	VIA TOSTI	19--20
VIA S. CROCE	20--21	VIA S. CROCE	20--21
VIA S. GERMANO	21--22	VIA S. GERMANO	21--22
VIA LOMBARDIA	22--23	VIA LOMBARDIA	22--23
VIA LOMBARDIA	23--24	VIA LOMBARDIA	23--24
VIA LOMBARDIA	24--25	VIA LOMBARDIA	24--25
VIA ZAMOSC (PART)	25--26	VIA ZAMOSC (PART)	25--26
VIA DONIZETTI	26--27	VIA DONIZETTI	26--27
VIA DONIZETTI (PART)	27--35	VIA G. PASCOLI	27--28
VIA ARNO	35--30	VIA PO	28--29
		VIA ARNO (PART)	29--30

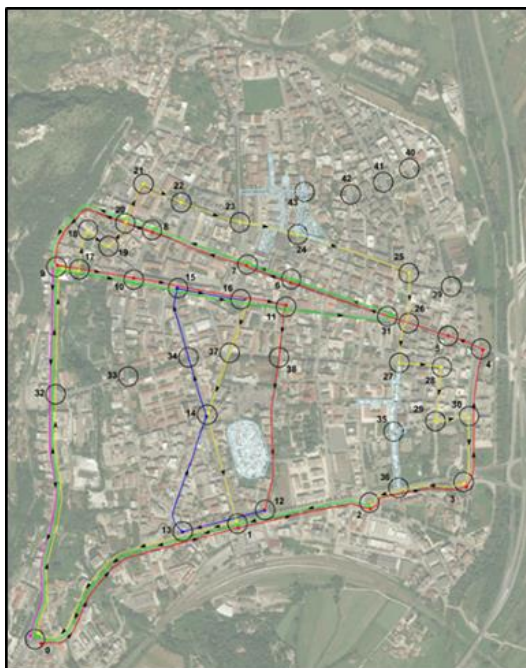
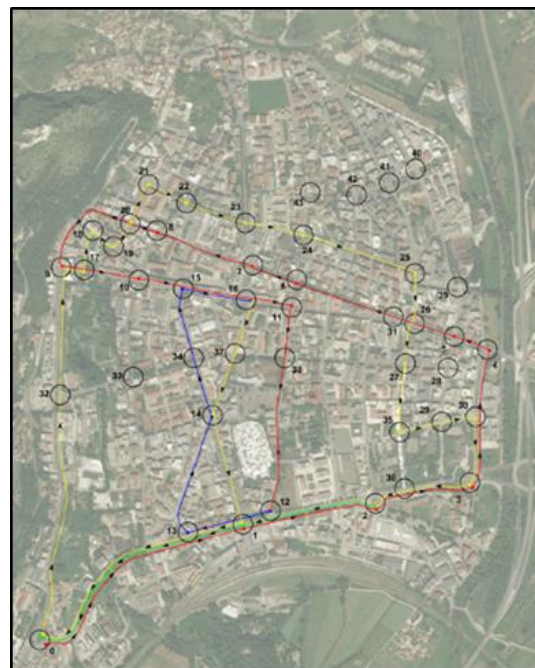


Figure 3.30 Pre-holiday route



Figures 3.31 Weekday route

The limitation of the survey with the manual technique of the mobile observer is the fact that the sampling takes place for less than one minute, therefore often there are

fewer data than in reality and they are more dispersed; for this reason it is necessary to carry out a greater number of surveys.

However, the aforementioned technique implies the use of several operators to fill in special forms created during the survey design phase; to overcome this problem and allow a single operator to carry out the search, it was decided to add technological support based on "detection with video images". In fact, a monitoring system has been devised installed onboard the vehicle and composed of devices that continuously capture and store data. These, in a subsequent phase, were processed and analyzed by the operator.

To carry out the survey, two smartphone devices (with an Android operating system) on which free apps were installed that would allow the collection of data of interest. Therefore, they have been installed:

- Free camera timestamp which is able to record high resolution video images (1280x720), to superimpose the date, time, street name, municipality, province and region in which it is located, as well as the GPS location; even if it is impossible to obtain the data in the form of editable files.
- GPS Logger, on the other hand, it allows to extrapolate data relating to the date, time, GPS position (expressed in latitude and longitude) of the observation vehicle moving along the route; as it stores and returns everything in easily processable files but cannot record video images.



*Figure 3.32 Placement of devices on the windshield*

Before proceeding with the surveys, tests were carried out. These highlighted some program malfunctions:

- Timestamp camera free returns inaccurate longitude and latitude values, therefore, it is not reliable on the identification of street names. To remedy

the problem, the incorrect data were ignored and integrated with those provided by GPS Logger and Google Earth.

- GPS Logger returns times according to the Greenwich time zone, not allowing them to be changed. To correct the time, an hour increase was made to obtain the time in the Italian zone and an additional hour due to the transition from solar time to summer time.

It was established which software the devices should operate with, how to physically set them up inside the passenger compartment and how to retrieve and store the data for subsequent analysis. The measurement campaigns were then conducted considering both weekdays and pre-holidays. The former made it possible to capture the movements associated with the presentation of schools, offices and shops. While in the pre-holidays the morning flows linked to the presence of the markets were recorded, while in the evening the movements influenced by the activation of the temporary pedestrian areas were recorded.

The time slots analyzed are the most loaded:

- on weekdays they go from 8.00 to 9.00, (for the arrival of students, employees, shopkeepers and artisans in the workplace), from 12.00 to 14.00 (time of exit from schools and lunch break) and in the evening from 18.00 at 19.00 (workers and any students still in the area return home).
- on the pre-holiday day, three time slots were analyzed in the morning (8.00-9.00, 9.00-10.00, 10.00-11.00) to facilitate the passage near the market areas and one in the evening (20.00-21.00) to cross the areas close to of the temporary pedestrian ones. Four complete laps were carried out on the itinerary set for the days examined.

In order to correctly detect the flows, where possible, and to have at least two points of view, the sections were traveled in both directions of a road section, maintaining speeds below 30 km/h.

By processing the survey data, the following were obtained:

- the number of pedestrians present on the sections (divided by categories: pedestrians on the right sidewalk, pedestrians on the left sidewalk and pedestrians crossing);
- the geo-localized positions of pedestrians (so as to know where they were detected);
- the times relating to the position of the pedestrian identified on the route.

The information was obtained by manually analyzing the video images in order to implement an Excel sheet.

A	B	C	D	E	F	G	H	I	J	K	L	M
LATITUDINE	LONGITUDINE	DATA - FUSO ORARIO GREENWICH	VIA/PIAZZA	VERSO DI PERCORRENZA	TRONCO STRADALE - NODI SEZIONE	FUSO ORARIO ROMA	PROGRESSIVA PERIODO TEMPORALE VIDEO	PEDONI DI SINISTRA FERMI	PEDONI DI SINISTRA IN MOVIMENTO	PEDONI CHE ATTRAVERSIANO	PEDONI DI DESTRA FERMI	PEDONI DI DESTRA IN MOVIMENTO
41.48223954	13.82505552	2019-06-29T05:57:23Z	VIALE BONONDI	EST	0 → 1	07:57:32	00:01:57					
41.48225801	13.82511855	2019-06-29T05:57:32Z	VIALE BONONDI	EST	0 → 1	07:57:33	00:01:58					
41.48226844	13.82511895	2019-06-29T05:57:32Z	VIALE BONONDI	EST	0 → 1	07:57:34	00:01:59					
41.48227508	13.82521515	2019-06-29T05:57:32Z	VIALE BONONDI	EST	0 → 1	07:57:35	00:02:00					
41.48227785	13.82521115	2019-06-29T05:57:32Z	VIALE BONONDI	EST	0 → 1	07:57:26	00:02:01					
41.48227199	13.82539159	2019-06-29T05:57:27Z	VIALE BONONDI	EST	0 → 1	07:57:27	00:02:02					
41.48225884	13.82454226	2019-06-29T05:57:28Z	VIALE BONONDI	EST	0 → 1	07:57:28	00:02:03					
41.48224059	13.82551583	2019-06-29T05:57:28Z	VIALE BONONDI	EST	0 → 1	07:57:29	00:02:04					
41.48223203	13.8255982	2019-06-29T05:57:30Z	VIALE BONONDI	EST	0 → 1	07:57:30	00:02:05					
41.48220993	13.82561446	2019-06-29T05:57:31Z	VIALE BONONDI	EST	0 → 1	07:57:31	00:02:06					
41.48219171	13.82567048	2019-06-29T05:57:32Z	VIALE BONONDI	EST	0 → 1	07:57:32	00:02:07					
41.48216544	13.82576804	2019-06-29T05:57:32Z	VIALE BONONDI	EST	0 → 1	07:57:33	00:02:08					
41.48219702	13.82581173	2019-06-29T05:57:32Z	VIALE BONONDI	EST	0 → 1	07:57:34	00:02:09					
41.48224064	13.82597844	2019-06-29T05:57:32Z	VIALE BONONDI	EST	0 → 1	07:57:33	00:02:10					
41.48229221	13.82608039	2019-06-29T05:57:32Z	VIALE BONONDI	EST	0 → 1	07:57:36	00:02:11					
41.48231707	13.82611981	2019-06-29T05:57:31Z	VIALE BONONDI	EST	0 → 1	07:57:37	00:02:12					
41.48234041	13.82614954	2019-06-29T05:57:31Z	VIALE BONONDI	EST	0 → 1	07:57:38	00:02:13					

Figure 3.33 EXCEL spreadsheet

Through the VLC multimedia player the videos were processed, adding video effects that allowed them to be zoomed.

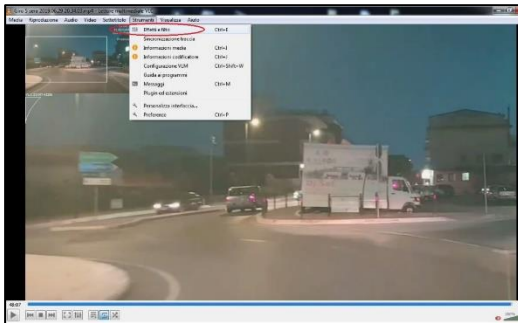


Figure 3.34 VLC media player, panel access: Video Effects.



Figure 3.35 VLC media player, Video Effects, Geometry, Interactive Zoom.

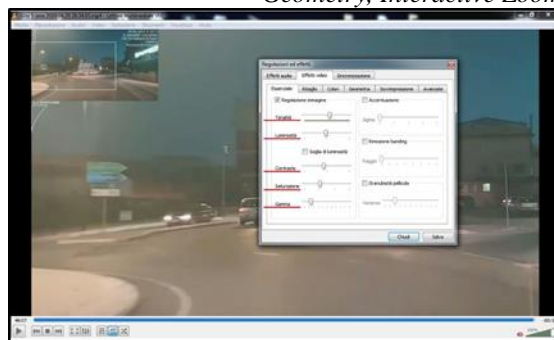
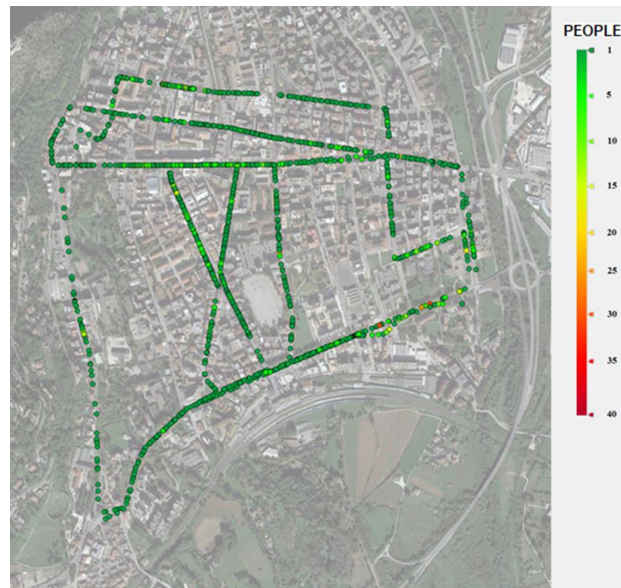


Figure 3.36 VLC Media Player, Video Effects, Essential.

The videos relating to the same road section were viewed at least three consecutive times, in order to verify the correctness of the information. Then the number of moving or stationary pedestrians were noted in correspondence with the progressive time period of the video. Having previously implemented the spreadsheet with the values deriving from GPSLogger (longitude, latitude and time zone) and synchronized the

shooting time, it was possible to position, within the sheet, the aforementioned parameters relating to pedestrians, obtaining a correspondence between them.

This was useful for having a QGIS representation of pedestrians within the study area.



*Figure 3.37 QGIS representation of pedestrians detected and present on the study path in the weekday scenario.*

### **3.2.3 Results of the forecast analysis**

From the analyzes with the Space Syntax different results are obtained according to the type of weight used. Below are the respective thematic representations of the network with a specific legend for distinguishing the values of the Integration parameter as the colors change. It was decided to focus on this parameter in particular since from experimental evidence it appears to be the one that most relates to the pedestrian movement actually observed on the network (Hillier & Iida, 2005) (Cutini, 1999).

## 1. Segment Analysis – unweighted

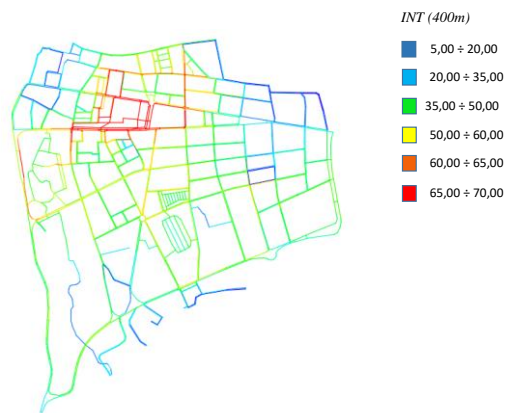


Figure 3.38 Thematic representation of the results of the unweighted analysis, with a legend of the Integration values based on the colors.

The unweighted analysis refers only to the geometric and topological characteristics of the network. The downtown area, with more interconnected sections, has the highest Integration values (red sections). These values decrease as you move away from the Central Business District (CBD) towards peripheral areas with less connectivity.

## 2. Segment Analysis - Pprox Weight

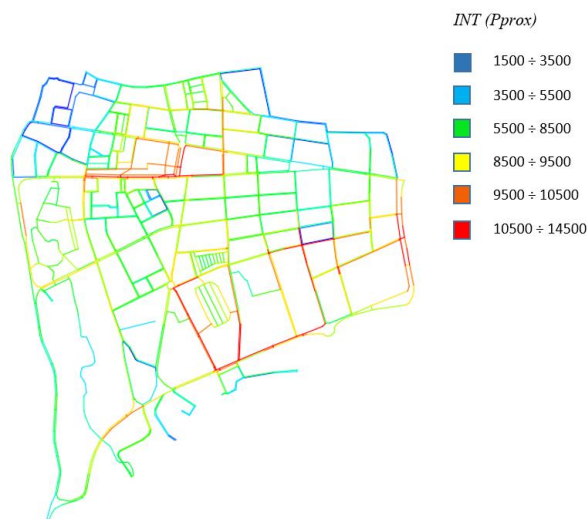


Figure 3.39 Thematic representation of the results of the weighted analysis with Pprox, with a legend of the Integration values based on the colors.

Unlike the previous analysis, the combined effect of the geographical distribution of the population and the pedestrian willing to move comes into play in the weighted analysis with Pprox. The central area continues to have high Integration values (10,000 - 12,000), due to the connectivity of the sections, however, lower values compared to

the redder areas located to the south (near the railway station) and the eastern limit of the study area. In fact, in these areas, there is a greater resident population, which necessarily defines a greater amount of daily movements.

### 3.2.4 Comparison between real and forecast data

The different thematic representations of the road networks (axial\_map\_cassino), analyzed in the GIS environment, allowed to carry out simulations with the Space Syntax forecasting model, thus obtaining data that were compared with the real ones, deriving from the surveys. Therefore, two tables linked to the survey scenarios, weekdays and pre-holidays, were created.

In order to understand how many major campaigns had to be carried out to make the model stable, different approaches were hypothesized considering the two major campaigns. The hypothesized criteria can be summarized as follows:

- approach1: the pedestrians detected in the single days of the different campaigns are entered (for example 3 days of survey return 3 points per section) to be compared with the forecast data returned by the Space Syntax;
- approach 2: enter the mediated pedestrians per survey campaign (for example, there are 2 survey campaigns corresponding to 2 points per section) to be compared with the forecast data returned by the Space Syntax;
- approach 3: the average of all pedestrians detected in the various campaigns is entered (for example, there is 1 point per stretch) to be compared with the forecast data returned by the Space Syntax.

This must be repeated separately for both weekdays and pre-holidays.

		Approach 1			Approach 2			Approach 3		
		Multiplicative	Exponent	R <sup>2</sup>	Multiplicative	Exponent	R <sup>2</sup>	Multiplicative	Exponent	R <sup>2</sup>
Weekday	Not weighed	26,284	1,0148	0,2733	26,673	0,9291	0,2643	28,033	0,9787	<b>0,3204</b>
	P(prox)	21,573	0,9696	0,2562	22,743	0,915	0,2632	23,602	0,9585	<b>0,3155</b>
	Not weighed - purified	39,305	0,546	0,6232	40,109	0,5268	0,6628	45,102	0,585	<b>0,7701</b>
	P(prox)- purified	44,398	0,5378	0,617	45,643	0,5228	0,662	49,688	0,5606	<b>0,752</b>

		Approach 1			Approach 2			Approach 3		
		Multiplicative	Exponent	R <sup>2</sup>	Multiplicative	Exponent	R <sup>2</sup>	Multiplicative	Exponent	R <sup>2</sup>
Pre-holiday	Not weighed	34,61	1,1286	0,2907	34,367	1,0431	0,2735	35,398	1,0895	<b>0,3157</b>
	P(prox)	23,071	0,8883	0,1815	23,929	0,8293	0,1751	23,69	0,8445	<b>0,1912</b>
	Not weighed - purified	106,02	0,8763	0,8945	106,1	0,8597	0,8903	102,39	0,8374	<b>0,9564</b>
	P(prox)- purified	51,195	0,615	0,5752	51,41	0,5992	0,5646	50,787	0,5855	<b>0,6104</b>

It was therefore observed that the third scenario allows having a stable model both in the weekday and pre-holiday scenario; this confirms the hypothesis that the model stabilizes with more days of observation.

The data were represented with a dispersion model, reporting on the abscissa the data from the simulations and on the ordinates those of the surveys. The data relating

to the number of pedestrians have been reported on the ordinates and the unweighted and weighted integration values (r400m and Prox) on the abscissas, scaled with the relative maximum value to obtain good readability on a graphical level.

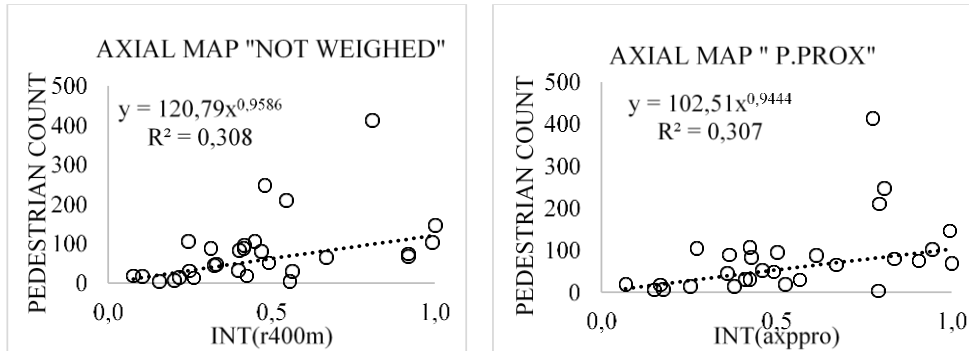


Figure 3.40 Resulting graphs of the survey on the working day

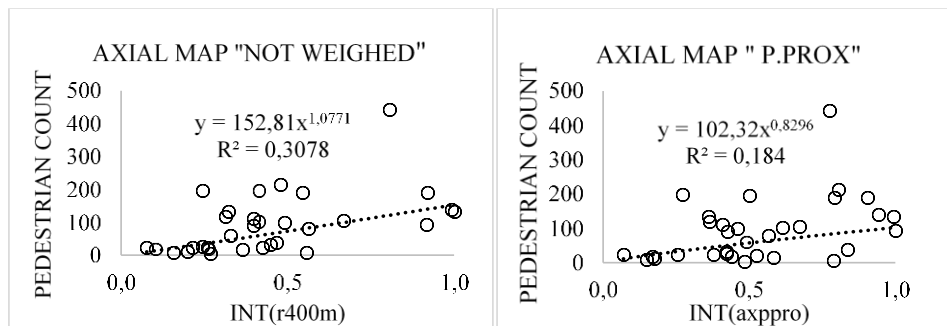


Figure 3.41 Graphs resulting from the survey on the day before holidays

From the graphs, it is possible to draw a trend line to obtain the coefficient of determination ( $R^2$ ). The  $R^2$  allows to understand how reliable the regression is in defining the variability of the data. Technically, this factor allows to determine the fit validity of the regression model as a function of the data.

Comparing the graphs it is observed that using the proximity weight compared to the “unweighted” model there is less dispersion of the data.

### 3.2.5 Data purification

In the unweighted scenarios, points that deviated from the regression line were identified and analyzed to understand the reason for these anomalies. It was found that these were linked to a high number of pedestrians in some areas of the network characterized by the presence of bus stops, a high concentration of commercial establishments or the presence of schools/universities.

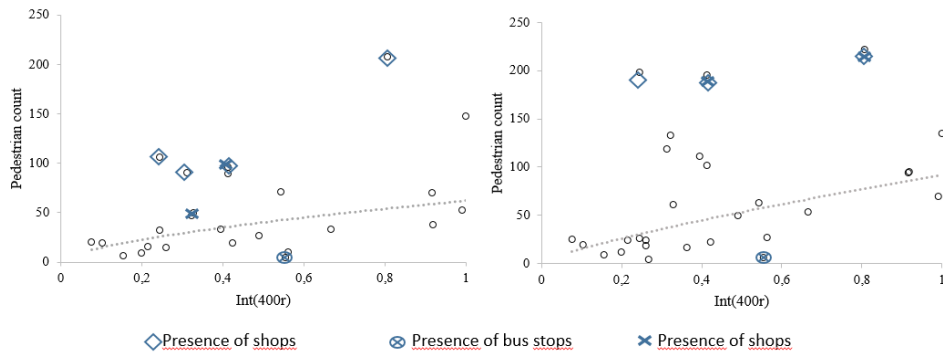


Figure 3.42 Graph resulting from the survey on the day before holidays (a) and weekdays (b) not weighted with the singular points to be purified.

The points related to the presence of educational institutions and bus stops were therefore excluded, obtaining worse  $R^2$  values than the previous model.

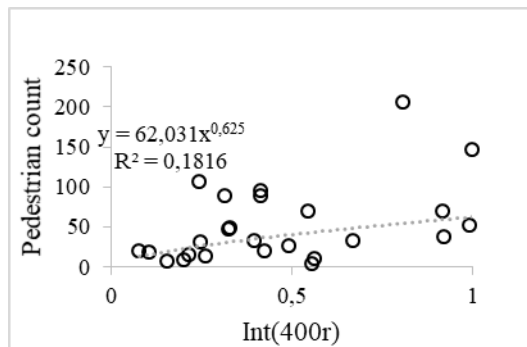


Figure 3.43 Graph resulting from the survey on the non-weighted working day without any singular points

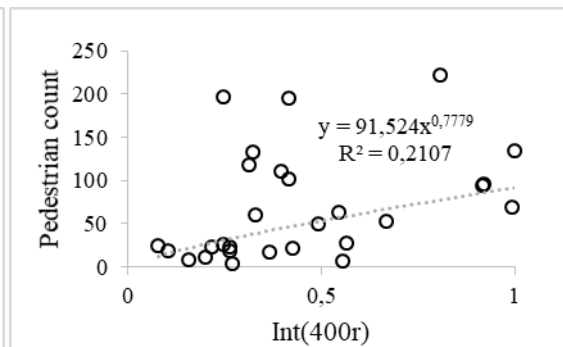


Figure 3.44 Graph resulting from the survey on the day before a holiday, unweighted without any singular points

### 3.2.6 Corrective weights

The idea of removing singular points has proved unsuccessful as the determination coefficients have worsened and the statistical number has been reduced. Therefore it was decided to identify all the attractors of the area through virtual surveys carried out with Google Maps. Considering that the transport user travels to these services on foot only if he is not forced to travel too much, the hybrid approach has been "corrected" by incorporating further K-factors, as described in the following paragraphs.



Then it is considered that the user uses these services on foot only if he is not forced to move too much, therefore starting from the proximity approach he was "corrected" by adding a  $K_{shop}$  multiplication factor.

This weight is evaluated considering not only the density of shops on each section of the network (expressed as the ratio between the number of shops present on the single section and the maximum number of shops evaluated on the entire network, in order to consider the attractiveness of the specific road section) but also the  $L_{average\ shops}$  exhibition length (expressed in terms of percentage of shops on the street front).

In the absence of commercial establishments along the route, the gravitational criterion has been proposed according to which the user tends to reach adjacent road sections where various services are provided. The gravitational weight  $P(\text{prox\_shop})$  is estimated considering the influence of the surrounding area. According to the proposed approach, the number of shops falling within the circular crowns of 300 m and one kilometer is evaluated, these are multiplied by their attractiveness (i.e. by the respective impedance coefficient (Kuzmyak, Walters, Bradley & Kockelman, 2014)) and normalized for the total number of shops in the area.

$$K_{shop} = \begin{cases} P(\text{prox\_shop}) * \frac{L_{average\ shops}}{L_{total\ treats}} & \text{if } n^{\circ}\text{ shops} = 0 \\ P(\text{prox\_shop}) * \frac{L_{average\ shops}}{L_{total\ treats}} * \frac{n^{\circ}\text{shops}}{n^{\circ}\text{maximum number of stores on the network}} & \text{if } n^{\circ}\text{ shops} \neq 0 \end{cases} \quad 3.3$$

Where  $P(\text{prox\_shop})$  is evaluated as:

$$P(\text{prox\_shop}) = \begin{cases} \frac{1 * n^{\circ}\text{shops}_{0-300\text{ m}} + 0.3 * n^{\circ}\text{shops}_{300-1000\text{ m}}}{n^{\circ}\text{total shops}_{0-1000\text{ m}}} & \text{if } n^{\circ}\text{ shops} = 0 \\ 1 & \text{if } n^{\circ}\text{ shops} \neq 0 \end{cases} \quad 3.4$$

Where  $n^{\circ}\text{shop}_{0-300\text{ m}}$  represents the number of shops falling within the radius of 300 m and  $n^{\circ}\text{shop}_{300-1000\text{ m}}$  is the number of shops falling in the buffer between 1000 m and the radius of 300 m.

The new  $K_{shop}$  factor can be incorporated into the weight evaluation following the configurational analysis in order to evaluate a correlation with pedestrian activity for each road section examined. With the hybrid approach, significantly better correlations are obtained with respect to the starting values. A Pearson correlation coefficient (P) of approximately 0.94 was also derived (see Figure 3.47). This shows that pedestrian flows are influenced not only by the configuration of the network but also by the

presence of particular attractors. Therefore the quantitative variables used are well correlated and the model is statistically significant.

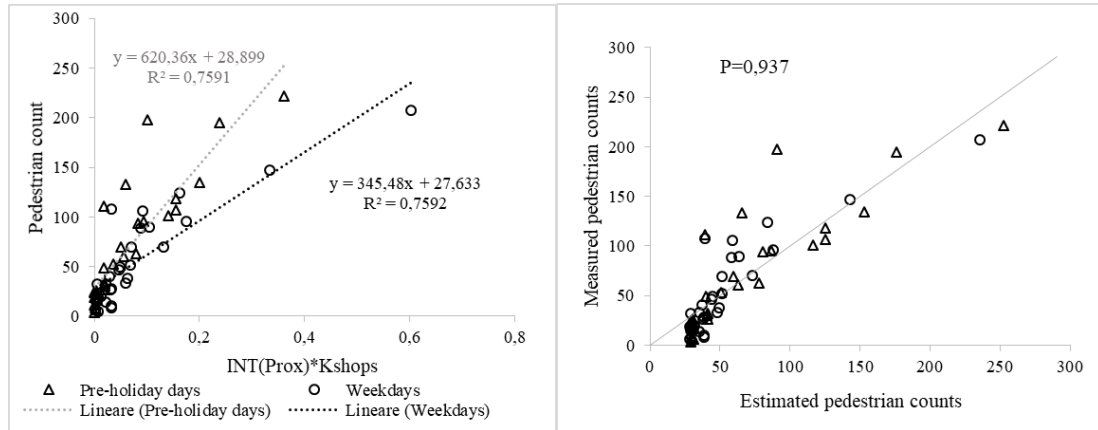


Figure 3.47 Results with weighted hybrid analysis

The corresponding regression statistics of the model obtained are also conveniently reported.

	Pre-holiday days $Y = ax + b$	Weekdays $Y = ax + b$
N <sup>o</sup> observations	32	29
Sum of residuals	-8,05407296411431E-10	-6,51939657814182E-09
Average residual	-2,51689780128572E-11	-2,24806778556615E-10
Residual sum of squares (Absolute)	27216,1823810779	15919,5603658666
Residual sum of squares (Relative)	27216,1823810779	15919,5603658666
Standard Error of the Estimate	30,119861875003	24,2819551701248
Coeff. of Multiple Determination (R <sup>2</sup> )	0,7590762769	0,7592199078
Proportion of Variance Explained	75,90762769%	75,92199078%
Adjusted coeff. of Multiple Determination (Ra <sup>2</sup> )	0,7510454862	0,7503021266
Durbin-Watson statistic	1,41447158255192	1,8936011290373

Variable	a) Regression Variable Results				b) Regression Variable Results			
	Value	St. Er.	t-ratio	Prob(t)	Value	St. Er.	t-ratio	Prob(t)
a	620,3528	63,8080	9,7221	0,00000	345,4754	37,4422	9,2268	0,00000
b	28,8985	6,5563	4,4077	0,00012	27,6331	5,4085	5,1091	0,00002

A statistical linear regression model was used to describe the correlation between the pedestrian count measured per single pass and the independent variable, INT(Prox) \* K<sub>shop</sub>.

It is worth noting that regression models other than linear did not show similar significant agreement (correlation) with the measured data. In fact, despite its naive nature, the linear model seems to highlight some important results for the two scenarios examined (weekdays and pre-holidays):

- the constant term is similar for both weekdays and days before holidays, thus providing evidence that there is a “basic level” of pedestrian activity that is independent of the specific day of the week;
- the slope of the model is apparently different; in fact, it is much higher for the days before holidays, proving a greater propensity of citizens to move on foot on the days before holidays (perhaps also due to the presence of different local market areas that are able to attract more customers even from neighboring municipalities).

### Corrective bus stops

To take into account the presence of bus stops scattered throughout the area, which generate aggregations of users at certain times of the day, an additional  $K_{bus}$  corrective factor was used. The latter has been multiplied by the correct hybrid approach:

$$INT (Prox) * K_{shop} * K_{bus} \quad 3.5$$

For the evaluation of the  $K_{bus}$  weight the procedure is similar to that for the  $K_{shop}$ . Urban and extra-urban transport stops were then identified on the network.

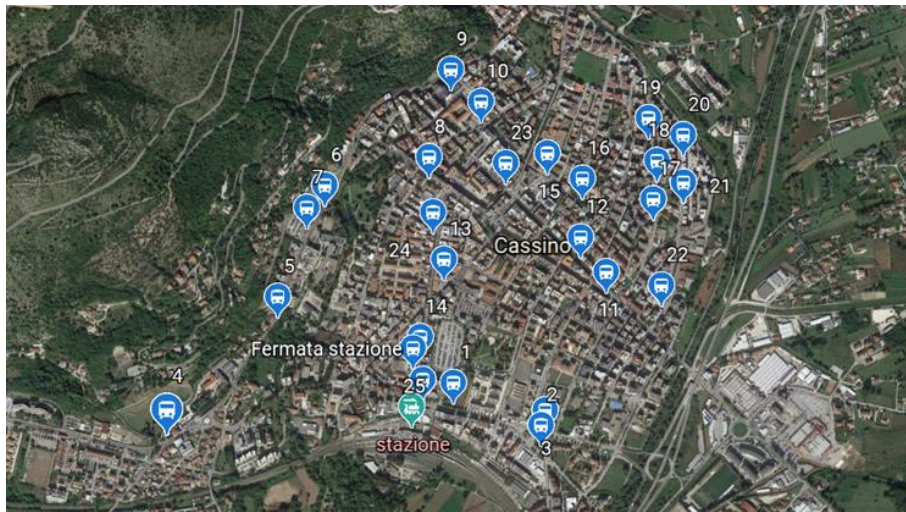


Figure 3.48 Urban and rural transport stops in Cassino

Then through the timetables on the sites (Cassino informa, 2019) (Cotral Spa, 2019) the number of buses crossing the analysis area in the different time slots were counted.

Also, in this case the gravitational criterion is applied according to which the user tends to move towards the bus stop next to him. The proximity weight  $P(\text{prox\_bus})$  takes into account the proximity to other sections where there are stops, so it can be estimated considering the impedance function (Kuzmyak, Walters, Bradley, &

Kockelman, 2014) and the bus stops present in the circular crowns between 0 and 1000 m. Summarizing, the  $K_{bus}$  is evaluated as:

$$K_{bus} = \begin{cases} P(\text{prox\_bus}) & \text{if } n^\circ \text{ bus stops} = 0 \\ P(\text{prox\_shop}) * \frac{n^\circ \text{urban buses} + n^\circ \text{extraurban buses}}{n^\circ \text{total bus on the network}} & \text{if } n^\circ \text{ bus stops} \neq 0 \end{cases} \quad 3.6$$

where  $P(\text{prox\_bus})$  is estimated as

$$P(\text{prox\_bus}) = \begin{cases} \frac{1 * n^\circ \text{bus stops } 0-300 \text{ m} + 0.3 * n^\circ \text{bus stops } 300-1000 \text{ m}}{n^\circ \text{bus stop } 0-1000 \text{ m}} & \text{if } n^\circ \text{ bus stops} = 0 \\ 1 & \text{if } n^\circ \text{ bus stops} \neq 0 \end{cases} \quad 3.7$$

Where  $n^\circ_{\text{bus stops } 0-300 \text{ m}}$  represents the number of stops falling within the radius of 300 m and  $n^\circ_{\text{stops } 300-1000 \text{ m}}$  is the number of shops falling in the buffer between 1000 m and the radius of 300 m.

With the new hybrid approach, by incorporating the  $K_{bus}$ , clearly, better correlations are obtained with respect to the starting values. Even if the correlation worsens compared to the use of  $K_{shops}$  alone; this may be due to the fact that the whole day was considered and not the time slots (therefore the reduction of bus trips on days before holidays or the non-homogeneous number of buses circulating on the network are not considered). A Pearson correlation coefficient (P) of 0.95 was also derived (see Figure 3.49). Therefore the quantitative variables used are well correlated and the model is statistically significant.

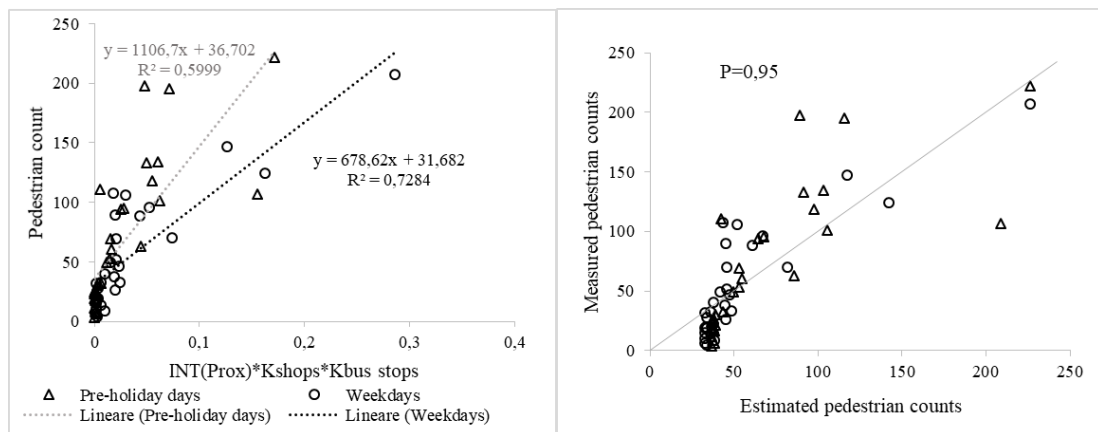


Figure 3.49 Results with weighted hybrid analysis

The corresponding regression statistics of the model obtained are also conveniently reported.

	Pre-holiday days				Weekdays			
Model	$Y = ax + b$				$Y = ax + b$			
N° observations	32				29			
Sum of residuals	4,11520773013763E-09				-2,73967515340701E-09			
Average residual	1,28600241566801E-10				-9,44715570140347E-11			
Residual sum of squares (Absolute)	45199,7628965921				17958,604940225			
Residual sum of squares (Relative)	45199,7628965921				17958,604940225			
Standard Error of the Estimate	38,8157025341515				25,7901825566364			
Coeff. of Multiple Determination ( $R^2$ )	0,599881607				0,7283797759			
Proportion of Variance Explained	59,9881607%				72,83797759%			
Adjusted coeff. of Multiple Determination ( $R_a^2$ )	0,5865443272				0,7183197676			
Durbin-Watson statistic	1,12647248708741				1,35504227151584			

Variable	a) Regression Variable Results				b) Regression Variable Results			
	Value	St. Er.	t-ratio	Prob(t)	Value	St. Er.	t-ratio	Prob(t)
a	1106,6745	165,0139	6,7065	0,00000	678,62360	79,7533	8,5090	0,00000
b	36,7018	8,1417	4,5078	0,00009	31,6824	5,52892	5,7303	0,00000

As also observed in the previous paragraph, the linear model seems to highlight some important results for the two scenarios examined (weekdays and pre-holidays):

- the constant term is similar for both weekdays and days before holidays, thus providing evidence that there is a “basic level” of pedestrian activity that is independent of the specific day of the week;
- the slope of the model is apparently different; in fact, it is much higher for the days before holidays, proof of a greater propensity of citizens to move on foot on the days before holidays (perhaps also due to the presence of different areas of the local market that are able to attract more customers even from neighboring municipalities and a reduction of extra-urban bus rides compared to weekdays).

### Corrective schools

Other singular points that attract many users are the schools. Therefore it was necessary to identify the schools of different types and levels (childhood, primary, secondary, university) and then report them geo-referenced on the network.

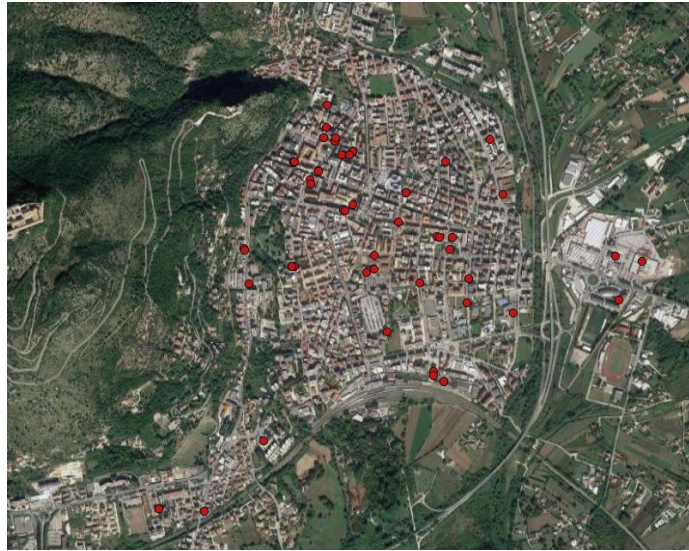


Figure 3.50 Schools present in the study area

Then through the ministerial sites (Ministero dell'Istruzione, 2020) or the schools themselves have evaluated the pupils enrolled in each school, this has made it possible to estimate the weight.

Also in this case it was considered that the user moves on foot only if the school is not very far from his home. A proximity weight  $P(\text{prox\_school})$  has been created which takes into account the proximity to other routes where there are schools. Then the impedance function was used (Kuzmyak, Walters, Bradley & Kockelman, 2014), considering the schools present in the circular crowns between 0 and 1000 m. Summarizing the weight linked to the presence of schools ( $K_{\text{school}}$ ) is evaluated as:

$$K_{\text{school}} = \begin{cases} P(\text{prox\_bus}) & \text{if } n^{\circ} \text{ schools} = 0 \\ P(\text{prox\_shop}) * \frac{n^{\circ} \text{ pupils enrolled in school}}{n^{\circ} \text{ total pupils enrolled in school on the network}} & \text{if } n^{\circ} \text{ schools} \neq 0 \end{cases} \quad 3.8$$

where  $P(\text{prox\_school})$  is evaluated as:

$$P(\text{prox\_school}) = \begin{cases} \frac{1 * n^{\circ} \text{ schools } 0-300 \text{ m} + 0.3 * n^{\circ} \text{ schools } 300-1000 \text{ m}}{n^{\circ} \text{ schools } 0-1000 \text{ m}} & \text{if } n^{\circ} \text{ schools} = 0 \\ 1 & \text{if } n^{\circ} \text{ schools} \neq 0 \end{cases} \quad 3.9$$

Where  $n^{\circ}_{\text{schools } 0-300 \text{ m}}$  represents the number of schools falling within the radius of 300 m and  $n^{\circ}_{\text{schools } 300-1000 \text{ m}}$  is the number of schools falling within the buffer between 1000 m and the radius of 300 m.

With the new hybrid approach, incorporating the  $K_{\text{schools}}$ , significantly better correlations are obtained with respect to the starting values; even if the correlation worsens compared to the use of  $K_{\text{shops}}$  alone; this may be due to the fact that the whole day has been considered and not the time slots (therefore the closure of schools on the days before holidays is not considered). A Pearson correlation coefficient (P) of approximately 0.96 was also derived (see Figure 3.51). Therefore the quantitative variables used are well correlated and the model is statistically significant.

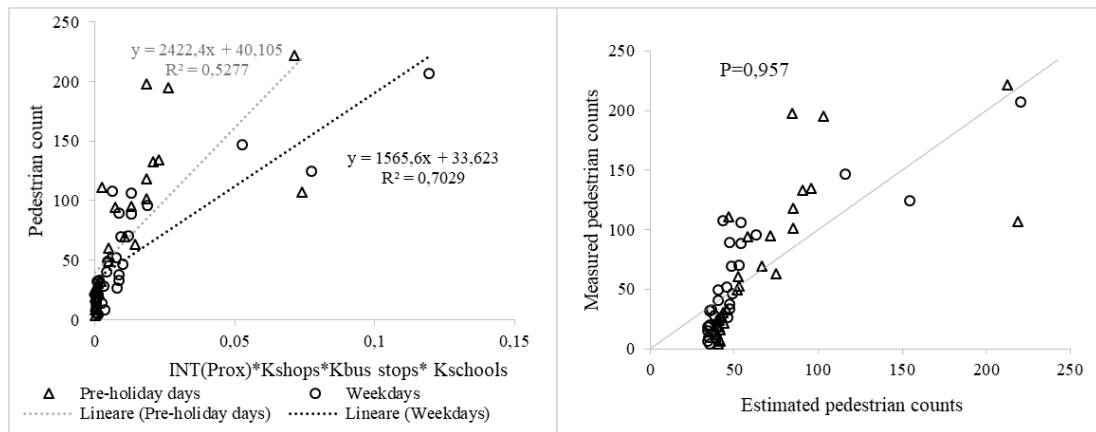


Figure 3.51 Results with weighted hybrid analysis

The corresponding regression statistics of the model obtained are also conveniently reported.

	Pre-holiday days	Weekdays
Model	$Y = ax + b$	$Y = ax + b$
N° observations	32	29
Sum of residuals	5,16440934461571E-09	-3,84617493409678E-09
Average residual	1,61387792019241E-10	-1,32626721865406E-10
Residual sum of squares (Absolute)	53358,9223547691	19646,0194344931
Residual sum of squares (Relative)	53358,9223547691	19646,0194344931
Standard Error of the Estimate	42,17381587145	26,9746241758003
Coeff. of Multiple Determination (R²)	0,5276549057	0,7028579771
Proportion of Variance Explained	52,76549057%	70,28579771%
Adjusted coeff. of Multiple Determination (Ra²)	0,5119100692	0,691852717
Durbin-Watson statistic	1,07169362803892	1,34616182524135

Variable	a) Regression Variable Results				b) Regression Variable Results			
	Value	St. Er.	t-ratio	Prob(t)	Value	St. Er.	t-ratio	Prob(t)
a	2422,3543	418,4386	5,789	0,00000	1565,6326	195,9098	7,9915	0,00000
b	40,1047	8,7025	4,6084	0,00007	33,6225	5,6899	5,9091	0,00000

Comparing the correlations obtained here with the previous ones, an improvement is observed. This highlights that the proximity approach alone, let alone the configurational approach, alone isn't able to represent pedestrian movements in a realistic way analyze data on an hourly basis, not on a daily average.

### 3.2.7 Generalization of the model

Known the functioning of the Space Syntax forecasting system, it was decided to generalize the model. A simulation was performed, with and without the use of weights, dividing the survey area into four quadrants identified by a buffer with a radius of 400 m.

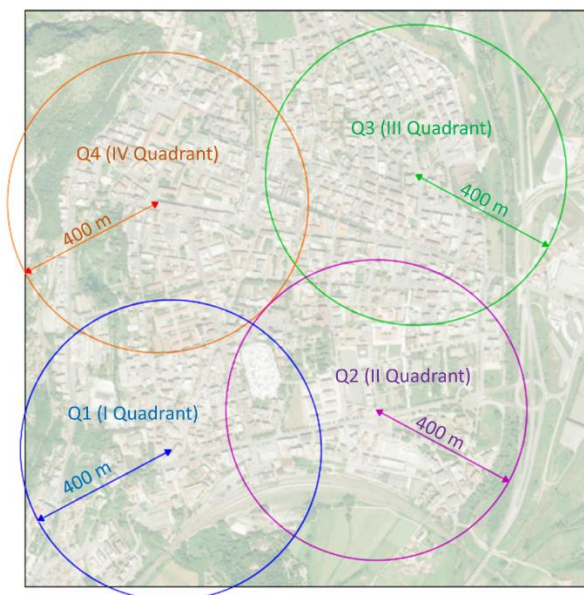


Figure 3.52 Cassino subdivision into four quadrants with buffer 400

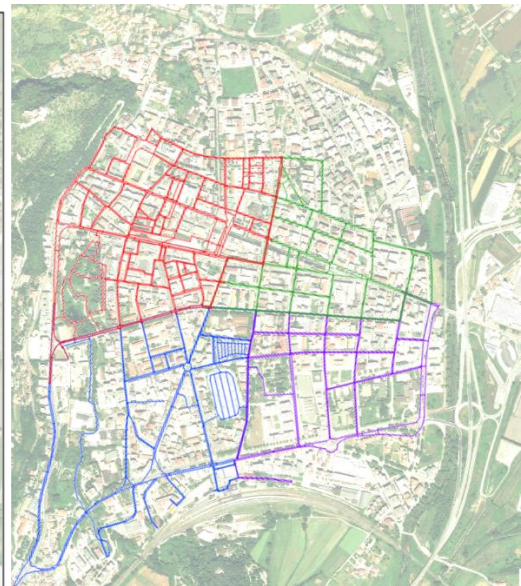


Figure 3.53 Qgis; Axial\_map: divided cassino.

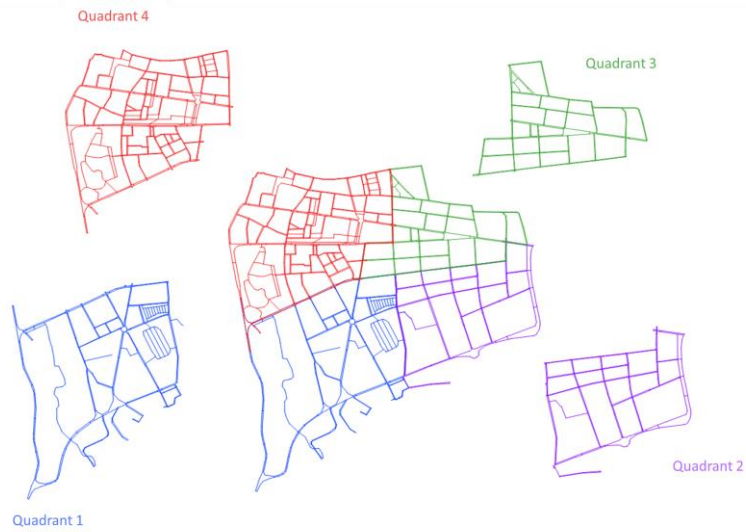


Figure 3.54 Qgis; Axial\_map\_cassino divided into four quadrants

The simulations were then carried out; the result was compared with the number of pedestrians in the sub-areas, extrapolated from the survey of the pre-holiday and weekday scenarios.

Weekdays - not weighed

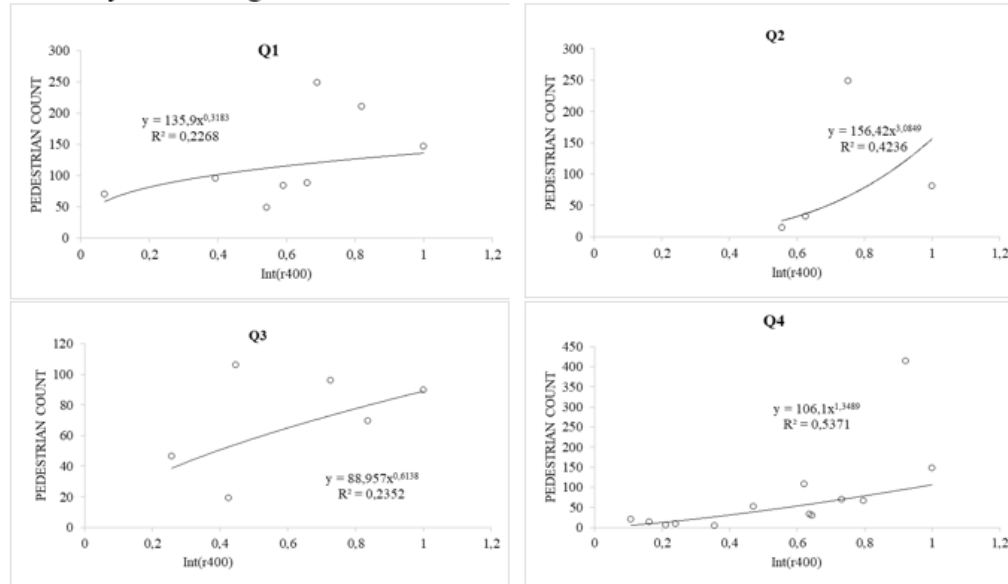


Figure 3.55 Resulting graphs relating to the survey on the weekday, simulation without weights.

Days before holidays - not weighed

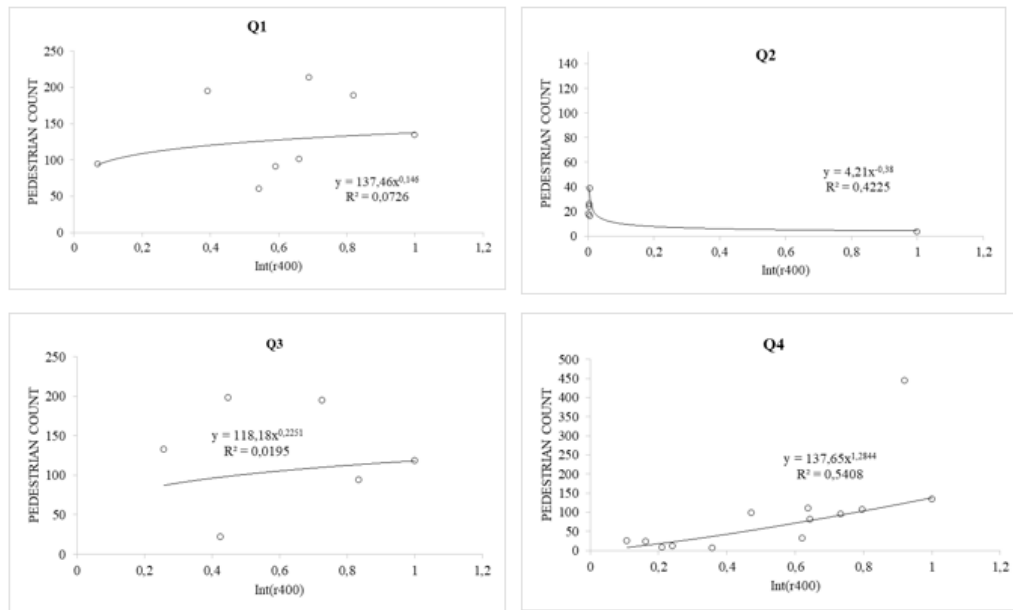


Figure 3.56 Resulting graphs relating to the survey on the day before holidays, simulation without weights.

As previously done, simulations with and without weights were performed with the Space Syntax first considering the quadrants individually (Q1, Q2, Q3, Q4) and then coupling the quadrants two by two (Q1Q2, Q2Q3, Q3Q4, Q1Q4).

By comparing the number of pedestrians with the Space Syntax forecast data using a power regression line, the following parameters were obtained.

ID site	Unweighted analysis						INT(prox)					
	Weekday			Pre-holiday			Weekday			Pre-holiday		
	A	B	R <sup>2</sup>	A	B	R <sup>2</sup>	A	B	R <sup>2</sup>	A	B	R <sup>2</sup>
Q1	135.9	0.3183	0.2268	137.46	0.146	0.0726	114.4	0.0479	0.4324	113.47	0.6857	0.16
Q2	156.42	3.0849	0.4236	4.21	-0.38	0.4225	73.463	1.6557	0.6248	31.298	0.02894	0.1843
Q3	88.957	0.6138	0.2352	118.18	0.2251	0.0195	48.533	-0.317	0.0495	62.632	-0.647	0.127
Q4	106.1	1.3489	0.5371	137.65	1.2844	0.5408	62.81	1.0305	0.3891	82.682	0.9827	0.4493
Study area	120.79	0.9586	0.308	152.81	1.0771	0.3078	102.51	0.9444	0.307	102.32	0.8296	0.184
Q1Q2	390.56	0.9571	0.6909	369.64	1.0771	0.3869	174.63	0.5988	0.3929	132.09	0.5954	0.1382
Q2Q3	131.24	0.7599	0.2707	85.532	0.542	0.0513	70.001	0.3303	0.0706	33.867	0.264	0.0129
Q3Q4	129.42	0.1888	0.07	331.61	0.2798	0.1512	73.21	0.9141	0.2841	112.07	0.9678	0.3326
Q1Q4	401.12	1.1553	0.3762	242.86	0.8324	0.3265	500.69	1.3293	0.4145	151.06	0.7652	0.3756

ID site	INT(prox)* K shop						INT(prox)* K shop*Kbus*Kschool					
	Weekday			Pre-holiday			Weekday			Pre-holiday		
	A	B	R <sup>2</sup>	A	B	R <sup>2</sup>	A	B	R <sup>2</sup>	A	B	R <sup>2</sup>
Q1	329.93	0.6477	0.8597	418.81	0.6739	0.9402	507.41	0.447	0.8747	403.4	0.3571	0.5821
Q2	248.29	0.4761	0.8692	160.46	0.2946	0.7366	313.89	0.3814	0.9323	167.36	0.2476	0.7105
Q3	284.49	0.5302	0.9318	367.7	0.4757	0.8504	1277.8	0.625	0.8367	1618.7	0.6396	0.9229
Q4	249.71	0.6643	0.7337	148.61	0.2852	0.5606	947.13	0.6609	0.8036	239.32	0.728	0.5226
Study area	88.562	0.6211	0.2453	229.78	0.3897	0.6483	94.432	0.7399	0.3373	242.27	0.3816	0.6222
Q1Q2	217.13	0.2881	0.5893	269.22	0.3344	0.7495	286.53	0.2461	0.6025	457.65	0.3249	0.6888
Q2Q3	228.13	0.416	0.8629	311.32	0.414	0.8137	506.45	0.4342	0.8704	570.53	0.4073	0.8079
Q3Q4	176.22	0.4904	0.6936	221.45	0.3332	0.6052	638.66	0.5462	0.8062	175.55	0.2341	0.4917
Q1Q4	1931	0.8735	0.649	196.4	0.2915	0.6236	8107.8	0.8166	0.6677	312.16	0.2767	0.5962

It is observed that the correct hybrid approach with the different weights (taking into account the attractors present in the area) turns out to be the one that best manages to estimate the pedestrian flows.

To generalize the model, it was decided to compare the multiplicative coefficients (A) and the exponents (B) of the regression lines (power-polynomial) with the population, the population density and their product and ratio.

By combining the data of the different scenarios, keeping the weekdays and the pre-holidays separate, regression lines were obtained (power in the population-density comparison with the multiplicative term and linear in the comparison with the exponent) with which the generalization was obtained:

$$N_{Pedestrians}^{\circ} = *A_{Population} (INT)^{B_{Population}}$$

$$N_{Pedestrians}^{\circ} = *A_{density} (INT)^{B_{density}}$$

$$N_{Pedestrians}^{\circ} = *A_{Population/density} (INT)^{B_{Population/density}}$$

$$N_{Pedestrians}^{\circ} = *A_{Population*density} (INT)^{B_{Population*density}}$$

where:

$A_{Population}$  = Multiplicative \* Population<sup>exponent</sup> (similarly applies to density and to the ratio / product of density and population);

$B_{Population}$  = Multiplicative \* Population + Known term (similarly applies to density and to the ratio / product of density and population);

INT = forecast value of pedestrians obtained with the Space Syntax (with and without corrective weights)

	Unweighted analysis						INT(proxy)					
	Weekday			Pre-holiday			Weekday			Pre-holiday		
	Multiplicative	Exponent	R <sup>2</sup>	Multiplicative	Exponent	R <sup>2</sup>	Multiplicative	Exponent	R <sup>2</sup>	Multiplicative	Exponent	R <sup>2</sup>
A-Population		0,1451	0,0191	0,0012	1,3385	0,2678	6,0775	0,3298	0,0581	3,8102	0,357	0,1029
A-Density	0,1395	-1,451	0,2619	738,11	0,3824	0,003	86,597	0,0438	0,0014	0,4623	-10,64	0,1254
A-Density*population	184,71	-0,041	0,002	2,4022	1,048	0,2179	86,597	0,0438	0,0014	44,759	0,1589	0,0271
A-Density/pop	1,2208	0,363	0,1134	1E-06	-1,358	0,0261	0,0206	-0,635	0,2039	0,0655	-0,531	0,2157

	INT(proxy)*K shop						INT(proxy)*K shop*Kbus*Kschool					
	Weekday			Pre-holiday			Weekday			Pre-holiday		
	Multiplicative	Exponent	R <sup>2</sup>	Multiplicative	Exponent	R <sup>2</sup>	Multiplicative	Exponent	R <sup>2</sup>	Multiplicative	Exponent	R <sup>2</sup>
A-Population	10646	-0,428	0,0718	130,5	0,0733	0,0113	88832	-0,581	0,0598	521,18	-0,045	0,0011
A-Density	1,0064	-1,156	0,0718	3390	1,0172	0,2986	21,169	-0,222	0,0012	0,000007	2,5215	0,4652
A-Density*population	1404	-0,442	0,1017	134,93	0,1604	0,0718	3404,1	-0,46	0,0499	153,6	0,2271	0,0365
A-Density/pop	12406	0,2846	0,0301	624	0,0701	0,0098	0,000006	0,581	0,0567	89536	0,4127	0,086

	Unweighted analysis						INTI(prox)					
	Weekday			Pre-holiday			Weekday			Pre-holiday		
	Multiplicative	Known term	R <sup>2</sup>	Multiplicative	Known term	R <sup>2</sup>	Multiplicative	Known term	R <sup>2</sup>	Multiplicative	Exponente	R <sup>2</sup>
B-Population	-0,00008	1,5207	0,0972	0,00007	0,1468	0,1816	0,00002	0,6364	0,0064	0,00005	0,1928	0,1009
B-Density	-191,34	2,5656	0,1384	-99,838	1,3583	0,092	-249,72	2,7133	0,4382	-231,71	2,341	0,5199
B-Density*population	-0,0123	1,618	0,1536	0,006	0,2838	0,0896	-0,0024	0,8393	0,0111	0,0021	0,3964	0,012
B-Density/popu	411465	0,3497	0,1353	-432311	1,2932	0,3645	-190633	1,0471	0,054	-444158	1,2452	0,4038

	INTI(ox)*K shop						INTI(ox)*K shop*Kbus*Kschool					
	Weekday			Pre-holiday			Weekday			Pre-holiday		
	Multiplicative	Known term	R <sup>2</sup>	Multiplicative	Known term	R <sup>2</sup>	Multiplicative	Known term	R <sup>2</sup>	Multiplicative	Known term	R <sup>2</sup>
B-Population	0,000001	0,5486	0,0005	-0,000005	0,4148	0,0144	0,00002	0,4235	0,1335	-0,00001	0,4766	0,0613
B-Density	-30,447	0,7987	0,0893	20,588	0,2242	0,0747	5,4526	0,5008	0,0024	29,851	1,621	0,0819
B-Density*population	-0,00005	0,5799	0,0065	-0,00002	0,3952	0,0011	0,0023	0,4381	0,1125	0,0009	0,4437	0,0219
B-Density/popu	-14200	0,5803	0,0041	43993	0,3139	0,0721	-59641	0,6446	0,0612	91973	0,2447	0,1644

From the calculations, it can be deduced that the coefficients A and B of the function have no direct link either with the population or with the density or their ratio/product. This depends both on the configuration of the network that falls within the quadrant, but also on the number of sections detected; that is, there are quadrants in which pedestrian surveys have been carried out on a greater number of sections unlike other quadrants. Therefore it will be appropriate to carry out further surveys on the network of the study area and apply this model to larger conurbations which will then be divided into neighborhoods.

### 3.3 The variation of non-motorized flows

The model presented so far allows to estimate the pedestrian flow, also called crowding, linked to the instant of detection and to the site. But to reorganize or design an area it is necessary to know the average daily use of structures, such as for vehicular traffic in which the Annual average daily traffic (AADT) is evaluated. Unfortunately, little is known about the variability of non-motorized traffic. The information available is limited because up to now very few public authorities have collected and analyzed continuous data on non-motorized traffic. This means that you have data relating to a single monitoring location with which you can illustrate the variability of the site, but may not be indicative for other locations. Therefore, models should be calibrated that consider, for example, the daily variation of non-motorized traffic based on the location and purpose of the trip. To simplify the problem, the daily pedestrian patterns has been used. From an analysis of the literature it is observed that these are stable and have similarities with the vehicular ones.

For example, by comparing the cycle and pedestrian patterns with the hourly vehicular patterns, peaks are observed in the same time bands even if the non-motorized peaks are less pronounced than the peaks of cars.

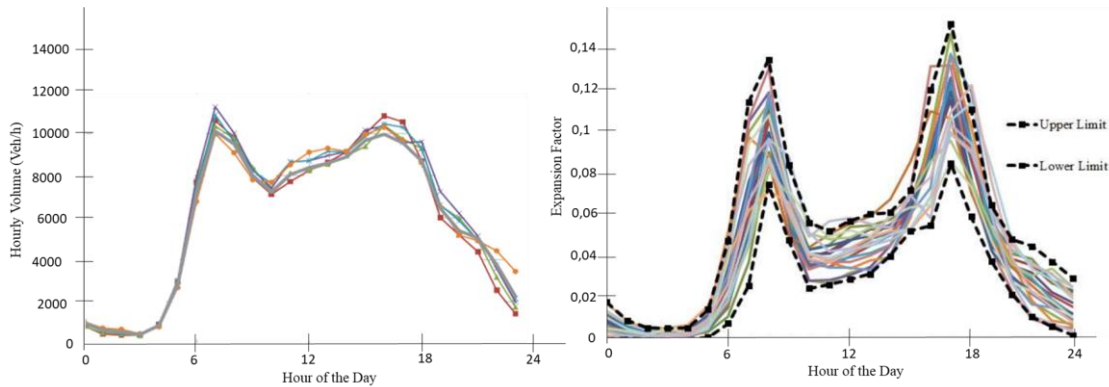


Figure 3.57 Comparative variability of the automobile (left)(taken from Ryuset al.,2014) and bicycle

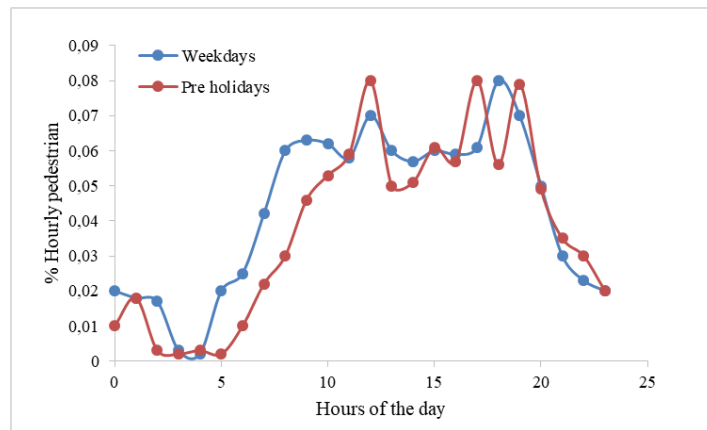


Figure 3.58 Pedestrian daily pattern(Lu, T. 2016)

In order to enter the patterns, however, it is necessary to know the flows. Assuming that the observer is stationary and observes the pedestrians proceeding at a speed equal to that of the vehicle with which the survey is carried out. In the travel time ( $t_p$ ) of the road section, a certain number of pedestrians are observed which follows a negative exponential distancing law. So it can be said that the range is the inverse of the average time spacing.

$$q_{ped} = \frac{1}{t_{average}}$$

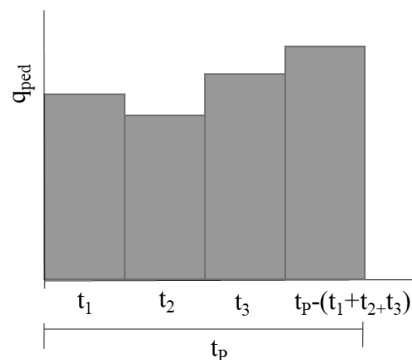
$$q_{ped} = \frac{1}{\frac{t_1+t_2+t_3+t_p-(t_1+t_2+t_3)}{4}}$$

where

$q_{ped}$  is the pedestrian flow along the road axis;

$t_i$  are the instants that make up the travel time;

4 represents the average spacing values



Leaving the section immediately after the final instant, there may be a last pedestrian that you cannot see. To capture this too, the average of the distances is considered (pedestrian count + 1).

Generalizing is obtained

$$q_{ped} = \frac{\text{pedestrian count} + 1}{t_p} \tag{3.10}$$

it is known that

$$t_p = \frac{\text{Length}_{\text{section } i}}{V_{\text{vehicle}}} \tag{3.11}$$

The pedestrian flow can be written as the product of pedestrian density and speed

$$q_{ped} = \rho_{ped} * V_{\text{vehicle}} \tag{3.12}$$

from which

$$\rho_{ped} = \frac{q_{ped}}{V_{\text{vehicle}}} \tag{3.13}$$

Note the flow rate or density for a defined time slot, you can enter a typical pattern and scale it using a single factor, the crowding ratio of the crossing, in order to obtain the pedestrian variation data for other time slots as well.

The crowding ratio allows to estimate the percentage of people crossing starting from the pedestrian flow along the road axis. By means of this factor it is, therefore, possible to identify the points in which, considering the concatenation with the site variables rather than with the vehicular flows, there is a greater vulnerability of vulnerable users.

To obtain the crossing crowding ratio, the crowding data with the pedestrians who crossed the road during the surveys were then compared, the following correlation was obtained:

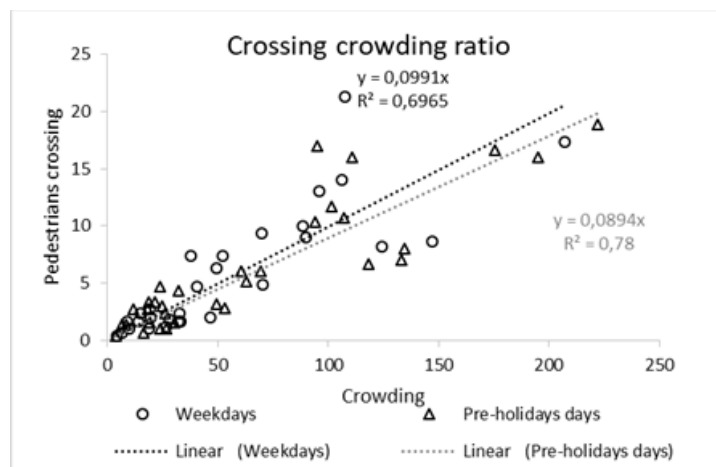


Figure 3.59 Crossing crowding ratio

Observing the correlations, it is highlighted that the coefficients of the model are similar in the two scenarios, this suggests that the propensity to cross is constant throughout the week.

Not knowing how the pedestrian flow is distributed on the pedestrian crossings, it is possible to calculate a crossing flow rate on the section on an hourly basis.

Note the length of the road section ( $S_g$ ), the average distance between the different crossings ( $k$ ) and the width of the crossing ( $L_i = 4.5\text{m}$ ), the exposure length for each crossing ( $L_{exp}$ ) can be evaluated. It is assumed that 50% of people use the stripes to cross and the remainder crosses out of these ( $g = 2$ ).

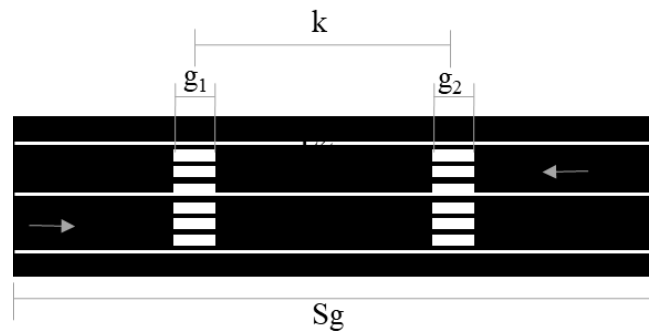


Figure 3.60 Representative quantities of the pedestrian crossing

$$L_{exp} = n^{\circ} \text{ pedestrian crossings on the section} * L_i * g \quad 3.14$$

$$L_{exp} = \frac{\text{Section length}}{k} + 1) * 4.5 * 2)$$

Therefore, it is possible to evaluate the crossing exposure time ( $T_{exp}$ ) by knowing the average speed of the car ( $V_{veh}$ ) with which the survey is carried out.

$$T_{exp} = \frac{L_{exp}}{V_{veh}} \quad 3.15$$

This allows evaluating the pedestrian crossing flow with which the pedestrian exposure is evaluated.

$$Q_{ped\_crossing} = \frac{(n^{\circ} \text{ of pedestrians crossing}/k) * 3600}{n^{\circ} \text{ pedestrian crossings on the section}} \quad 3.16$$

This will be one of the factors that will make it possible to evaluate a risk-based site prioritization index (see Paragraph 5.1).

### 3.4 Estimated cycle/pedestrian flow: demand driven model

Since the middle of the last century, researchers have been trying to solve the problems associated with vehicular outflow. Since the development of the motorized

transport system has highlighted the problem of maintaining and improving driving safety conditions, it is also necessary to start thinking about the safety of the "new" ways of getting around, namely walking or pedaling.

To properly manage and design the transport system it is necessary to estimate the demand for mobility; the latter represents the number of people who move in a certain period of time to take advantage of goods and services differently located in the territory.

The demand for mobility depends on numerous factors such as:

- the localization on the territory of the activities that the user uses on a daily basis;
- the offer of the transport system (the infrastructure is planned, sized and managed to satisfy the request for activities to be carried out and for trips to be made);
- the organization of the residences, depending on the level of accessibility that is adequate for the system of localized activities and the transport system offered.

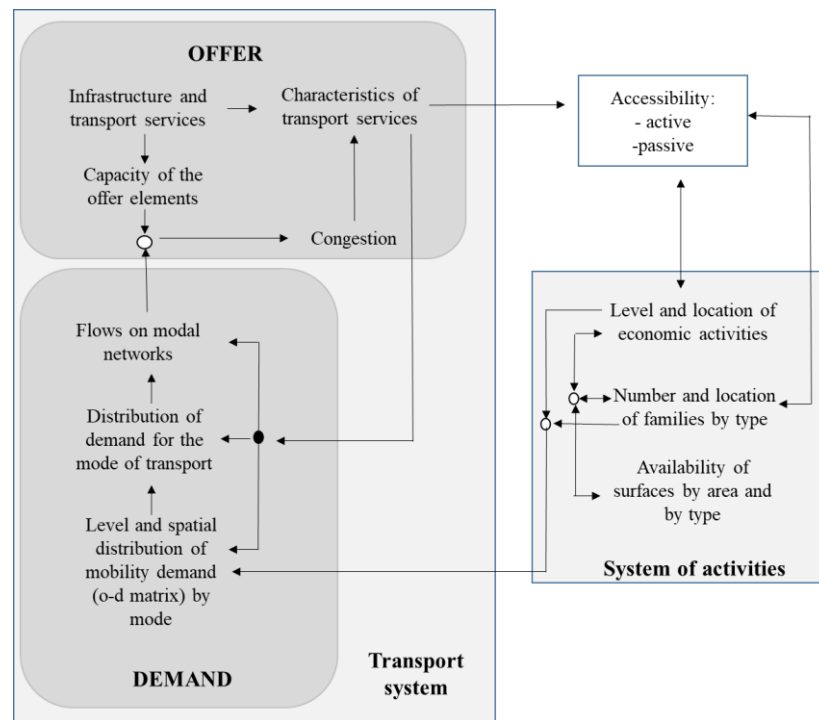


Figure 3.61 Operation of the transport system

Performing a mobility study means:

1. Identify the study area in which the effects produced by the changes made on mobility are exhausted;

2. Divide the study area into a finite number of zones (zoning). A centroid is associated with each zone; in the latter it is assumed that all the points of origin/destination of the movements are fictitiously concentrated.
3. Define an offering model of the transport system with which the infrastructure on which the transport services take place (road axes, railways, stations, etc.) is graphically represented by associating each element with precise quantitative characteristics (e.g. travel time, waiting time, costs, etc.)
4. Estimate (through surveys or models) the transport demand affecting the study area; this means building an OD matrix that represents the movements that affect the study area, in a certain period of time (hour, time slot, day, year), mode (foot, car, bus, etc.) and reason for the movement (home-work, home-acquired, etc.)
5. Simulate the demand/offer interaction (calculation of traffic flows on the different components of the system).

In this section, the estimate of demand will be analyzed, bearing in mind its variability over time (an element of greatest difficulty in estimating and forecasting analyzes). The question can be evaluated both with direct surveys and with mathematical models.

Direct surveys are interviews or counts that are carried out on a population sample, with the aim of verifying the current functioning of the Transport System and then calibrating or improving the mathematical models. The latter allows to estimate current and future demand according to the socio-economic and territorial characteristics of the study area and the transport system operating in it. Their use is justified by the difficulty of predicting the impacts resulting from the implementation of interventions on the system components or to carry out in situ experiments (for costs and organizational problems), as well as the complexity of the mobility phenomena.

In literature, for the motorized flows in order to estimate the demand either gravitational models or four-stage models (behavioral - descriptive) are used; the latter have also been adapted in studies to estimate the demand for non-motorized travel.

As is known, the four-stage model consists of the product of four sub-models, namely:

- generation or emission: simulates the choice of whether or not to move, from the origin zone O, for the reason s in the reference time period h,  $d_0(s, h)$ ;

- distribution: simulates the choice to go to destination  $d$ , having origin in  $O$  and the reason for the displacement  $s$  in the period  $h$ ,  $p$  ( $d/osh$ );
- modal choice: simulates the choice of the means to use to move from  $O$  to  $d$  for reason  $s$  in the time period  $h$ ,  $p$  ( $m/odsh$ );
- path choice: simulates the choice of the path used to move from  $O$  to  $D$  for reason  $s$  with mode  $m$  in time period  $h$ ,  $p$  ( $k/modsh$ ).

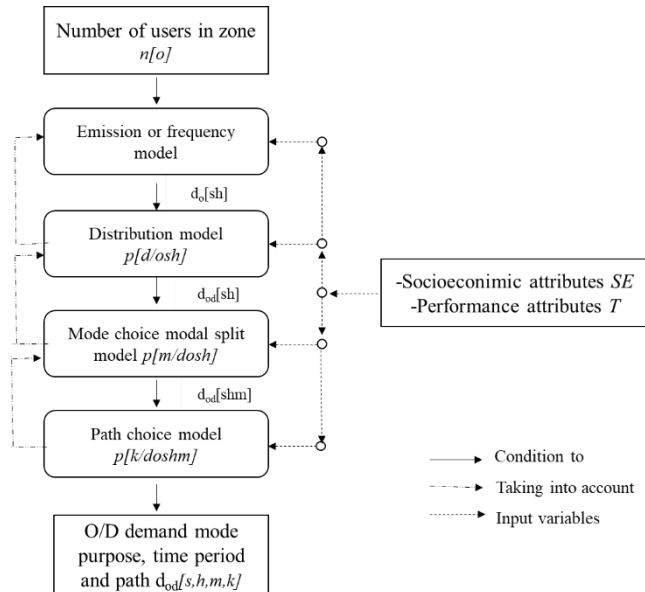


Figure 3.62 Four-stage model

### 3.4.1 Model of generation or emission

As already mentioned, the emission model allows to calculate the average number of trips issued from the area of origin  $O$  for the reason  $s$ , in a defined time reference period.

$$D^i(Osh) = n^i(O) * p^i(Osh) \quad 3.17$$

where is it:

$D_i(osh)$ : Number of users of category  $i$  who move in time interval  $h$ , for reason  $s$ , from zone  $O$ .

$n_i(O)$ : Number of members of category  $i$  who are in  $O$ .

$p_i(Osh)$ : percentage of users who move, therefore the average number of movements of users of category  $i$ , in the interval  $h$ , for the reason  $s$ , starting from zone  $O$ .

Therefore it is necessary to identify the reasons for the displacement, which can be of various kinds, such as:

- homebased
- accompaniment
- shopping
- medical visits
- sport
- handling practices
- leisure/free time.

In the case in question, the data of the emission model were extracted from Istat microdata 2011. Thus a commuting home-work/home-school commuting matrix is obtained; these must therefore be compared with those of the commuting matrix appropriately scaled for the reason (feet 17% of total journeys, bicycle 0.57% of total journeys) to verify whether they are comparable or scalable; this would allow the model to be used for other reasons as well.

### **3.4.2 Distribution model**

As already mentioned, this model is used to calculate the percentage of trips that, starting from the area  $o$ , for the reason  $s$ , goes to the destination  $d$ .

The distribution model schematizes the choice of destination for a shift between the possible destinations, allowing to evaluate the future scenarios linked to the urban changes that occur in the territory. Therefore, the destination actually chosen to carry out a certain activity is not a traffic area but one (or more) elementary destination (for example a shop, an office, etc.) contained therein.

Also, in this case, starting from Istat data, the activities present were identified for the various census sections, but since the distribution of users originally was not available, starting from the census on industries, an average distribution value was estimated over the entire study area imagining that this value can be spread uniformly in origin for all census areas.

### **3.4.3 Modal choice model**

The modal choice model allows to calculate the travel rate that chooses the mode  $m$ , going from the area of origin  $o$  to the destination  $d$  for the reason  $s$ . Usually, the term "mode" is used and not "means" of transport as in urban systems the possibility of moving on foot can also be considered.

The most used models are almost exclusively behavioral models; these can be developed with reference to the homogeneous categories of users adopted for the issue and distribution model.

To predict modal choice, it is necessary to understand the factors that predict travel behavior:

- *Time* is the variable that influences the perception of the trip, which influences the choice of the route; in fact the user chooses the mode that allows to minimize times and distances.
- *Capacity*: therefore the presence of adequately designed structures (such as wide sidewalks in commercial or densely residential areas, cycle paths in city center areas, presence of bus shelters, etc.);
- *Type of trip*: depending on the reason for the move, you are pushed to choose a different mode based on the distances in which the services are allocated;
- *Travel costs* that depending on the mode used, for example walking can be very cheap if not free while the use of the car requires maintenance costs, rather than fuel etc.
- *Environmental, health and safety considerations*: the use of motorized vehicles associated with sedentary life has led to the development of numerous diseases therefore the practice of using sustainable means is spreading which, in addition to reducing environmental impacts allows to improve health conditions.
- *The feeling of safety*: the fear of being in danger can be modified according to the presence of exclusive routes for the different ways, which allows users to increase or reduce the perception of safety.

Taking all these parameters into account in a model is not easy. This would require assessments that take into account a much more precise and detailed geographic level and also physical factors to measure network performance. But this data is not adequately processed in most large-scale survey tools (such as metropolitan travel surveys or the national personal transportation survey), so analysts often borrow data from analyzes usually scheduled for others purposes.

Also in the case in question, as detailed data deriving from the surveys were not available, the starting point was the Istat commuting matrix. This presents the data relating to commuting trips (home-based-work/home-based-school), diversified by the different modes of travel, referring to a municipal area, having a certain duration over time (up to 15 minutes, from 16 to 30 min, from 31 to 60 min, over 60). It has been hypothesized that the average behavior in terms of duration and modality, acquired on a municipal basis, can be considered valid at the scale of the single census area.

In reality, this is an approximation, since the choice of transport mode is influenced by:

- the cost of the journey both in terms of duration and ancillary costs (parking cost, subscription cost, etc.);
- family income that affects the possession of a means of transport;
- the offer of transport, therefore the road network, the pedestrian or cycle network, the offer of public transport, etc;

Furthermore, the time used to make the move is influenced by:

- congestion and configuration of the road network;
- territorial and orographic extension of the municipal territory.

Starting from a certain census area to understand how the movement is distributed over the other areas, knowing the centroid-centroid distances between the origin area and all possible destinations, one enters the impedance functions to derive the movements for the different modes of transport.

### **3.4.4 Route assignment or choice model**

The assignment model provides the percentage  $p$  ( $k/mods$ ) of displacements that use path  $k$ , relative to mode  $m$ , to go from  $o$  to  $d$  for the purpose  $s$ .

Once the actual movements on the different  $o-d$  pairs have been evaluated, it is necessary to load them on the road network to check whether the infrastructure is able to offer a satisfactory service to users, guaranteeing safety and full use. The interest of this study was to estimate the relative flows in order to understand which road sections should be redesigned with greater attention and using simplified methods to understand the distribution of these on the network.

#### **The cycle network**

After evaluating the cycle flow, as previously described, a matrix  $od$ . This was then loaded on the QGIS (only as an attribute table) and through the plugins Flow maps (ousins) the lines of desire relating to cycle journeys were represented (in graphic form).

	A	B	C	D
1	NSEZ_ORIG	NSEZ_DEST	spostamenti C	
2	3	297	0	
3	4	7	0,54	
4	5	7	0,54	
5	5	17	0,504	
6	5	297	0,551	
7	5	378	0,504	
8	10	7	0,6	
9	10	71	0,336	
10	10	107	0	
11	10	297	0,49	
12	10	374	0,168	
13	10	473	0,504	
14	12	107	0,65	
15	16	7	0	
16	16	372	0,522	
17	17	17	0	
18	17	357	0	
19	18	27	0,462	
20	18	297	0,54	
21	18	357	0,54	
22	21	7	0,504	
23	21	47	0,462	
24	21	97	0,455	
25	21	297	0,493	

Figure 3.63 Excel table origin-destination

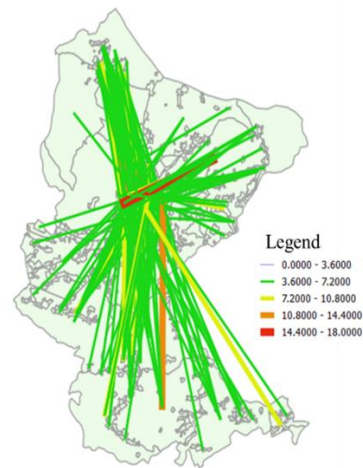


Figure 3.64. Graphic rendering of the lines of desire (taken from QGIS)

Following the construction of the linear layer, representing the road network broken down into sections (each of which is associated with an identification ID), the analysis was started to load the respective flow on each segment. To do this, the geoprocessing tools of the Qgis program have to be used with which a buffer has been built for each line of desire that intersects the road network. The size of the buffer, relative to each flow line, derives from a careful study in which the path obtained from the intersection (between the road and the buffer of the desire lines) was compared with that obtained on google maps.



Figure 3.65 Representation of the 'fixed distance buffer' (taken from QGIS)

The final choice fell on a buffer width ranging from 0 to 45 meters in radius. Using the 'intersection' tool of the Qgis, it was possible to obtain for each road section all the origins-destinations that intersected the section of interest.

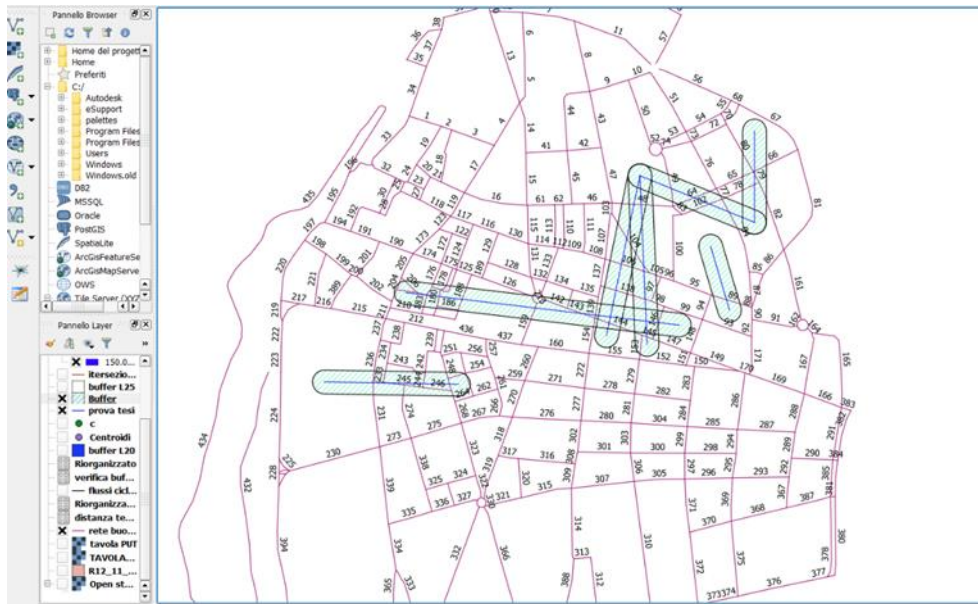


Figure 3.66 Representation of the 'fixed distance buffer'. (taken from QGIS)

Once the geoprocessing tools have been applied, the program returns, in the form of analytical data, the results in tabular form, showing the ids of the roads affected by the flow, the origins, the destinations and the value of the flow itself.

	id	ORIGINE	DEST	FLUX
1	48	302	12	1.30000
2	48	302	36	1.30000
3	49	302	42	1.30000
4	64	302	42	1.30000
5	65	62	42	1.30000
6	66	62	42	1.30000
7	77	302	42	1.30000
8	78	62	42	1.30000

Figure 3.67 Attribute table returned upon application of the 'intersection' geoprocessing tool

By combining the flow data relating to the same identifier, the total flow on the single section was obtained. It can be observed that with a buffer at a radius of 0 m, an underestimation of the flows is obtained, while with a radius of 45 m, flows are overestimated. Therefore, to obtain more realistic flows, the data obtained with buffers 0 and 45 m were averaged.

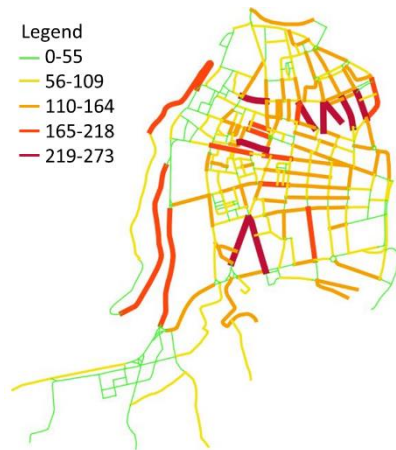


Figure 3.68 Estimated flows with zero buffer

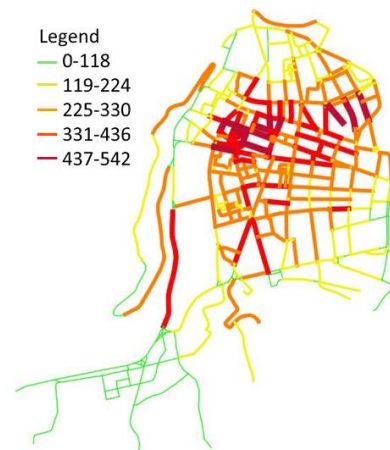


Figure 3.69 Estimated flows with 45 m buffer

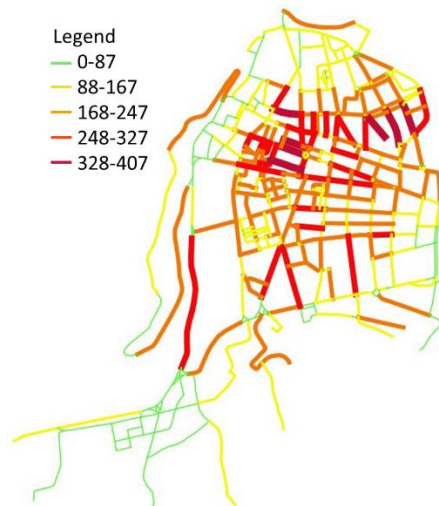


Figure 3.70 Flows estimated as the average of the flows obtained with buffers at 0 and 45 m radii

The data thus obtained show that the areas that are most heavily loaded by cycling flows are those of the central area or characterized by the presence of attractors (schools, shops, bars, etc.). These preliminary data make it possible to assess whether the network currently manages to safely contain these movements or whether improvements should be proposed.

Then the flow file is loaded into QGIS in order to make a comparison with the urban traffic plan (PUT). The PUT is a set of coordinated interventions for improving the conditions of road traffic in the urban area, pedestrians, public transport and private vehicles, which can be carried out in the short term, a two-year period, and in the hypothesis of providing infrastructure and means of transport substantially unchanged. In this perspective, the PUT is aimed at obtaining:

1. the improvement of traffic conditions;

2. the improvement of road safety;
3. the reduction of atmospheric and acoustic pollution;
4. the containment of energy consumption;
5. respect for environmental values.

The New Highway Code (art. 36, Legislative Decree 30/04/1992 n ° 285) (ACI - Automobile club of Italy, sd) provides for the drafting of the Urban Traffic Plan for municipalities that meet one of the following conditions:

- i. population over 30,000 inhabitants;
- ii. seasonal presences exceeding 10,000 units;
- iii. municipalities where there are high requirements for environmental protection.

The objective is therefore to assess whether the urban plan envisaged by the PUT satisfies the demand for cycle transport which has been assessed through the analysis of ISTAT data relating to the 15th census.

By superimposing the flows on the PUT (urban traffic plan) it was observed that the central areas, where most of the flows are concentrated, are used as a cycle-pedestrian area and that the planned tracks seem to cover most of the heavily loaded section. From these estimates of flows, however, it can be observed that the area adjacent to the mother church and the covered market seems to be devoid of a cycle path, therefore, probably the network could be integrated with further sections that would close the city center mesh.

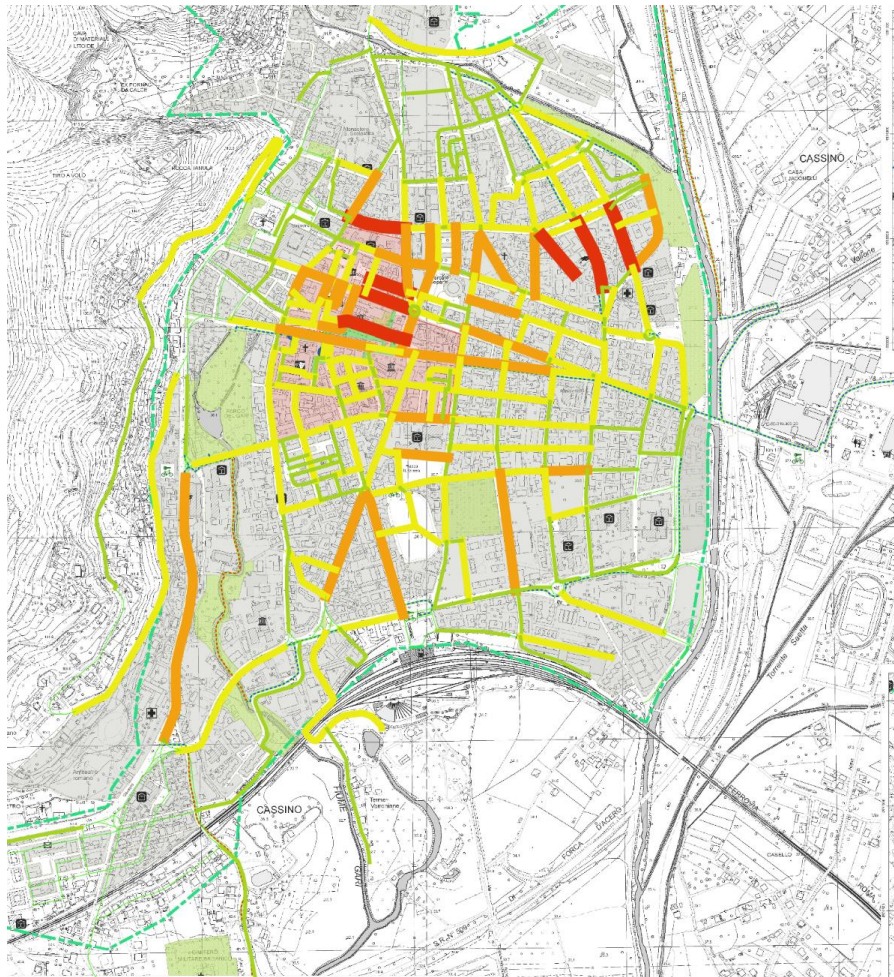


*Figure 3.71 Loaded cycle network representation of flows compared with the geographical reference of the PUT: (taken from QGIS)*

### **The pedestrian network**

A procedure similar to that described for the cycle network was carried out for the pedestrian network; even if it was necessary to observe that the movements carried out on foot are independent from the direction of travel and are reversible (i.e. the movement can be the same if one moves from A to B or from B to A) therefore the network has been discretized in way denser than the cycle path.

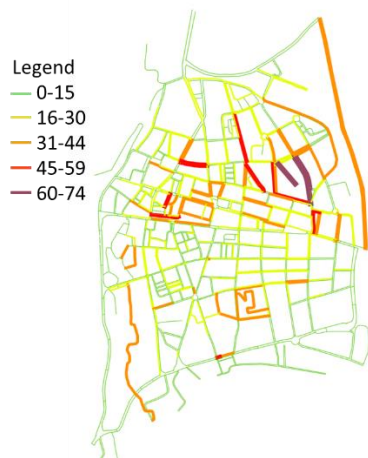


Figure 3.72 Estimated flows with zero buffer

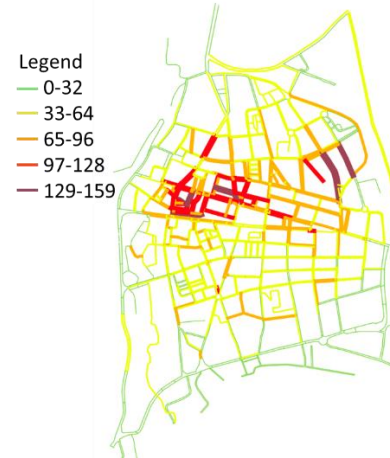


Figure 3.73 Estimated flows with 45 m buffer

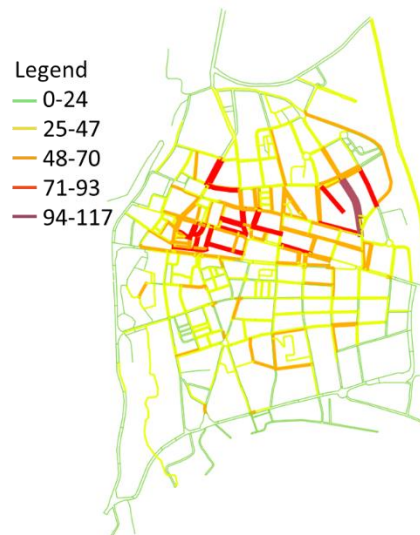


Figure 3.74 Flows estimated as the average of the flows obtained with buffers at 0 and 45 m radii

Observing the graphic outputs, as for the cycle path, it can be observed that the estimated flows with buffer at radius 0 are underestimated, with radius 45 they are overestimated, so the right compromise is the average of the two flows. Also in this case, the greatest flows are concentrated in the central area of the city or in areas where particular attractors are present.

### 3.5 Conclusions

Given the ever-increasing need to design routes dedicated to vulnerable users in the urban environment, two models have been proposed and calibrated:

- for the estimation of the pedestrian flow an original hybrid approach has been calibrated which employs a combined configurational analysis of the

aptitude for use of the land. The results of the simulations were compared with the pedestrian counting conducted in the central area of Cassino.

- for the estimation of cycling and pedestrian flows, a demand-driven model has been calibrated, ie a model similar to the four-stage vehicle.

The idea is to integrate the vehicle traffic component with pedestrian and cycle flows. This requires a reduction in the risk of contrast which requires exposure estimation. To do this, an exposure forecasting methodology was developed that would allow planners to take a more proactive role in risk assessment when real collision data are not available.

Further improvements are planned regarding:

- i. increase the number of pedestrians detected to improve statistical significance;
- ii. experimentally validate the proposed methodological approaches;
- iii. extend the proposed methodologies to different urban contexts.

However, the preliminary results obtained seem quite promising and allow us to state that the developed approaches can provide a qualitative and satisfactory estimate of pedestrian/cycling movements compared to what has been obtained so far in the scientific literature. It is believed that the assessment of pedestrian and cycling movements can constitute valid support for the study of injuries related to vulnerable users of the urban area.

## References

- 1,000 Friends of Oregon. 1993. Making the Land Use Transportation Air Quality Connection. The Pedestrian Environment, Volume 4A.
- Abdelghany, A., Adbelghany, K., Mahmassani, H., & Al-Zharani, A. 2012. Dynamic Simulation Assignment Model for Pedestrian Movements in Crowded Networks. Transportation Research Record 2316, pp. 95–105.
- Abedi, N., Bhaskar, A., & Chung, E. 2013. Bluetooth and Wi-Fi MAC address based crowd data collection and monitoring: benefits, challenges and enhancement.
- ACI- Automobile club d'Italia. Art. 36. Piani urbani del traffico e piani del traffico per la viabilità extraurbana. Tratto da <http://www.aci.it/i-servizi/normative/codice-della-strada/titolo-ii-della-costruzione-e-tutela-delle-strade/art-36-piani-urbani-del-traffico-e-piani-del-traffico-per-la-viabilita-extraurbana.html#:~:text=E%20SEGNALETICA%20STRADALE-,Art.,traffico%20per%20>

- Agens, Anav, Asstra. 2019. 16°Rapporto sulla mobilità degli italiani. Roma.
- Al\_Sayed, K. 2018. Space Syntax Methodology. London, UK: Bartlett School of Architecture, UCL.
- Annesley, T., Dix, M., Beswick, A., & Buchanan, P. 1989. Development and Application of Pedestrian Assignment Models In London Railway Station Studies . Traffic Engineering and Control. Vol. 30, p. pp. 345–352.
- Ashford, N., O'Leary, M., & McGinity, P. 1976. Stochastic Modelling of Passenger and Baggage Flows through an Airport Terminal. Traffic Engineering and Control 17 , pp. 207-10.
- ATECO. 2007. Classificazione delle attività economiche. Tratto da <https://www.istat.it/it/archivio/17888>
- Batty, M. 2001. Agent-based pedestrian modeling. Environment and Planning B: Planning and Design 28 , pp. 321-326.
- Blue, V., & Adler, J. 1999. Using Cellular Automata. Microsimulation to Model Pedestrian Movements. . Proceedings of the 14th International Symposium on Transportation and Traffic Theory. Elsevier Science .
- Blue, V., & Adler, J. 2000. Cellular Automata Microsimulation of Bidirectional Pedestrian Flows. Transportation Research Board 1678, pp.135-141.
- Bongiorno, C., Santucci, D., Kon, F., P., S., & Ratti, C. 2019. Comparing bicycling and pedestrian mobility: Patterns of non-motorized human mobility. Greater Boston Journal of Transport Geography 80 102501.
- Bu, F., Greene-Roesel, R., Diogenes, M., & Ragland, D. 2007. Estimating Pedestrian Accident Exposure: Automated Pedestrian Counting Devices Report. Berkely, CA: Safe Transportation Research and Education Center.
- Burstedde, C., Klauck, K., Schadschneider, A., & Zittartz, J. 2001. Simulation of pedestrian dynamics using a two-dimensional automation. Physica A: Statistical Mechanics and its Applications, 295, pp. 507-525.
- Cascetta, E. 1993. L'ingegneria dei sistemi di trasporto: metodi quantitativi per la pianificazione e la gestione. Sistemi di trasporto, 1.
- Cassino informa. 2019. Tratto da Orari bus urbani: <https://www.cassinoinforma.it/vivi-cassino/orari-bus-urbani/>
- Cervero, R., & Radisch, C. 1995. Travel Choices in Pedestrian versus Automobile Oriented Neighborhoods. Working Paper 644. Berkeley, CA: University of California at Berkeley.
- Clifton, K. J., Singleton, P. A., Muhs, C. D., Schneider, R. J., & Lagerwey, P. 2013. Improving the Representation of the Pedestrian Environment in Travel

- Demand Models, Phase I. Transportation Research and Education Center (TREC), <http://dx.doi.org/10.15760/trec.120>.
- Corazza, M. 1999. IL DISEGNO DELLO SPAZIO URBANO PER L'INDIVIDUAZIONE DELL'ISOLA AMBIENTALE / Spazio collettivo, disegno di strade e controllo del traffico per un nuovo concetto di mobilità . Università degli Studi di Roma "La Sapienza".
- Cotral Spa. 2019. Tratto da [https://moovitapp.com/index/it/mezzi\\_publici-line-COTRAL-Roma\\_e\\_Lazio-61-870562-446071-0](https://moovitapp.com/index/it/mezzi_publici-line-COTRAL-Roma_e_Lazio-61-870562-446071-0)
- Cutini, V. 1999. Spazio urbano e movimento pedonale. Uno studio sull'ipotesi configurazionale. Italia.
- Dai, W., & Yu, X. 2013. A configurational exploration of pedestrian and cyclist movements: using Hangzhou as a case study, China. Proceedings of the Ninth International Space Syntax Symposium.
- di Pinto, V. 2013. Tesi di dottorato: Leggere e comunicare il Paesaggio per un modello interpretativo dello spazio urbano percepito.
- Dobler, G., Vani, J., & Dam, T. 2019. Patterns of urban foot traffic dynamics.
- Federal Highway Administration (FHWA). 2016. Travel Monitoring Guide.
- Federal Highway Administration. 1999. Guidebook on Methods to Estimate Non-Motorized Travel: Overview of Methods. Virginia: United States Department of Transportation, Publication No. FHWA-RD-98-165.
- Federal Highway Administration. 2013. Traffic Monitoring Guide. U.S Department of Transportation.
- Geogek.xyz. 2018. Tratto da How to add Google Maps layer in QGIS 3: <https://geogek.xyz/how-to-add-google-maps-layers-in-qgis-3.html>
- Greene-Roesel, R., Diogenes, M., Ragland, D., & Lindau, A. 2008. Effectiveness of a Commercially Available Automated Pedestrian Counting Device in Urban Environments: Comparison with Manual Counts (Revised). . Tratto da <http://safetrec.berkeley.edu/news/08-0503session240ryanposter.pdf>
- Hamacher, H., & Tjandra, S. 2001. Mathematical modeling of evacuation problems: a state of the art. *Pedestrian and Evacuation Dynamics*, pp. 59–74.
- Helbing, D., Molnár, P., Farkas, I., & Bolay, k. 2001. Self-Organizing Pedestrian Movement. *Environment and Planning B: Planning & Design* 28, pp.361-83.
- HfcQGIS. Tratto da <http://hfcqgis.opendatasicilia.it/it/latest/>
- Hiller, B., Penn, A., Hanson, J., Grajewski, T., & Xu, J. 1993. Natural movement: or configuration and attraction in urban pedestrian movement. *Environment and Planning B:planning and design*, vol 20 pp.29-66.

- Hillier, B. 1996, 2007. *Space is the Machine: A Configurational Theory of Architecture*. Space Syntax. London, UK.
- Hillier, B., & Iida, S. 2005. Network effects and psychological effects: a theory of urban movement. *International Conference on Spatial Information Theory, COSIT 2005*, September 14-18, pp. 475-490. Ellicottville, NY, USA: Springer.
- Hjelkrem, O., & T., G. 2009. *A Comparative Study of Bicycle Detection Methods and Equipment*. Presented at the 16th ITS World Congress and Exhibition on Intelligent Transport Systems and Services. Stockholm, Sweden.
- Hoodgendoorn, S., & Bovy, P. 2004. Pedestrian route-choice and activity scheduling theory and models. *Transportation Research Part B*, volume 38, pp. 169–190.
- Hoogendoorn, S. P. 2004. Pedestrian Route-Choice and Activity Scheduling Theory and Models. *Transportation Research Part B*, no. 38 , pp. 169-90.
- Hoogendoorn, S., & Bovy, P. 2004. Pedestrian Route-Choice and Activity Scheduling Theory and Models. *Transportation Research Part B*, no. 38, pp. 169-90.
- Hughes, R. 2002. A continuum theory for the flow of pedestrians . *Transportation Research Part B: Methodological* 36, pp. 507–535.
- Hyde-Wright, A., Graham, B., & Nordback, K. 2014. Counting Bicyclists with Pneumatic Tube Counters on Shared Roadways. *ITE Journal*, p. pp. 32–37.
- Isfort. (020. 17°Rapporto sulla mobilità degli italiani- Tra gestione del presente e strategie per il futuro.
- ISTAT. 2011. Basi territoriali e variabili censuarie. Tratto da <https://www.istat.it/it/archivio/104317>
- ISTAT. 2015. Atti del 9° Censimento generale dell'industria e dei servizi e Censimento delle istituzioni non profit, 5 - Le sezioni di censimento. Italia.
- ISTAT. 2019. Gli indici dei prezzi al consumo. Tratto da <https://www.istat.it/it/archivio/226761>
- ISTAT. Basi territoriali e variabili censuarie. Tratto da <https://www.istat.it/it/archivio/104317>
- J., E., Olson, J., & Spring, D. 1997. Sketch-Plan Method for Estimating Pedestrian Traffic for Central Business Districts and Suburban Growth Corridors. *Transportation Research Record* 1578.
- Jacobsen, P. 2003. Safety in numbers: more walkers and bicyclists, safer walking and bicycling. *Injury Prevention*, Vol. 9, pp. 205-209. .
- Jiang, B., & Claramunt, C. 2002. Integration of space syntax into GIS: new perspectives for urban morphology . *Transactions in GIS* 6 , PP. 151-162.

- Jiang, B., Claramunt, C., & Klarqvist, B. 2013. An Integration of Space Syntax into GIS for Modelling Urban Spaces in International Journal of Applied Earth Observation and Geoinformation .
- Jones, M., Ryan, S., Donlon, J., Ledbetter, L., Ragland, D., & Arnold, L. 2010. Seamless Travel: Measuring Bicycle and Pedestrian Activity in San Diego County and its Relationship to Land Use Transportation. Safety and Facility Type. Report No. UCB-ITS-PRR-2010-12, Final Report for Task .
- Kitamura, R., Mokhtarian, P. A., & Laidet, L. A micro-analysis of land use and travel in five neighborhoods in the San Francisco Bay Area. Transportation, Vol. 24, 1997, pp. 125-158.
- Kurkcu, A., & Ozbay, K. 2017. Transportation Research Record, 2644(1), pp.72-82. Estimating pedestrian densities, wait times, and flows with wi-fi and bluetooth sensors. .
- Kurose, S., & Satoshi, H. 1995. A Method for Identifying Accessibility Properties of Pedestrian Shopping Networks. Journal of Retailing and Consumer Services 2, no. 2, pp. 111-18.
- Kuzmyak, J. R., Walters, J., Bradley, M., & Kockelman, K. M. 2014. Estimating bicycling and walking for planning and project development: A guidebook.
- Kuzmyak, J., Walters, J., Bradley, M., & Kockelman, K. 2014. NCHRP REPORT 770 - Estimating Bicycling and Walking for Planning and Project Development: A Guidebook.
- Landis, B., Ottenberg, R., & Vattikuti, V. 1999. The Roadside Pedestrian Environment: Toward A Comprehensive Level of Service. Paper 990570. Washington, D.C.: TRB, National Research Council.
- Leden, L. 2002. Pedestrian risk decrease with pedestrian flow. A case study based on data from signalized intersections in Hamilton, Ontario. Accident Analysis and Prevention, Vol. 34, pp. 457-464.
- Lerman, Y., Rofè, Y., & Omer, I. 2014. Using Space Syntax to Model Pedestrian Movement in Urban Transportation Planning. Geographical Analysis, vol 46 pp. 392–410.
- Lovas, G. 1994. Modelling And Simulation Of Pedestrian Traffic Flow. Transportation Research B. Vol. 28 , p. pp. 429–443.
- Lu, T. 2016. Bicycle and Pedestrian Traffic Monitoring and AADT Estimation in a Small Rural College Town. Master Thesis. Faculty of the Virginia Polytechnic Institute.

- McNally, M. 2000. The Four-step Model in Hensher and Button, Handbook of Transport Modelling . New York: Pergamon.
- McNally, M. 2000. The Four-step Model. Hensher and Button, eds., Handbook of Transport Modelling.
- Ministero delle infrastrutture e dei trasporti . SISTEMI DI MONITORAGGIO DEL TRAFFICO / LINEE GUIDA PER LA PROGETTAZIONE .
- Ministero dell'Istruzione. 2020. Tratto da Scuola in chiaro: <https://cercalatuascuola.istruzione.it/cercalatuascuola/>
- Navin, P., & Wheeler, R. 1969. Pedestrian Flow Characteristics. Traffic Engineering Vol. 39, p. pp. 31–36.
- Nordback, K. J., & Koonce, P. 2014. Using Signal Controllers to Count Bicycles. . Presented at the North American Travel Monitoring Exposition and Conference . Chicago.
- Nordback, K., & Janson, B. 2010. Automated Bicycle Counts . Transportation Research Record: Journal of the Transportation Research Board, No. 2190, p. pp. 11-18.
- OCSE. 2000. Environmentally Sustainable Transport, futures, strategies and best practices, Relazione di sintesi del progetto sul trasporto sostenibile da un punto di vista ambientale dell'OCSE, ! tenutas. Est International Conference , Organizzazione per lo sviluppo e la cooperazione economica. Vienna, Austria.
- Ostwald, M. 2011. The Mathematics of Spatial Configuration: Revisiting, Revising and Critiquing Justified Plan Graph Theory. Nexus Network Journal 13, PP. 445–470.
- Pushkarev, B., & Zupan, J. 1971. Pedestrian Travel Demand. Highway Research Record Vol. 355.
- Raford, N., & Ragland, D. 2003. Space Syntax: An innovative pedestrian volume modeling tool for pedestrian safety. Paper 04-2977. Annual Meeting of the Transportation Review Board.
- Raford, N., & Ragland, D. 2005. Pedestrian Volume Modeling for Traffic Safety and ExposureAnalysis .
- Robertson, H., Hummer, J., & Nelson, D. 1994. Manual of Transportation Engineering Studies. Englewood Cliffs, NJ: Prentice Hall and the Institute of Transportation Engineers (ITE).
- Roess, R., Prassas, E., McShane, & William, R. 2004. Traffic Engineering. Third Edition. Upper Saddle River, NJ: Pearson Prentice Hall.

- Rossi, T., Lawton, T., & Kim, K. 1993. Revision of Travel Demand Models to Enable Analysis of Atypical Land Use Patterns. Cambridge Systematics, Inc. and Metropolitan Service District.
- Ryus, P., Ferguson, E., Laustsen, K. M., Schneider, R. J., Proulx, F. R., Hull, T., & Miranda-Moreno, L. 2014. NCHRP REPORT 797 Guidebook on Pedestrian and Bicycle Volume Data Collection.
- Schadschneider, A. 2002. Traffic Flow: A Statistical Physics Point of View. *Physica A*, Vol. 313, p. pp. 153–187.
- Schadschneider, A., Kirchner, A., & Nishinari, K. 2002. CA Approach to Collective Phenomena in Pedestrian Dynamics. *Proceedings of ACRI 2002*, (p. pp. 239–248).
- Sener, I., Ferdous, N., Bhat, C., & Reeder, P. 2009. Tour-based Model Development for TxDOT: Evaluation and Transition Steps. Technical Report, prepared for the Texas Department of Transportation (TxDOT), October 2009.
- Southern California Association of Governments (SCAG). 2016. Regional Travel Demand Model and 2012 Model Validation. Report from the Federal Highway Administration (FHWA) and Federal Transit Administration (FTA).
- Systematics, C. 1994. Short-Term Travel Model Improvements, Travel Model Improvement Program. U.S. Department of Transportation; DOT-T-95-05, p. pp. 2-1 to 2-7.
- Teklenburg, J., Timmermans, H., & van Wageningen, A. 1993. Space Syntax: Standardised Integration Measures and Some Simulations. *Environment and Planning B* 20(3) , p. pp.347–357.
- Timms, P. 1992. Putting Pedestrians into Network Planning Models. 6th World Conference on Transport Research. Lyon.
- Traumueller, M., Johnson, N., Malik, A., & Kontokosta, C. 2018. Digital footprints: Using WiFi probe and locational data to analyze human mobility trajectories in cities. *Computers, Environment and Urban Systems*, 72, pp.4-12.
- Volchenkov, D., & Blanchard, P. 2008. Scaling and Universality in City Space Syntax: between Zipf and Matthew. *Physica A-statistical Mechanics and Its Applications* 387, pp. 2353-2364.
- Wang, T., & Chen, J. 2009. An improved cellular automation model for urban walkway bi-directional pedestrian flow. *International Conference on Measuring Technology and Mechatronics Automation*. China: IEEE.
- Xu, Y., Rollo, J., Jones, D., Esteban, Y., Tong, H., & Mu, Q. 2020. Towards Sustainable Heritage Tourism: A Space Syntax-Based Analysis Method to

Improve Tourists' Spatial Cognition in Chinese Historic Districts. Buildings ,  
pp.10-29.

Ziye, N. 2011. The Analytical Tools For Pedestrian Mobility Design . POLITECNICO  
DI MILANO - Facoltà di Architettura.

## **CHAPTER 4. ROAD USER VULNERABILITIES**

According to world statistics, most accidents involving vulnerable users occur in urban areas. This happens because the spaces shared between motorized traffic and are not reduced or poorly managed. In order to protect pedestrians and cyclists, but indirectly also motorists, it is advisable to analyze all the points or sections of the road network in which the greatest number of accidents have occurred over the years. This makes it possible to identify the most recurrent accident scenarios but to foresee the measures to be implemented to reduce or eliminate them it is necessary to start risk-based engineering investigations. Therefore, data on the number, recurrence, localization and dynamics of accidental events (Ebner A., 2010) (Ebner, Samaha, Scullion & Helmer, 2010) should be found, as well as the severity of the consequences for people.

Such data, in Italy, are often difficult to find and the ISTAT database is not useful since it does not provide a detailed location of the accident or a precise description of the dynamics.

Instead in many European countries, in-depth accident databases (GIDAS, 2010) (UMTRI, 2005) are already available to help understand the mechanisms of injury and tolerance of the human body to provide an operational framework for investigating real-world pedestrian accident scenarios (Bahman SR, 2005) (Kong CY, 2010) (Naif AS, 2009) (Olukoga IA., 2003) (Otte D, 2003).

These data together with the biomechanical knowledge (with which it is possible to know the tolerance of the human body to stresses and to attribute criteria that classify the injuries suffered by the occupants of the vehicle) have made it possible to start studies whose purpose was to define the vulnerability prediction functions (Helmer T., 2009).

Evaluating vulnerability means defining the results of an impact, this means examining what in the reconstruction of an accident is called the post-impact phase.

Before this, the pre-impact and impact phases may be encountered; in the first, the driver of the car detects the presence of the pedestrian and activates the maneuvers to avoid the accident, while in the second there is a collision.

According to the trajectories followed by the pedestrian in the post-impact phase, vehicle-pedestrian accidents are differentiated into non-free trajectories (due to the presence of obstacles) or free ones (the final position of the pedestrian is determined only by the configuration of the impact).

Numerical analyzes based on empirical formulations are usually used for the reconstruction of accidents involving pedestrians, although the use of software that makes use of multi-body simulation is increasingly widespread. By means of the multi-body simulation codes, once the initial conditions have been imposed, it is possible to describe the motion of the bodies involved and, as a function of the dynamics, allowing to evaluate of the induced damage. The help of the software allows you to perform calculations quickly and to obtain a 2D or 3D graphic representation that faithfully reproduces the real scenario. In order to obtain realistic analyzes, the software allows to carry out direct analysis, called Forward Calculation, in which the simulation of an accident is repeated iteratively by varying the initial parameters.

In this chapter a new methodology aimed at enriching the existing pedestrian vulnerability prediction functions by the information on kinematic (acceleration, speed, etc.) and mechanical (moments, cuts, normal stresses, etc.) outcomes provided by multi-body simulation codes is proposed.

## **4.1 Dynamic vehicle-pedestrian collisions**

Reconstructing the dynamics of the pedestrian-vehicle collision is not a simple task as this depends on the concatenation of many factors such as the physical ones of the vehicle (type, speed, etc.) and of the pedestrian (characteristics, the position taken at the moment of impact, age, etc.), the atmospheric, urban, legislative, psycho-physical ones of the driver, etc.

### **4.1.1 Pedestrian-vehicle collisions**

Kinematics and pedestrian injuries in vehicle accidents are affected by numerous factors such as impact speed, vehicle type, stiffness and shape of the vehicle front (such as bumper height, hood height and length, windshield frame), age and build of pedestrians, as well as the pedestrian's starting position relative to the front of the vehicle (Yang J.K., 1997).

In this work, the "free trajectories" were analyzed. These allow to model the collision between vehicle-pedestrian and the subsequent motion of the pedestrian in a series of consecutive phases.

During the first phase, called contact, the pedestrian collides with a part of the body the car; based on the extent of the impact, the pedestrian is subject to acceleration. In this phase, the car, depending on the shape of the front, lifts the body which is loaded on the bonnet. According to the speed, the body is projected forward or sideways and finally there is a rolling or sliding phase on the ground.

### 4.1.2 Types of free trajectories

Basically, it is possible to distinguish two types of free trajectories:

- Forward projection;
- Wrap or winding.

The Wrap trajectory, the most common, allows to identify three other types of trajectories that can be considered particular cases of the same, namely:

- Fender Vault;
- Roof Vault;
- Somersault.

In Forward Projection the height of the center of gravity of the pedestrian ( $h_{CG}$ ) is placed below the height of the upper edge of the front of the vehicle ( $H_c$ ). It is substantially realized in all those cases in which the pedestrian is hit in full, that is the central area of the front of the vehicle where the collision occurs.

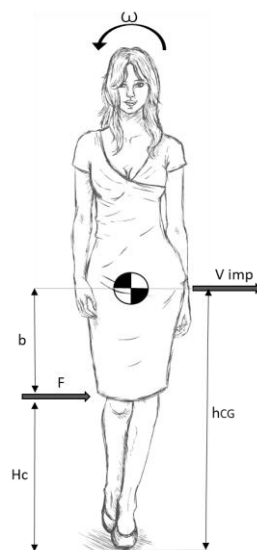


Figure 4.1 Center of gravity and diagram of the forces acting on the pedestrian with subsequent motion

The typical cases are those in which the collision between an adult pedestrian and a truck or bus occurs, or in the case in which there is a collision between a child and a vehicle that has a higher front than its center of gravity.

Therefore, the individual phases of the trajectory can be summarized as follows:

- a primary impact;
- the acceleration of the pedestrian in the horizontal direction up to the exit speed from the impact, close to that of the vehicle;
- free flight, with the almost horizontal direction of launch;
- ground impact;
- motion on the ground to the position of rest.

If the vehicle does not break, the pedestrian may roll or drag with a consequent change in the state of rest.

In the Wrap-type trajectory when the pedestrian is fully hit, the height of the center of gravity of the pedestrian is greater than that of the height of the upper edge of the vehicle front.

By schematizing the pedestrian as a rigid body, the motion that is given to it following the impact is a horizontal translation and a rotation around the center of mass.

Consequently, the pedestrian wraps around the hood of the vehicle with the subsequent impact of the head on it or on the windshield. In this regard, a fundamental parameter is introduced, the Wrap Around Distance (WAD).

It is defined as the distance from the point of contact with the front of the bumper to the ground at the point furthest from the front. This parameter is influenced by the impact speed of the vehicle, the length of the hood and the height of the pedestrian.

There is a direct proportionality between the WAD and the impact speed ( $V_{imp}$ ), as shown in the figure below.

$$WAD = ab + bc + cd$$

4.1

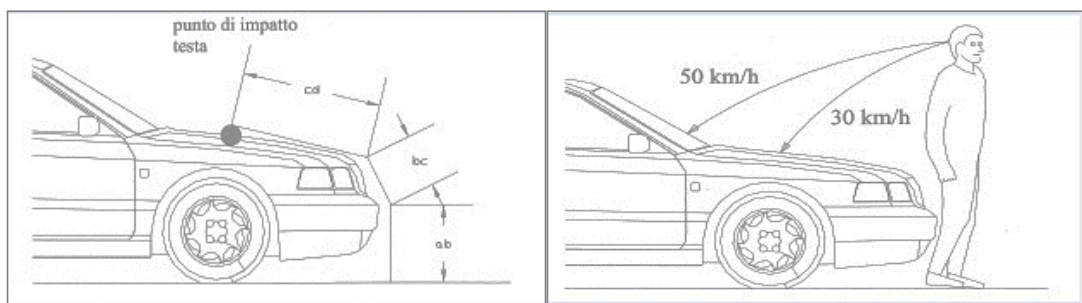


Figure 4.2 Analysis of the WAD (Taken from the text (Vangi & al., 2008))

With the same shape of the front of the vehicle and the height of the pedestrian, the higher the speed, the greater the WAD.

Summarizing the individual phases of the Wrap trajectory, they are:

- primary impact;
- acceleration of the pedestrian in the horizontal direction;
- pedestrian rotation around its center of gravity with loading on the hood;
- pedestrian motion on the hood;
- secondary impact of the head and/or shoulders on the bonnet or windscreen,

depending on the impact speed of the vehicle at the moment of impact;

- pedestrian unloading, with launch angle dependent on the geometry of the vehicle front and on the unloading method;
- free fly;
- ground impact;
- motion on the ground to the position of rest.

If the vehicle brakes during or immediately upon impact, the pedestrian does not have a high acceleration transverse to the direction of the vehicle, therefore a frontal discharge is observed; while if the vehicle brakes with delay or does not brake at all, the pedestrian has a high transversal speed with respect to the direction of the vehicle and there is a lateral discharge.

The Fender Vault-type trajectory occurs when the height of the center of gravity of the pedestrian is greater than the height of the upper edge of the front of the vehicle, but the impact occurs on the end or side of the latter, so it is not hit in full but only on one leg. This trajectory typically occurs with speeds that are around 40 km/h. As in the Wrap-type trajectory, the act of motion transmitted from the vehicle to the pedestrian is the roto-translational type, but in this case, the main rotation occurs around the vertical axis and is free and not hindered by the front of the vehicle. Consequently, the pedestrian rotates towards the side of the vehicle, where the secondary impact occurs, which varies according to the speed of the car.

If the speed is low, the secondary impact occurs on the front part of the hood, on the other hand, if the speed is higher it occurs at the rear.

In conditions similar to the Wrap type trajectory, therefore with the height of the center of gravity of the pedestrian higher than the height of the upper edge of the front of the vehicle, but with high impact speed and in the absence of braking, it is possible to witness the Roof Vault type trajectory. It takes place in a speed range between 50 km/h and 60 km/h. A higher speed gives the pedestrian a greater vertical thrust, with a consequent flight phase of the same following the primary impact, during which the

pedestrian twirls in the air due to the effect of the rotational motion component acquired by the impact.

The secondary impact of the pedestrian occurs against the roof of the vehicle or the top of the vehicle. By further increasing the vehicle's impact speed, i.e. greater than 60 Km/h, the trajectory of the Sommersoult type is passed, in which the secondary impact is not observed since the pedestrian undergoes a greater vertical thrust which gives rise to a phase of flight during which the vehicle moves much faster under the pedestrian. In this case, the final resting position of the pedestrian is always behind the vehicle stop position.

Given the variability of each influencing parameter in each phase, it is more convenient to classify the types of impact on the basis of the overall trajectories (pre-impact, impact, post-impact). As already mentioned, in this work the post-impact phase was mainly which is influenced by the characteristics of the impact phase such as the geometry of the front of the vehicle related to the height, position and motion of the pedestrian in the per-impact phase, the braking characteristics of the vehicle and the impact speed.

### 4.1.3 Vehicles characteristics

In recent years, many car manufacturers have been carrying out tests to estimate the behavior of the bonnet both in terms of shape and stiffness to improve its performance and offer better protection for pedestrians.

Three fundamental geometric parameters are used to define the shape of the vehicle's front.

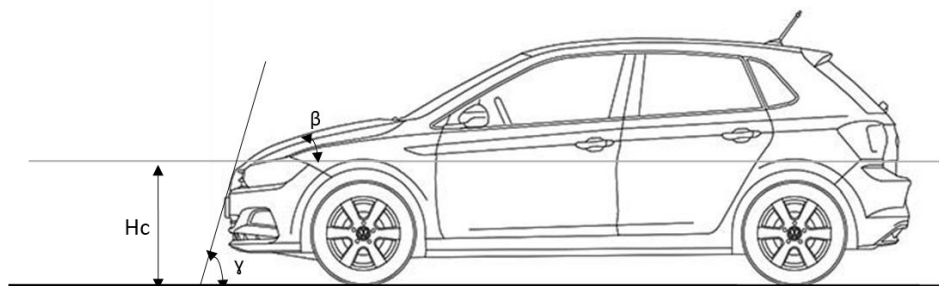


Figure 4.3 Geometric parameters for defining the front of the vehicle

Where:

- *Lead Angle* ( $\gamma$ ) loading angle which determines the amount of vertical thrust on the pedestrian in the primary impact;

- *Bonnet Angle ( $\beta$ )* angle of inclination of the bonnet which affects both the loading and the direction of launch of the pedestrian, and the way in which the pedestrian hits the bonnet in the secondary impact;
- *Height of the front edge of the "Lead Edge" hood ( $H_c$ )* which together with the height of the center of gravity of the pedestrian determines the arm of the rotational moment ( $\omega$ ).

According to the relationship between the height of the pedestrian and the front of the vehicle, three types of front are identified:

- *Low Front Vehicles*, in which the height  $h$  of the frontal is less than 0.55m, or the value corresponding to the fiftieth percentile of the knee height of the adult population;
- *High Front Vehicles*, in which the height of the front  $h$  is between 0.55 m and 1.05 m, that is the value corresponding to the fiftieth percentile of the height of the center of gravity of the adult population;
- *Vertical front vehicles*, whose front height  $h$  is greater than 1.05m.

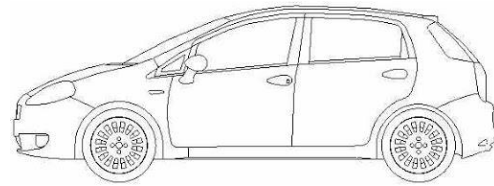


Figure 4.4 Example of a vehicle with a low front

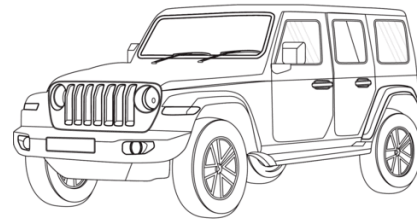


Figure 4.5 Example of high front vehicle



Figure 4.6 Example of a vehicle with a vertical front

The height of the front edge of the hood and its combination with other parameters have an influence on the head or torso injuries of the vulnerable user; in fact, increasing the height of the front edge of the hood can potentially reduce the risk of head injuries.

Further consideration should be made on the profile of the front of the vehicle seen from above which can be classified into rectangular, triangular or arched.

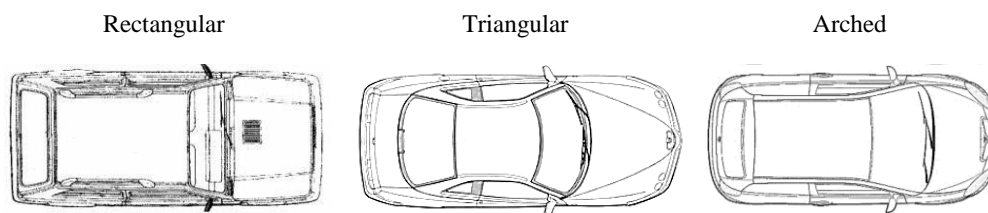


Figure 4.7 Type of front with top view

The latter classification has a considerable influence on the speed component of the pedestrian transversal to the direction of the vehicle.

In fact, for rectangular type fronts, the speed remains unchanged, with the consequent variation of the momentum of the pedestrian in the direction of advancement of the vehicle itself, neglecting the friction during contact.

While for triangular or arched fronts, the transverse motion of the pedestrian can undergo a deceleration or acceleration depending on the area in which the impact occurs. But it is known that the risk of injury, especially to the head, is a function of both the shape of the bonnet and the speed of impact (Liu, Yang & Lövsund, 2002); in fact, with an adult pedestrian a reduction in the impact speed, from 40 km/h to 30 km/h and an increase in the height of the bonnet have a positive effect on the risk of head injuries. While in the impact with children a reduction in impact speed from 40 km/h to 30 km/h has a great influence on the severity of the injury, while the vehicle design parameters show contrasting effects due to the variability in childhood anthropometry.

One of the many studies presenting different lesions based on the type of hood is that of Han et al. (2013) in which the authors investigated the kinematics of impact between a 50th percentile dummy and three vehicles (a sedan car, a mini-car and an SUV). With the same position of the dummy with respect to the vehicle, they observed that the speed of the head is higher in the case of a sedan, followed by “minicars” and SUVs. This result is closely related to the rotation of the whole body during the loading phase: the greater the rotation, the greater the final speed of the head.

Others (Fredriksson, Rosen, & Kullgren, 2010) (Rosen et al., 2010) (Otte, 1994) have shown that short hoods cause more head impacts to the vehicle's windshield than a long hood, resulting in more severe head injuries for pedestrians. In addition to the conditions of impact with the head, it is evident that the contact time of the head during the impact decreases as the speed of impact with the vehicle increases from 20 to 50 km/h.

The hood therefore affects:

- the loading phase;

- the amount of vaulting during the loading phase, since it depends on the height from the ground of the upper edge of the bonnet (this is greater for low edges, lower for high edges);
- the parts of the body that impact on the front of the vehicle, vary according to the height from the ground of the front edge of the bonnet and its length.

#### 4.1.4 Pedestrian's characteristics

Pedestrians are characterized according to their age, their build as well as their position with respect to the vehicle at the moment of impact.

Many of the results published by the NHSTA (2001), by the FARS (Fatality Analysis Reporting System) and by the General Estimates System (GES) of the National Automotive Sampling System, show the risk based on age; in fact, it is observed that middle-aged and elderly people are more likely to die in a pedestrian accident, while young people and children are more likely to be injured.

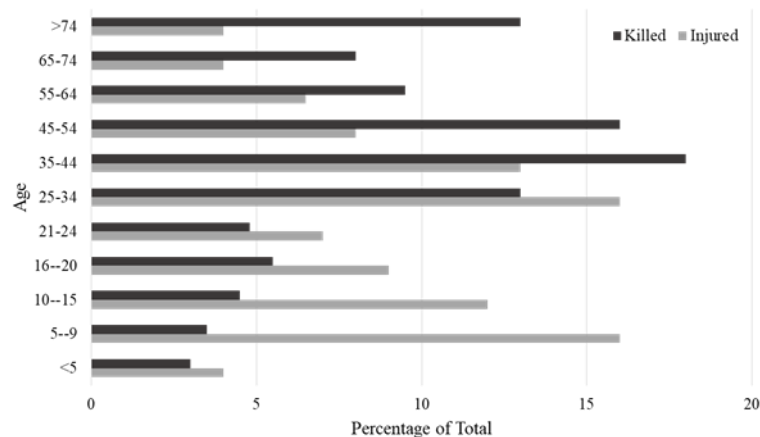


Figure 4.8 Risk of death/injury based on age

On the other hand, when the position is considered, the angle of impact has a great influence since the sequence of the parts of the body that collide with the vehicle and therefore of the relative injuries is different (Chen H., 2015) (Yang J.K., 1997).

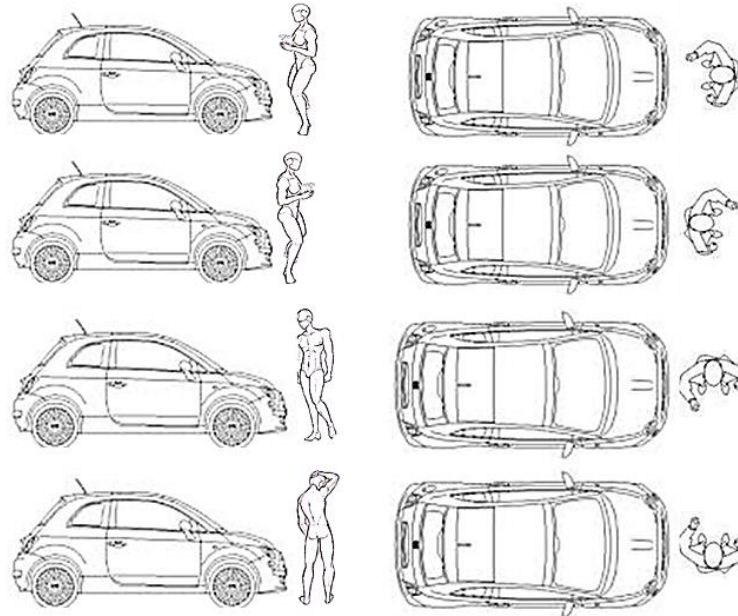


Figure 4.9 Positions of the pedestrian with respect to the front of the vehicle

Many studies (Carollo F., 2018) (Virzi Mariotti G., 2014) confirm that the frontal position is more dangerous than the lateral one because the contact of the head and thorax occurs directly on the hood; while the pedestrian in the lateral position hits the hood with the shoulder, this limits the injuries to the fatal parts. The above is confirmed by the analysis of the data on accidents.

## 4.2 Proposed Methodology for pedestrian injuries evaluation

To determine the pedestrian injuries, both in terms of location and severity, following an impact, several factors must be considered. They never occur individually but combined with each other.

In order to identify the outcomes of the impact, vulnerability functions are often used. These, however, consider only two parameters, not allowing to take into account the mechanical behavior of the bodies during the impact. To make the results of the analyzes more realistic, once the various factors have been defined, a model can be built and then multi-body simulations can be started, from which the mechanical or kinematic parameters useful for defining the lesions will be obtained.

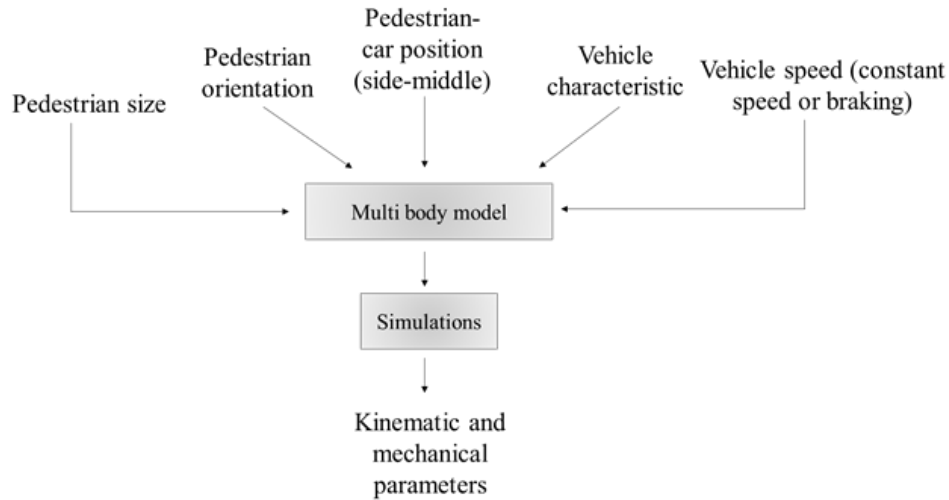
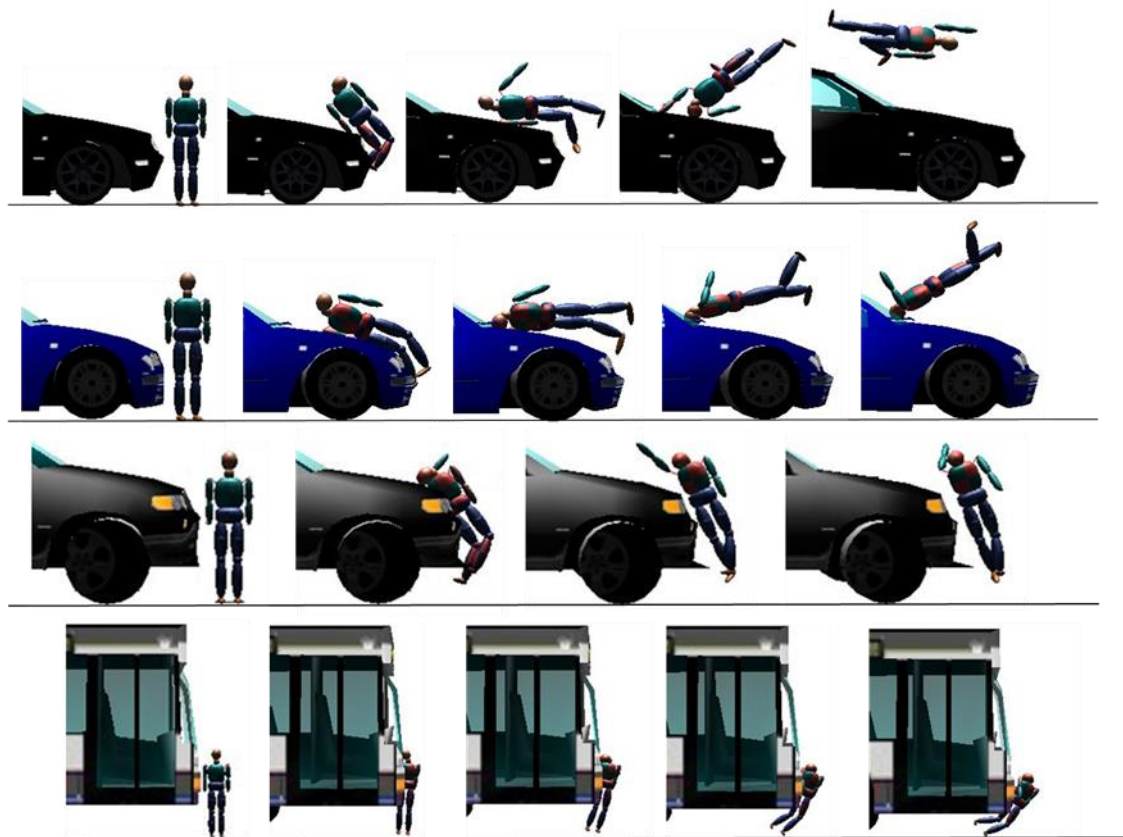


Figure 4.10 Conceptual scheme adopted in the numerical simulations

The vehicle-pedestrian collision generates damages of a different nature, due to the primary impact, the secondary impact and finally those due to the impact on the ground. In this work, the focus was on the injuries suffered by a pedestrian in the primary impact. Usually, in these cases, there are bruises, fractures, or trauma and they vary according to the speed of the vehicle and the pedestrian and whether it is an adult or a child. In the case of adults, these damages are caused by the bumper and/or by the front edge of the hood and are localized at the height of the legs or pelvis; and have different gravities depending on the speed (Vangi et al., 2008).

In children, on the other hand, the primary impact generates localized damage to the torso and/or head. It is essential to determine the area in which the injuries caused by the primary impact occur as these allow in the reconstructive phase to determine the orientation of the pedestrian at the moment of impact.

By observing the different frames of the multibody simulations it is clearly visible that as the vehicle front and the respective shape vary, there are impact conditions and therefore different outcomes and injuries in the different parts of the body.



*Figure 4.11 Pedestrian kinematics after various vehicle impacts*

This is easily found by observing the different frames of the multibody simulations. In fact, in these, it is clearly visible that when the front of the vehicle and the respective shape vary, there are impact conditions and therefore different outcomes and injuries in the different parts of the body.

Nowadays pedestrian-vehicle impact outcome in terms of injury level can be evaluated by means of vulnerability prediction functions employing a logistic approach (Helmer, T., 2015). Logistic models are stochastic models that do not allow us to know the outcome of an accident but only to estimate the probability of a certain degree of injury and they are calibrated on detailed accident data collected with-in in-depth accident databases (GIDAS,2010) (UMTRI,2005). Unfortunately, most of the existing vulnerability logistic models (VLM) is based on few statistically significant explanatory variables (namely, vehicle speed and pedestrian age) since the size of the in-depth accident database is very limited.

However, in order to analyse pedestrian safety according to a risk-based approach a better understanding of how pre-impact conditions (in term of pedestrian, vehicle and site characteristics and possible evasive manoeuvres) may affect accident outcome

is needed. The basic idea underlining this work is therefore to develop and calibrate a multi-body pedestrian-vehicle model in order to provide an additional analysis tool that may complement the prediction yield by VLM by producing reliable synthetic accident data that will allow to enrich VLM with additional and new explanatory variables.

In order to accomplish this task, the following procedure has been pursued:

1. review of existing relationships between kinematic and mechanical quantities provided by multibody/fem accident numerical simulations and pedestrian injury scales;
2. assessment of numerical reliability of the developed multibody model by calibration with scientific literature data;
3. experimental calibration of the proposed methodology by comparison with results provided by existing VLM based on real accident data.

### 4.2.1 Injury scales

Based on the type and severity of the lesions, they are classified with different scales based on the area of use. The main ones can be grouped into three categories:

- anatomical scales: classify the lesion in terms of anatomical location, type and severity. These scales assess the extent of the injury rather than the long-term consequences. The most famous and widespread of these scales is the “Abbreviated Injury Scale” (AIS);
- physiological scales: that describe the physiological state of the patient based on the change in functionality caused by the lesion. The status and its numerical rating may vary during the period of care. This type of scale is widely used in the clinical setting;
- scales based on damage, disability and social cost. In this case, the long-term consequences and the influence that the injuries have on the patient's quality of life are assessed.

The first two types are medical, while biomechanics is concerned with scales that belong to the third group.

All scales assign trauma points, which were originally designed with the aim of standardizing injury descriptions and classifying their severity. Following the trauma scores have been modified to support research in risk assessment and to predict the probability of survival (Baker, O'Neill, Haddon & Long, 1974) (Champion, Copes, Sacco, Lawnick & al., 1990).

Today the purpose of trauma scores is becoming to allow for predicting damage (MacKenzie, Damiano, Miller & S., 1996), improving user quality and safety (Boyd, Tolson, & Copes, 1987) (Hannan, Hicks Waller, Szypulski Farrell, & Cayten, 2005) (Meredith, Evans, Kilgo, MacKenzie, & al., 2002).

### Abbreviated Injury Scale

The most common injury scale worldwide is the Abbreviated Injury Scale (AIS). This is commonly used to assess the severity and describe the types of injuries (AAAM, 2008) as a function of the severity of the injury, as described in the international literature (Virzi Mariotti G., 2014) (Battaglia S., 2006) (Bellavia GVM, 2009) (Bellavia GVM, 2009).

AIS has provided standard terminology for describing injuries. This scale divides the body into nine regions: head, face, neck, chest, spine, abdomen/pelvis, upper extremities, lower extremities and unspecified. A consensus-derived scale was developed for each region to classify injuries from 1 (minor) to 6 (practically insurmountable).

*Table 4.1 Damage related to the severity of the injury*

AIS	Level	Description
0	null	No injury
1	minor	Slight brain injury, with headache, dizziness and no loss of consciousness; slight cervical injury, whiplash and bruises.
2	moderate	Bruises with or without skull fracture, less than 15 minutes of unconsciousness, small corneal cracks, retinal detachment, nose fracture and facial damage.
3	serious	Bruises with or without skull fracture, more than 15 minutes of unconsciousness without severe neurological damage, compound or no compound skull fracture, without loss of consciousness, or other damage such as loss of vision, fracture of the facial bones, the cervical fracture without damage to the spinal cord.
4	severe	Fracture of the skull with severe neurological damage.
5	critic	Concussions with or without skull fracture, more than 12 hours of unconsciousness, with haemorrhage near the skull and / or critical neurological damage.
6	not survivable	Death, partial or total damage to the brain stem or upper cervical area due to pressure or rupture, fracture or twisting of the upper cervical region, with damage to the spinal cord

For each level there is, as shown in (Shojaati M., 2003), different damage to different parts of the body.

AIS is universally used in the analysis of road accidents, in evaluating the effectiveness of safety systems and as a justification for the biomechanical limits used in regulations and ratings. (Plan L., 2013).

The maximum value of AIS is known as MAIS (Maximum Abbreviated Injury Scale) and indicates the most severe damage a patient has suffered (European Commission).

Some scholars have highlighted the relationship between the frequency of injuries by body region and the severity of injuries (Helmer, Ebne et al., 2010) (Mizuno, 2005) (Martin, Lardy et al., 2011) (Yang, 2005) showing that torso injuries are second only to head injuries.

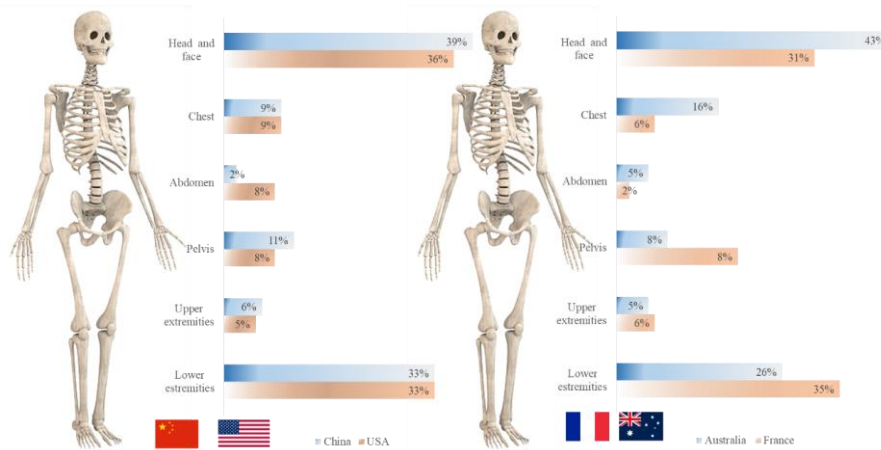


Figure 4.12 Percentage of AIS 2 injuries per body region in different countries

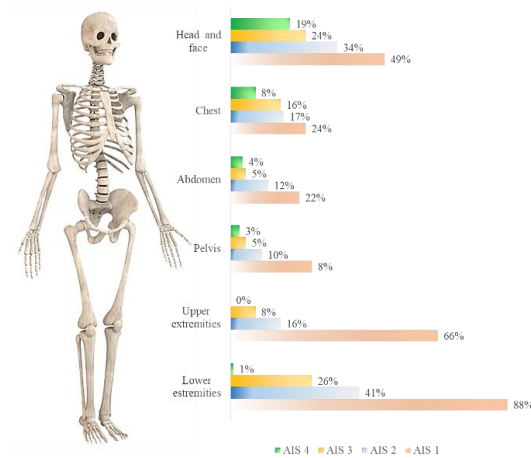


Figure 4.13 Percentage of AIS injuries by body region

Unfortunately, AIS does not take into account the cumulative effect of injuries in different regions of the body, so in 1974 Baker proposed the ISS, an AIS-based algorithm designed to improve AIS's ability to predict injury severity (Baker & O'Neil, 1976). The ISS divides the injuries into six body regions compared to the nine AIS and it is calculated by taking the sum of the squares of the highest AIS from each of the three most severely injured body regions. This generates a score ranging from 0 to 75, with a breakdown into levels as shown below.

*Table 4.2 ISS levels*

ISS	Level
1-8	Minor
9-15	Moderate
16-24	Serious
> 25	Very serious

By definition, a very severe injury with an AIS of 6 is assigned an ISS of 75.

However, both the AIS and the ISS require high costs and time for the training of the personnel involved in data acquisition and scoring (manual coding (Stephenson, Langley & Civil, 2002)).

To determine the AIS it is necessary to extract the lesions from the medical record and the trauma encoder by assigning the AIS Codes to each lesion. Depending on the software used to implement the algorithm and the skills of the personnel who analyzes it, there may be significant differences in the calculation of the AIS and the ISS. This limits the ability to compare results with data derived from different institutional practices.

ISS is statistically problematic because it is neither linear nor monotonous, so mortality does not necessarily increase with subsequent ISS values (Copes, Champion, Sacco, Lawnick, & al., 1988).

For this reason, AIS remains the foundation of most trauma scoring systems. Thanks to the availability of the ICD mapping software and its lesion descriptors, this scale is used extensively, allowing data to be extracted even from non-trauma administrative databases. This is because it has been found that trauma scoring systems that consider only injury severity are useful, but insufficient for risk adjustment.

To easily combine trauma log data with other relevant research databases and define treatment and injury prevention in advance, it would be necessary to acquire the data

accurately and completely, automatically update the trauma logs, and use a standardized procedure for evaluating lesion descriptors.

### **Head Injury Criterion**

In this study, statistical data was used to identify relationships between the injury criteria and the probability that the same occurs. In particular, the risk criterion for the head was considered in several studies (Mizuno, 2005) (Yang, 2005) (Martin, Lardy, & al., 2011) which show that in patients with multiple injuries, following an accident, the head is the most commonly injured part. Therefore, being a very delicate part of the human body, many have taken care of evaluating the injuries and the consequences that these can generate. When considering head injuries they can be distinguished according to the affected part:

- the skin may have bruises, lacerations and abrasions;
- the skull may show bone fractures;
- the brain, due to the direct impact of the head, can compress, generating even permanent injuries.

It is difficult to define a criterion that is able to take into account all the different modes of injury. But the international literature comes in support by providing on the various risk criteria (Virzi Mariotti G., 2014) (Bellavia GVM, 2009).

The Abbreviated Injury Scale (AIS) (Association for the Advancement of Automotive Medicine, 2001) for the head assigns a score of 1 for minor scalp injuries such as abrasions, bruises and lacerations. Longer and deeper lacerations are rated 2, while scalp injuries accompanied by significant blood loss or characterized by total loss of the scalp are classified as 3. Cranial nerve injuries are coded as 2. Injuries to major cerebral vessels are generally coded as 3 or 4 for thrombosis or traumatic aneurysm formation, or as 4 or 5 for a laceration.

Small single or multiple bruises receive a score of 3, as well as edema or heart attack directly related to the trauma. Hematomas are rated 4 or 5, depending on their size. Massive destruction or crush injuries lead to a score of 6.

The duration of loss of consciousness and the presence of associated neurological deficits can be used to assess the severity of the injury by assigning scores ranging from 2 to 5, sometimes exceeding those attributed for anatomical lesions.

Table 4.3 Abbreviated Injury Scale for Head Injury

Score	Injury Severity	Head injury examples
1	Minor	Minor scalp injuries
2	Moderate	More severe scalp injuries Cranial nerve injuries Post-traumatic amnesia
3	Serious	Worst scalp injuries Cerebral vascular injuries Skull base fractures
4	Severe	Worst cerebral vascular injuries Worst skull fractures
5	Critical	Worst cerebral vascular injuries Larger hematomas
6	Lethal	Massive destruction Crush injuries

However, the most used criterion for head injuries in impact with the various areas of the vehicle and to find correlations between the deformations observed in the vehicle and acceleration is the Head Injury Criterion (HIC).

Changing the formula leads to the definition of the Head Injury Criterion, also known as Head Performance Criterion (HPC):

$$\text{HIC} = \max\left\{(t_2 - t_1) \left[ \frac{1}{(t_2 - t_1)} \int_{t_1}^{t_2} a(t) dt \right]^{2.5}\right\} \quad 4.2$$

where:

- (t) is the resultant of the acceleration evaluated in the center of gravity of the head, measured in g;
- $t_1$  and  $t_2$  are two points on the time axis which, during impact, maximize the HIC. Time is measured in seconds;
- the exponent 2.5 is the slope of the curve in bilogarithmic coordinates.

The calculation of the HIC involves an iterative process characterized, for each instant of time, by an integration carried out over a time interval equal to 36 msec or 15 msec (NHTSA), depending on the threshold value that you decide to take into account. In the integration,  $t_1$  increases by 0.1 millisecond, at each step, and  $t_2$  is defined as  $t_1 + 36$  msec, therefore, for each step, a curve is obtained as  $t_2$  varies. For each of them, the maximum value is taken, which contributes to the definition of the

local maximum curve. To proceed quickly, a Matlab spreadsheet has been implemented as shown in Appendix A.

The NHTSA proposed a 36 millisecond interval to evaluate HIC since it observed reduced brain injury in long-lasting events. But to better assess the danger of short-term collisions, the interval has been reduced to 15 milliseconds, which is associated with limit HIC values of 700.

The European legislation has adopted this criterion in fact the FMVSS directive (1998), provides that the HIC15 must not be greater than 1000 because there is a very serious accident, with a high probability of lethality. In collisions with surfaces that are not excessively rigid (bonnet, airbag, etc.) there is an increase in the HIC with the increase of the interval  $t_2-t_1$ , with reduced peaks. If the peaks increase, exceeding 100g, the peak value of the HIC is obtained in intervals of a few milliseconds.

Therefore the Head Injury Criterion indicates the threshold beyond which the individual undergoes fatal injuries, inversely correlating the intensity of the acceleration and its duration. But the HIC does not provide any information regarding the extent of the injury. This is precisely why the HIC-AIS correlation is used.

### **Thoracic Trauma Index**

For the evaluation of thoracic trauma, one of the most common injury criteria, especially for lateral impact cases, is the Thoracic Trauma Index (TTI). This is evaluated as expressed in the following equation

$$TTI = 1.4 * \text{age} + 0.5 * (\text{RIBy} + \text{T12y}) * \frac{m_c}{M_{std}} \quad 4.3$$

where;

- age is the age of the pedestrian;
- RIBy is the maximum lateral acceleration of the abdominal spine (12th spinal segment) [g];
- T12y is the maximum lateral acceleration of the 12th thoracic vertebra [g];
- $m_c$  is the mass of the pedestrian [Kg];
- $M_{std}$  is the standard mass equal to 75 Kg.

In the case under examination, having a simplified model of a dummy, the vertebral and thoracic accelerations were hypothesized to be similar to the resulting acceleration in the chest.

### Spine injury criterion

Another injury found recurrently in accidents is that of the spine; although the injured in most cases make a full recovery within short periods, there are prolonged medical problems. So the socio-economic cost of these injuries is enormous.

The part of the spine most involved in collisions is the cervical one. In this, the stresses are due to the contact forces acting on the head or to inertial forces related to the mass of the same. Therefore, several combined loads must be considered to estimate neck injuries (Myers, et al., 1994) (Belwadi & Yang, 2008) between them so that these do not exceed certain limits.

In this preliminary study, spinal injuries are assimilated to those of the torso.

### 4.2.2 Conversion of injury thresholds to AIS scale

Not having available complete data that would allow to evaluate the precise AIS values, the lesion level was evaluated starting from the relationship between AIS and the different lesion parameters found in the literature. For example, I know the HIC has entered the interval and assigned a level of AIS (National Highway Traffic Safety Administration, 1981).

*Table 4.4 HIC-AIS relationship*

HIC	AIS	Brain and head injury level
135 - 519	1	Headache or dizziness
520 - 899	2	Loss of consciousness for less than 1 hour - linear fracture
900 - 1254	3	Loss of consciousness from 1 to 6 hours - depressed fracture
1255 - 1574	4	Loss of consciousness from 1 to 24 hours - open fracture
1575 - 1859	5	Loss of consciousness for more than 25 hours - diffuse hematoma
> 1860	6	Not survivable

Similarly, it was done for the other injury parameters. After evaluating the AIS for the different parts of the body, the three maximum values are taken and the ISS is estimated:

$$ISS = AIS_1^2 + AIS_2^2 + AIS_3^2 \quad 4.4$$

The next step was to define the probability of having an injury using both deterministic and stochastic models.

## 4.3 Damage to the vehicle

The damage to the vehicle following an impact with a pedestrian, in turn, can be classified into those caused by the primary impact and those caused by the secondary

impact. The damage due to the primary impact is substantially concentrated in the frontal area of the vehicle, caused by the impact against the legs and/or pelvis of the pedestrian. The front area of the vehicle means the bumper, the grill, the hood, the cowl and the windshield.



*Figure 4.14 Impact zones in the primary impact*

The extent of the damage varies according to the impact speed and the position of the center of gravity of the pedestrian. For low collision speeds, on the vehicle there are only small traces due to contact with the pedestrian, in correspondence with the bumper and/or the bonnet and then there is the possibility of the presence of small scratches due to metal objects such as buckles or studs, if worn by the pedestrian.

At high speeds, on the other hand, the front grille breaks and the front part of the hood deforms. Possibly if the point of impact is at one of the ends of the front of the vehicle, the headlights will break.

In some cases, for higher impact speeds with a careful visual analysis, it is possible to recognize the footprints of the fabric worn by the pedestrian at the moment of collision, especially for more resistant fabrics such as jeans. This is useful for recognizing the point of impact on the vehicle and for identifying the orientation of the pedestrian at the moment of impact.

As for the damages due to the secondary impact, if present they are caused by the head and/or the upper part of the torso of the pedestrian which, as previously mentioned, their extent and position are influenced by many factors. They vary according to the type of free trajectory, the speed, the mechanical resistance of the area of the vehicle where the impact occurs, in fact the deformation that occurs in the central area of the bonnet is greater than that which occurs in correspondence with the side area of the bonnet, or at the base or on the windscreen pillars which are more rigid.



*Figure 4.15 Example of damage due to the impact of the head on the windshield (Taken from Google images)*

In some cases, it is possible to find a double trace of impact on the bonnet and or on the windscreen due to the impact with the head and a subsequent impact on the shoulders or arm or vice versa.

The traces are the fracture lines, which if studied it is possible to reconstruct the temporal succession of collisions. The fracture lines due to the first impact can be recognized because they are instantaneous and propagate undisturbed, while the fracture lines of the second impact terminate at the intersection with the fracture lines of the first impact.

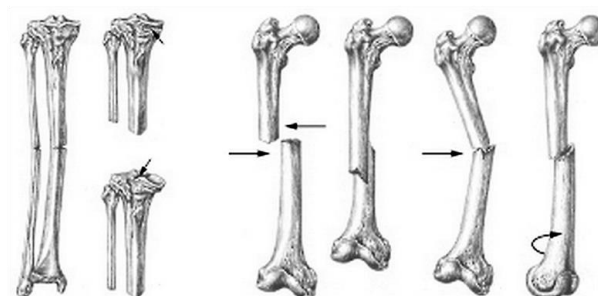


*Figure 4.16 Example of a fracture caused by the vehicle's bumper*

### **4.3.1 Correlations between vehicle damage and collision speed**

The damage on the vehicle can be useful in the reconstruction phase of the accidents to identify the type of trajectory of the post-impact motion of the pedestrian even if it is difficult to assess the speed of the vehicle at the time of the collision due to the multiple variables that come into play.

To design the safety measures for vulnerable users, it is essential to assess the damage to the vehicle but also the injuries to pedestrians. For example, it is evident

that the rounded shapes of the bumper and front of recently built vehicles are certainly less aggressive towards the pedestrian, furthermore their greater compliance contributes to the absorption of part of the impact energy which is therefore not transferred to the pedestrian.

Therefore, the probability of injury or mortality on the pedestrian is evaluated according to the speed of impact (Anderson, McLean, & al., 1997) (Davis, 2001) (Pasanen & Salmivaara, 1993) (Rosen & Sander, 2009) (Oh, Kang et al., 2008) (Hannawald & Kauer, 2004).

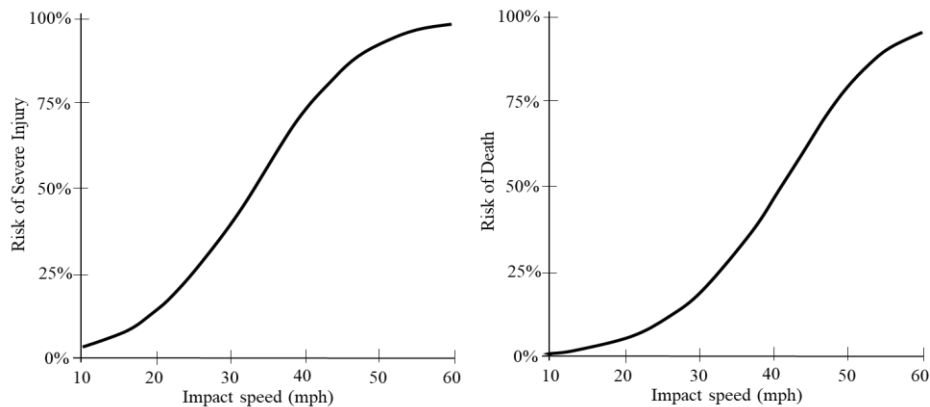


Figure 4.17 Impact speed and a pedestrian's risk of severe injury or death

Once the probabilities have been assessed, the devices are put in place which, once tested, allows to check whether the damage is reduced.

For this reason, over the years assessment bodies have been created such as USNCAP (United States New Car Assessment Program) in the USA, EuroNCAP (European New Car Assessment Program) in Europe, in Australia the ANCAP (Australian NewCar Assessment Program), in Japan the JNCAP (Japan New Car Assessment Program), in the countries of Latin America and the Caribbean LatinNCAP (NewCar Assessment Program for Latin America and the Caribbean), which have recently been joined by initiatives in developing countries such as the BharatNCAP (Bharat New Vehicle Assessment Program), and the Asean NCAP (NewCar Assessment Program for Southeast Asian Countries) under the guidance of the Global NCAP organization promoted by the FIA (International Federation of Motorists).

## 4.4 Euro NCAP

To estimate the safety of motor vehicles, crash-tests, or impact tests, are carried out, considering the various risk conditions to improve prevention techniques. In Europe,

the body that manages these tests is EuroNCAP. This project verifies the active and passive safety devices on cars with destructive tests that follow specific test protocols.

In particular, for the evaluation of pedestrian safety, the EuroNCAP carries out tests that simulate the impact of a person and then detect the degree of "aggressiveness" of the front part of the body towards the impactor (adult and child), but also the risk of injury to the head, pelvis, thighs and calves of the latter.

The tests carried out analyze front, side and rear impacts, tests for the head and for pedestrians.

Impact tests for pedestrian safety are carried out by impacting a car at a speed of 40 km / h against dummies equipped with special equipment in order to define the damage suffered and give it an assessment. The damage is classified into five levels each identified with a different color.

Green = good
Yellow = adequate
Orange = marginal
Brown = relevant
Red = severe

*Figure 4.18 Euro NCAP rating levels*

To evaluate the safety of pedestrians, numerical values and green stars with a variable number from 0 to 4 are used.



*Figure 4.19 Green star rating*

This also allows the front of the vehicle to be represented with cells of different colors depending on the influence that is found in the impact with the pedestrian. Then five variations of green, yellow, orange, brown and red color are observed.

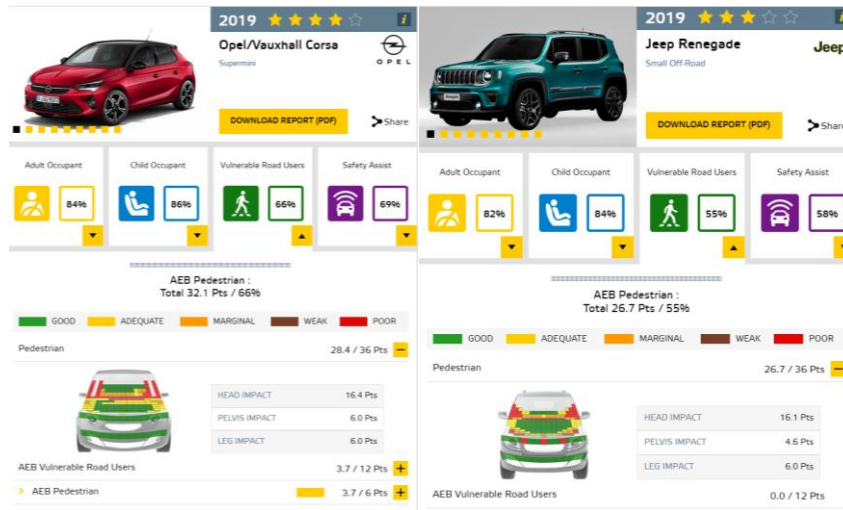


Figure 4.20 Example mapping of the front of the vehicle in relation to pedestrian safety passenger car (Opel corsa) b) SUV (Jeep Renegade) (taken from (EuroNCAP, <https://www.euroncap.com>, sd))

Thus the test results are correlated with damage scales such as HIC<sub>15</sub>.

Table 4.5 HIC- influence of the hood (EuroNCAP, 2012)

HIC <sub>15</sub>	<650	650-1000	1000-1350	1350-1700	≥1700
Head Injury Criterion	Green	Yellow	Orange	Brown	Red
	1 point	0.75 point	0.5 point	0.25 point	0 point

### 4.4.1 Pedestrian crash tests carried out by Euro NCAP

Crash tests are performed using standardized dummies and cars with different hood shapes. In the past, different dummies were used for each type of impact (front, side, etc.), but the most common is the Hybrid III with standardized characteristics.

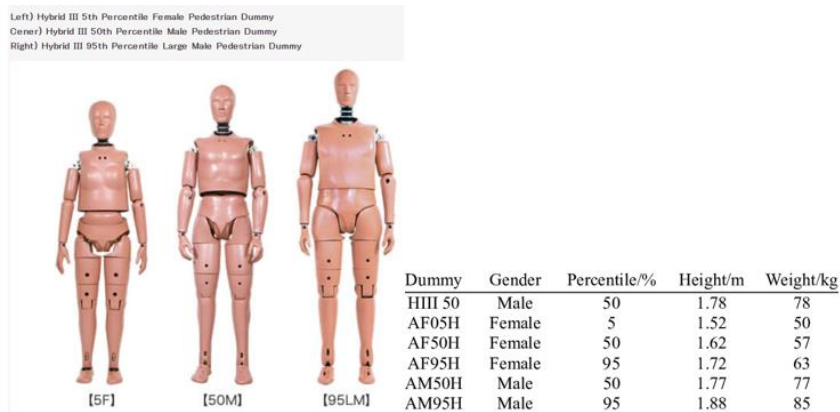


Figure 4.21 Hybrid III mannequins and features

The simulations are recorded by means of high-performance cameras in order to identify the real movements of the pedestrian following the impact, these are also detected by means of accelerometers placed on the vehicle.



*Figure 4.22 Crash test simulation*

From the processing of the frames and from the data obtained from the accelerometers it is possible to evaluate the influence of the different shapes of the hood on the movement of the dummy following the impact.

EuroNCAP for impact testing with pedestrians uses a standardized simulation procedure which is described in bulletin TB024 "Pedestrian Human model certification version 1.1 October 2018".

The pedestrian has defined dimensions deriving from physical tests and numerical simulations with "Human Body Model" (HB). This is a virtual geometric-mechanical representation of the human body, therefore it must consider the anatomy of the body consisting of a bone skeleton and soft tissues (feet, hands, face and ears are simplified).

Before proceeding with the vehicle-pedestrian impact simulations, it is necessary to certify the HBM (as foreseen in the CoHerent project (Klug et al., 2017)), to ensure that the results obtained can be comparable and reproducible.

In the HBM certification procedure, the kinematic response of the model is compared with those of known models in which there are pedestrian impacts of generic vehicles moving at speeds between 30 and 50 km/h.

In practice, a check of the robustness of the generic vehicle is carried out, with a series of tests in which a rigid cylindrical device is used.

Generic vehicles can be represented with four categories, namely:

- Family Cars (FC)
- Multi-Purpose Vehicles and Superminis (MPV)
- Roadsters (RDS)
- Sport Utility Vehicles (SUV)

The EuroNCAP simulations can be schematized with a sequence of phases reported in the bulletin. Following the simulation, the data are processed to extract the graphical and numerical outputs with which the quality criteria checks are carried out.

#### 4.4.2 The dummies used in crash tests

The dummies used in crash tests are built according to biomechanical criteria and are composed of numerous sensors that allow to verify acceleration of the head, tension, bending and rotation of the neck, the acceleration and compression of the chest, the acceleration of the pelvis, compression of the femur, pressure on the knees, pressure on the tibia, the integrity of ankles and feet. The arms are not instrumented due to the uncontrolled movement they undergo during frontal tests.

There are two types of sensors, the accelerometers that measure the accelerations of important parts of the body (such as brain, lung and heart) and the load cells that are positioned on the areas at risk of breaking due to compression (the bones).

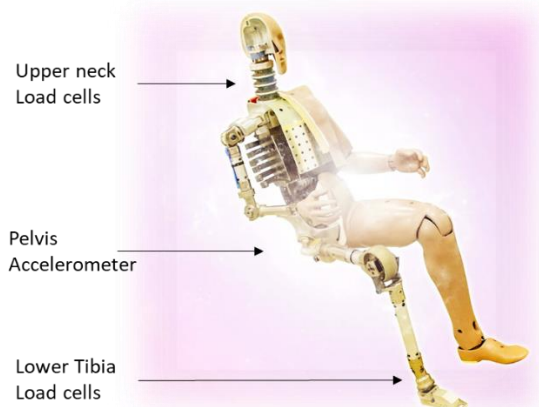


*Figure 4.23 Dummy sensors*

Both sensors are made up of resistors which, as a result of shocks, provide a series of voltages that are processed in real-time by particular acquisition equipment.

As for the accelerometer, each voltage corresponds to a certain well-defined acceleration value during the calibration phase and is measured in grams.

The load cells provide voltages which will then be compared with a tension-force scheme. These control devices allow the evaluation of forces (measured in N) and moments in the three xyz directions (measured in Nm).

In the past, dummies were differentiated according to the type of impact in order to obtain better dynamic responses. In fact, Hybrid III 50th, 95th and 5th (used for children) percentile were used for frontal impacts, today Thor is used which is similar to Hybrid III 50th percentile but with advanced features and instrumentation.

While the EUROSID 2 (ES-2) models in the EU are used for side impacts, (Sicurauto, sd), Rib Extension in the USA or the SID-II. Lately, the dummy called WorldSID is being introduced, with a view to harmonizing the world standard of mannequins for side impacts.

However, the most common is still the Hybrid III 50th percentile (which represent the physiognomic properties of 50% of the population). The appropriately instrumented dummy allows to verify: the acceleration of the head, the tension, the bending and rotation of the neck, the acceleration and compression of the chest, the acceleration of the pelvis, the compression of the femur, the pressure on the knees, the pressure on the tibia and the integrity of the ankles and feet (Sicurauto, sd).

To give response very similar to that of the human neck, the neck of the HYBRID III is equipped with a series of aluminum discs interposed with rubber discs, which represent the vertebrae, in addition, a cable runs along the vertical axis of the neck and acts by limiting lateral rotation.

From the experimental tests carried out on a 50 percentile HYBRID III dummy carried out by Arosio et al (2020) it can be seen that the accelerations increase as the fall height increases, moreover the maximum acceleration peak shifts over time as the fall height increases. A similar trend is recorded for the forces in the neck. Therefore, starting from the acceleration data, the injuries are correlated.

## **4.5 Calibration of numerical multi-body model for the reconstructions of vehicle-pedestrian impacts**

In order to reconstruct the vehicle-pedestrian collision phenomena, numerical analyzes are started using a pedestrian model based on the multibody system, while the vehicle is schematized as a rigid body.

The "multibody" simulation was used in this study to carry out the numerical analysis of pedestrian-vehicle collisions in a direct way, "forward calculation", by means of an iterative process that allows simulating both the pre and post-impact kinematic phase and the real bump. Ultimately, by carrying out more simulations and varying the input data it is possible to faithfully reproduce what happens in reality.

For the vehicle-pedestrian impact simulations, the model of dummy used is a "HYBRID III 50 percentile" which represents an average man with a height of 175 cm and a weight of 77 kg.

The multibody model proposed by the software considers a mannequin consisting of a series of rigid parts (such as head, torso, arms and legs interconnected by means of joints or joints) represented by ellipsoids.

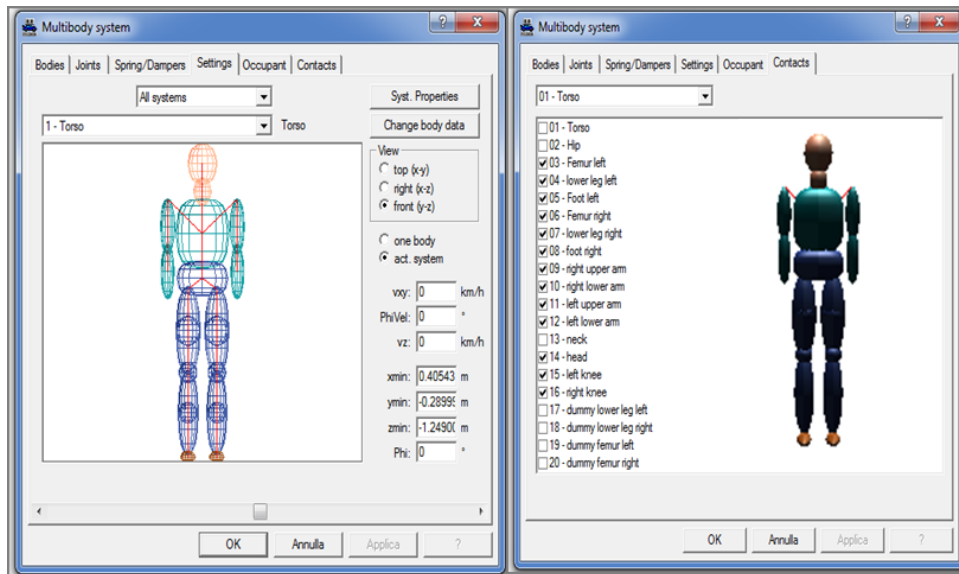


Figure 4.24 Multibody model proposed by the software (image taken from the software)

The software allows you to change the angles of each of the individual rigid parts of the body, making the dummy take the desired position and to set the height, weight and age.

According to the position that the dummy assumes with respect to the direction of travel of the car, the interconnections along the x, y and z axes must be stiffened (blocking).

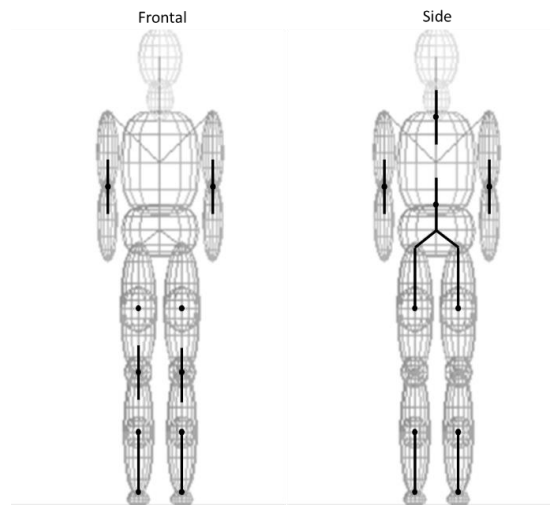


Figure 4.25 In black the parts to be selected and locked

This model automatically calculates the collisions between the individual parts considering that the system reacts to the force of gravity and the forces of collision with the ground vehicle; the weak point is the impossibility of simulating the movement of the pedestrian who will be positioned in the desired way in front of the front hood of the vehicle.

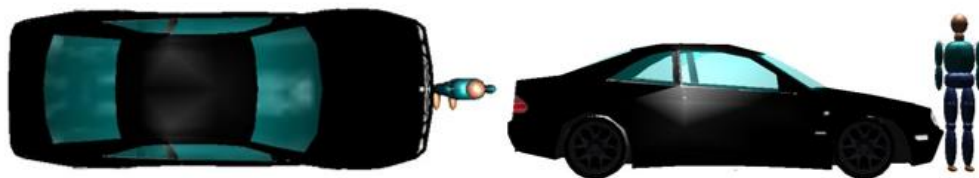


Figure 4.26 Top view and side view of the dummy placement (Taken from the Software)

In order to start the simulations, the initial conditions of the vehicle (speed, trajectory, braking), of the pedestrian (age, height, weight, position with respect to the car) and the type of simulation to be started (kinetics or kinematics) have been defined.

Furthermore, the coefficients of friction must also be entered. Specifically, there is the "Frict. Ground" coefficient between the multibody and the ground and the "Frict. Cars" which represents the coefficient of friction between the multibody and the vehicle. Therefore, a coefficient of 0.3 was chosen for Friction cars (EuronCAP, 2018) while for the Friction Ground 0.6 was chosen (Astrid, Clay, Anthony, Brian, & al., 2005).

The software assigns two different colors to the dummy, which appear on the quadrants of each ellipsoid, and which, following the impact, change to red for the parts that have been damaged.



*Figure 4.27 Color of the single covers in the pre-impact phase and colors of the single bodies in the post-impact phase. (Taken from the software)*

In addition to the dummy, it is also necessary to define the type of vehicle to be used, this can be done by defining it from scratch or by taking it from one or more databases contained in it.

The databases contained in the software are:

- DSD or standard DSD database;
- KBA or German Department of Transport database;
- DSDJapan2000 or DSD standard Japanese database;
- ADAC95 or European database of 1995;
- Spe that is Canadian Specs database, it includes most passenger cars and light trucks marketed in North America.

For this work, the DSD 2006 database was used.

The initial conditions of the vehicle (speed, trajectory, braking), of the pedestrian (age, height, weight, position with respect to the car) and the type of simulation to be started (kinetics or kinematics) have been defined.

The simulation allows the graphic visualization of the crash dynamics, thanks to a 3D representation, which can be immediately compared with that of the crash tests actually performed in order to evaluate its reliability.

Once the simulation is complete, the graphs associated with the dynamic interaction between vehicle and pedestrian can be viewed.

The software, for each of the 16 components of the multibody pawn, allows you to view graphs that allow you to consider:

- Distance;
- Speed;
- Acceleration;
- Rotation angle;

- Angular speed;
- Angular Acceleration;
- Kinetic energy);
- Contact forces;
- Elastic forces.

For all items, except for energy, four values are provided along the x, y and resultant axes for each component of the multibody system.

## 4.6 Software calibration and parametric analysis

### 4.6.1 Software calibration

The study conducted by Corallo F. et al. (2018) was used to calibrate the software; in which the reconstruction of an impact with multibody modeling between a teenage pedestrian and an SUV is considered. In the simulation, the pedestrian dummy is stationary and it is positioned in a lateral or frontal respect to the bonnet of the car which is advanced at a constant speed and then with vigorous breaking upon impact. The speeds of the car are made to vary from 20 to 50 Km/h (with the ace of 10 Km/h, as proposed by EuroNCAP) imagining that the collision takes place in an urban environment.

From these simulations, the maximum acceleration values to the head and torso at different speeds were obtained, from which the HIC and TTI were obtained; both the injuries and the accelerations obtained were then compared with those of the article.

#### Input data for simulation setup

To calibrate the simulation that allows you to determine the motion of the pedestrian following the impact with the vehicle at a certain speed, the following parameters have been implemented in the software:

- Vehicle

Template:	<i>BMW X5d &amp; G- 160Kw, 01.2003-12.2005 E53</i>
Kw Weight of the car:	<i>2270 Kg</i>
Length:	<i>4.67m</i>
Width:	<i>1.88m</i>
Height:	<i>1.71 m</i>
Type of front:	<i>high front vehicle</i>

As the type of vehicle requested was not available in the database, the one with similar characteristics was taken and the mass was subsequently modified.

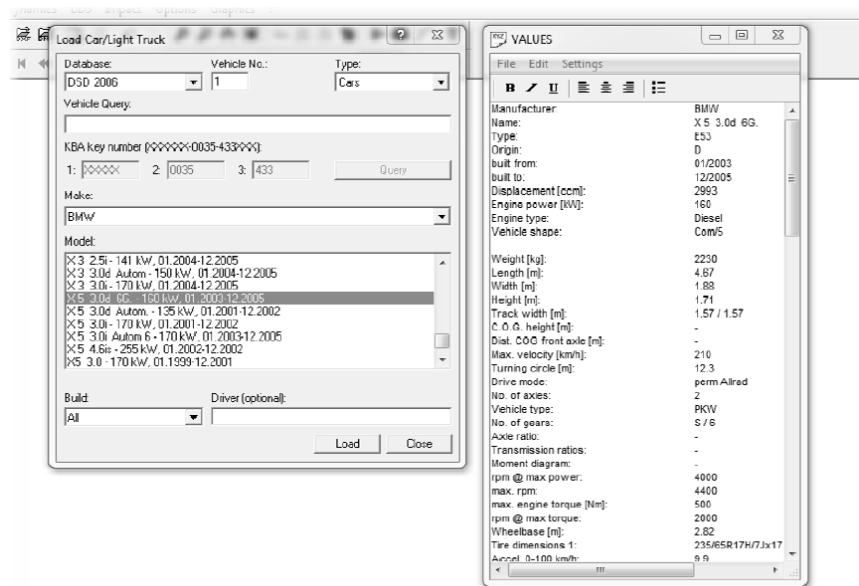


Figure 4.28 Characteristics of the car

- Pedestrian

Type of mannequin:	<i>Hybrid III 50th percentile</i>
Weight:	<i>45 Kg</i>
Height:	<i>1.45 m</i>
Age:	<i>15 years</i>
Multibody Speed:	<i>0 Km / h</i>
Return:	<i>0.10</i>
Friction with the ground:	<i>0.60</i>
Vehicle friction:	<i>0.30</i>

The following simulation scenarios were assumed:

- scenario 1: the vehicle proceeds at a constant speed, without slowing down following the impact;
- scenario 2: the vehicle brakes vigorously at the moment of impact with the pedestrian until it stops. To set the forceful braking in the person in which the car collides with the pedestrian, a deceleration of 6.47 m/s<sup>2</sup> is required to stop, with a perception and reaction time of the driver equal to 1.2 seconds and a time of response of the braking system equal to 0.2 seconds.

In each of the two scenarios, the different position of the pedestrian with respect to the windshield was considered, so it can be schematized as follows:

- ✓ Scenario 1.1T constant speed vehicle and teenager pedestrian in front, upright and central position with respect to the vehicle hood;
- ✓ Scenario 1.2T constant speed vehicle and teenager pedestrian in lateral, upright and central position with respect to the vehicle hood;
- ✓ Scenario 2.1T vehicle that initiates vigorous braking at the instant of impact with the teen pedestrian who is in front, upright and central position with respect to the vehicle hood;
- ✓ Scenario 1.2T vehicle that initiates vigorous braking at the instant of impact with the teen pedestrian who is in a lateral, upright and central position with respect to the vehicle hood;

The position of the dummy was set by blocking, as previously described, the components of the multibody in the appropriate section of the "multibody system" software. Once the simulation has been started, the vehicle is made to proceed under the desired conditions and through the 3D view it is possible to compare the resulting frames with those taken from the article.

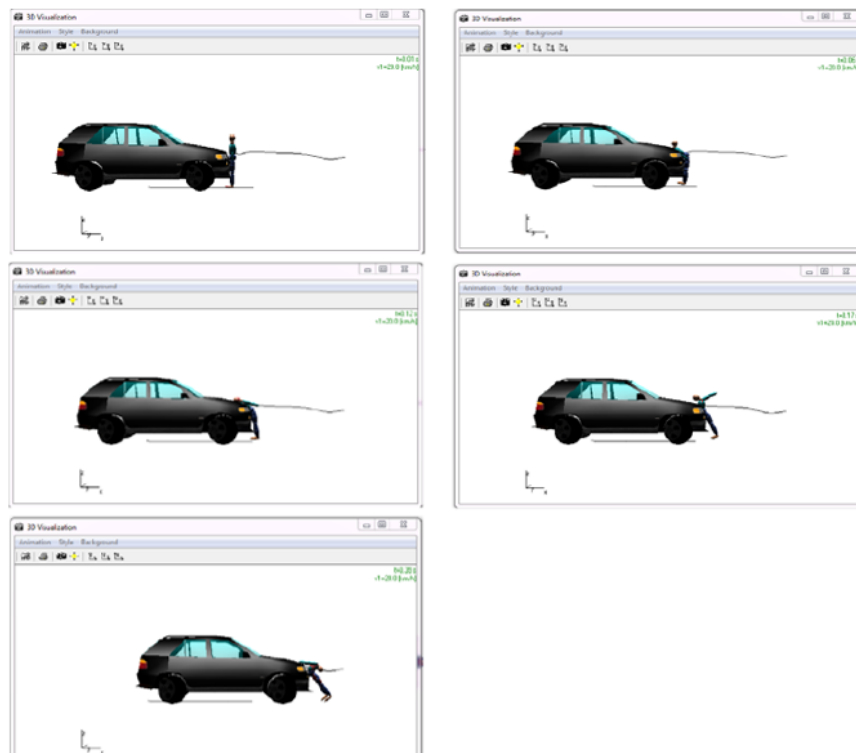


Figure 4.29 Sequence of images that compare the simulated crash-test with that of the article

The succession of images highlights how the movement of the pedestrian in the simulation is very similar to the real one.

After the simulation, the graphs relating to the resulting accelerations to the head and torso as a function of time were obtained.

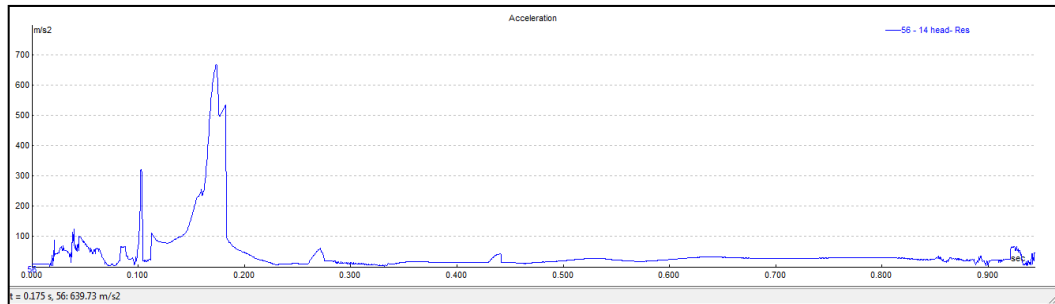


Figure 4.30 Graphic-analytical determination of the head's accelerations provided by the numerical simulation

On the graph, it is possible to observe that acceleration occurs on the ordinate axis (m/s<sup>2</sup> but must be converted into g) and time (seconds) on the abscissa axis.

It should be noted that around 0.2 seconds there is always the maximum acceleration peak at the head, which represents the moment of impact of the head against the windscreen of the vehicle.

The goal was to carry out the simulations by implementing the same input data available to then verify the graphical and numerical feedback by comparing the sequence of frames as well as the graphical-analytical response relating to the accelerations of the head.

Once the simulations were started, the resulting acceleration graphs at the head were obtained from which the maximum acceleration of the primary impact was obtained and, as previously described, the HIC was evaluated.

These simulation parameters are then compared with those in Corallo F. et al. (2018) and it can be observed a fairly good correlation with Pearson's values equal to 0.92 with the SUV and to 0.89 for the sedan, whereas those for HICs seems lower (0.73 for the SUV and 0.84 for the sedan).

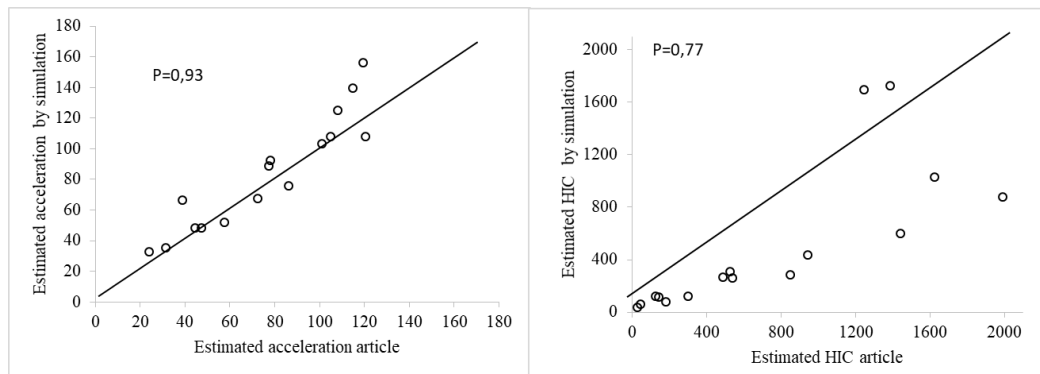


Figure 4.31 Comparison of data from simulation and those reported in (Carollo F., 2018) (teenager-SUV)

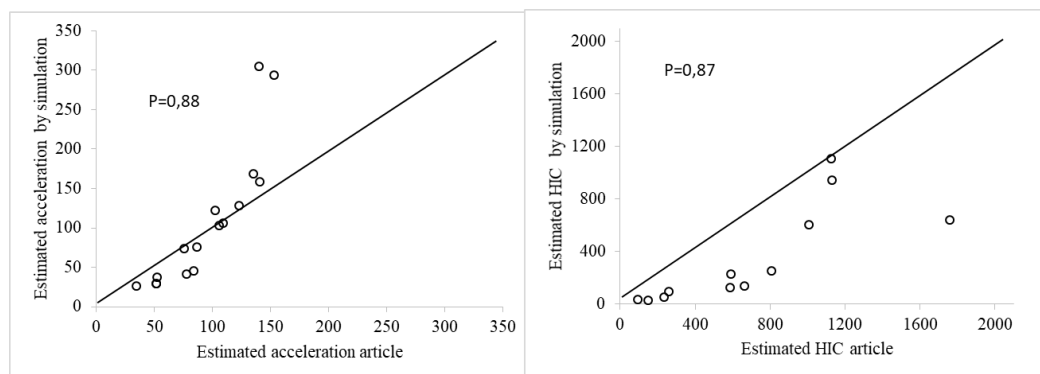


Figure 4.32 Comparison of the simulation results with those reported in (Carollo F., 2018) (teenager-sedan)

This allows to say that the results obtained in terms of accelerations are not dissimilar from each other therefore the model is calibrated correctly, but there are differences in terms of HIC that can be attributed to a different accelerometric trace. This can be attributed to a greater rigidity of the dummy, therefore to the different degrees of constraint, used in the simulations which gives more precautionary results.

## 4.6.2 Other simulations

Once it was verified that the parameters used made the simulations reliable and that the calculation methods to estimate the parameters of injury were correct, further simulations were carried out.

The aim is to study the influence of the impact speed and the shape of the front of the vehicle on the kinematic response and the risk of injury to pedestrians in collisions with different vehicles.

Five types of vehicles (coupe, SUV, sedan, van and bus) and four pedestrian models (child, teenager, 50th percentile adult and big adult) were used in various impact speed

simulations. The general kinematics and impact conditions were analyzed for different speeds and pedestrian positions.

Initially, new simulations were carried out while keeping the car unchanged but using an adult pedestrian placed frontally and sideways to the SUV instead of a teenager.

- Vehicle

Template:	<i>BMW X5d &amp; G- 160Kw, 01.2003-12.2005 E53</i>
Kw Weight of the car:	<i>2270 Kg</i>
Length:	<i>4.67m</i>
Width:	<i>1.88m</i>
Height:	<i>1.71 m</i>
Type of front:	<i>high front vehicle</i>

- Pedestrian

Type of mannequin:	<i>Hybrid III 50th percentile</i>
Weight:	<i>75 Kg</i>
Height:	<i>1.70 m</i>
Age:	<i>30 years</i>
Multibody Speed:	<i>0 Km / h</i>
Return:	<i>0.10</i>
Friction with the ground:	<i>0.60</i>
Vehicle friction:	<i>0.30</i>

Also, in this case, four simulation scenarios were considered, called:

- Scenario 1.1 At constant speed - frontal adult pedestrian;
- Scenario 1.2 At constant speed - side adult pedestrian;
- Scenario 2.1A vehicle braking - frontal adult pedestrian;
- Scenario 2.2A braking vehicle - side adult pedestrian.

Subsequently, other simulations were carried out, varying the type of car and pedestrian, always considering the four scenarios, both for the adult pedestrian and for the adolescent in order to compare the damage based on the front part of the car.

- Vehicle

Template:	<i>BMW X5d &amp; G- 160Kw, 01.2003-12.2005 E53</i>	<i>(C208) Coupé CLK 200 2.0 16V-100Kw, 01.1999-12.2001</i>	<i>Sedan Fiat Stilo 1.6 16V Dynamic-76 KW 01.2001-12.2002</i>	<i>Bus. MAN Doppeldecker ND 202 162 Kw, 01.1995-12.1999</i>	<i>Van IVECO Daily 35-12V-90 KW, 01.1996-12.2002</i>
Vehicle weight:	<i>2270 Kg</i>	<i>1300 Kg</i>	<i>1270 Kg</i>	<i>11500 Kg</i>	<i>2320 Kg</i>
Length:	<i>4.67m</i>	<i>4.57m</i>	<i>4.18 m</i>	<i>11.74m</i>	<i>6.89 m</i>
Width:	<i>1.88m</i>	<i>1.72m</i>	<i>1.78 m</i>	<i>2.48 m</i>	<i>2.10 m</i>
Height:	<i>1.71 m</i>	<i>1.37 m</i>	<i>1.47 m</i>	<i>3.52m</i>	<i>2.63 m</i>
Type of front:	<i>high front vehicle</i>	<i>low front vehicle</i>	<i>low front vehicle</i>	<i>flat front vehicle</i>	<i>flat front vehicle</i>

## - Pedestrian

	<i>Adult</i>	<i>Big adult</i>	<i>Teenager</i>	<i>Child</i>
Type of dummy:	<i>Hybrid III 50th percentile</i>	<i>Hybrid III 50th percentile scaled</i>	<i>Hybrid III 50th percentile scaled</i>	<i>Hybrid III 50th percentile scaled</i>
Weight:	<i>75 Kg</i>	<i>100 Kg</i>	<i>45 Kg</i>	<i>20 Kg</i>
Height:	<i>1.70 m</i>	<i>1.88 m</i>	<i>1.45 m</i>	<i>1.15 m</i>
Age:	<i>30 years</i>	<i>50 years</i>	<i>15 years</i>	<i>6 years</i>
Multibody Speed:	<i>0 Km / h</i>	<i>0 Km / h</i>	<i>0 Km / h</i>	<i>0 Km / h</i>
Return:	<i>0.10</i>	<i>0.10</i>	<i>0.10</i>	<i>0.10</i>
Friction with the ground:	<i>0.60</i>	<i>0.60</i>	<i>0.60</i>	<i>0.60</i>
Vehicle friction:	<i>0.30</i>	<i>0.30</i>	<i>0.30</i>	<i>0.30</i>

### 4.6.3 Parametric analysis

Once the 3D simulations were started, all the output graphs relating to the acceleration of the dummy for the different pedestrians in relation to the speeds were analyzed. It is observed that the peaks present different accelerations depending on the part of the body and the frontal area of the car (bonnet or windshield) affected.

To assess the extent of the injury suffered by a pedestrian following a collision with a vehicle, not only the peak value of the acceleration is sufficient but also its duration over time. In fact, it can be noted that a very high peak acceleration of a very short duration does not produce an appreciable displacement of the head and vital organs, for this reason, reference has been made to the various parameters of injury.

So as described above (par 4.2), the extent of the injury suffered by the pedestrian was assessed with the acceleration parameters, therefore the corresponding AIS and ISS were estimated for the various scenarios.

## 4.7 Evaluation of injury level by existing prediction function

To define the injury risk functions, logistic models were used, obtained as a result of laboratory experiments, with which it is possible to determine the biomechanical response and the level of tolerance to injuries.

The logistic regression models, which are used to estimate the effect of one or more factors on the probability of injury, are binary.

$$P_i = \frac{1}{1 + \exp(a + b \cdot Y_{ped} + c \cdot V)} \quad 4.5$$

where:

$P_i$ , probability of a specific injury level;

a, b, c are the calibration parameters;

$Y_{ped}$  is the age of the pedestrian;

$V$  the speed of the car (considered constant).

Therefore by means of these function it is possible to estimate the probability that following an injury the pedestrian can reach or exceed a certain level of severity. Starting from the vulnerability functions for assigned ISS (Helmer, 2015), implemented on GIDAS data (2010), the five degrees of severity of the lesion and the respective probability estimates were identified, as shown in the table

Table 4.6 Probability of injury based on severity

Severity of the injury	ISS range	P (ISS)
Minor	0-8	$1 - P(ISS_{9+})$
Mild	9-15	$P(ISS_{9+}) - P(ISS_{16+})$
Moderate	16-25	$P(ISS_{16+}) - P(ISS_{25+})$
Serious	26-75	$P(ISS_{25+})$
Not survivable	$> 75$	$P(\text{fatalities})$

These models estimate the probability of an injury considering two explanatory variables, namely the age of the pedestrian and the speed of the car.

Starting from these models, the probabilities associated with the different levels of injury were assessed.

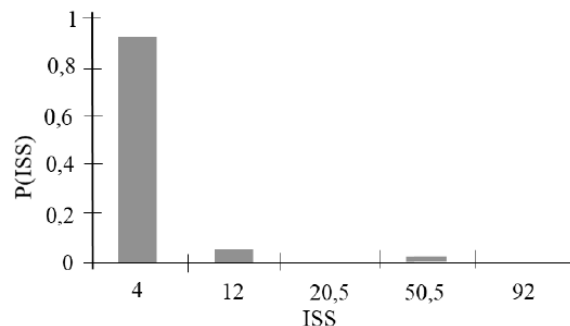


Figure 4.33 Example of ISS probability distribution derived from vulnerability prediction functions

From this for each age-speed pair the expected value was obtained:

$$ISS_{\text{vulnerability model}} = \sum P(ISS) * ISS_{\text{average of the interval}} \quad 4.6$$

Then different input parameters such as the age of the pedestrian and the travel speed of the car (steady mode), the position of the pedestrian (front or side with respect to the bonnet of the car) and the type of car (SUV, sedan, cabrio) have been changed and an overall ISS average value,  $ISS_{\text{average}}$  has been evaluated to be compared with that provided by the vulnerability prediction functions,  $ISS_{\text{vulnerability model}}$ . The comparison between the two ISS, taking into consideration an adult pedestrian of 30

years and a 15-year-old teenager is reported below for several vehicle (steady) speed values.

Table 4.7 ISS vulnerability model-ISSaverage comparison

Pedestrian's age	V (Km/h)	ISS vulnerability model	ISSaverage
15	20	5.16	3.07
	30	6.40	5.4
	40	8.84	12.3
	50	13.44	27.72
30	20	5.76	0.85
	30	7.35	1.9
	40	10.79	7.35
	50	17.32	25.075

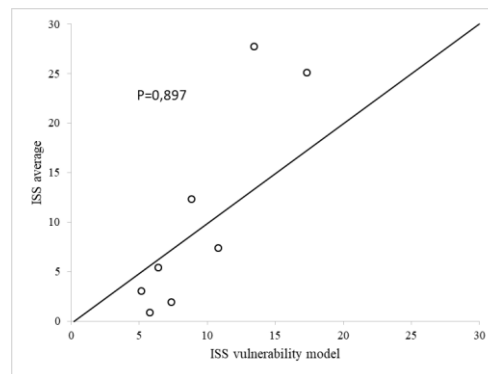


Figure 4.34 ISS vulnerability model-ISSaverage comparison (teenager-adult pedestrian)

The agreement between the average outcome provided by the simulation models and that derived from vulnerability prediction functions seem fairly acceptable. However further simulations are needed in order to improve it.

## 4.8 Conclusions

The aim of the work is to analyze the vehicle-pedestrian impact dynamics, as recent national and international accident reports provide evidence for an increase of crashes involving pedestrians. In this connection, refined pedestrian vulnerability prediction tool are needed to help road safety engineers. It is believed that multibody accident reconstruction models may offer a significant contribution in improving existing pedestrian vulnerability predictions functions.

To this purpose, a multibody pedestrian vehicle impact model has been developed. Following an initial calibration by a comparison with data provided by technical and

scientific literature, a parametric analysis has been carried out by varying several pedestrian and vehicle related impact parameters. From kinematic and mechanical results obtained by numerical simulations, injury level evaluation has been performed and an estimation of an average values of ISS has been derived. This value obtained for several vehicle speed and pedestrian type has been compared with an average ISS value derived from existing pedestrian vulnerability prediction functions that have been calibrated on real accident data collected in a German in-depth accident database (GIDAS).

The comparison is fairly acceptable and more simulations are needed in order improve the modelling framework. However, basing on these preliminary results, the multibody pedestrian-vehicle impact developed seems to be able to capture the complexity of this accident scenario and to provide a reliable estimation of possible outcomes.

The results of the simulations allow us to observe that:

- the geometry of the vehicles greatly affects pedestrian injuries, and therefore there is a need to classify the types of impact not only based on the speed of impact but also based on the geometry of the front. In fact, short fronts with a relatively high hood edge and large windshield area (like that of the minicar) could result in a head impact closer to the central area of the windshield reducing fatal head injuries in pedestrians.
- the impact speed of the vehicle has a significant influence on the severity of the injury, especially in adult pedestrians. Reducing the speed of impact is an effective means of mitigating the severity of pedestrian injuries in impacts with various types of vehicles. The simulation results show that the likelihood of a fatal head injury is low at speeds of 30 km/h or less; it follows that if the impact speed of the vehicle is less than 30 km/h, the accident parameters can be reduced.
- the shape of the front of the vehicle and the size of the pedestrian are the factors that influence the risk of injury of each region of the body. Head impact speed decreases with an increase in the height of the hood edge and a center height of the lower bumper. The stiffness of the area that comes into contact with the head greatly affects the resulting severity of the injury.

It will therefore be necessary to extend the analyzes by considering additional injury parameters, for example to the lower extremities or the chest, in order to better understand the effects of a vehicle-pedestrian collision. Through the simulations, it will therefore be possible to get to know a priori the effects of particular impact

scenarios and thus prevent them by affecting the characteristics of the environments that users go through.

By an extensive use of the proposed model it is believed that it will be possible to add a better understanding of the complex kinematic of impacted pedestrians and provide more significant explanatory variables in the existing pedestrian vulnerability prediction functions. This will allow safety engineers to highlight site conditions affecting the initial pedestrian-vehicle impact parameters and therefore to study mitigations countermeasures.

## References

- AAAM. 2008. The Abbreviated Injury Scale (AIS) 2005.
- Anderson, R., McLean, A., & et al. 1997. Vehicle travel speeds and the incidence of fatal pedestrian crashes. *Accid Anal Prev* , 29(5): 667-74.
- Arosio, B., Benetton, D., Mongiardini, M., Mattos, G., Gzerbieta, R., Anghileri, M., & et al. 2020. *Biomeccanica Forense. Confronto tra Hybrid III e modello di corpo umano in lesioni alla testa in impatti con pendolo e test di caduta verticale.*
- Association for the Advancement of Automotive Medicine. 2001. The Abbreviated Injury Scale. 1990 rev., update 1998. Barrington, IL: Association for the Advancement of Automotive Medicine.
- Astrid, L., Clay, D., Anthony, C., Brian, F., & et al. 2005. Mathematical simulations of real world pedestrian-vehicle collisions. 19th International Technical Conference on the Enhanced Safety of Vehicles (ESV). Washington DC, United States, Date.
- Bahman SR, C. N. 2005. An evaluation of the association between vehicle type and the source and severity of pedestrian injuries. *Traffic Inj Prev.* , 6: 185–192.
- Baker, S., & O'Neil, B. 1976. The injury severity score: an update. *J Trauma*.16: 882-885.
- Baker, S., O'Neill, B., Haddon, W., & Long, W. 1974. The injury severity score: a method for describing patients with multiple injuries and evaluating emergency care. *J Trauma*, 14:167–196.
- Battaglia S., D. I. 2006. The sports bicycle. Geometric and inertial characteristics. Dynamic simulation. Rome: Aracne.
- Bellavia G., V. M. 2009. Development of an Anthropomorphic model for Vehicle - Pedestrian Crash Test, *Automotive Engineering. XXI Science and Motor*

- Vehicles 2007, JUMV international Conference with Exhibition, 62, p. 48-56; (3/4). Belgrade, Serbia.
- Bellavia G., V. M. 2009. Multibody Numerical Simulation For Vehicle - Pedestrian Crash Test, Motor vehicle engineering ATA. XXI Science and Motor Vehicles 2007, JUMV international Conference with Exhibition, Vol. 62, 11/12, pp 40-49.
- Belwadi, A., & Yang, K. 2008. Response of the cadaveric lumbar spine to flexion with and without anterior shear displacement. Proceedings of IRCOBI conference, (p. pp 397–410).
- Boyd, C., Tolson, M., & Copes, W. 1987. Evaluating trauma care: the TRISS method. Trauma Score and the Injury Severity Score. *J Trauma*, 27: 370–378.
- Carollo F., V. M. 2018. Head, chest and femur injury in teenage pedestrian – SUV crash; mass influence on the speeds. *Journal of Automobile Engineering, Part D*.
- Champion, H., Copes, W., Sacco, W., Lawnick, M., & et al. 1990. The Major Trauma Outcome Study: establishing national norms for trauma care. *J Trauma*, 30:1356–1365.
- Chen H, P. D. 2015. Pedestrian response with different initial positions during impact with a mid-sized sedan. Paper presented at: 24th International Technical Conference on the Enhanced Safety of Vehicles (ESV).
- Copes, W., Champion, H., Sacco, W., Lawnick, M., & et al. 1988. The injury severity score revisited. *J Trauma*, 28:69–77.
- Davis, G. 2001. Relating severity of pedestrian injury to impact speed in vehicle pedestrian crashes - Simple threshold mode. *TRB Distinguished Lecture, Pt 1 - Bicycle and Pedestrian Research, Pt 2(1773): 108-113*.
- Ebner A., S. R. 2010. Methodology for the development and evaluation of active safety systems using reference scenarios: Application to preventive pedestrian safety. . In *Proceedings of the International Research Council on Biomechanics of Injury (IRCOBI)*, 155-168.
- Ebner A., Samaha RR, Scullion P., Helmer T. 2010. Identifying and analyzing reference scenarios for the development and evaluation of preventive pedestrian safety systems.
- EuroNCAP. 2012. European New Car Assessment Program - Assessment Protocol Pedestrian Protection. [www.euroncap.com](http://www.euroncap.com) .
- EuronCAP. 2018. Pedestrian Human Model Certification ,Version 1.1.
- EuroNCAP. (s.d.). <https://www.euroncap.com>.

- European Commission. (s.d.). Road traffic accidents statistics.
- FMVSS 201U. 1998. Occupant Protection in Interior Impact. Upper Interior Head Impact Protection.
- Fredriksson, R., Rosen, E., & Kullgren, A. 2010. Priorities of pedestrian protection—a real-life study of severe injuries and car sources. *Accid Anal Prev.*, 42:1672–1681.
- GIDAS. 2010. German In-Depth Accident Study. Tratto da [http://www.gidas.org/files/GIDAS\\_eng.pdf](http://www.gidas.org/files/GIDAS_eng.pdf)
- Han, Y., Peng, Y., Peng, Q., Huang, H., & Mizuno, K. 2013. A Study on Kinematic Behavior and Head Injury Risk in Vehicle to Pedestrian Collisions. Fifth International Conference on Measuring Technology and Mechatronics Automation. Hong Kong, China.
- Hannan, E., Hicks Waller, C., Szypulski Farrell, L., & Cayten, G. 2005. A comparison among the abilities of various injury severity measures to predict mortality with and without accompanying physiologic information. *J Trauma*, 58:244–251.
- Hannawald, L., & Kauer, F. 2004. Equal Effectiveness Study on Pedestrian Protection. Technische Universität Dresden. Dresden, Germany.
- Helmer T., E. A. 2009. Präventiver Fußgängerschutz - Anforderungen und Bewertung. Aachen:18. Aechener Kolloquium Fahrzeug- und Motorentechnik.
- Helmer, T. 2015. Development of a Methodology for the Evaluation of Active Safety using the Example of Preventive Pedestrian Protection, Doctoral Thesis accepted by Technische Universität Berlin, Germany. DOI 10.1007/978-3-319-12889-4.
- Helmer, T., Ebner, A., & et al. 2010. Injury risk to specific body regions of pedestrians in frontal vehicle crashes modeled by empirical, in-depth accident data. *Stapp Car Crash J*, 54: 93-117.
- Klug, C., Feist, F., Raffler, M., Sinz, W., Petit, P., Ellway, J., & van Ratingen, M. 2017. Development of a Procedure to Compare Kinematics of Human Body Models for Pedestrian Simulations. IRCOBI. 2017 IRCOBI Conference Proceedings. (p. pp. 509–30). Università di Tecnologia.
- Kong CY, Y. J. 2010. Logistic regression analysis of pedestrian casualty risk in passenger vehicle collisions in China. *Accid Anal Prev.*, 42:987-993.
- Liu, X., Yang, J., & Lövsund, P. 2002. A Study of Influences of Vehicle Speed and Front Structure on Pedestrian Impact Responses using Mathematical Models. *Traffic Injury Prevention*, 3(1): 31-42.

- MacKenzie, E., Damiano, A., Miller, T., & S., L. 1996. The development of the Functional Capacity Index. *J Trauma*, 41:799–807.
- Martin, J., Lardy, A. et al. 2011. Pedestrian injury patterns according to car and casualty characteristics in france. *Ann Adv Automot Med*, 55: 137-46.
- Meredith, J., Evans, G., Kilgo, P., MacKenzie, E. et al. 2002. A comparison of the abilities of nine scoring algorithms in predicting mortality. *J Trauma*, 53:621–628.
- Mizuno, Y. 2005. Summary Of IHRA Pedestrian Safety WG Activities (2005) - Proposed Test Methods To Evaluate Pedestrian Protection Afforded By Passenger Cars. . The 19th International Technical Conference on the Enhanced Safety of Vehicles. . Washington, DC.
- Mizuno, Y. 2005. The 19th International Technical Conference on the Enhanced Safety of Vehicles. Summary Of IHRA Pedestrian Safety WG Activities (2005) -Proposed Test Methods To Evaluate Pedestrian Protection Afforded By Passenger Cars. Washington, D.C.
- Myers, B., Arbogast, K., Lobaugh, B., Harper, K., Richardson, W., & Drezner, M. 1994. Improved assessment of lumbar vertebral body strength using supine lateral dual-energy X-ray absorptiometry. *J Bone Min Res* , 9(5):687–693.
- Naif AS, S. B. 2009. In-depth analysis of pedestrian crashes in Riyadh. *Traffic Inj Prev.*, 10: 552–559.
- National Highway Traffic Safety Administration. 1981. Report: Issue 9. Part 2.
- NHTSA. (s.d.). Tratto da U.S. Department of Transportation: <http://www.nhtsa.gov/cars/rules/.../PEA/pea-III.n.pdf>
- NHTSA. 2001. Traffic Safety Facts 2001: A Compilation of Motor Vehicle Crash Data from the Fatality Analysis Reporting System and the General Estimates System. Washington, DC:US: Department of Transportation National Highway Traffic Safety Administration.
- Oh, C., Kang, Y. et al. 2008. Development of probabilistic pedestrian fatality model for characterizing pedestrian-vehicle collisions. *International Journal of Automotive Technology*, 9(2): 191-196.
- Olukoga IA. 2003. Pedestrian casualties and fatalities in road traffic crashes in a South African municipality. *Traffic Inj Prev.* , 4: 355–357.
- Otte D, K. C. 2003. Scientific approach and methodology of a new in-depth-investigation study in Germany so called GIDAS. Paper presented at: ESV Conference . Nagoya, Japan.

- Otte, D. 1994. Influence of the front hood length for the safety of pedestrians in car accidents and demands to the safety of small vehicles. SAE Technical Paper No.942232.
- Pasanen, E., & Salmivaara, H. 1993. Driving speeds and pedestrian safety in the city of Helsinki. *Traffic Eng. Control*, 34: 308-310.
- Perry, J. 1992. *Gait analysis: Normal and pathological function*: Slack.
- Piano L. 2013. Passive safety of motor vehicles. Design and experimentation criteria.
- Rosen, E., & Sander, U. 2009. Pedestrian fatality risk as a function of car impact speed. *Accid Anal Prev* , 41(3): 536-42.
- Shojaati M. 2003. Correlation between injury risk and impact severity index ASI. In: *Proceedings of the 3rd Swiss Transport Research Conference*, pp. 19–21.
- Sicurauto. (s.d.). Tratto da <https://www.sicurauto.it/crash-test-video/test-speciali/tutti-i-manichini-da-crashtest-presenti-nel-mondo-automotive|hybrid-3.htm>
- Stephenson, S., Langley, J., & Civil, I. 2002. Comparing measures of injury severity for use with large database. *J Trauma*, 53:326–332.
- UMTRI. 2005. 1994–1998 NASS pedestrian crash data study (PCDS) codebook. . Version 03 Mar01. UMTRI Transportation Data Center.
- Vangi, D. et al. 2008. *Ricostruzione della dinamica degli incidenti stradali*. Firenze University Press.
- Virzi Mariotti G., G. S. 2014. Determination and analysis of the head and chest parameters by simulation of a vehicle-teenager impact. *Journal of Automobile Engineering*, 228(1):3-20(DOI:10.1177/0954407013501487).
- Yang JK. 1997. Injury biomechanics in car-pedestrian collisions: development, validation and application of human-body mathematical models. Doctoral Dissertation, Department of Injury Prevention, Chalmers University of Technology. Sweden.
- Yang JK, a. L. 1997. Development and validation of a human body mathematical model for simulation of car pedestrian collisions. . In *Proceedings of IRCOBI Conference*, pp. 133–149.
- Yang, J. 2005. Review of injury biomechanics in car-pedestrian collisions. *Int. J. Vehicle Safety*. Vol. 1 (1/2/3): 100-117.

# **CHAPTER 5. COUNTERMEASURES: DESIGN CHOICES FOR THE PROTECTION OF PEDESTRIANS AND CYCLISTS**

Globally, as explained in detail in the introduction, countries are striving to reorganize transport networks by promoting a new form of mobility that is sustainable and healthy for citizens. The task assigned to the designers is to create interconnected, safe, attractive and comfortable routes so that users begin to change their habits by preferring alternative modes of transport to motorized ones. In this chapter a preliminary procedure was defined for the choice of the different types of pedestrian and cycling routes starting from the characteristics of the area but above all from the flows that interest it. Once the interventions that can be implemented have been defined, through a benefit-cost analysis and with the help of technical guides, it is possible to evaluate which are the most convenient and effective.

## **5.1 Risk-based prioritization**

Most roads must accommodate a wide range of users. Each of these has different needs, which often conflict, so a balance must be sought between allocating limited space and the level of service provided to each user group.

To obtain an integrated approach, a hierarchy is used that strives to:

- plan the environments by identifying the importance of each mode of travel;
- identify the importance of each travel modality based on local needs. In some cases, the user hierarchy might even change at different times of the day (for example before and after school).

This approach involves understanding the interaction of different modes of transport and requires awareness of the impacts they have on the transport network.

Then the benefits and costs of the different planning or treatment decisions for each group of road users have to be evaluated.

Before choosing the measure to be carried out, it is necessary to identify the high-risk areas, therefore where more accidents occur. These are usually found mainly in built-up areas where there are high flows that are in conflict. A synthetic index was therefore devised to privilege the intervention sites.

### 5.1.1 Synthetic index based on risk analysis

Evaluating a synthetic index does not mean estimating the actual probability of death, but identifying the areas of high risk in a relative way. In fact, not having enough information, in evaluating the various factors that make up the index it was assumed that every time a pedestrian and a vehicle meet, there is an impact; this hypothesis is only partially true.

The synthetic index is intended as the probability that on the  $j^{\text{th}}$  section the vehicular and pedestrian capacity of the crossing enter into a contract. Therefore, to estimate the probability of death, the following data must be available:

- peak hour vehicular flow and its daily variation pattern;
- pedestrian flow rate at rush hour crossing (Eq. 3.16) and daily variation pattern on an hourly basis
- site characteristics (Lu, S, W, I, X, f) Eq 2.9

So it can be defined as:

$$P(\text{death}) = \iint_{Q_V, Q_P} P(D|V) * P(V|Q_V) * P(Q_V) * P(Q_P) d Q_V d Q_P \quad 5.1$$

The term  $P(D|V)$  represents the conditional probability of death that occurs when a pedestrian of age  $Y$  impacts with a vehicle that velocity  $V_i$  on the  $j^{\text{th}}$  segment. From which one has:

$$P(D|V) = \frac{1}{1 + \exp(a + bV_{ij} + cY)} \quad 5.2$$

Where

- $a$ ,  $b$  and  $c$  are coefficients of the vulnerability functions taken from literature (Helmer, T. 2015)
- $V_{ij}$  is the speed estimated with the model described in Chapter 2
- $Y$  understood as the average age derived from the distribution of ages in the area (in this case on Cassino). it was considered that elderly people have a lower propensity to make movements so the average age of pedestrian users is calculated for an age range between 6 and 70 years.

The second term  $P(V | Q_v)$  represents the probability of having a certain speed given a vehicular flow; therefore, for what has been said in Chapter 2, this probability is a normal distribution as the flow rate varies.

To simplify, the probability is expressed in discrete terms, so the double integral becomes a sum. This makes it possible to consider the probability of death on the  $i^{th}$  segment as a product of the vulnerability function, of the vehicular and pedestrian flow rates of the stretch relative to the specific time of day. To consider a typical day this is multiplied by a factor  $f = n^{\circ} \text{ type } i \text{ hours over a year} / n^{\circ} \text{ total hours of a year} = 1/24$

$$P(\text{death})_j = \sum_{l=1}^{24} \frac{1}{1 + \exp(a + bV_{ij} + cY)} Q_{V_{ij}} Q_{P_{ij}} * f \tag{5.3}$$

Where: the logistics function represents the vulnerability function while  $Q_v$  e  $Q_p$  the vehicular and pedestrian flows of crossing the section.

Having available both pedestrian and vehicular patterns diversified for the weekdays and pre-holidays scenarios, the probabilities  $P(\text{death\_weekdays})_j$  and  $P(\text{death\_pre holidays})_j$  are evaluated. To obtain a single index, an average is evaluated:

$$P_{(\text{death})_j} = P_{(\text{death\_weekdays})_j} \frac{n^{\circ} \text{ weekdays}}{n^{\circ} \text{ total days of the year}} + P_{(\text{death\_pre holidays})_j} \frac{n^{\circ} \text{ pre holidays}}{n^{\circ} \text{ total days of the year}}$$

Once the index is obtained, it is normalized to the maximum value and the segments are prioritized. Below is a result of the prioritization of the main segments of the Cassino network.

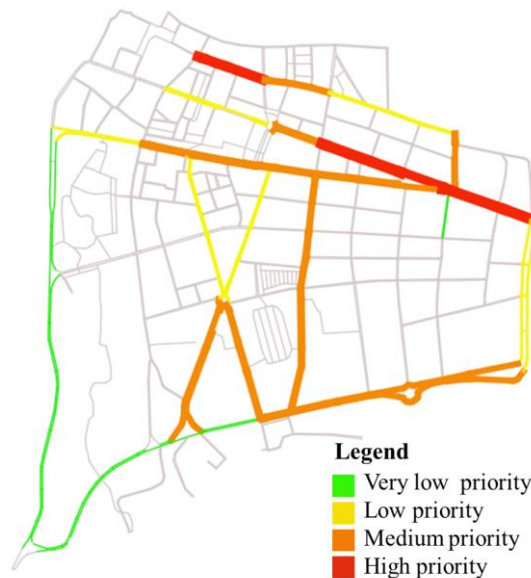


Figure 5.1 Sections prioritization

As shown in Figure 5.1, the sections in which it is necessary to intervene with priority are those of the main access road to the city center and the area where schools,

post offices and the municipality are concentrated (in red). The medium priority area is linked to the presence of numerous roadside parking spaces with appreciable vehicular and pedestrian flows (in orange).

## 5.2 The pedestrian areas

When it comes to pedestrian environments according to international literature, 3 main macro-categories can be identified:

- **Shared zones** is a residential or commercial street that has been designed to prioritize residents and pedestrians by significantly reducing the dominance of motor vehicles. The path for vehicles is physically constrained by street furniture and restrictions, with no delimitation between the sidewalk and the carriageway. Shared zones are suitable for compact areas with low traffic flows. Their maximum size is limited by the need to reduce response times for emergency services and to limit the extent of the carriageway that must be traveled by motorists at low speed.



*Figure 5.2 Shared zone example (taken from Google Images)*

- **Pedestrian precincts:** are areas dedicated to the exclusive use of pedestrians. These are created by restricting access or closing roads to traffic. Pedestrian zones are advantageous where there is strong pedestrian activity, commercial or mixed development, a high number of pedestrian/vehicle conflicts, and motor traffic can be accommodated elsewhere.



Figure 5.3 Pedestrian precincts example (taken from Google Images)

- Living streets:** are streets where pedestrians have priority and vehicles are not excluded. This makes it possible to balance the needs of residents, businesses, pedestrians and cyclists with cars, thus encouraging a better quality of life and a wider range of community and street activities. However, this solution requires high costs and possible delays in motorized traffic.



Figure 5.4 Living street example (taken from Google Images)

In Italy these areas are called environmental islands; in these, a series of measures are put in place to inhibit vehicular traffic in order to favour cycle and pedestrian circulation. The measures for traffic and speed control, which are usually adopted in these areas, are:

- Limited Traffic Zones (LTZ)* to limit the number of vehicles in circulation in a specific area;
- Residential Areas (or PPTA - Privileged Pedestrian Traffic Areas);*

- c) *Pedestrian areas* in the case of spaces intended for pedestrian transit only and therefore directed to the protection of central places such as squares or spaces, even if peripheral, in any case conceived and organized for exclusively pedestrian use.

In this study, the focus was mainly on pedestrian areas. There is a ban on transit and parking with the forced removal of all vehicles with hours 0.00 - 24.00. Notwithstanding the prohibition, vehicles in emergency service (police forces, rescue, firefighters, etc.), cycles, vehicles serving disabled people (bearing the mark referred to in art. . 381 of Presidential Decree 405/92), zero-emission vehicles, having dimensions and speeds such as to be assimilated to cycles, electric mini-busses.

In order to dimension these areas, as well as the simple sidewalks, reference is made to the Highway Capacity Manual 2000 in order to identify its quality in terms of service level. So a good design considers as performance parameters:

- the space available for pedestrians (area of influence of each pedestrian, approximately 0.75 m<sup>2</sup>) or that which can be observed directly on the field by measuring the sample area of the infrastructure in question and determining the maximum number of pedestrians that this area can accommodate at any given time;
- the speed of pedestrians observed or estimated based on age group.
- the average pedestrian flow, or the count of pedestrians in the fifteen minutes rush hour.

This makes it possible to estimate, according to the useful width, the level of service of the sidewalk

*Table 5.1 Level of service of the sidewalk*

LOS	Average space (m <sup>2</sup> / p)	Flow unit width (ped/ min/m)	Average speed ( m/s)	V / c ratio	Description
A	> 5.5	≤16.7	> 1.3	> 5.5	Ability to move along the desired path without deviating the trajectory
B	3.7÷5.5	16.7 ÷23.3	1.4 ÷1.3	3.7÷5.5	Occasional need to deviate the trajectory to avoid conflicts
C	2.2÷3.7	23.3 ÷33.3	1.2 ÷1.3	2.2÷3.7	Frequent need to deviate the trajectory to avoid conflicts
D	1.7÷ 2.2	33.3÷50	1.1 ÷1.2	1.4÷2.2	Reduced speed and reduced chance of

					overtaking slower pedestrians
E	0.7÷1.4	50÷76.7	0.8÷1.1	0.7÷1.4	Reduced speed and very limited ability to overtake slower pedestrians
F	≤ 0.7	variable	≤ 0.8	≤ 0.7	Very slow speed and frequent contact with other pedestrians

Once the dimensions of the area on which to intervene have been evaluated, the costs are estimated starting from the unit price lists. This allows, based on the available budget, to prioritize the areas in which to intervene and to what extent. Certainly, in all areas where there is the promiscuity of modes of transport, it is necessary to secure the crossing areas of the carriageway. Therefore, pedestrian crossings must be designed with particular attention.

### 5.2.1 Pedestrian crossings

The areas of the road where the pedestrian is most likely to come into conflict with the vehicular flow, therefore in which the exposure to risk is greatest, are the crossings. This requires careful planning and the need to pursue the following objectives:

- accessibility, safety and comfort for pedestrians;
- perceptibility of pedestrian crossing;
- reduction of vehicle speed;
- reciprocal pedestrian-vehicle visibility.

As regards accessibility, safety and comfort of pedestrians, attention must be paid to the type of flooring, the quality of the safety equipment to facilitate the crossing in the indicated place, to ensure the continuity of the pedestrian crossing with the pedestrian path/cycle path and the sidewalk and, finally, also the elimination of architectural barriers for the disabled.

The second objective is the perceptibility of the pedestrian crossing, whose shape, size and location must derive from an integration project between the road and local functions.

The third goal is to reduce vehicle speed without compromising mobility. In the presence of areas in which the different traffic components share the same spaces, there is a need for each of them to behave correctly. To control the conduct of drivers and reduce speed, various interventions are implemented such as signs, narrowing of the carriageway, speed bollards, works to raise the pavement, etc.

Finally, reciprocal visibility must always be guaranteed or improved, by intervening above all on the elimination of the side stop near crossings, or by advancing the sidewalks, or by using retro-reflective systems, or by enhancing public lighting with LED solutions.

The optimal design of a pedestrian crossing, both from a functional and a geometric point of view, presupposes the knowledge of data or estimates relating to pedestrian and vehicular traffic. In this regard, in accordance with the sector bibliography, the following minimum conditions are required to create a pedestrian crossing:

- vehicular traffic in transit on the crossing is 200-250 vehicles/hour per lane during rush hour;
- pedestrian frequency is 50 pedestrians/hour during rush hour or 100 pedestrians during the busiest 3-5 hours of the day.

### 5.2.2 Total kinetic energy of the vehicular flow

To fully describe the traffic that characterizes a site, it is necessary to define a quantity that takes into consideration both the estimated vehicular flow and the speeds that characterize the trunk. This quantity, improperly called the kinetic energy of the vehicular flow, is the synthesis of the two quantities described above. In this specific case, it is possible to consider the kinetic energy as a quantity that takes into account not only the vehicular flow of the observed trunk but also the speeds that vehicles can take along it.

The kinetic energy of the vehicular flow has been defined as the following quantity:

$$K = m_{vehicle} \cdot Q_{vehicle} \cdot V_{vehicle}^2 + m_{hv} \cdot Q_{hv} \cdot V_{hv}^2 \quad 5.4$$

Where:

$K$  = Kinetic Energy of the flow [J];

$m_{vehicle}$  = mass of light vehicles [kg];

$Q_{vehicle}$  = vehicular flow [veh/s];

$V_{vehicle}$  = speed of light vehicles [m/s].

$m_{hv}$  = mass of heavy vehicles [kg];

$Q_{hv}$  = heavy vehicle flow [veh/s];

$V_{hv}$  = speed of heavy vehicles [m/s].

The kinetic energy thus defined can be used as an input value for the choice of the type of crossing.

### 5.2.3 Proposed procedure

In choosing the type of pedestrian crossing, the volumes of vehicular and pedestrian traffic present, the speeds and the type of road involved must be evaluated.

Pedestrian crossings can be classified into macro-categories (in ascending order of economic investment; costs are purely representative as they vary greatly locally and even more nationally)

*Table 5.2 Average cost of a pedestrian crossing*

<b>Type of crossing</b>	<b>Average cost of realization (€ per crossing)</b>
marked crosswalk	500
raised pedestrian crossing	6000
pedestrian crossing on request	15000
pedestrian overpasses/underpasses	35000

In the event that the pedestrian traffic component is not allowed (rural area) and in the case of high vehicle flows and high vehicle speeds, it is recommended to resort to the choice of crossings at staggering levels.

The selection criterion proposed here is reported in Table 5.3, which presents a synoptic table of the applicable types of pedestrian crossing, in relation to the pedestrian flow and the energy of the vehicular flow (estimated with the pedestrian flow per lane).

*Table 5.3 Choice of the type of crossing based on flow assessments*

<b>Pedestrian flow (peak h) [ped / h]</b>	<b>Energy of the vehicular flow (peak hours) [J]</b>		
	<12860	<38580 and>12860	> 38580
> 300	level / on request	on request/ raised	on request / overpasses
<300 and> 100	level / on request	level / on request	on request / overpasses
<100	level	level/ on request	on request / raised

The above matrix indicates general criteria that cannot be separated from site analysis and the designer's discretion.

Once the type of crossing has been identified, in order to define the construction details, additional factors must be considered, such as:

- *signs*: in the event that, within a hundred meters of the site under study, there are more than five advertising billboards in order to highlight the vertical signs relating to the crossing, it is appropriate to signal it with luminous devices;
- *brightness*: if existing or to be built, it should be adapted as reported in the UNI 10439 and EN 13201 standards (UNI 10439 “Illuminotecnica - Requisiti illuminotecnici delle strade con traffico motorizzato”. 31/07/2001, Ente Italiano di Normazione) from which the following table has been extrapolated
- *location of pedestrian crossings* must achieve the right balance between the needs of pedestrians and those of vehicular traffic.

Generally, the choice of location derives from safety studies based on the surrounding area, therefore a geometric analysis of the stretch of road on which you want to make the pedestrian crossing is required, paying particular attention to:

- number of lanes to cross which affects the length of the pedestrian crossing and the possible insertion of a pedestrian life jacket in the middle;
- longitudinal slope of the pedestrian crossing (slope transversal to the direction of travel of vehicles) which, if higher than 5%, could represent an obstacle to the accessibility of vulnerable users.
- transversal slope of the pedestrian crossing (longitudinal slope to the direction of travel of the vehicles) necessary to ensure the flow of rainwater on the section used for the crossing itself.
- analysis of the visibility distance for stopping.

Particular attention must be paid to the design and definition of the equipment of the single crossing.

#### **5.2.4 Pedestrian crossing categories**

In the previous paragraphs, the preliminary analyzes useful for choosing the type of pedestrian crossing most suitable for the case study have been presented, below are the possible positions and furnishings of the crossing in particular cases:

- marked crosswalks;
- raised pedestrian crossings;
- pedestrian crossings on request;
- pedestrian crossings near public transport stops;
- pedestrian crossings near cycle paths;
- pedestrian overpasses.

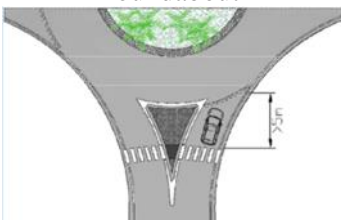
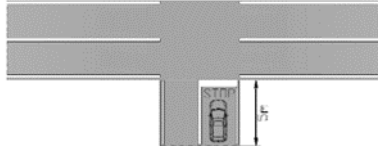
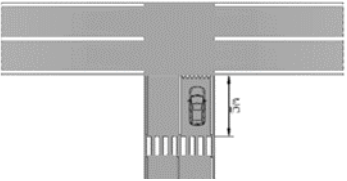
In the following paragraphs, the types of pedestrian crossing are presented separately, presenting the most important characteristics.

### Marked crosswalks

#### DESCRIPTION

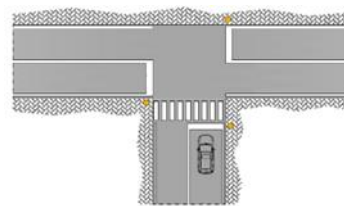
A marked crosswalk is a classic zebra. Depending on the case, it is positioned as shown in the following table:

*Table 5.4 Safe positioning of a marked crosswalk*

DESCRIPTION	STANDARD	ADDITIONAL INFORMATION
Positioning near roundabouts	<p><math>\geq 5</math> m upstream of the roundabout</p> 	the pedestrian crossing must be set back by 5 meters with respect to the outer edge of the circular ring so that pedestrians can pass behind the first stationary car waiting to enter the crown.
Positioning near intersections regulated by the STOP sign	<p><math>\geq 5</math> m upstream of the intersection</p> 	
Positioning near intersections with precedence rule	<p>Positioning near intersections with precedence rule <math>\geq 5</math> m upstream of the intersection</p> 	

Positioning near  
traffic-light  
intersections

After the stop line of the  
traffic light



### LOCATION

The pedestrian crossing must always be made orthogonally to the sidewalk to facilitate the orientation of visually impaired people who tend to make a trajectory perpendicular to the sidewalk itself. If this were not the case, they would risk finding themselves crossing outside the pedestrian crossing with the danger of being in the center of the intersection. The location of the pedestrian crossing takes into account both the average traffic of vehicles and the needs of pedestrians. Possibly it is placed away from curves and bumps at least at a distance equal to the stop distance.

### **Raised pedestrian crossing**

#### DESCRIPTION

The raised pedestrian crossing is an elevation of the carriageway, with connecting ramps in the longitudinal direction to the movement of the vehicles, created to give continuity of height to the sidewalk and to the pedestrian path in correspondence with a pedestrian crossing. This type cannot be used on roads where emergency services pass frequently.

In the raised pedestrian crossing, the pedestrian has priority over the vehicles. In fact, it is not the pedestrian who gets off the sidewalk to “invade” the carriageway used by the vehicles, but the vehicle in transit that rises to the level of the sidewalk where the pedestrians are; in the raised pedestrian crossing the intruder is the vehicle.

The raising of the carriageway to the level of the sidewalk, in correspondence with the pedestrian crossings, allows further benefits in terms of safety and accessibility as it moderates the speed of passing vehicles and eliminates the need to create access ramps.



Figure 5.5 Example of raised crossing (source Google Images)

The slope of the connecting ramps must not exceed 15% in the case of speeds less than or equal to 50 km/h. In “zone 30”, where the maximum speed of vehicles is 30 km/h, the slope of the connecting ramp can be raised to 17.5%. To make the connecting ramp more visible, between the level of the carriageway and the level of the sidewalk, it is advisable to provide stripes of alternating color, White/Black or Yellow/Black.

It is necessary to provide suitable vertical warning signs for raising.

The width of the raised area must be proportional to the extent of pedestrian flows and, in any case, must not be less than 3.50 m, i.e. the minimum width of the crossing plus two lateral clearances of at least 0.50 m each.

#### LOCATION

The pedestrian crossing must always be made orthogonally to the sidewalk to facilitate the orientation of visually impaired and blind people who tend to follow a trajectory perpendicular to the sidewalk itself. Pedestrian crossings can be located near intersections or anywhere else on the road. In some cases, the authorities may associate the pedestrian crossing right with a fixed lighting system. The location of the pedestrian crossing takes into account both the average traffic of vehicles and the needs of pedestrians. Possibly it is placed away from curves and bumps at least at a distance equal to the stopping distance. This typology is strongly recommended near school and attractive recreational areas (cinemas, parks, etc).

### **Pedestrian crossing on request**

#### DESCRIPTION

A pedestrian crossing on request is characterized by the presence of lanterns of two colors:

- the green, meaning the go-ahead, which allows pedestrians to use the roadway to cross;

- red, meaning stop, which does not allow pedestrians to cross, nor to engage the carriageway.

On the other hand, the transition phase is not envisaged but alternatively, two solutions are envisaged:

- countdown device (art. 60, paragraph 1, of law no. 120 of 29 July 2010) which marks the remaining time of the green and red pedestrian phase; the device can be positioned, for example, in place of the current yellow lantern. These have a minimum height of 120 mm for lights with a diameter of 200 mm and 185 mm for lights with a diameter of 300 mm;
- an animated pictogram (pedestrian traffic lights in the shape of a colored pedestrian on a black background):



Figure 5.6 Countdown device (source Google Images)



Figure 5.7 Example animated pictogram (source Google Images)

In the pedestrian red phase, the pedestrian pictogram is static and colored red, while in the pedestrian green phase the pedestrian pictogram is animated; it moves at a normal pace and accelerates the pace in the last period of pedestrian green.

The calculation of the pedestrian green area presupposes the knowledge of the pedestrian speed during the crossing phase. Usually, a speed of 1 m/sec is considered and compared to the length of the crossing (for example: for a carriageway of 10 m it is estimated that it takes 10 sec to cross it). The duration of the pedestrian green time calculated in this way can be corrected, at the discretion of the designer, by means of coefficients that take into account the specific characteristics of the pedestrians who use the crossing; for example, elderly or disabled users who have a pace slower than 1 m/sec.

### LOCATION

The pedestrian crossing must always be made orthogonally to the sidewalk to facilitate the orientation of visually impaired and blind people who tend to follow a trajectory perpendicular to the sidewalk itself. Pedestrian crossings can be located near intersections or anywhere else on the road. In some cases, the authorities may associate

the pedestrian crossing right with a traffic light, a fixed or flashing lighting system, or an artificial bump to slow down the speed of vehicles. The location of the pedestrian crossing takes into account both the average traffic of vehicles and the needs of pedestrians. Possibly it is placed away from curves and bumps at least at a distance equal to the stopping distance. In the case of traffic light intersections, the crossing must be placed in front of the vehicle stop line.

### **Pedestrian crossing near public transport stops**

#### DESCRIPTION

In the case of crossings at public transport stops, depending on how they are made (on the carriageway or off the carriageway), the characteristics of the road (one-way, two-way, one or more lanes in each direction, ...), the crossing can be set back from the public transport stop in the following cases:

- a) In the event of a public transport stop on the carriageway, on a two-way street and crossing without traffic lights; the retreat must allow for a suitable distance of visibility between pedestrians and oncoming vehicles.



Figure 5.8 Crossing at the public transport stop on the cat carriageway

- b) In the event of a public transport stop outside the carriageway, on a two-way street and traffic light crossing, the setback depends on the geometry of the recess intended for the stop.



Figure 5.9 Crossing near public transport stops

Or directly behind the public transport stop in the following cases:

- c) Public transport stop on the carriageway, on a one-way street and crossing without traffic lights.

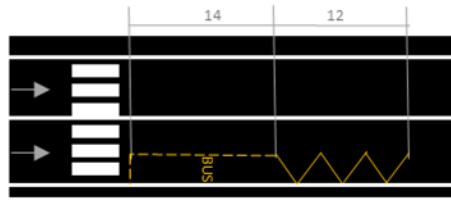


Figure 5.10 Crossing near public transport stops

- d) public transport stop on the carriageway, on a two-way street but where there is a traffic island in the center of the carriageway and crossing without traffic lights.



Figure 5.11 Crossing near public transport stops

- e) public transport stop in the carriageway, on two-way roads and in the presence of traffic lights.



Figure 5.12 Crossing near public transport stops

Solution (d) is possible because the traffic island guarantees pedestrian protection from traffic currents coming from the opposite direction, which are not easily visible.

In the event of significant constraints, the crossing can also be made advanced with respect to the bus stop, but always to such an extent as to ensure the necessary visibility between pedestrians and traffic currents.

### LOCATION

The pedestrian crossing must always be made orthogonally to the sidewalk to facilitate the orientation of visually impaired and blind people who tend to follow a trajectory perpendicular to the sidewalk itself. If this were not the case, they would risk finding themselves crossing outside the pedestrian crossing, and in the event of an intersection, with the danger of being in the center of it. In the presence of level intersections without traffic lights, the pedestrian crossing, if existing, must be

positioned 5 meters before the intersection itself to avoid that the driver does not pay sufficient attention to the pedestrian about to cross, as he is busy carrying out his maneuver. The distance chosen is also such as to allow the crossing back behind the first vehicle. The location of the pedestrian crossing takes into account both the average traffic of vehicles and the needs of pedestrians. Possibly it is placed away from curves and bumps at least at a distance equal to the stopping distance.

### **Pedestrian crossing near cycle paths**

#### DESCRIPTION

In the event of a pedestrian crossing at the cycle lane stops, it is advisable to separate the two user modes, creating the external cycle crossing alongside the pedestrian one.

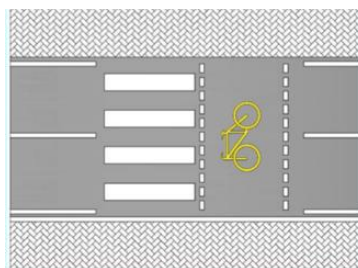


*Figure 5.13 Crossing positioning in the presence of cycle paths*

If the cycle path is one of the lanes of the carriageway, the crossing must start before the track itself, the track must be considered as a normal lane to cross, especially in the case of traffic lights.

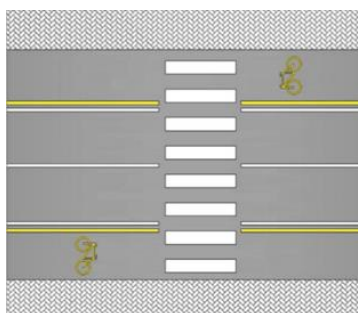


*Figure 5.14 Crossing positioning in the presence of cycle paths*

#### LOCATION

The pedestrian crossing must always be made orthogonally to the sidewalk to facilitate the orientation of visually impaired and blind people who tend to follow a trajectory perpendicular to the sidewalk itself. If this were not the case, they would

risk finding themselves crossing outside the pedestrian crossing, and in the event of an intersection, with the danger of being in the center of it. In the presence of level intersections without traffic lights, the pedestrian crossing, if existing, must be positioned 5 meters upstream of the intersection itself to avoid that the driver does not pay sufficient attention to the pedestrian about to cross, as he is busy making his maneuver. The distance chosen is also such as to allow the crossing back behind the first vehicle. The location of the pedestrian crossing takes into account both the average vehicle traffic and the needs of pedestrians. Possibly it is placed away from curves and bumps at least at a distance equal to the stopping distance.

### **Pedestrian overpasses/underpasses**

#### DESCRIPTION

In the case of roads with separate lanes or characterized by a strong traffic component, in order to allow the crossing, it is advisable to think of an altimetrically staggered crossing model with stairs that allow overcoming the difference in height between the level of the walking surface and that of the deck of the bridge.

In order to break down the architectural barriers constituted by the stairs, the installation of side lifts was planned in such a way as to allow the outflow of pedestrian traffic even in the presence of the disabled. Please refer to Ministerial Decree 11/5/2001 (n. 6792).



*Figure 5.15 Example of an altimetrically staggered crossing (source google Maps loc. Grotte Celoni, RM)*



Figure 5.16 Example of an altimetrically staggered crossing (source google Maps loc. Grotte Celoni, RM)

### 5.2.5 Benefit-cost analysis

Once the type of crossing to be implemented has been chosen, and the pedestrian and vehicular flows known, it is necessary to consider the characteristics of the site to ensure that it is clearly identified by users. Road policies and characteristics can help promote active transport, such as the use of orientation signs or crossing signs. So the environments need to be redesigned to make these ways safer and more enjoyable. To do this, the designers must choose, based on the available budget, one or more measures to be installed, taking into account both the implementation and operating costs. The infrastructure costs reported in this paragraph are intended to help and encourage the improvement of these environments but are only indicative, as they are known to vary greatly from city to city and from state to state.

Table 5.5 Average cost estimated by type of pedestrian crossing

	Type of measurement	Average cost (€)
Pedestrian crossing at level	high visibility road markings	50 €/ml
	road markings	10 €/ml
	asphalt pavement	30 €/ml
	brick sidewalk	50 €/ml
	concrete sidewalk	20 €/ml
	ramp from the pavement to the carriageway	600 €/ml
	single street lamp lighting	250 €
	ground lighting	5000 €/m
Raised pedestrian crossing	roadway elevation in asphalt	7000 €/ml
Pedestrian crossing on request	flashing beacon	8000 €
	hybrid pedestrian beacon	15000 €
	automatic pedestrian detection devices	350 €
	pedestrian detection devices with push button	300 €
	flashing with countdown	600 €
	audible pedestrian signal	650 €
Overpass / underpass	wooden bridge	100 €/m
	prefabricated steel bridge	170 €/m
	protective railing	400 €/m
	lifter	3500 €

After the installation of a particular treatment it is possible to estimate the expected number of accidents, with respect to a basic condition (Gross, Persaud, & Lyon, 2010); This multiplying factor of estimation, which in Italy does not yet exist, is called Crash Modification Factor (CMF) overseas. When the CMF is greater than 1.0 there is an expected increase in the number of accidents after treatment is implemented, while a CMF of less than 1.0 indicates a decrease in the number of accidents. Then CMFs are used to estimate the safety benefits of alternative treatments and/or identify cost-effective strategies.

The FHWA (2009) has created an online CMF archive where it uses a star quality rating system to evaluate the quality of the individual CMF (then they consider sample size, standard error, potential bias and source quality some data). The rating scale ranges from 1 to 5, with 1 being the lowest rating and 5 being the best possible rating.

Countermeasure: Install raised pedestrian crosswalks

Compare	CMF	CRF(%)	Quality	Crash Type	Crash Severity	Area Type	Reference	Comments
<input type="checkbox"/>	0.64	36	★★★★☆	All	A (serious injury),B (minor injury),C (possible injury)	Urban and Suburban	ELVIK, R. AND VAA, T., 2004	
<input type="checkbox"/>	0.55	46	★★★★☆	Vehicle/pedestrian	A (serious injury),B (minor injury),C (possible injury)	Urban and Suburban	ELVIK, R. AND VAA, T., 2004	
<input type="checkbox"/>	0.7	30	★★★★☆	All	A (serious injury),B (minor injury),C (possible injury)	Urban and Suburban	ELVIK, R. AND VAA, T., 2004	

Compare Reset Compare

\*NOTE: You can compare CMFs across countermeasures, subcategories, and categories.

Figure 5.17 Example of a CMF table for installing a raised pedestrian crosswalks (from (Federal Highway Administration, 2009))

### 5.3 Cycling network design

The design of a short-distance transport network depends on historical characteristics and land use evolution, thus knowledge of the land use layout, topography, climate and lifestyle of the population is required. In addition, it is necessary to have traffic data (flow of motor vehicles, cyclists and pedestrians) and injury rates, highlight the presence of attractions (schools, universities, commercial or recreational activities, tourist areas, etc.) and existing structures with their respective geometric characteristics.

Known the land use characteristics, the different origins and destinations must be taken into consideration to identify the paths that users could choose to meet their needs.

This allows you to hierarchize the network in:

- Main cycling paths, for long distances, with city or interurban connection function;
- Secondary roads that connect adjacent neighborhoods;
- Local routes, for short distances, which allow movement within the neighborhoods.



### 5.3.1 Types of cycling path layouts

Before defining the proposed methodology for the design cycling infrastructure for given area characteristics and flows, the most common cycling path layouts are briefly presented. Although this is not an exhaustive review, given the different legal definitions and terminologies used in EU countries.

Depending on whether or not cyclists share the infrastructure with other users, three situations can occur:

1. *total sharing of road space* between bicycle and vehicular traffic; this is usually a one-way lane, but there may be situations where the bicycle can travel in the opposite direction (for example, zone 30).



Figure 5.18 Example of sharing street space (zone 20)

2. *visual separation* with simple indication with horizontal signs on the sidewalk of the runway. The space intended for bicycles is an integral part of the carriageway, unidirectional, generally in the direction of the traffic flow.



Figure 5.19 Visual separation of the cycle path by means of horizontal signs

3. *physical separation*: it is a lane, one or two-way, dedicated to bicycles (with the possibility of sharing with non-motorized modes) separated by obstacles from the road for other ways.



Figure 5.20 physical separation of the cycle path by railing

By reviewing the different guidelines of European countries (Meschik, 2008), (Mobility, 2006), (Celis, 2014), (Julien, 2000), (Ciclável, 2011), (Government of Catalonia, 2008), (Landsting, 2010), (Eidgenossenschaft, 2010), (Officials, 2014) albeit with different names, cycle paths can be grouped as shown below.

### Greenway

It is a "multipurpose" route reserved for non-motorized users, separated from traffic and independent from main roads, which passes through open spaces, parks, gardens and woods and must respect the surrounding environment. Sharing the lane by different users can cause conflicts so it is recommended to physically separate the different parts intended for different users.

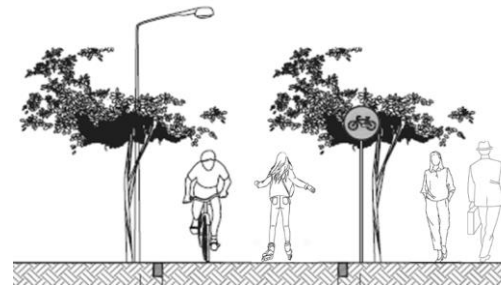


Figure 5.21 Greenway example

### Cycle lane

It is a cycle path with independent lane, separated from the carriageways, designed for the exclusive use of bicycles.

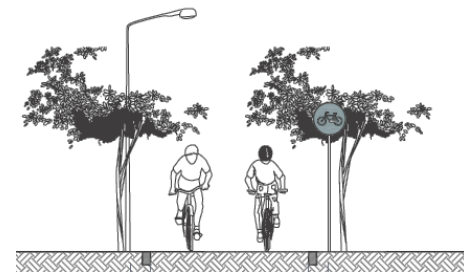


Figure 5.22 Example of cycle lane

### Protected cycle path

They are protected lanes designed exclusively for bicycles with physical separation from motorized traffic. Usually neither pedestrians nor skaters are allowed. This can be one-way (one lane on each side of the main road) or two-way (one lane with both directions on one side of a main road) usually near a road with high motorized traffic.

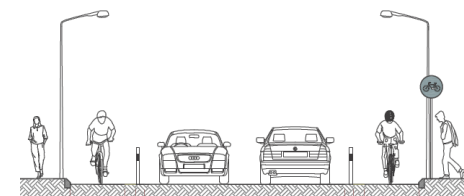


Figure 5.23 Example of one-way Protected cycle path

### Cycle path

It is reserved for bicycles separated from the rest of the circulation by horizontal signs. It is designed for roads at low speed and with reduced transit of heavy vehicles.

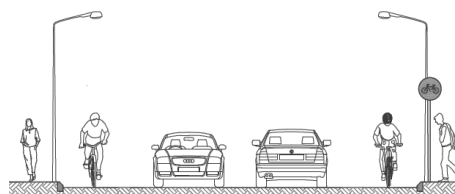


Figure 5.24 Example of cycle path

### Road of 30 km / h zone

In this both bicycles and cars share the carriageway without any access restrictions.

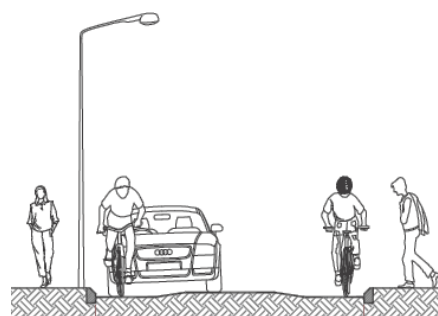


Figure 5.25 Example of road of 30 Km/h zone

### Cycle track

In which pedestrians and cyclists share the sidewalk. The part intended for the bicycle must have the relative signs. As there is not always enough space, this usually takes place in pedestrian areas or in common routes where the speed limit for cyclists is 20 km/h.

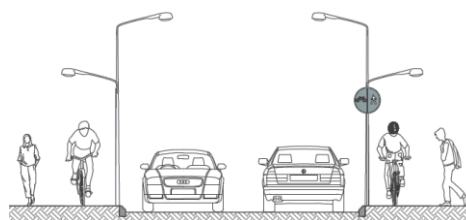


Figure 5.26 Example of cycle track

### Shared-use path

It is a shared between pedestrians and cars. These roads are also suitable for cycling, but with a speed limit of 20 km/h and with pedestrians always having priority.



Figure 5.27 Shared-use path example

## 5.3.2 Choice of the specific cycling path layout to be adopted

Since there is no absolute rule for the application of the different solutions for the choice of cycle paths, it is necessary to take into account the density and speed of the vehicles (to define the type of protection on the cycle path), the expected number of

cyclists (to define the width of the track), the existing space and the urban environment (to identify the type of cycle path and its characteristics).

Once that cyclic flows have been evaluated as described above, it is possible to use a decision matrix, such as the one shown below (Dufour D., Ligtermoet and the Netherlands Partners, 2010), and define the type of cycling path layout solution suitable for each specific road section.

Table 5.6 Decision matrix

		Speed (Km/h)		Intensity (vehicles/day)	Density of cyclists (bike/day)		
					<750	500-2500	>2000
		Not applicable		0	Greenway		
Function traffic road	Local access road	Walking space or 30 Km/h		1-25000	Shared-use path	Cycle lane or cycle path	
				2000-5000			
				>4000	Cycle lane or cycle track		
	Distribut or road	50 Km/h	2x1 lanes	not applicable	Cycle track (adjacent or separated)		
			2x2 lanes				
		70 Km/h					

In order to choose the ideal solution from among the possible solutions, it is necessary to take into account the characteristics of the road, the flows, the speeds, the surrounding space, the hierarchy of the roads but also the economic resources available.

This means that planners and decision-makers must carry out cost-benefit analyzes that may represent an effective help to use the funds in a targeted way and to justify the investment on one choice rather than another. According to Elvik (2000), the cost-benefit analysis of pedestrian and cycle infrastructures should use methodologies similar to those used for transport projects in general, keeping in mind that the costs associated with the design and construction of the cycling infrastructure improvements are relatively low compared to road projects of similar lengths.

Although apparently simple, it is not so straightforward to estimate the costs for the installation of cycle networks as these are often part of a larger maintenance project, such as the resurfacing of a road. So while it is quite simple to describe the cost of purchasing and installing the bike path material (vertical signs, paints, etc), the other elements are grouped together in the larger project and difficult to detail.

Each cycling path layout type has a series of possible variable costs, determined by the different measures implemented, which are linked to the design, operation of the work and its maintenance.

The costs presented in this paper, relating to the design of cycle networks in Italy, are purely representative as they vary greatly locally and even more nationally. The purpose is only that of identifying a series of possible interventions to increase cycling of a generic area, but the evaluation of each to determine which are the most convenient will require further research and the development of an assessment framework appropriate to the context.

*Table 5.7 Cost estimates for the design of the different solutions*

	Type of separator	Cost (€ / Km)	
		Unidirectional	Bidirectional
Cycle path	Road markings	50000	40000
	Colored bitumen	125000	100000
Protected cycle path	Curbstone	210000	120000
	Creasing	100000	60000
	Flower bed	210000	120000
	Parking stalls	260000	140000
	Horizontal signs	170000	120000
Cycle track	Sidewalk with staggered floors	165000	120000
	No separation on the sidewalk	40000	35000
Road of 30 Km/h	No separation on the road		60000
Cycle lane	Calcestre	\	330000
	Bitumen	\	195000

It is intuitive to understand that optimizing the existing network by inserting a horizontal and vertical signaling system that delimits the route requires moderate financial resources (400 to 600 €/Km). Just as expanding an existing cycle network involves lower costs than new construction. Similarly, it is more convenient to create multi-purpose cycle paths than dedicated ones.

Many authors (Bushell, Poole, Zegeer & Rodriguez, 2013) (NACTO, 2014) (Benni, Macaraig & Malmo-Laycock, 2019) (Nuno Lopez, Cannone, Drufuca & Dondè, 2006) (Weigand, McNeil & Dill, 2013) have dealt with defining the costs of the different solutions, sometimes lacking details on the different components of the project. All the studies analyzed refer to specific manuals to define the costs according to the characteristics of the work to be carried out.

Once the costs have been defined, the benefits due to the construction of the work must therefore be assessed in terms of reduction of material damage caused by

accidents, reduction of pollutant emissions, improving the quality of life and social profitability. The best solution will be the one that, over time, will lead to benefits that exceed the costs.

## 5.4 Conclusions

Zero impact travel is still not very common in people's daily lives. Many people prefer to use their private vehicle even for short trips. Although in recent years the idea has become increasingly widespread that promoting walking or the use of bicycles as a mode of transport allows improving health conditions, supporting sustainability and facilitating access to different areas. It has been shown (Monsere, Dill, McNeil & Clifton, 2014) that, by installing dedicated infrastructure, users are able to perceive a greater level of comfort and safety which encourages them to use these "new" modes of transport in urban areas.

In this chapter, an original methodology has been suggested that is able to identify the optimal layout between the different solutions within a specific study area. Since there is no absolute rule for the application of the different solutions for the choice of cycle/pedestrian routes, it is necessary to take into account the density and speed of the vehicles (to define the type of protection to be provided to separate the flows), the expected number of vulnerable users (to define the width of the area dedicated to pedestrians and cyclists), of the existing space and of the urban environment (to identify the type of cycle path or pedestrian area and its characteristics). Once these quantities have been identified, by combining them, it is possible to choose the one suitable for the context among the different solutions. This procedure is aimed both at guiding the designers (also on the basis of the available budget) in the choice of the countermeasure but also at providing them with a valid tool to justify the choice of one investment rather than another. This would make it possible to obtain a network that satisfies the needs of both users and managing bodies.

## References

- Celis, C. 2014. Danish handbook for cycle traffic. Denmark: HÅNDBOG CYKELTRAFIK.
- Ciclável, R. 2011. Princípios de Planeamento e Desenho. COLEÇÃO DE BROCHURAS TÉCNICAS / TEMÁTICAS. IMT.
- D'Apuzzo, M., Santilli, D., Evangelisti, A., Pelagalli, V., Montanaro, O., & Nicolosi, V. 2020. An exploratory step to evaluate the pedestrian exposure in urban

- environment. 20th International Conference on Computational Science and Applications (ICCSA 2020) and its associated workshops, held ONLINE in collaboration with the University of Cagliari, Italy, 1 – 4 Giugno 2020. Part VII, LNCS 12255. pp.645-657. DOI:10.1007/978-3-030-58820-5\_47. ISBN:978-3-030-58819-9  
[https://link.springer.com/chapter/10.1007/978-3-030-58820-5\\_47](https://link.springer.com/chapter/10.1007/978-3-030-58820-5_47)Dufour D., Ligtermoet and the Netherlands Partners. (2010). PRESTO Cycling Policy Guide- Cycling Infrastructure.
- Dufour D., Ligtermoet and the Netherlands Partners. (2010). PRESTO Cycling Policy Guide- Cycling Infrastructure.
- Eidgenossenschaft, S. 2010. Handbuch Wegweisung für Velos, Mountainbikes und fahrzeugähnliche Geräte . Switzerland.
- Elvik, R. 2000. Which are the relevant costs and benefits of road safety measures designed for pedestrian and cyclist? Accident Analysis Prevention, 32:37-45.
- Government of Catalonia. (2008). Manual for the Design of Cyclepaths in Catalonia. Spain.
- Helmer, T. 2015. Development of a Methodology for the Evaluation of Active Safety using the Example of Preventive Pedestrian Protection, Doctoral Thesis accepted by Technische Universität Berlin, Germany. DOI 10.1007/978-3-319-12889-4.
- Julien, A. 2000. Cycling infrastructure design and urban public space- a comparison of cycling design manuals. Association Metropolis. France: PREDITMELT/DRAST.
- Landsting, T. 2010. Guideline on configuration, operation and maintenance of pedestrian, cycling and moped traffic. Handbok – Utformning, drift och underhåll med gång-, cykel- och mopedtrafik I fokus .
- Meschik, M. 2008. Planungshandbuch radverkehr. Wien, Austria: Springer-verlag. .
- Mobility, B. 2006. Vademecum Velo en Region de Bruxelles-Capitale. <https://mobilite-mobiliteit.brussels/en/node/265>. Brussels, Belgium.
- Monsere, C., Dill, J., McNeil, N., & Clifton, K. (2014). Evaluation of Innovative Bicycle Facilities: SW Broadway Cycle Track & SW Stark/Oak Street Buffered Bike Lanes.
- Officials, N. A. 2014). Urban Bikeway Design Guide. USA.

# **CHAPTER 6. PUNCTUAL COUNTERMEASURES: TRAFFIC CALMING**

In recent years, the number of accidents has assumed such high proportions that it has become a major cause of death and disability in Europe and the rest of the world, causing high social and economic costs. It is therefore legitimate to ask what is meant by road safety. In Italy, there is no universally accepted definition of road safety. The latter could be defined as the set of measures and methodologies aimed at preventing or reducing the risk of injury and death for road users (drivers, passengers and pedestrians). As noted in Chapter 2, speed is one of the underlying elements of the safety problem. Numerous countermeasures have been created over the years to influence the behavior of drivers, inducing them to reduce speed. Among the many, traffic calming allows obtaining this result with reduced costs and a minor modification of the road environment. Once the regulatory framework has been analyzed and the different types of devices have been identified (see Appendix B), the disturbance effects have been studied with simplified models. In fact, when these devices are crossed, they generate stresses in the occupants of the vehicle which can be reduced by moderating the speed. It has been highlighted that these interventions, if correctly applied, lead to greater accessibility of public space by vulnerable road users, favoring non-motorized mobility precisely because greater safety conditions have been restored.

## **6.1 State of art**

Speed management has become a major issue over the past century. For this reason, more and more often, horizontal and vertical devices are installed (for example speed humps, gateways, speed humps, speed cushions, etc.); which serve precisely to force the drivers to maintain the speed set according to the type of the road. However, traffic calming does not guarantee that you will always obtain speeds that comply with the

imposed limits. This has encouraged researchers from various countries to start evaluating the effect of such measures, to determine their effectiveness based on size (height, length, gradient and radius) and shapes. Efficiency is evaluated by means of speed reduction or accident rate decrease and, sometimes, road capacity.

The first studies were conducted since 1980 (Waltz, Hoefliger & Fehlmann), (Van Houten & Van Hutten, 1987), later different devices were studied from various points of view: efficacy studies, standards, guidelines.

In this Paragraph the devices with altimetric effect were mainly analyzed considering the experimental and theoretical studies.

### **6.1.1 Experimental studies**

In the experimental studies, before-after analyzes are carried out, in which the sites before and after the installation of the devices are compared in order to evaluate the variation in speed and traffic flows, thus determining the effectiveness of the installed measurement.

As is known, traffic calming deviates traffic volumes on the roads adjacent to those in which they are installed, therefore many scholars (Werner, 2012) (Berthod, 2011) (Johansson, Rosader, & Leden, 2011) have set themselves the objective of evaluating the impact they have on the surrounding areas or at different times of the day (Jagerbrand, Johansson, & L., 2018).

Depending on the type of device and its geometry (Webster & Layfield, 1998) (Marek & Walgren, 1993) (Kirkpatrick, 1996) (Klyne, Mie & Maitpm, 1998) (Parkhill, Sooklall, Geni, & Bahar, 2001) (Ziolkowski, 2014) (Traffic Engineering South Carolina Department of Transportation, 2006) different speed reductions are generated (Smith, Knapp & Dr. Hallmark, 2002) (Shauna, Keith, Gary, & S., 2002) (Moreno, Garcia & Romero, 2011) (Giffod, 1973) (Chadda, Asce, & Cross, 1985) (Russell & Godavarthy, 2010) also due to the different area of influence in which the slowdown occurs (Basil, 2012). This suggests that in order to obtain significant speed reductions, one could think of inserting the devices in series (Richard, et al., 2016), therefore one would no longer evaluate the punctual speed but a speed profile (Heloisa, Miles, Tight & May, 2000) (Latoya & Nedzesky, 2003) (Gunwoo, Shinhye, Cheol, & Keechoo, 2013) (Namee & Witchayangkoon, 2011), (Sayer & Parry, 1994). To obtain the desired speed reductions it is necessary to correctly space the devices, in fact at a shorter distance lower speeds are expected; since, between a bump and another, it would not be possible to reach high speeds (García, Torres, Romero, & Moreno, 2011)

(Aya & Hisashi, 2011) (Siti & Hamsa, 2016) (Garcia, Torres, Romero & Moreno, 1987) (Brindle, 2005), (Canale & Leonardi, 2005).

Other problems related to the use of these devices may be due to noise (Khairum, Hamsa, Mohdzin Bin & Mansor, 2016) produced by cars by surmounting them or by the load on the pavement (Talaat & Hassan Hashim, 2017) or the vibrations produced (Transport, 2005).

In the last twenty years, thanks to new technologies, the experiments have not only been carried out in the field, but also through driving simulators (Compte & Jamson, 2000) (Kennedy, Gorell, Crinson, Wheeler & Elliot, 2005) (Pyne, Dougherty, Carsten & Tight, 1995) (Alley, 2000) with which the effects of the devices on the driver's choices using photomontages and driving simulators

### **6.1.2 Theoretical studies**

Another approach used to evaluate speed reduction is the theoretical one. This allowed the development of models with  $n$  degrees of freedom with the aim of evaluating kinematic quantities such as displacements, accelerations (Al-Nassr, 1982) (Bahram, Masoud & Mansour, 2007) or rotation of the vehicle (Hessling & Zhu, 2008) and/or driver (Khorshid & Alfares, 2004).

Other more articulated models allow to evaluate the vibrations transmitted to the ground (D'Apuzzo, 2007) (Toplak, Sever, Ivanič, Mohorić & Lubej, 2016) (Mhanna, Sadek & Shahrour, 2011) and their relationship with the road profile (Oke, Salauz, Adeyefaj, Akanbi & Oyawale, 2007) (Krylov, 1998).

Sometimes, to calibrate the theoretical models, the results of the field campaigns were taken into consideration and then compared with those deriving from the experimentation (Fwa & Liaw, 1992) (Hassen et al., 2017); this allowed to derive the empirical speeds (Vlahogianni, 2006) (Barbosa, 1995), the characteristics of the hump and the road (Pau M. , 2001) (Riviera, Bassani, & Dalmazzo, 2010); thus, knowing only the dimensions of the devices, it is possible to predict the speeds, without going through experimental observations (Philip & Weber, 1998) (Amirarsalan & Ali, 2014) (Sahoo, 2009) (Moreno & García, 2013), in order to reduce deaths and serious injuries (Babak, Zohn & Muennig, 2018).

Some evaluate with statistical formulations, after before-after studies, the changes in volume (Persaud, Retting, Garder Per & Lord, 2006)), rather than the influence on accident reduction (Yannis, Kondyli & Georgopoulou, 2014) (Damsere et al., 2019).

Other factors to consider are the damage to the flooring (Talaat & I., 2017) using as input data the speeds and volumes of traffic, or the vibrations transmitted to

buildings (Watts & Krylov, 2000) and the driver (Khorshid & Alfares, 2007) to define the geometry of the device.

Further studies determine the distance between devices using mathematical models (Tajudeen, Adebayo, & Sunday, 2004) (Basil, 2012) in order to predict the speed of crossing over the bumps.

In environmental terms, formulations have been built to evaluate the impacts of the devices both on vehicle dynamics in fuel consumption (Ribeiro, 2015) that in terms of exhaust emissions (Elumala & Suresh, 2017) (Boulter, 2001)).

## **6.2 Vibrations' effects on the human body**

During motion in a vehicle, the body is subject to vibrations. Vibration is a mechanical movement around a fixed point intended as a mechanical wave and, like all waves, it transfers energy and not matter. Vibration needs a mechanical structure to travel. Such a structure could be a vehicle, a tool or even a person, but if a mechanical coupling is lost, the vibration will no longer propagate.

Waves can be divided into:

1. deterministic, when the future oscillations can be predicted from the knowledge of the previous waves;
2. stochastic, commonly called random waves, can be characterized by some statistical properties.

Deterministic waves can be divided into periodic and non-periodic; the former, in turn, are divided into simple sinusoidal or multi-sinusoidal waves, which have the characteristic of being able to be represented analytically in a closed-form. The latter, the non-periodic ones, on the other hand, can in turn be divided into transient waves or shocks.

In most cases the waves to which the human body is exposed during work and leisure are stationary and non-stationary random waves.

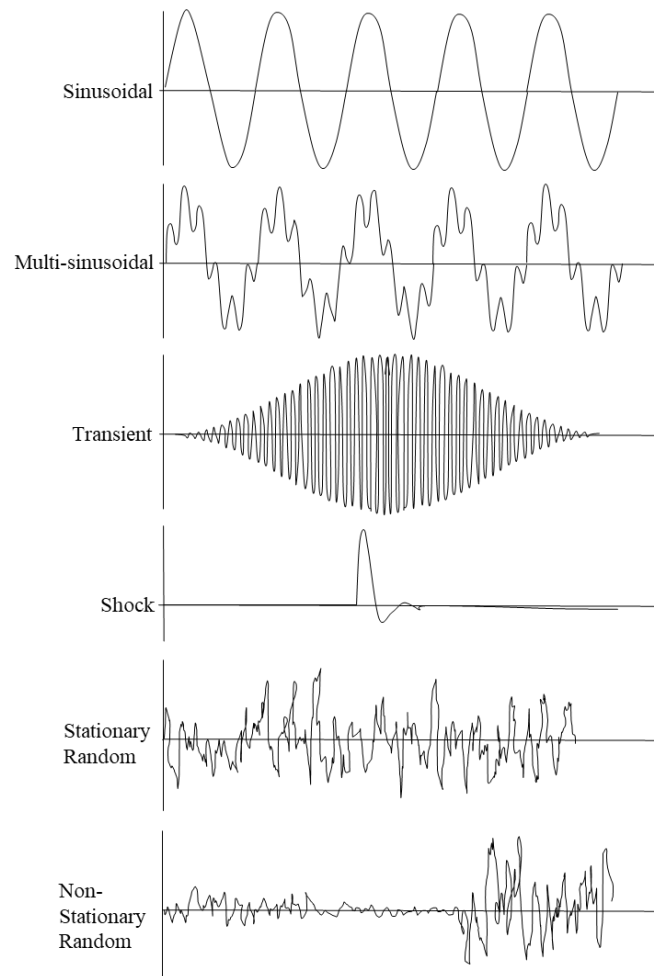


Figure 6.1 Various types of waves

The most basic type of wave is mathematically defined by the formula:

$$a(t) = A \sin(2\pi ft) \quad 6.1$$

In which:

$a(t)$  is the quantity represented as a function of time;

$A$  represents the amplitude, the maximum value that this quantity can have over time;

$f$  represents the frequency (expressed in Hertz, that is 1/s), that is the number of cycles that a periodically variable quantity completes in the unit of time; it could also be said that it represents the number of times in which this quantity reaches a certain value in the unit of time.

Amplitude is the representative quantity in a period, defined as the time interval corresponding to the wavelength and is indicated with  $T$ . This wavelength is the spatial distance between two crests. The period is also defined as the inverse of the frequency,

which is the number of pulses in one second. This frequency can be expressed in radians per second through the relationship in which the pulsation appears ( $\omega$ ):

$$\omega = 2\pi f \quad 6.2$$

The sine wave, in the most complete form, can be written as reported in the following equation:

$$a(t) = A \sin(\omega t + \phi) \quad 6.3$$

In which  $\phi$  is the initial phase, which is the fraction of the elapsed period with respect to a fixed time and is measured through an angle, called the phase angle. This phase angle is a function of the boundary conditions, such as displacement and initial speed; this represents the fraction of the period elapsed with respect to a fixed time (in our case the time in which  $t$  is equal to 0).

In reality, however, it is difficult to encounter a simple wave, so more complex wave descriptions are required than the sine wave. Such complex waves can be processed by superimposing multiple sine waves with different amplitudes, frequencies and phases. This superposition principle consists in the fact that if the single waves interact, the resulting vibration is equal to the sum of all the components, that is, the sum of different waves will generate a complex wave. The usefulness of this principle is that the superposition process can be reversed using mathematical techniques so that a complex wave can be resolved into simple waves with different amplitudes, frequencies and phases.

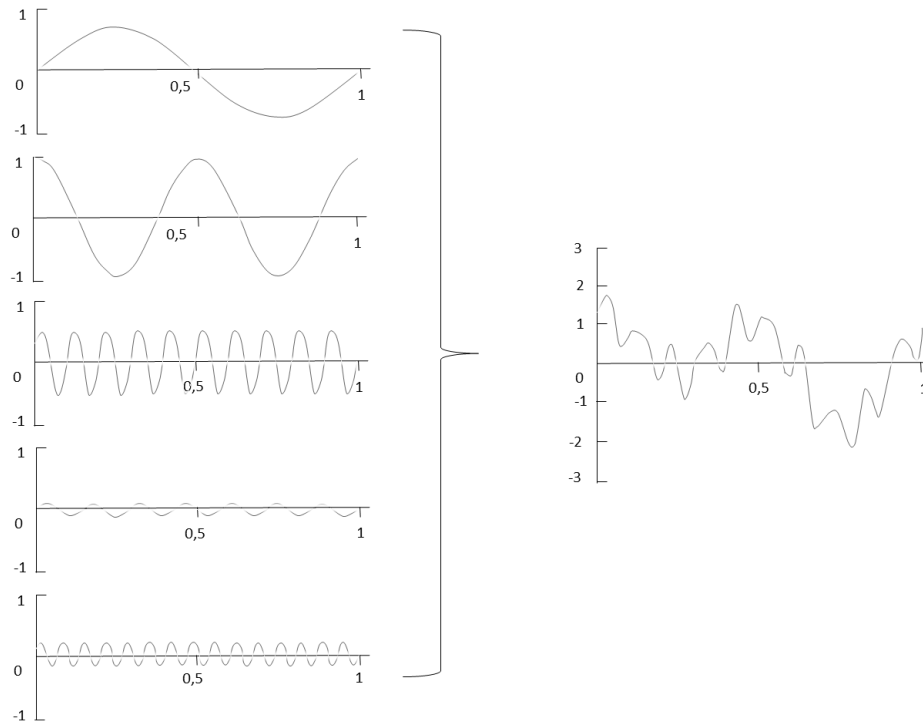


Figure 6.2 principle of superposition (taken from the Handbook of human vibration by MJGriffin)

This principle is the basis of the Fourier transform; in which given as input a complex signal the Fourier transform returns as output data a frequency response spectrum, which has frequency as independent variable and amplitude as dependent variable. It allows you to write a time-dependent function in the frequency domain, to do this it decomposes the function into the basis of exponential functions with a scalar product.

$$X(f) = \int_{-\infty}^{+\infty} x(t)e^{-j2\pi ft} dt \quad 6.4$$

This Fourier transform can only be used for finite signals, in short, the signal must be absolutely summable, therefore the following equation must hold:

$$\lim_{T \rightarrow \infty} \int_{\frac{-T}{2}}^{\frac{T}{2}} x(t) dt < \infty \quad 6.5$$

Vibration can be described in three quantities: displacement, velocity and acceleration. In the case of sine waves it is possible to pass analytically from one quantity to another simply by deriving or integrating. In particular, it is possible to pass from the displacement  $x(t)$  to the velocity  $v(t)$  by deriving the function  $x(t)$ ; deriving further obtains the acceleration  $a(t)$ . If, on the other hand, one wants to pass from the

acceleration  $a(t)$  to the speed  $v(t)$  and to the displacement  $x(t)$  just integrate. Since they are periodic functions, they can be integrated into closed form, so you can pass from one function to another by simply dividing or multiplying by the constant  $\omega$ , as the formula of this wave is given by:

$$x(t) = A \sin(\omega t) \quad 6.6$$

To have the first derivative it will be enough to multiply  $x(t)$  by the opposite of  $\omega$ , to have the second derivative just multiply  $x(t)$  by  $\omega^2$ .

In correspondence with the maximum displacement, the velocity equal to zero and the minimum acceleration will be found; in correspondence of the maximum speed, the displacement and zero acceleration will be obtained, instead in correspondence with the maximum acceleration there will be the minimum displacement and zero speed, as shown in the following graph in the Handbook of Human Vibration (Griffin MJ, 1990).

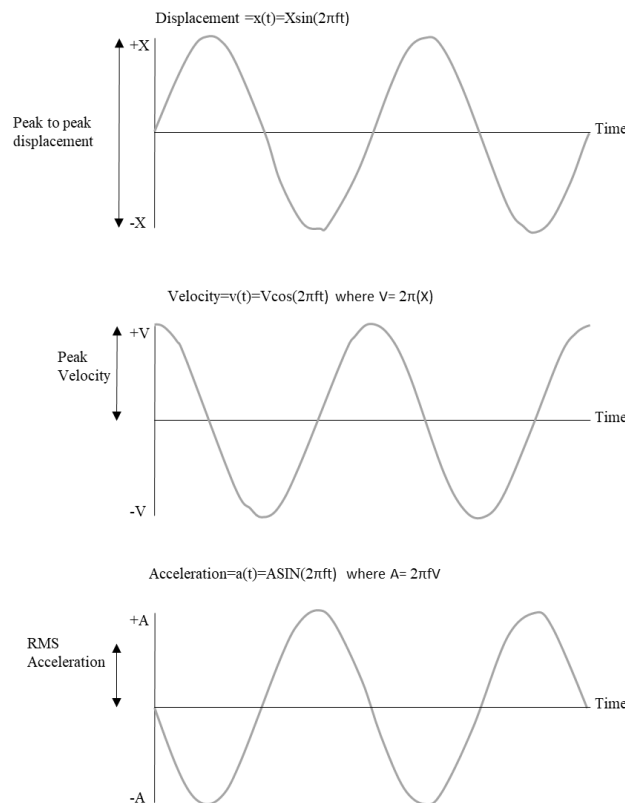


Figure 6.3 comparison of displacement, speed and acceleration

The magnitude of the acceleration of a vibration can be expressed in terms of peak to peak acceleration (acceleration calculated as the difference between the amplitude of the positive peak and the amplitude of the lower peak) and in terms of peak

acceleration (acceleration calculated by going to just takes a peak). The acceleration measure used most often in engineering is the RMS (root mean square) value, which is the square root of the standard deviation. This quantity can be calculated as the square root of the mean of the squares of the acceleration values, that is, the square root of the square mean. For a sinusoidal signal, the peak to peak acceleration is worth twice the amplitude, while the peak amplitude is worth the amplitude, while the peak amplitude is worth the amplitude, instead, the RMS value is worth the amplitude divided by the square root of 2.

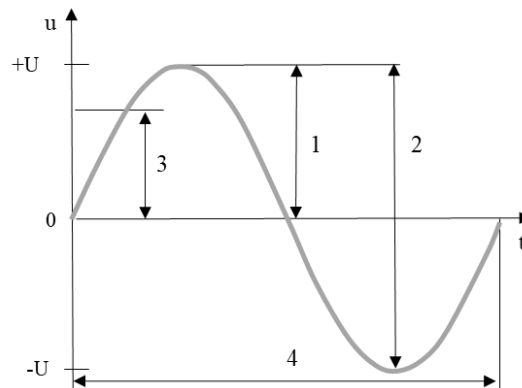


Figure 6.4 difference between peak acceleration, peak to peak and effective value (RMS).

The previous image shows the peak amplitude graphed with 1, the peak-to-peak amplitude with 2, the RMS represented with 3, while 4 depicts the period.

In the cases in question, not having to do with simple sine waves, this RMS value was determined through the PSD (power density spectrum), representing the vibration in the frequency range. Once this vibration was represented, the PSD for each frequency was calculated; this is obtained from the square of the ratio between the relative acceleration value divided by the respective frequency, as reported in the following formula; note the PSD, the RMS is nothing more than the area subtended by that PSD.

$$PSD(f_i) = \frac{acc_i(f_i)}{f_i} \quad 6.7$$

The acceleration measurement values described so far do not take into account the duration, or rather the exposure time. With the same peak to peak value, peak amplitude or RMS, it is easy to understand that the response of the human body varies according to the exposure time in which our body is subject to this vibration. Another measure comes into play, namely the vibration dose value in which these measures will be correlated with the duration.

The ISO 2631 standard suggests two formulas for evaluating this vibration dose based on the crest factor, ie the ratio between peak acceleration and RMS acceleration. This new quantity is useful because to evaluate the exposure to vibrations it is not only the acceleration value that is important, but the duration in which the human body is exposed to this vibration.

If this crest factor is greater than six, the VDV will be used, while if the crest factor is less than three, the eVDV will be used, these values have dimensions of  $\text{ms}^{-1.75}$ . They are calculated with the following formulas:

$$VDV = \left[ \int_{t=0}^{t=T} a^4(t) dt \right]^{\frac{1}{4}} \quad 6.8$$

$$eVDV = 1.4 \text{ r. m. s. } (duration)^{\frac{1}{4}} \quad 6.9$$

The crest factor is less than three (Pahansen De Alwis, 2014), then the second formula was used, in which the RMS must be weighted based on frequency as the body responds differently to vibrations not only based on amplitude but also based on frequency. This is the reason why the analysis of this vibration induced to the human body will be conducted in the frequency domain rather than in that of time, also because the human body reacts differently from the mechanical point of view.

The human body responds differently depending on the frequency of the vibrations. This is why vibration is sometimes described in the frequency domain instead of the time domain. To do this, the Fourier transform (FFT) is used. The FFT breaks down a random signal into a series of simple sinusoidal signals; therefore a frequency response spectrum is obtained in which there will be frequencies associated with the respective amplitudes.

To assess the exposure of the human body to vibrations according to the direction from which the vibrations originate, reference is made to ISO 2631 (for more information, see Appendix B2).

### 6.3 Simulation models

Traffic calming devices cause a strong vertical acceleration in the transiting vehicle due to the dynamic interaction between the vehicle and the irregularity. This acceleration causes a strong disturbance in the driver who is thus forced to reduce speed. It is evident that in order to operate an effective and continuous control of the speed of the vehicles, it is necessary to establish in series a certain number of such devices according to a specific spacing.

Various car models were used to evaluate this vertical acceleration that occurs as a result of the dynamic interaction between the vehicle and the irregularity of the road profile and then evaluate the acceleration perceived by the driver:

- 2-degree-of-freedom vehicle model (quarter-car)
- 4-degree-of-freedom vehicle model (half-car)
- 5-degree-of-freedom vehicle model (half-car plus driver insertion)

The substantial difference between the quarter-car and half-car model lies in the portion of the car that is considered, in the first case only a quarter of a car is considered, in the second case half the car is considered (for further information see Appendix B.3).

### 6.3.1 Input data

From the three models presented above, acceleration as a function of time was obtained. These signals must be transformed from the time domain to the frequency domain. Known the accelerogram in the time domain, to carry out an analysis on the effects it is necessary to evaluate the acceleration in the frequency domain, this means making a change of variables through the use of the DFT (fast discrete Fourier transform). To evaluate this frequency response it was first necessary to take only part of the accelerogram as this algorithm only works if a vector of  $2k$  elements is entered as input data. In practice, the data must be a power of 2, so once the size of the accelerogram is known,  $2k$  points are taken so that  $2k$  is less than the size of the accelerogram; by truncating this signal it is possible to represent it in the frequency range. The FFT returns the Fourier transform that is a vector in which the  $k$ -th element:

$$c_j = \frac{1}{n} \sum_k \left[ v_k e^{-i\left(\frac{2\pi j}{n}\right)k} \right] \quad 6.10$$

Where  $n$  is the number of elements of  $v$  and  $i$  is the imaginary unit, all this is scaled by  $n$ , the number of data of the vector  $v$ .

Of particular importance is the sampling theorem formulated by Nyquist; according to this theorem, a continuous-time signal  $x(t)$  with spectral content limited to  $F_b$  can be reconstructed, starting from its sampled version, if the sampling frequency  $F_c$  (i.e. the inverse of the sampling time step) is such that  $F_c > 2 F_b$ .

Once the sampling time step is known, the sampling frequency can be known, which allows the signal to be represented in the frequency domain up to a frequency equal to half the sampling frequency.

From this FFT comes out as a result of the acceleration values and the corresponding frequencies. The step with which the frequency domain  $df$  is discretized is equal to the ratio between  $f_s$  (sampling frequency) and the number of points of the signal sampled in base  $2^k$ .

The kinematic quantity that represents the vibration is the acceleration of the signal computed as RMS (Root mean square) which is calculated as the square root of the area subtended by the PSD (function of the power density). The PSD is evaluated, for each frequency, by dividing the relative acceleration squared by the respective frequency. Once the PSD for all  $2^k$  was calculated, the frequency domain was discretized by frequency bands and the band by third octaves was chosen; the minimum frequency of the  $i$ -th band is equal to the maximum frequency of the  $i$ -th-1 band. The minimum frequency of the  $i$ -th band increases with respect to the previous one by a factor equal to  $\sqrt[3]{2} \cong 1.26$ , the higher frequency will therefore be equal to the product between  $\sqrt[3]{2}$  and the lower frequency, instead, the center frequency will be equal to  $\sqrt{f_l f_s}$ . The table below shows the discretization by bands, in which  $f_c$  is the central frequency,  $f_1$  the lower frequency,  $f_2$  the upper frequency and  $df$  the difference between the upper and lower frequency:

*Table 6.1 Discretization by bands*

<b>fc [Hz]</b>	<b>f1 [Hz]</b>	<b>f2 [Hz]</b>	<b>df [Hz]</b>
0.5	0.445449	0.561231	0.115782
0.629961	0.561231	0.707107	0.145876
0.793701	0.707107	0.890899	0.183792
1	0.890899	1.122462	0.231563
1.259921	1.122462	1.414214	0.291752
1.587401	1.414214	1.781797	0.367584
2	1.781797	2.244924	0.463127
2.519842	2.244924	2.828427	0.583503
3.174802	2.828427	3.563595	0.735168
4	3.563595	4.489848	0.926253
5.039684	4.489848	5.656854	1.167006

6.349604	5.656854	7.12719	1.470335
8	7.12719	8.979696	1.852507
10.07937	8.979696	11.31371	2.334012
12.69921	11.31371	14.25438	2.940671
16	14.25438	17.95939	3.705013
20.15874	17.95939	22.62742	4.668024
25.39842	22.62742	28.50876	5.881342
32	28.50876	35.91879	7.410027
40.31747	35.91879	45.25483	9.336048
50.79683	45.25483	57.01752	11.76268
64	57.01752	71.83757	14.82005
80.63495	71.83757	90.50967	18.6721

Since the following study is based on a frequency range between 0.5 Hz and 80 Hz, 23 bands have been identified. Then the PSD was evaluated in a frequency range ranging from 0.445449 Hz and 90.50967 Hz and subsequently, the average of the PSDs falling in each band was evaluated.

The PSD before and after discretization by one-third octave bands has been graphically reported below; it can be seen that after this discretization there is a smoothed effect of the PSD, to make a better visualization of this effect a logarithmic scale has been chosen for the ordinates.

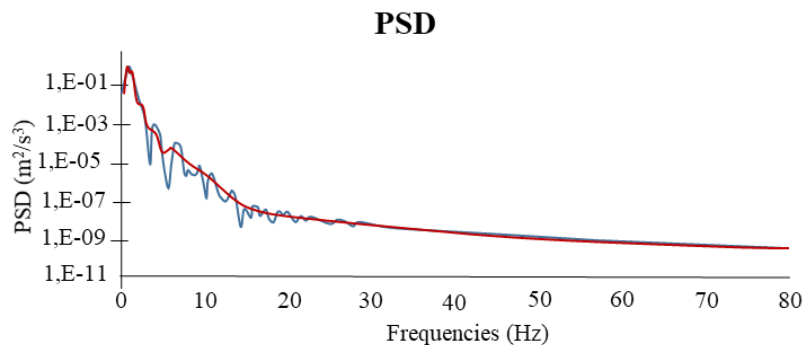


*Figure 6.5 Difference between PSD as a function of time and its representation in one-third octave band frequencies*

In this way, a spectral representation of the accelerations in bands of one third of an octave was obtained. The RMS was calculated as the square root of the area subtended by the PSD for each band, or the square root of the product of the average PSD was evaluated for the difference between the maximum and minimum frequency

of each band. Once the RMS has been obtained, it is appropriate to make some considerations on the response of the human body based on the frequencies. With the same amplitude the human body has a different perception based on the frequency with this logic it is necessary to weigh the RMS according to its own frequency. It is appropriate to put a reduction factor for the frequencies that are at the extremes of our domain of interest, therefore the ISO2631 standard (International Organization for Standardisation, 1986) suggests the use of multiplying factors for each frequency and for each x, y, z axis. In the case under analysis, being interested in acceleration along the z axis, the weighting values  $W_k$  were taken into consideration.

fc [Hz]	Wk
0.5	0.418
0.629961	0.459
0.793701	0.477
1	0.482
1.259921	0.484
1.587401	0.494
2	0.531
2.519842	0.631
3.174802	0.804
4	0.967
5.039684	1,039
6.349604	1,054
8	1,036
10.07937	0.988
12.69921	0.902
16	0.768
20.15874	0.636
25.39842	0.513
32	0.405
40.31747	0.314
50.79683	0.246
64	0.186
80.63495	0.132

To evaluate a single indicative value of the discomfort level, the effective weighted acceleration was calculated with the following equation:

$$a = \sqrt{\sum_i^{23} (W_{ki}RMS_i)^2} \quad 6.11$$

Once these models were developed, the crossing of four different types of vehicles, representative of the entire vehicle fleet, was simulated on some traffic calming altimetric devices.

The four macro-categories of vehicles can be summarized in:

- small cars represented with the designation A;
- medium-sized cars called category C cars;



- sedans represented with the designation D;
- off-road vehicles falling into category E.



Road profiles were then selected, with a spatial pitch of 0.02 cm in order to have a sufficiently high sampling frequency to be able to represent the relative acceleration at frequencies above the analysis range (between 0.5 Hz and 80 Hz). Particular attention must be paid to choosing the length of the profile. Once the spatial step of integration has been defined, the number of points must be arbitrarily defined; this should not be too small, because the signal is truncated when the phenomenon has not yet been exhausted, nor too high, otherwise the RMS would be underestimated. A fair compromise must be found between these two limit situations, in the case in the analysis a number of data equal to 1500 was considered, therefore road profiles with a length of 30 m were constructed. In the evaluation of the FFT, not all points are taken into consideration, remembering the rule of construction of the signal based on  $2^k$ , therefore only 1024 points will be considered, corresponding to a length of 20.48 m. In summary, with this choice, the signal runs out or is close to exhaustion after 20.48 m.

The profiles initially implemented are parabolic, for the representation of these the literature gives the dimensions for points with a step of 0.3048 m (1 foot), but since the step of the following study is equal to 0.02 m, it was preferred to evaluate this profile in closed form. With the help of the Maple18 calculation program, the formula for the parabolic profiles was obtained and then solved a system of 3 second degree equations, imposing the passage of this parabola by three points (at the starting point of the bump, in the middle and in the final point).

```

> L:=3.6576;
> h:=0.0635;
> eq1:=0=A*0^2+B*0+C;
> eq2:=h=A*(L/2)^2+B*(L/2)+C;
> eq3:=0=A*(L)^2+B*L+C;
> sol:=solve({eq1,eq2,eq3},{A,B,C});
> A:=-4*h/(L^2);
> B:=4*h/L;
> C:=0;

```

$L = 3.6576$   
 $h = 0.0635$   
 $eq1 := 0 = C$   
 $eq2 := h = \frac{1}{4}AL^2 + \frac{1}{2}BL + C$   
 $eq3 := 0 = AL^2 + BL + C$   
 $sol := \left\{ A = -\frac{4h}{L^2}, B = \frac{4h}{L}, C = 0 \right\}$   
 $A = -\frac{4h}{L^2}$   
 $B = \frac{4h}{L}$   
 $C = 0$

As you can see, to calculate the profile of the parabola it will be enough to know the height and length of the hump, as from them it is possible to obtain the coefficients A, B, C:

$$A = -\frac{4h}{L^2} \qquad B = \frac{4h}{L} \qquad C = 0$$

Then you can trace the profile of the bump as a function of the progressive with the equation:

$$h = ax^2 + bx + c \qquad 6.12$$

On the other hand, as regards the trapezoidal profiles (speed tables), they too have been determined through analytical functions, as the slopes of the ramps have been calculated as a ratio between the height of the device and the length of the ramp.

Then the profile in the first ascending section was calculated with the equation:

$$h = ax \quad 6.13$$

In the central section the height is constant, while in the descending section the formula is used:

$$h = h_{MAX} - ax \quad 6.14$$

The profiles have been inserted starting from the 200th point, i.e. 4 m from the beginning of the progressive, since the half-car model proposed has a finite length wheelbase, therefore a portion of the initial profile having a constant height and equal to 0, the minimum length is that of the centre distance. The 200 points have been entered, so that any vehicle with a 4m wheelbase can be used in modelling. To improve the representation of the phenomenon, however, the starting point was taken as the one in which the front wheel begins to overcome the bump, therefore the  $n$  superfluous points calculated as the difference between 4 m and the length of the wheelbase have been eliminated. All this allows you to have a more precise signal because you are going to eliminate null values that would lead to underestimating the final result.

The following are the characteristics of the vehicles used in the modelling.

Vehicle	A	C	D	E
Elastic stiffness of the front suspension (N/m)	12400	12800	12950	13400
Elastic stiffness of the rear suspension (N/m)	10600	13800	14720	17000
Linear coefficient of kinematic viscosity of the front suspension (N s/m)	1550	1600	1618	1675
Linear coefficient of kinematic viscosity of the rear suspension (N s/m)	1325	1725	1840	2125
Suspended mass (kg)	893	963	1220	1700
Front unsprung mass (kg)	80	92	105	115
Rear unsprung mass (kg)	72	120	110	130
Elastic stiffness of the front tire (N/m)	165000	170000	180000	200000
Elastic stiffness of the rear tire (N/m)	150000	150000	170000	200000
Moment of inertia	1018.76	1284	2313.21	3264
Wheelbase length (m)	2.35	2.47	2.69	2.85
Total length (m)	3.70	4.0	4.77	4.80
Tire imprint length (m)	0.12	0.14	0.16	0.2

Length of the distance between the center of gravity of the car and the driver (m)	1	1.2	1.3	1.6
--	---	-----	-----	-----

These quantities were taken from the technical data sheets (Dixon, 1986), but it should be noted that the masses must be halved because this study is conducted on a Half-car model while the reported masses relate to the entire vehicle; instead the elastic stiffnesses and the linear viscosity coefficients reported are relative to the single wheel and therefore must be taken as they are written. Clearly, the wheelbase lengths, total length and the distance of the driver from the centre of gravity will also be taken whole.

### 6.3.2 Model validation with irregular profile

To validate the method and make assessments on the possibility of applying this method also in other fields, another completely different scenario has been proposed. The dynamic response of the vehicle was studied on a generic uneven road profile.

A portion of the profile of equal length with respect to the one in which the bump was inserted was therefore studied; however, rather than having a singularity, such as a hump, it has an irregular but homogeneous profile:

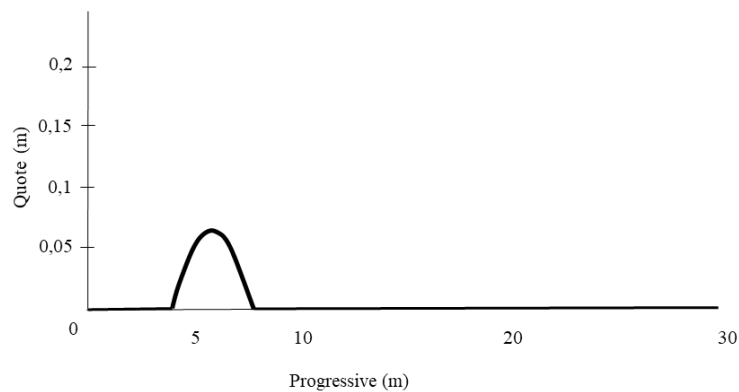


Figure 6.6 Road profile with a bump 12 feet long and 3 inches high

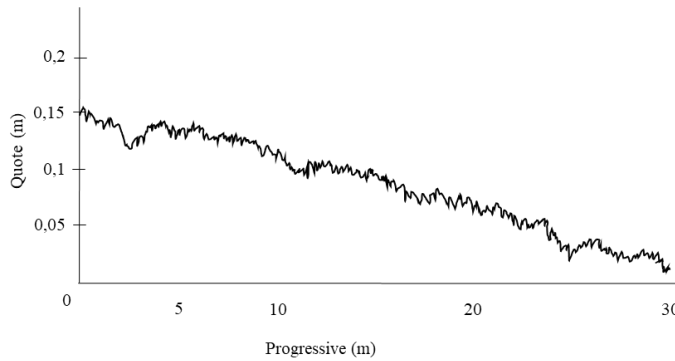


Figure 6.7 Irregular profile

Both the R.M.S. that the eVDV vibration dose for the four types of vehicle at different speeds in a range between 20 km / h and 60 km / h, presumed speeds with which this profile could be traveled.

From an operational point of view, the same Mathcad worksheet was used, inserting the profile with a spatial pitch of 0.02 m (therefore the analyzes were conducted in the same conditions with which the analyzes on the bumps were conducted).

Below is a summary table of the results in terms of RMS and eVDV.

Speed	A		B		D		E	
	RMS	eVDV	RMS	eVDV	RMS	eVDV	RMS	eVDV
20	0.084571	0.160158	0.095888	0.18332	0.083032	0.015992	0.077435	0.146327
30	0.109479	0.019077	0.122485	0.212682	0.098955	0.172562	0.087931	0.0150548
40	0.119479	0.196696	0.134377	0.221	0.10417	0.086094	0.086094	0.136246
50	0.129031	0.198623	0.144369	0.0223481	0.112445	0.090744	0.90744	0.134943
60	0.138003	0.203517	0.154274	0.225432	0.122934	0.097919	0.097919	0.13225

From a graphic point of view instead:

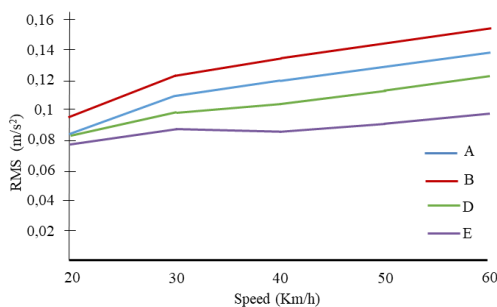


Figure 6.8 RMS as a function of speed for different vehicles

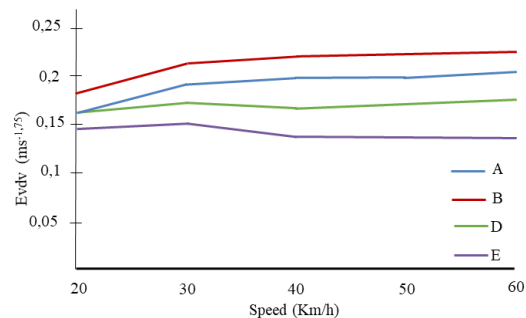


Figure 6.9 Speed-dependent eVDV for different vehicles

Interpreting these graphs it can be seen that the RMS acceleration increases as the travel speed of the profile increases, while the eVDV remains almost constant, this is because the eVDV is given by the following equation:

$$eVDV = 1.4 a_{RMS} d^{0.25} \quad 6.15$$

Therefore, as the speed increases, the RMS acceleration increases while the duration in which the vehicle is exposed to these stresses decreases.

There is also a translation between the responses of the various vehicles; in particular, if the vehicles were classified according to the acceleration they undergo, it is observed that the vehicle that is subject to the greatest vibration is vehicle A, then vehicle C, vehicle D and lastly vehicle E.

The percentage reduction in vibration with respect to vehicle A is shown below, highlighting that this reduction increases with increasing speed, as they are designed to have the best possible comfort at high travel speeds.

*Table 6.2 Percentage reduction of vibration compared to vehicle A*

Speed	Reduction %			
	RMS	eVDV	RMS	eVDV
20	86.59283	87.23553	80.75621	79.82049
30	80.78981	81.13581	71.7891	70.78533
40	77.52036	75.12159	64.06916	61.64948
50	77.88711	76.71669	62.85591	60.38233
60	79.68558	78.32152	63.47047	59.9849

These results are very useful in verifying the validity of the model applied. In fact, the E-type vehicles are designed to travel on roads with very irregular profiles, so a lower response in terms of acceleration is expected than the classic small cars. In the same way, the vehicles falling into the D segment are designed for longer journeys and with higher speeds than the small cars, so in this design the driver's comfort has a significant thickness. The results of this model show that segment E vehicles undergo less acceleration than type A vehicles, thus increasing comfort.

Ultimately it can be said that the results deriving from these analyzes are comforting in evaluating the goodness of the model that can also be applied in other fields. One can imagine being able to use it in the future to evaluate the discomfort on bumpy roads.

### 6.3.3 Case study

So far it has been explained how to obtain the weighted acceleration (RMS) known the characteristics of the vehicle, the geometry of the bump and the speed with which the vehicle passes through it. The initial objective of this work is to evaluate for a given bump and for a given vehicle, a relationship that links acceleration to speed. You can intuitively imagine that acceleration increases with increasing speed and height of the bump as well as decreasing vehicle characteristics. An analysis was carried out below to evaluate how the input parameters can vary the acceleration understood as a disturbance index.

In this study, the entire vehicle fleet of cars for private use (described above) was represented. 5 types of bumps have been implemented in the model, 4 of which are parabolic and 1 trapezoidal. The geometric characteristics of each bump are shown below:

1. Parabolic speed hump (length 12 feet (3.65 m); height 2.5 inches (0.0635 m));

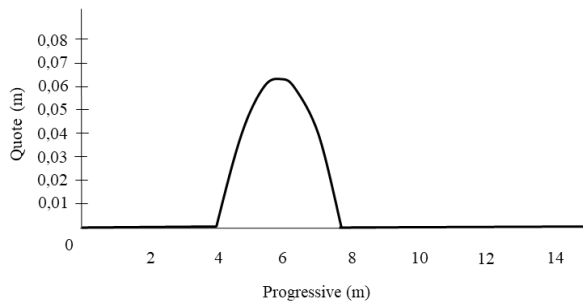


Figure 6.10 Speed hump (12 feet; 2.5 inch)

2. Parabolic speed hump (length 12 feet (3.65 m); height 3 inch (0.0762 m));

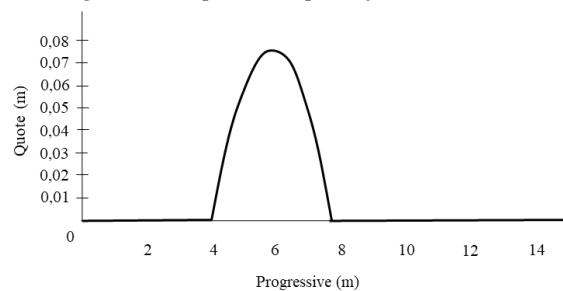


Figure 6.11 Speed hump (12 feet; 3 inch)

3. Parabolic speed hump (length 22 feet (6.70 m); height 3 inch (0.0762 m));

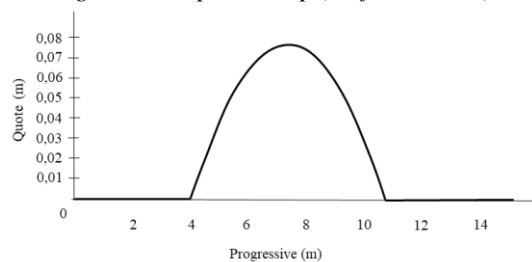


Figure 6.12 Speed hump (22 feet, 3 inch)

- 4. Parabolic speed hump (length 22 feet (6.70 m); height 3.5 inches (0.0889m));

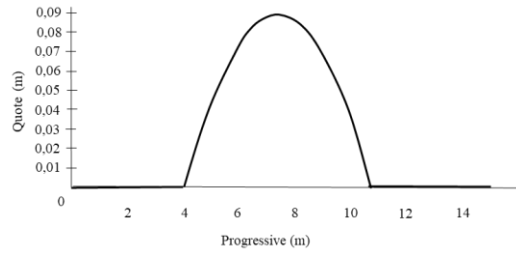


Figure 6.13 Speed hump (22 feet; 3.5 inch)

- 5. Trapezoidal speed hump (length 22 feet (6.70 m); height 3 inch (0.0762 m));

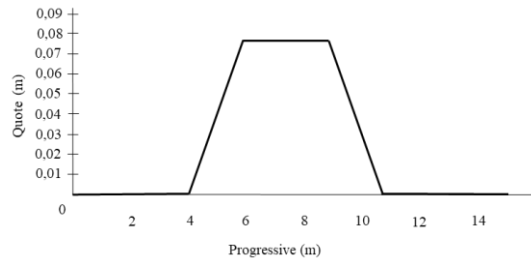


Figure 6.14 Speed table (22 feet, 3 inch)

The analyzes were conducted in a speed range between 0 km/h and 40 km/h, with a speed step of 5 km/h for each vehicle on each bump.

Thus the acceleration diagrams were obtained, in terms of RMS or the eVDV, as a function of speed. In total, 20 diagrams (V-RMS) and 20 diagrams (V-eVDV) were obtained.

The results for each vehicle on each type of bump are shown below in both numerical and graphical form:

**Vehicle A**

Table 6.3 Correlation between speed and accelerations (RMS and eVDV) on the vehicle A

Speed	1		2		3		4		5	
	RMS	eVDV								
5	0.0150	0.0265	0.0181	0.0324	0.0096	0.0148	0.0111	0.0183	0.0126	0.0215
10	0.0522	0.0930	0.0627	0.1126	0.0383	0.0701	0.0447	0.0834	0.0522	0.0989
15	0.0795	0.1304	0.0954	0.1579	0.0596	0.1052	0.0695	0.1237	0.0891	0.1580
20	0.1289	0.2105	0.1547	0.2596	0.1089	0.1831	0.1270	0.2173	0.1372	0.2304
25	0.2014	0.3338	0.2417	0.4044	0.1929	0.3316	0.2251	0.3898	0.2193	0.3697
30	0.2761	0.4516	0.3313	0.5483	0.3009	0.5154	0.3510	0.6045	0.3312	0.5685
35	0.3496	0.5699	0.4196	0.6903	0.4230	0.7184	0.4935	0.8413	0.4578	0.7790
40	0.3692	0.5975	0.4430	0.7242	0.4831	0.8150	0.5636	0.9544	0.5239	0.8859

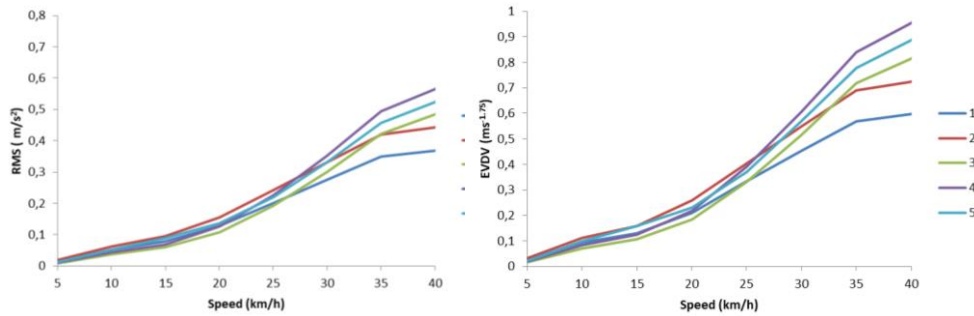


Figure 6.15 Graphic representation of the correlation between speed and accelerations (RMS and eVDV) on vehicle A

**Vehicle C**

Table 6.4 Correlation between speed and accelerations (RMS and eVDV) on the vehicle C

Speed	1		2		3		4		5	
	RMS	eVDV								
5	0.0157	0.0275	0.0189	0.0337	0.0101	0.0153	0.0117	0.0192	0.0139	0.0243
10	0.0573	0.1013	0.0688	0.1228	0.0425	0.0775	0.0496	0.0920	0.0604	0.1162
15	0.1044	0.1767	0.1253	0.2174	0.0731	0.1304	0.0853	0.1532	0.1186	0.2129
20	0.1524	0.2494	0.1828	0.3049	0.1163	0.1984	0.1356	0.2359	0.1629	0.2830
25	0.2195	0.3652	0.2635	0.4425	0.1922	0.3301	0.2242	0.3874	0.2319	0.3992
30	0.2943	0.4845	0.3531	0.5861	0.2990	0.5117	0.3489	0.5995	0.3383	0.5778
35	0.3695	0.5969	0.4433	0.7238	0.4252	0.7200	0.4961	0.8505	0.4645	0.7892
40	0.3907	0.6310	0.4688	0.7640	0.4929	0.8292	0.5751	0.9709	0.5388	0.9084

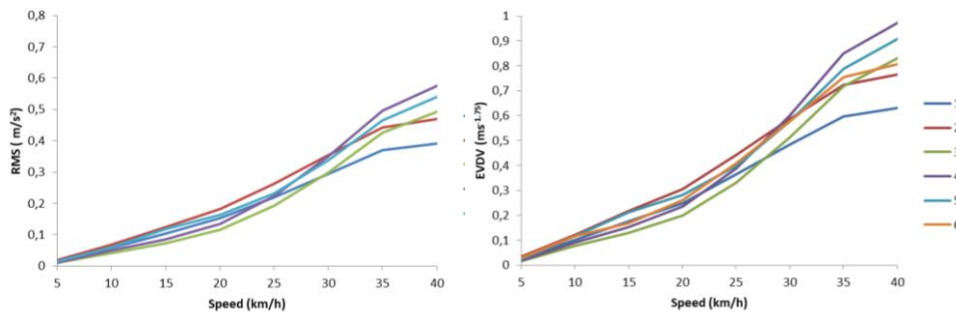


Figure 6.16 Graphic representation of the correlation between speed and accelerations (RMS and eVDV) on vehicle C

**Vehicle D**

Table 6.5 Correlation between speed and accelerations (RMS and eVDV) on the vehicle D

Speed	1		2		3		4		5	
	RMS	eVDV								
5	0.0142	0.0245	0.0170	0.0301	0.0097	0.0147	0.0113	0.0184	0.0137	0.0245
10	0.0582	0.1056	0.0698	0.1277	0.0429	0.0782	0.0501	0.0928	0.0693	0.1343
15	0.1131	0.1932	0.1357	0.2328	0.0755	0.1352	0.0880	0.1588	0.1293	0.2337
20	0.1611	0.2697	0.1933	0.3293	0.1167	0.2011	0.1361	0.2386	0.1732	0.3029
25	0.2123	0.3515	0.2548	0.4259	0.1837	0.3188	0.2144	0.3744	0.2278	0.3969
30	0.2648	0.4405	0.3177	0.5333	0.2775	0.4787	0.3238	0.5623	0.3169	0.5429
35	0.3183	0.5245	0.3820	0.6351	0.3853	0.6608	0.4496	0.7737	0.4231	0.7275
40	0.3311	0.5355	0.3973	0.6487	0.4404	0.7475	0.5138	0.8742	0.4831	0.8213

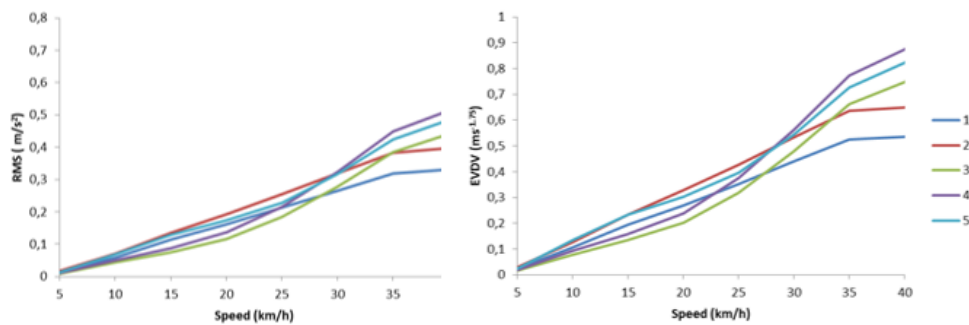


Figure 6.17 Graphic representation of the correlation between speed and accelerations (RMS and eVDV) on vehicle D

**Vehicle E**

Table 6.6 Correlation between speed and accelerations (RMS and eVDV) on the vehicle E

Speed	1		2		3		4		5	
	RMS	eVDV								
5	0.0124	0.0198	0.0149	0.0244	0.0094	0.0139	0.0109	0.0172	0.0129	0.0220
10	0.0681	0.1263	0.0817	0.1538	0.0456	0.0844	0.0532	0.1002	0.0796	0.1552
15	0.1352	0.2435	0.1623	0.2950	0.0781	0.1410	0.0912	0.1657	0.1322	0.2427
20	0.1779	0.3110	0.2134	0.3772	0.1209	0.2137	0.1410	0.2525	0.1744	0.3139
25	0.2097	0.3605	0.2517	0.4366	0.1765	0.3069	0.2060	0.3611	0.2166	0.3821
30	0.2392	0.4051	0.2870	0.4910	0.2473	0.4343	0.2885	0.5097	0.2819	0.4944

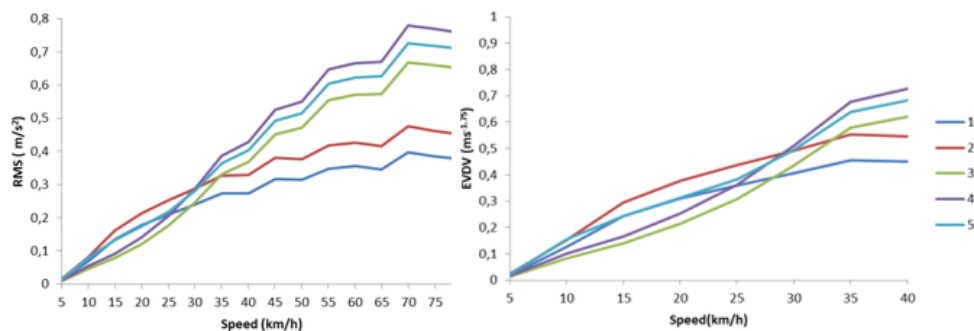


Figure 6.18 Graphic representation of the correlation between speed and accelerations (RMS and eVDV) on vehicle E

From the graphs, it is possible to deduce how the response in terms of RMS and eVDV varies with the variation of the geometric characteristics of the device (height and length).

It should be noted that at the same speed, the device that causes greater acceleration, for all vehicles, both in terms of RMS and in terms of eVDV, is the fourth device (length equal to 6.70 m and height 8.89 cm).

The height plays an important role in fact if attention is paid to the comparison between devices of equal length and it is observed that at the same speed, the device with a greater height causes greater acceleration. This result can be seen in all types of vehicles. In particular, it was found that for the same length, an increase of 1/2 inch (0.0127 m) shows an increase in acceleration of about 20% of the acceleration on the first bump. By way of example, the increase in percentage terms caused by crossing the bump of a single-vehicle at a single speed is shown below (but this is valid for all speeds and for all vehicles):

	1	2	
Speed	RMS	RMS	%
30	0.276054	0.331264	20.00

	3	4	
Speed	RMS	RMS	%
30	0.300871	0.351016	16.67

	1	2	
Speed	eVDV	eVDV	%
30	0.451627	0.548292	21.40

	3	4	
Speed	eVDV	eVDV	%
30	0.515403	0.604497	17.29

The accelerations, caused by the same bump, on the different vehicles were then compared. Then the diagrams (V-RMS) and (V- eVDV) will be shown in which the two values evaluated for each car on a given bump will be compared.

1. SPEED HUMP

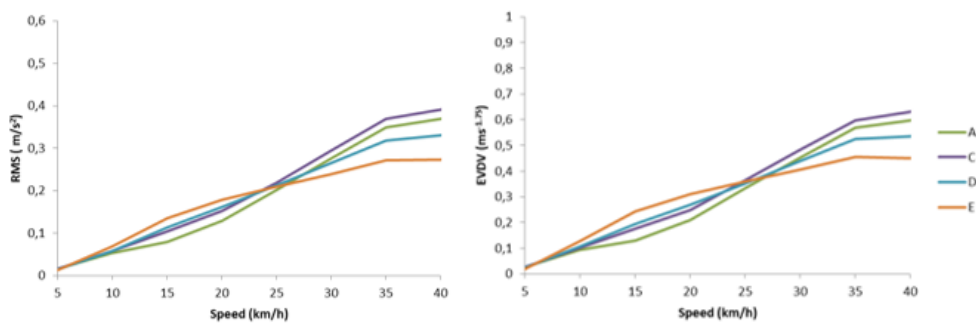


Figure 6.19 Correlation between speed and accelerations (RMS and eVDV) of the different vehicles on the speed hump

2. SPEED HUMP

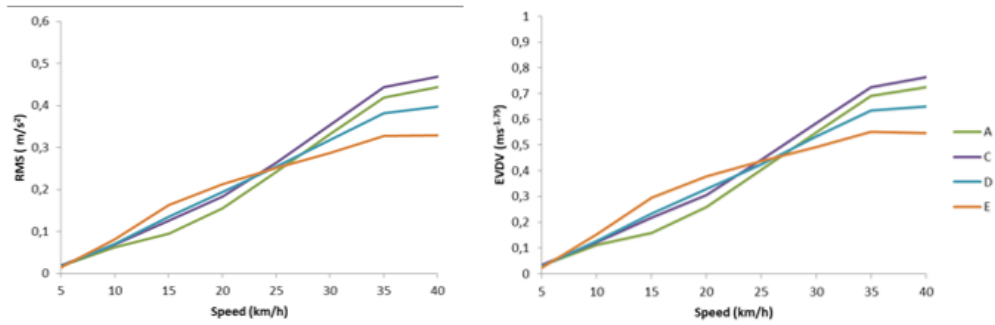


Figure 6.20 Correlation between speed and accelerations (RMS and eVDV) of the different vehicles on the speed hump

3. SPEED HUMP

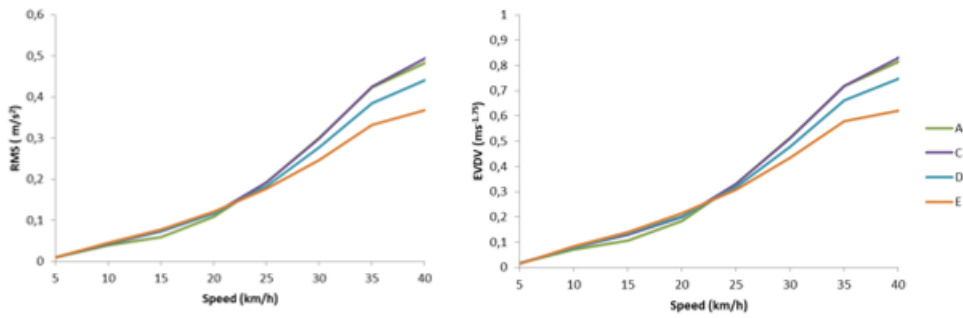


Figure 6.21 Correlation between speed and accelerations (RMS and eVDV) of the different vehicles on the speed hump

4. SPEED HUMP

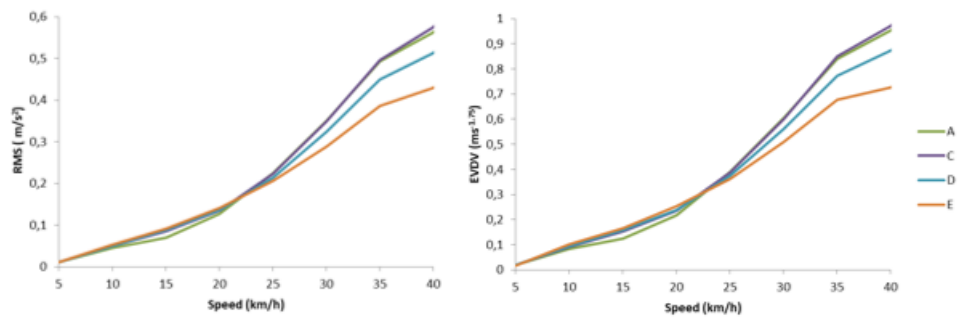


Figure 6.22 Correlation between speed and accelerations (RMS and eVDV) of the different vehicles on the speed hump

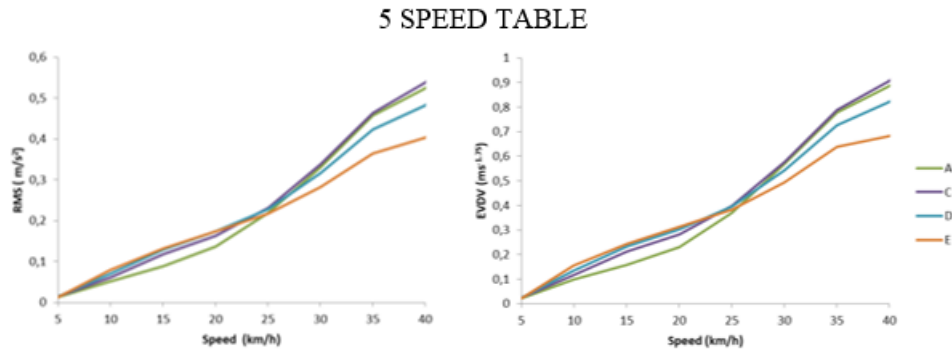


Figure 6.23 Correlation between speed and accelerations (RMS and eVDV) of the different vehicles on the speed table

It can be deduced from these comparisons that the disturbance (intended both as vertical acceleration RMS and as vibration dose eVDV) is very similar for all speeds up to 25 km / h, after this value it can be seen that the vehicles of segment E and segment D suffer less stress than vehicles in segment A and segment C.

In the literature, there are several works that evaluate the speeds according to the category of vehicle that crosses them, but some estimate that the speeds of crossing the bumps remain unchanged regardless of the type of vehicle (Latoya & Nedzesky, 2003) (Namee & Witchayangkoon, 2011).

Comparing the results obtained with those from the literature, it is confirmed that at certain speeds, under a certain threshold, the induced accelerations do not vary with the type of vehicle; in fact on a bump the crossing speeds of each vehicle category are the same.

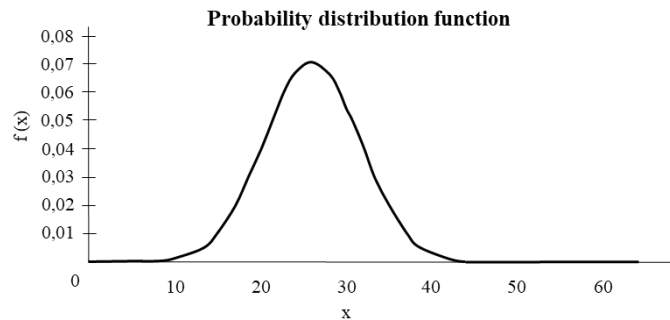
Once the relationships between speed-RMS and speed-eVDV have been identified, an attempt has been made to determine an RMS acceleration threshold or eVDV vibration dose beyond which the driver experiences discomfort and tends to be below this threshold. The goal was to evaluate this threshold and, known the geometry of the device, identify the corresponding crossing speed.

To do this, it was necessary to identify from the literature the speed distributions, as well as the average speed, of crossing the bump.

Among the many studies consulted, reference was made to those of Smith (2002) in which two temporary devices (speed hump and speed table) were considered on which average speed and a V85 were obtained (taken a speed sample, 85% of the population travels a given space with a speed lower than this value of V85). To

represent the probability function, that is the function that assigns a probability of the event to each value of the independent variable (in the case in question, the velocity), was used a normal continuous probability distribution, commonly called Gaussian.

$$f(x) = \frac{1}{\sqrt{2\pi}\sigma} e^{-\frac{1}{2}\left(\frac{x-\mu}{\sigma}\right)^2} \quad 6.16$$



To identify this distribution it is necessary to enter two characteristic values (mean  $\mu$  and standard deviation  $\sigma$ ). The data that you have only the average speed ( $\mu$ ) and V85, so the mean is known while the standard deviation remains to be calculated.

To calculate this value was used the distribution function of the standardized continuous random variable. This has the particularity of having zero mean and unit standard deviation. A standardization must be performed, which consists in identifying a quantity  $Z$  given by the equation:

$$Z = \frac{x - \mu}{\sigma} \quad 6.17$$

in which  $\mu$  is the average, while  $\sigma$  is the standard deviation. To each value of  $Z$  will be associated therefore a value will be associated with a probability value of not exceeding, clearly for  $Z$  zero, it means that  $x$  is equal to the average therefore the probability of exceeding a is equal to 0.5; while for  $Z$  which tends to infinity, that is, when one moves away from the mean  $Z$ , the probability of non-exceedance approaches asymptotically to 1 since this threshold is almost certain not to be exceeded. There are tables that associate the probability of not exceeding to each value of  $Z$ . Then the data in possession is a V85, so it will be necessary to enter these tables with the value of 0.85 of the probability of not exceeding and take the relative value of  $Z$ , in the case in question it will be equal to 1.05.

Known Z, the standard deviation ( $\sigma$ ) will be given by the inverse formula:

$$\sigma = \frac{x - \mu}{Z} \tag{6.18}$$

Where x will be the value of V85 while  $\mu$  is the average value of the speed (V50).

Daniel J. Smith (2002) reports for three sites the V50 and V85 for the two temporary devices inserted and the standard deviation calculated as previously described.

As a first step, the acceleration (RMS) and the vibration dose (eVDV) as a function of speed was calculated, building the V-RMS and V-eVDV diagrams for each vehicle on the two bumps.

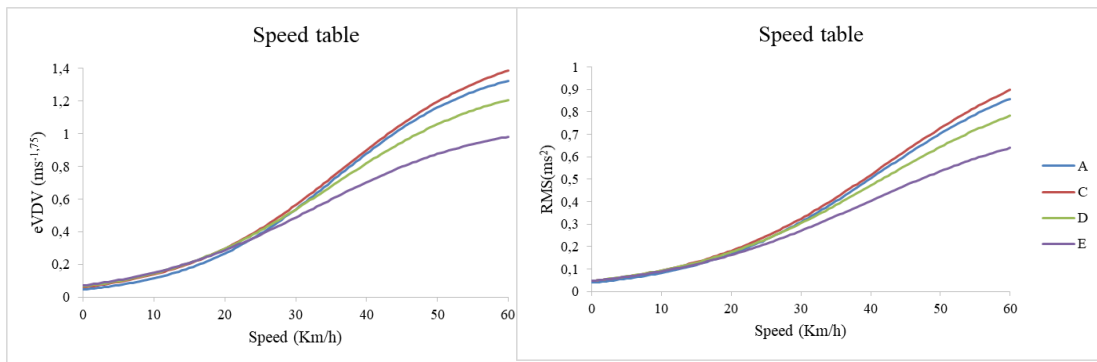


Figure 6.24 The V-RMS and V-eVDV diagrams for each vehicle on the speed table

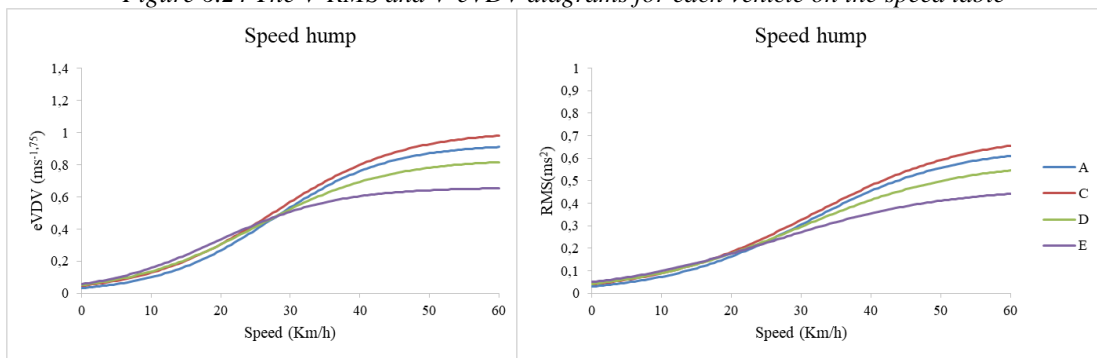


Figure 6.25 The V-RMS and V-eVDV diagrams for each vehicle on the speed hump

These graphs are the result of analyzes conducted in a speed range between 0 km/h and 60 km/h with a pace of 5 km/h.

The V-RMS and V-eVDV curves were then represented from an analytical point of view so as to be able to derive the acceleration as a function of speed for any speed and not only for certain speeds. Paying attention to these curves, it has been noted that they tend to have a horizontal asymptote for speed tending to 0 and a horizontal asymptote for speeds tending to 60 km/h. The aim is to identify a family of curves that

best approximates the experimental data. With the above considerations, the curve that best approximates these data is a logistic-sigmoidal function, an example is shown below:

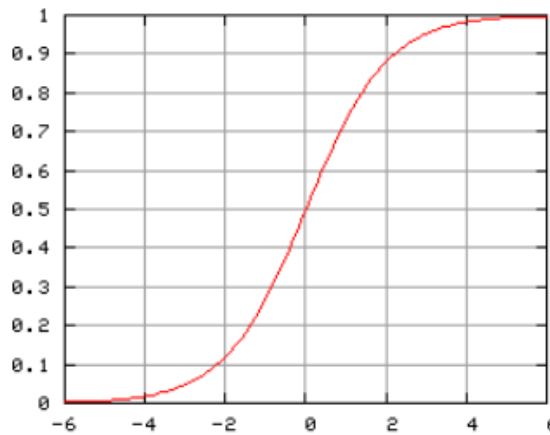


Figure 6.26 The curve that approximates the V-RMS and V-eVDV bonds is a logistic-sigmoidal. The analytical formula of this function, which has exactly this S-shape with two horizontal asymptotes, is shown below:

$$f(x) = \frac{a}{(1 + be^{-cx})} \quad 6.19$$

Executing the limits for the independent variable that tends to zero will result in the denominator tending to infinity, since the numerator is a finite number, so  $f(x)$  tends to 0. The limit for the independent variable tending to infinity instead will be precisely at 1, as the denominator tends to 1. Having found the qualitative form that best approximates our data series, it remains to find the coefficients  $a$ ,  $b$  and  $c$ .

These values were calculated with a software in which the experimental values of the  $x$  and  $y$  were entered, as in the example proposed below:

	X	Y
1	0	0
2	5	0.013875819
3	10	0.060365633
4	15	0.11857039
5	20	0.1629189
6	25	0.231902279
7	30	0.338311704
8	35	0.464526132
9	40	0.538823945
10	45	0.672774919
11	50	0.71650858
12	55	0.837891022
13	60	0.868539588
14		

The software calculates the  $a$ ,  $b$ ,  $c$  values that best approximate this data series. In the “result” window you can see these results. Furthermore, to evaluate the goodness

of this approximation, the determination coefficient R2 is estimated or it is possible to see the graphical representation as well as the residual waste.

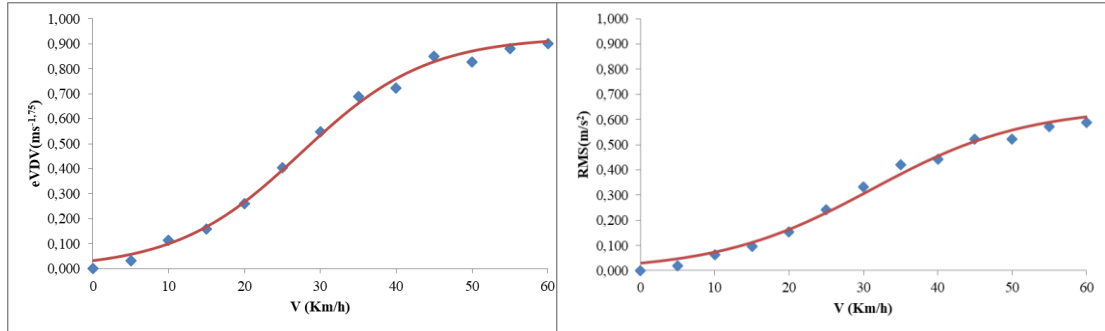


Figure 6.27 Figure 6.28 The approximation curve of V-RMS and V-eVDV

Then these triples of values were obtained for each bump for each vehicle, in total 8 triples were obtained for the 8 V-RMS curves and 8 triples for the 8 V-Evdv curves.

The values for the V-RMS curves for the different vehicles are shown below

**SPEED TABLE**

Table 6.7 Coefficients of the logistic function on the different vehicles passing through the speed table

	<b>A</b>	<b>C</b>	<b>D</b>	<b>E</b>
<b>a</b>	0.871387	0.949209	0.832933	0.69
<b>b</b>	43.0433	35.13953	26.28365	18.51
<b>c</b>	0.106973	0.09	0.09	0.08

**SPEED HUMP**

Table 6.8 Coefficients of the logistic function on the different vehicles passing through the speed hump

	<b>A</b>	<b>C</b>	<b>D</b>	<b>E</b>
<b>a</b>	0.584591	0.631796	0.52313	0.40555
<b>b</b>	30.67273	24.13194	17.16027	11.65780
<b>c</b>	0.121221	0.112627	0.108795	0.11555

The values for the V-Evdv curves are shown below:

**SPEED TABLE**

Table 6.9 Coefficients of the logistic function on the different vehicles passing through the speed table

	<b>A</b>	<b>C</b>	<b>D</b>	<b>E</b>
<b>a</b>	1.317267	1.426886	1.251	1.01
<b>b</b>	44.55743	32.8945	23.72679	16.05
<b>c</b>	0.115781	1.04E-01	9.75E-02	0.09

**SPEED HUMP**

Table 6.10 Coefficients of the logistic function on the different vehicles passing through the speed hump

	<b>A</b>	<b>C</b>	<b>D</b>	<b>E</b>
<b>a</b>	0.895652	0.962834	0.800534	0.62296
<b>b</b>	32.83901	24.28596	17.15509	12.60163

c	0.1312	0.120802	0.118449	0.13898
---	--------	----------	----------	---------

Given these values, it is now possible to calculate both the RMS and the eVDV for each vehicle on each bump. The accelerations and vibration doses were calculated precisely in correspondence with the values of V50 and V85 as determined by Daniel J. Smith (2002) in his work.

It is expected to find similar values of accelerations as the speed with which the crossing of a bump is approached. The goal is to identify an acceleration value beyond which the driver perceives discomfort.

The RMS and e-VDV values for each type of vehicle are shown below:

*Table 6.11 RMS and eVDV as a function of V50 and V85 generated by vehicle A when crossing speed hump and speed table*

	Vehicle A					
	Roonsvelt nord		Roonsvelt sud		Redwood	
	SPEED HUMP	SPEED TABLE	SPEED HUMP	SPEED TABLE	SPEED HUMP	SPEED TABLE
<b>V50 (Km/h)</b>	32.34	30.25	31.05	31.70	28.48	28.16
<b>RMS</b>	0.3634	0.3236	0.3416	0.3557	0.2965	0.2795
<b>e-VDV</b>	0.6086	0.5624	0.5746	0.6170	0.5024	0.4861
<b>V85 (Km/h)</b>	41.35	39.10	37.17	37.48	36.84	32.66
<b>RMS</b>	0.4855	0.5259	0.4366	0.4892	0.4322	0.3776
<b>e-VDV</b>	0.7825	0.8889	0.7163	0.8331	0.7101	0.6535

*Table 6.12 RMS and eVDV as a function of V50 and V85 generated by vehicle C when crossing speed hump and speed table*

	Vehicle C					
	Roonsvelt nord		Roonsvelt sud		Redwood	
	SPEED HUMP	SPEED TABLE	SPEED HUMP	SPEED TABLE	SPEED HUMP	SPEED TABLE
<b>V50 (Km/h)</b>	32.34	30.25	31.05	31.70	28.48	28.16
<b>RMS</b>	0.3871	0.3368	0.3650	0.3682	0.3197	0.2937
<b>e-VDV</b>	0.6469	0.5863	0.6130	0.6388	0.5414	0.5132
<b>V85 (Km/h)</b>	41.35	39.10	37.17	37.48	36.84	32.66
<b>RMS</b>	0.5140	0.5379	0.4622	0.5006	0.4576	0.3896
<b>e-VDV</b>	0.8268	0.9070	0.7566	0.8503	0.7501	0.6740

*Table 6.13 RMS and eVDV as a function of V50 and V85 generated by vehicle D when crossing speed hump and speed table*

	Vehicle D					
	Roonsvelt nord		Roonsvelt sud		Redwood	
	SPEED HUMP	SPEED TABLE	SPEED HUMP	SPEED TABLE	SPEED HUMP	SPEED TABLE
<b>V50 (Km/h)</b>	32.34	30.25	31.05	31.70	28.48	28.16
<b>RMS</b>	0.3467	0.3181	0.3299	0.3447	0.2948	0.2812
<b>e-VDV</b>	0.5834	0.5580	0.5584	0.6020	0.5041	0.4959
<b>V85 (Km/h)</b>	41.35	39.10	37.17	37.48	36.84	32.66
<b>RMS</b>	0.4392	0.4854	0.4021	0.4548	0.3988	0.3677
<b>e-VDV</b>	0.7097	0.8209	0.6615	0.7753	0.6570	0.6312

Table 6.14 RMS and eVDV as a function of V50 and V85 generated by vehicle E when crossing speed hump and speed table

	Vehicle E					
	Roonsvelt nord		Roonsvelt sud		Redwood	
	SPEED HUMPS	SPEED TABLE	SPEED HUMPS	SPEED TABLE	SPEED HUMPS	SPEED TABLE
V50 (Km/h)	32.34	30.25	31.05	31.70	28.48	28.16
RMS	0.3174	0.2840	0.3066	0.3047	0.2828	0.2549
e-VDV	0.5461	0.5073	0.5332	0.5410	0.5021	0.4588
V85 (Km/h)	41.35	39.10	37.17	37.48	36.84	32.66
RMS	0.3693	0.4115	0.3499	0.3885	0.3481	0.3186
e-VDV	0.5989	0.7026	0.5811	0.6697	0.5793	0.5632

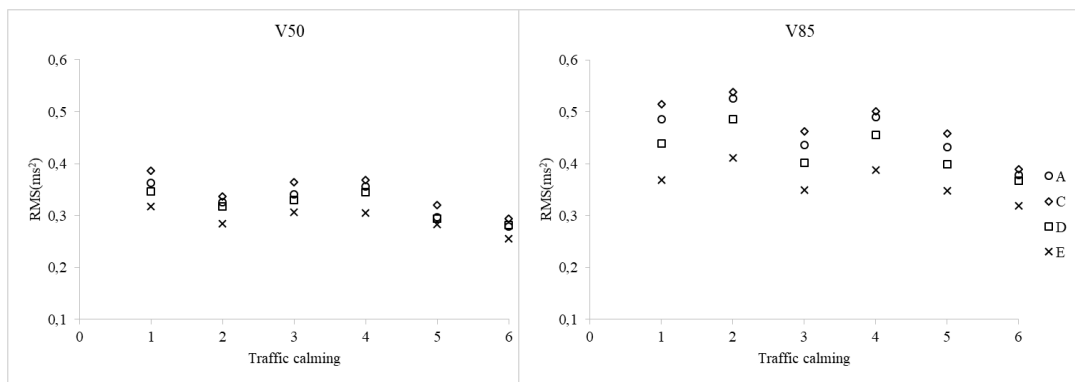


Figure 6.29 RMS on traffic calming according to V50 and V85

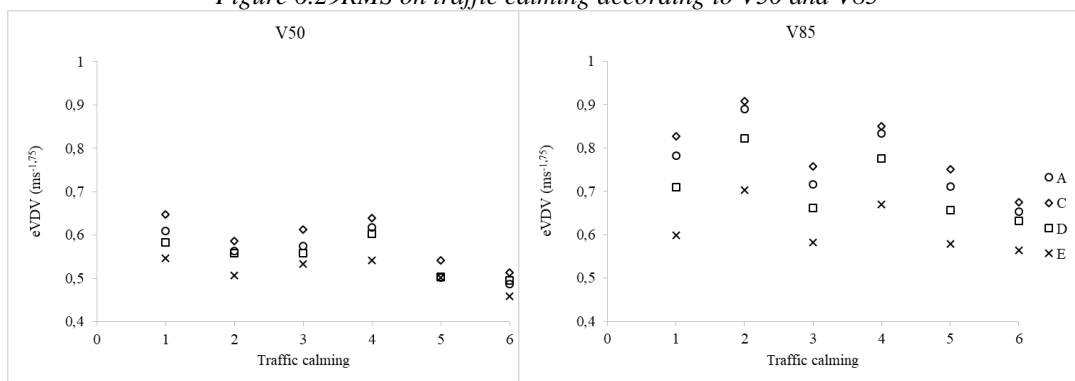


Figure 6.30 Evdv on traffic calming according to V50 and V85

As can be seen from these results, both in numerical and graphical form, the RMS and Evdv values do not vary much depending on the site, the bump and the speed with which they are crossed. The differences, albeit minimal, are due to external site factors.

Analyzing the results, it turns out that drivers undergo acceleration in terms of RMS in a range between 0.30 m/s<sup>2</sup> and 0.35 m/s<sup>2</sup>. If, on the other hand, the results referring to V85 are analyzed, the values are in a range between 0.40 m/s<sup>2</sup> and 0.45 m/s<sup>2</sup>. If you pay attention to the diagrams where the vibration doses are reported

(VDV) the values referring to the V50 are around 0.6 ms<sup>-1.75</sup> and the values related to the V85 are around 0.8 ms<sup>-1.75</sup>.

The set objective has been reached, that is to find a characteristic value of RMS and generalized e-VDV that does not vary as the device changes.

It was subsequently thought to evaluate a distribution of the RMS and e-VDV starting from the distribution of the velocities and from the analytical link that exists between the velocities and accelerations. A transformation of the random variables was required to calculate the probability distribution of the accelerations.

Given a continuous random variable (X) with  $f(x)$  continuous, in the present case  $f(x)$  is the probability distribution function of the velocities, both  $g(x)$  continuous and differentiable, in the present case  $g(x)$  is the RMS (V) or e-VDV (V) function, defined as the inverse function of  $g(x)$  as follows:

$$x = \varphi(y) = g^{-1}(y) \quad 6.20$$

Then the new distribution function  $f(y)$  where  $y$  is the new independent variable (RMS or e-VDV) will be given by the following formula:

$$f_Y(y) = \frac{f_X(g^{-1}(y))}{\frac{dg}{dx}(g^{-1}(y))} \quad 6.21$$

So first the inverse function of  $g(x)$  or  $g^{-1}(y)$  was computed.

With some mathematical passages:

$$\begin{aligned} RMS(V) &= \frac{a}{(1 + be^{-cV})} \\ 1 + be^{-cV} &= \frac{a}{RMS} \\ be^{-cV} &= \frac{a}{RMS} - 1 \\ e^{-cV} &= \left(\frac{a}{RMS} - 1\right) \frac{1}{b} \\ -cV &= \ln\left(\left(\frac{a}{RMS} - 1\right) \frac{1}{b}\right) \\ V &= -\frac{1}{c} \ln\left(\left(\frac{a}{RMS} - 1\right) \frac{1}{b}\right) \end{aligned}$$

the inverse function has been obtained, it is therefore possible to obtain the speed as a function of the RMS or similarly the speed as a function of the e-VDV.

Then the derivative of  $g(x)$  with respect to  $x$  was calculated:

$$\frac{d(RMS)}{d(V)} = \frac{-a(-cbe^{-cV})}{(1 + be^{-cV})^2} \quad 6.22$$

Subsequently, the expression as a function of RMS was substituted for the V:

$$\frac{d(RMS)}{d(V)} = \frac{-a \left( -cbe^{-c \left( \frac{1}{c} \ln \left( \left( \frac{a}{RMS} - 1 \right) \frac{1}{b} \right) \right)} \right)}{\left( 1 + be^{-c \left( \frac{1}{c} \ln \left( \left( \frac{a}{RMS} - 1 \right) \frac{1}{b} \right) \right)} \right)^2} \quad 6.23$$

Ultimately then it will be that:

$$fY(RMS) = \frac{f(x) = \frac{1}{\sqrt{2\pi}\sigma} e^{-\frac{1}{2} \left( \frac{-\frac{1}{c} \ln \left( \left( \frac{a}{RMS} - 1 \right) \frac{1}{b} \right) - \mu}{\sigma} \right)^2}}{-a \left( -cbe^{-c \left( \frac{1}{c} \ln \left( \left( \frac{a}{RMS} - 1 \right) \frac{1}{b} \right) \right)} \right)}{\left( 1 + be^{-c \left( \frac{1}{c} \ln \left( \left( \frac{a}{RMS} - 1 \right) \frac{1}{b} \right) \right)} \right)^2} \quad 6.24$$

Therefore, to know the RMS distribution it will be necessary to know the data of the speeds V50 and V85, and the coefficients a, b and c of the sigmoidal function that approximates the V-RMS curve. Analogous speech for the eVDV in which the formula for calculating the probability distribution will be given by:

$$fY(eVDV) = \frac{f(x) = \frac{1}{\sqrt{2\pi}\sigma} e^{-\frac{1}{2} \left( \frac{-\frac{1}{c} \ln \left( \left( \frac{a}{eVDV} - 1 \right) \frac{1}{b} \right) - \mu}{\sigma} \right)^2}}{-a \left( -cbe^{-c \left( \frac{1}{c} \ln \left( \left( \frac{a}{eVDV} - 1 \right) \frac{1}{b} \right) \right)} \right)}{\left( 1 + be^{-c \left( \frac{1}{c} \ln \left( \left( \frac{a}{Evdv} - 1 \right) \frac{1}{b} \right) \right)} \right)^2} \quad 6.25$$

As an example, the comparison between the speed probability distribution and the RMS probability distribution for a case is shown. As previously mentioned, to carry

out this transformation it is necessary to have the V50 and V85 and the values of the sigmoid coefficients a, b and c.

V50 (km / h)	30.25
V85 (km / h)	39.1
DEV (km / h)	8.428571

a	0.686985
b	18.507974
c	0.084905

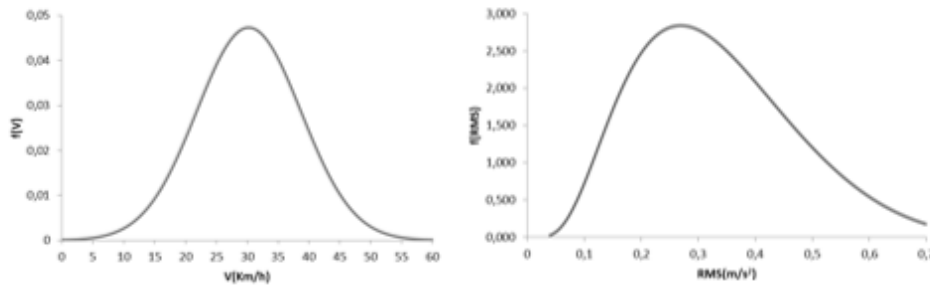
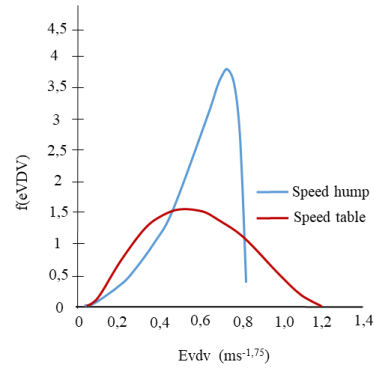
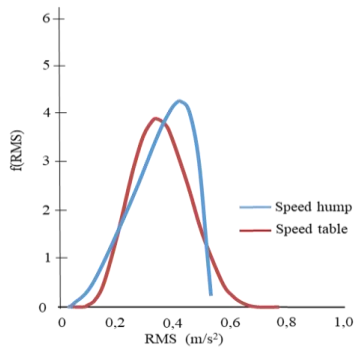


Figure 6.31 Speed probability distribution and the RMS probability distribution

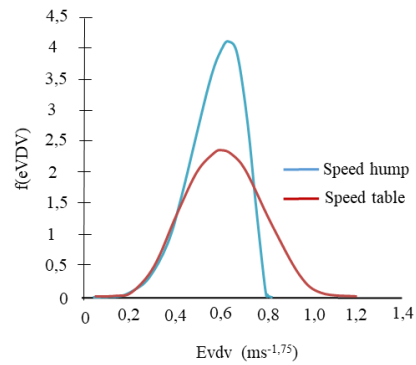
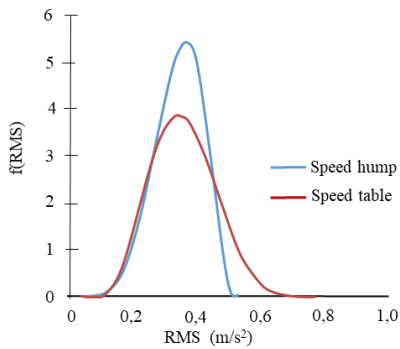
From the first graph, having a symmetrical shape due to an intrinsic characteristic of the Gaussian, it can be seen that the points around the average (30.25 km/h) are arranged symmetrically with respect to it. Once this transformation has taken place, it is clear that the curve will no longer be symmetrical, in fact, the probability distribution function of the velocity has been divided by the derivative of the sigmoid which has a shape that is anything but constant. To obtain a RMS probability distribution function, one should choose a linear function rather than the sigmoid one, in order to obtain a constant derivative for each velocity value.

Below are the comparative curves on the two devices, only one curve was calculated for each bump, assuming that each vehicle affects vehicular traffic in the same way, i.e. each vehicle category represents 25% of the entire vehicular flow. In this way, it was possible to switch from four different curves on a given device to a single curve.

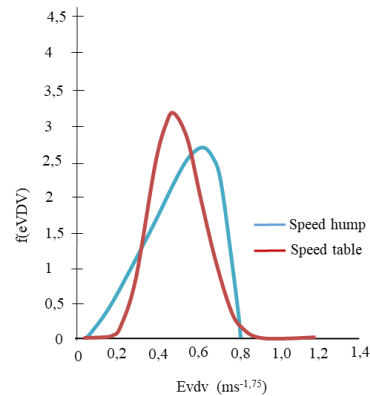
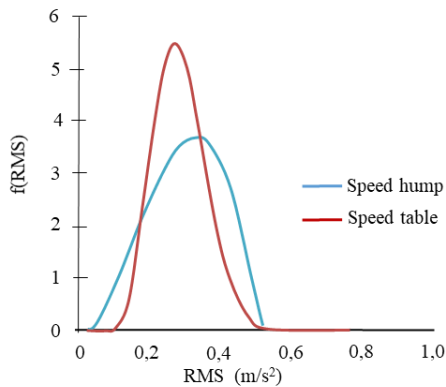
### ROOSEVELT NORTH



**ROOSEVELT SOUTH**



**REDWOOD**



The data analyzed so far refer to a job in which the devices were temporarily inserted. Now to see the difference with permanently inserted devices and evaluate what the difference is in the behaviour of the drivers.

In this case, data relating to the work conducted by Reid Edwing were taken (2001). In this, the author aims to identify the average speeds and standard deviations in different types of devices present in the United States. The data that were taken refer to two types of devices: two speed humps with a length of 12 feet and 14 feet and a

height of 3 inches. With the same methodology used for temporary devices, the V-RMS and V-Evdv curves were obtained and then the RMS (V) and Evdv (V) functions, also in this case the function that best approximates these series of points is sigmoid. Once these curves were known, the RMS and Evdv values were obtained in correspondence with the V50 and V85 and then moving on to a representation of the probability distribution of the RMS and Evdv.

The data in possession are the V50 and the standard deviations from which the V85 were obtained, as shown in the table:

	V50 (km/h)	$\sigma$ (km/h)	V85 (km/h)
Speed hump 12 feet	25.95	5.63	31.86
Speed hump 14 feet	25.25	3.37	28.80

The logistic coefficients a, b and c were then calculated for each vehicle on each single bump:

SPEED HUMP 12 FEET (V-RMS)

	A	C	D	E
a	0.503893	0.531718	0.4243	0.3251
b	40.44146	30.4383	22.9307	19.7045
c	0.146109	0.1384	0.1454	0.1816

SPEED HUMP 12 FEET (V-EVDV)

	A	C	D	E
a	0.8222	0.8607	0.6917	0.5372
b	37.9297	27.7442	21.4153	20.0710
c	0.1453	0.1375	0.1466	0.1966

SPEED HUMP 14 FEET (V-RMS)

	A	C	D	E
a	0.5402	0.5761	0.4755	0.3630
b	55.6097	44.8314	35.2147	22.9738
c	0.1520	0.1420	0.1410	0.1485

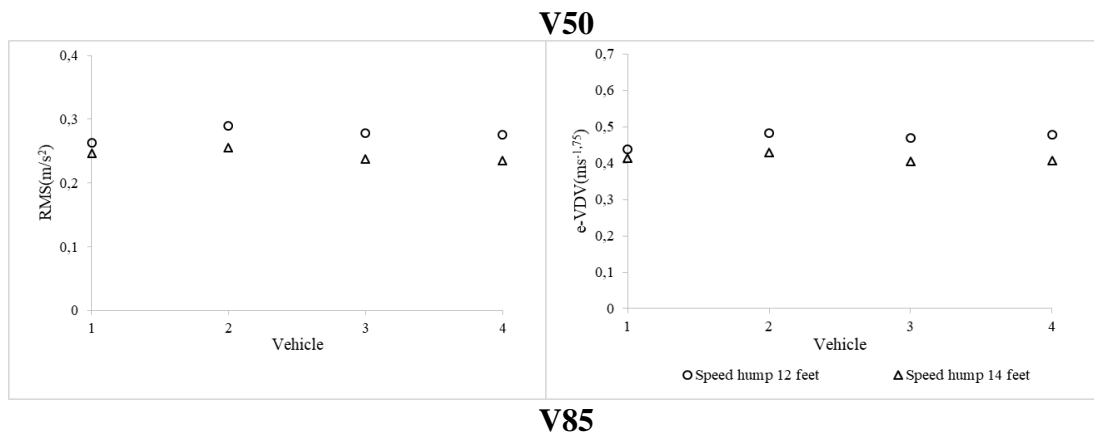
SPEED HUMP 14 FEET (V-EVDV)

	A	C	D	E
a	0.8898	0.9497	0.7833	0.6007
b	52.4988	40.8372	32.3852	20.5985
c	0.1511	0.1394	0.1403	0.1495

Below are the RMS and Evdv values for each type of vehicle on each single bump in correspondence with the speed at which they are crossed:

	Vehicle A		Vehicle C	
	Speed hump 12 feet	Speed hump 14 feet	Speed hump 12 feet	Speed hump 14 feet
<b>V50 (Km/h)</b>	25.95	25.25	25.95	25.25
<b>RMS</b>	0.2635	0.2460	0.2893	0.2561
<b>e-VDV</b>	0.4387	0.4128	0.4830	0.4299
<b>V85 (Km/h)</b>	31.86	28.8	31.86	28.8
<b>RMS</b>	0.3639	0.3183	0.3882	0.3282
<b>e-VDV</b>	0.6001	0.5397	0.6390	0.5467

	Vehicle D		Vehicle E	
	Speed hump 12 feet	Speed hump 14 feet	Speed hump 12 feet	Speed hump 14 feet
<b>V50 (Km/h)</b>	25.95	25.25	25.95	25.25
<b>RMS</b>	0.2779	0.2372	0.2763	0.2356
<b>e-VDV</b>	0.4682	0.4043	0.4788	0.4078
<b>V85 (Km/h)</b>	31.86	28.8	31.86	28.8
<b>RMS</b>	0.3469	0.2954	0.3066	0.2752
<b>e-VDV</b>	0.5761	0.4991	0.5175	0.4699



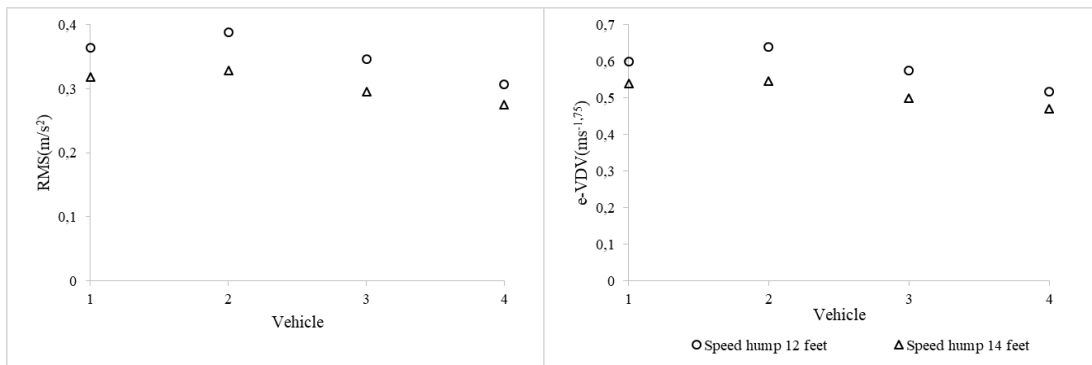


Figure 6.32 RMS and Evdv on speed hump (12-14 feet) according to V50 and V85

The probability distribution was then represented for both the RMS acceleration and the vibration dose Evdv.

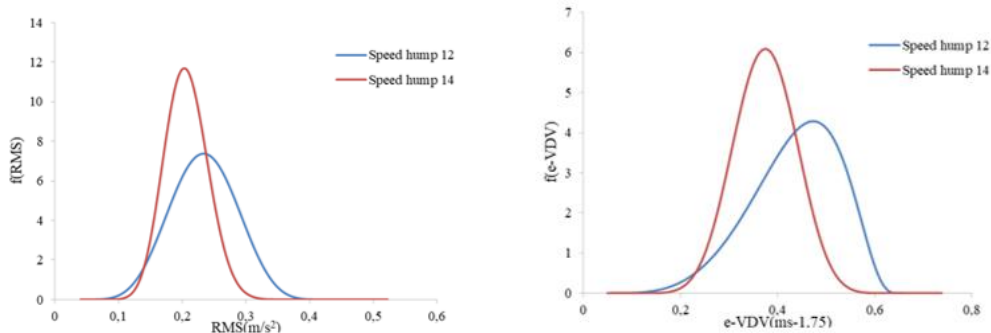


Figure 6.33 The probability distribution of RMS and eVDV

As you can see, the RMS and Evdv values are lower than in the case of temporary devices, this is due to the fact that the driver changes his behaviour after several passages by choosing a lower crossing speed that gives him comfort. It can be said that the effect of these devices is not noticed immediately after installation since the driver can learn to vary his speed according to the desired comfort.

In fact, the temporary devices are crossed with speeds even higher than 30 km/h while the permanent devices are crossed at a lower speed, about 25 km/h; in fact by reducing the vertical acceleration going from values of about 0.35 m/s<sup>2</sup> to values of 0.25 m/s<sup>2</sup>.

The results derived from the approximation of the V-RMS and V-EVDV curves to logistics do not give satisfactory results when one passes to the representation in terms of probability function of the quantities to be represented. To represent the V-RMS and V-EVDV curves, the same procedure was used to identify the RMS and EVDV,

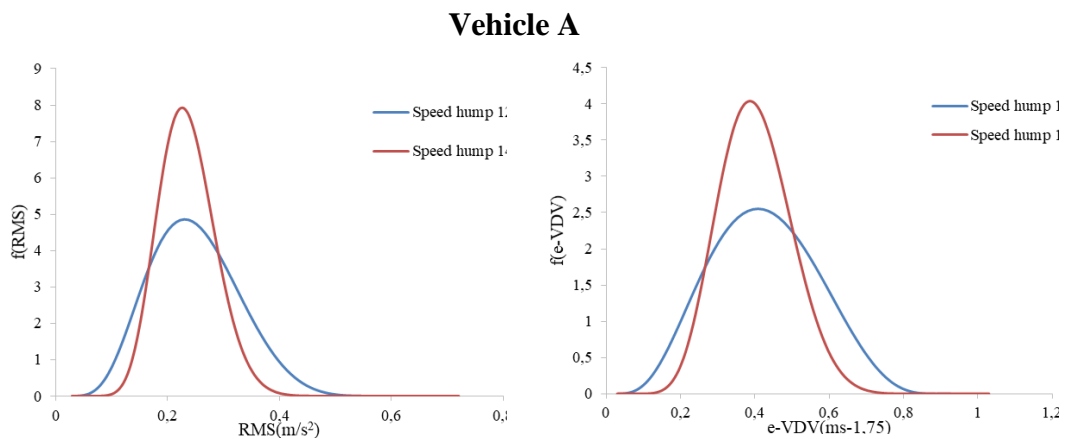
using a linear function rather than a logistic function. This is because it has been observed that these curves (V-RMS and V-EVDV) follow a mostly linear trend in the velocity range of interest.

Below are the acceleration and vibration dose values measured at V50 and V85 for all types of vehicle on the two types of bump:

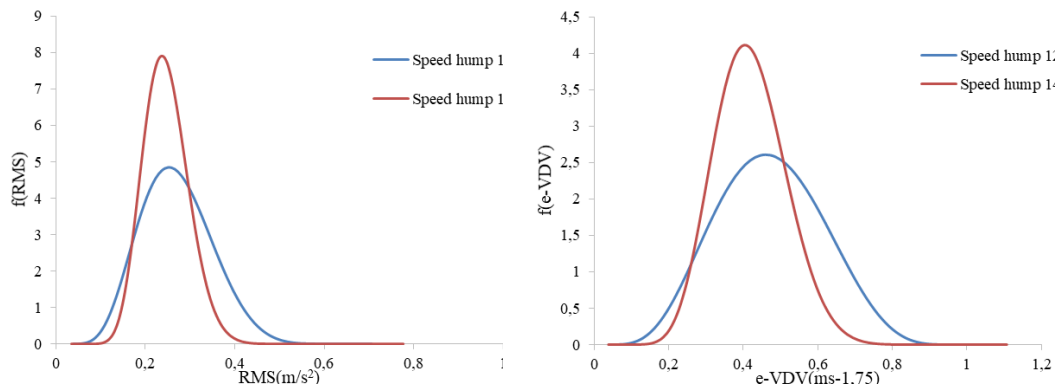
		A		C		D		E	
		RMS	eVDV	RMS	eVDV	RMS	eVDV	RMS	eVDV
1	V50	0.27496	0.458	0.28684	0.4775	0.25343	0.4253	0.2446	0.4111
	V85	0.35119	0.584	0.36544	0.537	0.3208	0.537	0.3007	0.5016
2	V50	0.26035	0.431	0.28253	0.4228	0.25678	0.4228	0.2342	0.3773
	V85	0.30366	0.502	0.32832	0.4867	0.29618	0.4867	0.2669	0.4337

As can be seen, the acceleration and vibration dose values received on the first and second devices, crossed at different speeds, are very similar for each type of vehicle. This result had already been found with the logistic function, the difference between the two approximations can be seen on the probability distributions of the accelerations and vibrations doses.

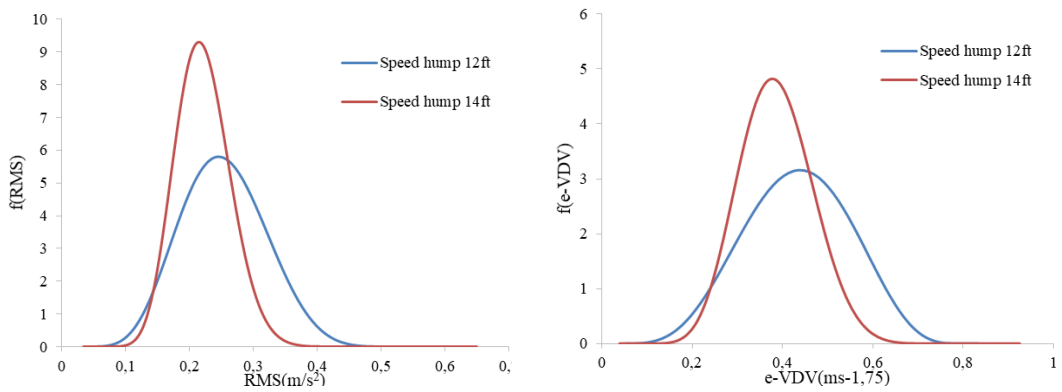
Below are the comparisons for each vehicle of the RMS and EVDVs on the two types of devices:



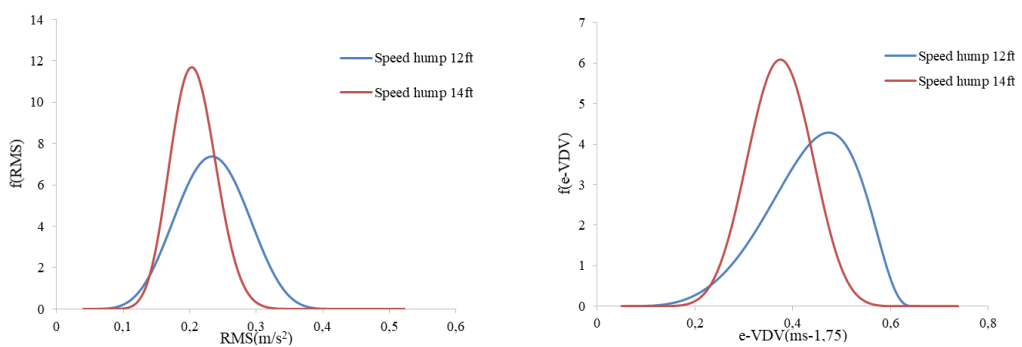
**Vehicle C**



**Vehicle D**



**Vehicle E**



It can be noted that the difference between the RMS and EVDV distribution functions on the two bumps is minimal if the average values are considered; even if there is greater dispersion in the curve of the 12 feet length device, due to the fact that the detected speed distribution function has a greater dispersion than that of the device at 14 feet.

The standard deviation in temporary devices is higher than in permanent devices as the driver takes time to adapt to the device, therefore the distribution of speeds is wider, while in permanent devices all drivers tend to assume the same comfort speed.

Devices in series have been evaluated to bring about a speed reduction that is no longer punctual but in a longer stretch of road. By inserting a series of devices the driver does not tend to accelerate too much, so it is possible to contain speeds. In this regard, RMS and EVDV were evaluated expecting, as found by LaToya Jhonson (2003), that drivers tend to maintain the same speed on the bumps in succession.

For example, two roads are taken where two speed humps with a height of 3 inches and a length of 12 feet have been inserted in series.

Below are the measured values of V50 and V85 in the two roads considered both on the first and on the second bump. Then the standard deviation was obtained assuming a normal distribution:

	First speed humps			Second speed humps		
	V50 (km/h)	V85 (km/h)	$\sigma$ (km/h)	V50 (km/h)	V85(km/h)	$\sigma$ (km/h)
1st site	16.25	19.63	3.22	16.41	19.79	3.22
2nd site	15.12	19.15	3.84	15.12	19.63	4.51

Below are the logistics coefficients a, b, and c which best approximate the data series of the V-RMS and V-eVDV curves for each vehicle (A, C, D and E) on a speed hump of 12 feet length and 3 inch height.

	A		C		D		E	
	RMS	e-VDV	RMS	e-VDV	RMS	e-VDV	RMS	e-VDV
<b>a</b>	0,503893	0,8222	0,531718	0,8607	0,4243	0,6917	0,3251	0,5372
<b>b</b>	40,44146	37,9297	30,4383	27,7442	22,9307	21,4153	19,7045	20,071
<b>c</b>	0,146109	0,1453	0,1384	0,1375	0,1454	0,1466	0,1816	0,1966

Now these curves are known and the speeds are known, the RMS acceleration and vibration dose EVDV have been calculated in correspondence with the V50s and V85s for each vehicle category:

	A				C			
	First speed humps		Second speed humps		First speed humps		Second speed humps	
	1° site	2° site	1° site	2° site	1° site	2° site	1° site	2° site
V50 (Km/h)	16,25	15,12	16,41	15,12	16,25	15,12	16,41	15,12
RMS	0,1107	0,0989	0,1125	0,0989	0,1297	0,1171	0,1316	0,1171
e-VDV	0,1829	0,1623	0,186	0,1623	0,2183	0,1961	0,2216	0,1961
V85 (Km/h)	19,63	19,15	19,79	19,63	19,63	19,15	19,79	19,63
RMS	0,1522	0,14577	0,1544	0,1522	0,1733	0,1666	0,1756	0,1733
e-VDV	0,2559	0,2445	0,2597	0,2559	0,2947	0,2829	0,2987	0,2947

	D				E			
	First speed humps		Second speed humps		First speed humps		Second speed humps	
	1° site	2° site	1° site	2° site	1° site	2° site	1° site	2° site
V50 (Km/h)	16,25	15,12	16,41	15,12	16,25	15,12	16,41	15,12
RMS	0,1331	0,1213	0,1349	0,1213	0,1457	0,1337	0,1838	0,1337
e-VDV	0,2285	0,2073	0,299	0,2073	0,2688	0,2451	0,2722	0,2451
V85 (Km/h)	19,63	19,15	19,79	19,63	19,63	19,15	19,79	19,63
RMS	0,1728	0,1667	0,1748	0,1728	0,1474	0,1782	0,1856	0,1838
e-VDV	0,2316	0,2884	0,3025	0,299	0,3417	0,3313	0,3451	0,3417

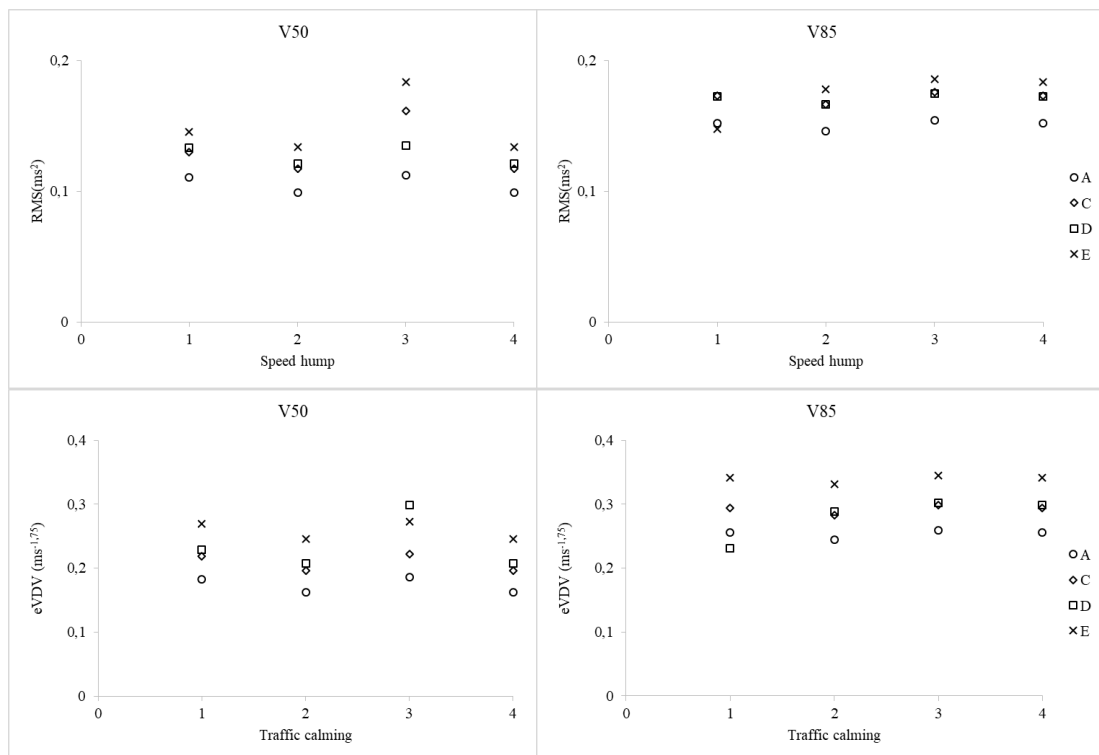
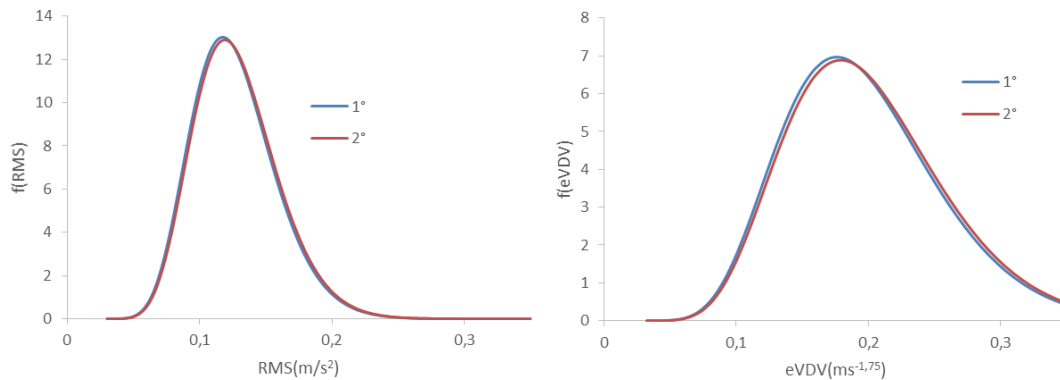


Figure 6.34 RMS and Eadv on traffic calming according to V50 and V85

Subsequently, the probability distribution was represented for both the RMS and the VDV. Each curve represents the distribution on a given bump:



From the study of the devices in series, it can be deduced that the accelerations in terms of RMS and EVDV are similar for both the first and the second bump; this means that the driver tends to assume the same behavior on two bumps in succession, keeping an unchanged speed.

## 6.4 Conclusions

The aim of this Chapter was to understand the behavior of drivers in the vicinity of traffic calming. The attention was placed on altimetric devices (speed hump and speed table) which exploit vertical acceleration; this causes discomfort in the driver who tends to moderate the speed below a certain threshold to reduce the disturbance. An analytical link was then identified between velocity and vertical acceleration, using a vehicle model with five degrees of freedom. With this model, vertical displacement and acceleration received by the driver as a function of time have been evaluated.

The perceived discomfort is a very complex problem, which also affects vibrations. Numerous literature studies consulted have shown that a very important factor in characterizing the effects on the human body of vibrations is their frequency. With the same amplitude of accelerations, the human body behaves differently since there is a different perception threshold depending on the frequency itself. This highlighted that stopping to evaluate only the acceleration as a function of time was reductive, for this reason the acceleration was represented as a function of the frequencies, subsequently identifying a single parameter (the acceleration expressed in weighted RMS or the vibration dose eVDV) also function of the duration. Relationships between speed and accelerations were then derived, demonstrating, as daily experience suggests, that acceleration increases as speed increases.

The final goal was to define acceleration or vibration dose thresholds beyond which the driver feels discomfort. Therefore, starting from the literature, the speeds with which the bumps are crossed have been experimentally calculated. Thus, for each bump, relations were obtained between velocity and vertical accelerations (different according to the bump), after which the speed was known, the level of acceleration received was calculated. In order to understand if there is a common value of acceleration as the bump varies, different scenarios were studied with bumps with variable geometry crossed at different speeds. This made it possible to obtain a common value of acceleration and vibration dose for the different scenarios; which allows predicting the crossing speed on any type of hill.

Specifically, note the geometry of the bump, it is possible to evaluate the relationship between speed and acceleration. Subsequently, once this acceleration threshold has been set, it is possible to analytically determine the speed with which that given acceleration is received.

Traffic calming (regardless of geometry), inserted in some sites for prolonged times, has been found to produce a greater reduction in speed than temporary devices. This is because the driver does not perceive a priori what the appropriate speed is to overcome the bump, but it is necessary that he cross them several times before this identifies a comfort speed.

It was also observed that by using the bumps in series it is possible to control the speed of a certain road section and that if they have the same size they are crossed at the same speed (producing the same discomfort effects as the bump varies).

Ultimately, this work can support the design for placing traffic calming on a road section; since once the travel speed has been established, it is possible to evaluate the vibration value beyond which the driver complains of discomfort and therefore vary the geometry and the number of devices.

## References

Alley, B. 2000. Confusing People into Slowing Down: Perceptual Countermeasures at Rural/Urban Thresholds. MS thesis, University of Waikato, New Zealand.

- Al-Nassr, E. K. 1982. Dynamic consideration of speed control humps”, *Transportation Research-B* Vol. 16B, No 4. Mechanical engineering department, university of petroleum & minerals, Saudi Arabia, 291-302.
- Amirarsalan, M., & Ali, A. 2014. Optimization of speed hump profiles based on vehicle dynamic performance modelling. *Articol Journal Of Transportation Eng.*
- Annunziata, F., Cecere, E., Coni, M., Maltint, F., Pinna, F., & Portas, S. 2007. *Progettazione Stradale. Manuale pratico di progettazione.* DARIO FLACCOVIO.
- Associates, K. H. (s.d.). *A guide to roundabouts (two lane).* State of Florida: Department of Transportation.
- Aya, K., & Hisashi, K. 2011. Effectiveness of speed humps ranged at different intervals considering roadside environment including vehicle speed, noise and vibration. *Journal Of The Eastern Asia Society For Transportation Studies*, Vol 9.
- Babak, M., Zohn, R., & Muennig, P. 2018. The impact of urban speed reduction programmes on health system cost and utilities. *Injury Prevention* vol 24:, p. 262-266.
- Bahram, H., Masoud, S., & Mansour, N. 2007. Multiobjective shape optimization of speed humps. *Struct Multidisc Optim* DOI 10.1007/s00158-008-0226-7.
- Barbosa, H. M. 1995. Impact of traffic calming measures on speed on urban roads.
- Basil, D. 2012. The influence of width of road humps on operating speed. Malaysia: Faculty Of Civil And Environmental Engineering.
- Berthod, C. 2011. Traffic calming speed humps and speed cushions. *Annual Conference Of Transportation Association Of Canada.* Edmonton, Alberta.
- Boulter, P. 2001. The impacts of traffic calming measures on vehicle exhaust emissions. PhD thesis. Middlesex University.
- Brindle, R. 2005. Speed-based design of traffic calming schemes. *75th ITE Annual Meeting And Exhibit.* Melbourne, Victoria.
- British Standard institution. 1984. BS 6473: Evaluation of human exposure to vibration in buildings.
- Canale, S., & Leonardi, S. 2005. Verifica sperimentale degli interventi di traffic calming.
- Chadda, H. S., Asce, M., & Cross, E. 1985. Speed (road) bumps: issue and opinions. *Journal transportation engineering*, vol 111, no.4, USA.
- Compte, S., & Jamson, A. 2000. Traditional and innovative speed-reducing measures for curves: an investigation of drivers. *Safety Science* 36.
- D.Zaidel, A. H. 1992. The use of road humps for moderating speeds on urban streets. *Accid. Anul.* vol24 .no.1, Great Britain, 45-56.

- D'Apuzzo, M. 2007. Some remarks on the prediction of road traffic induced ground-borne vibrations. 4th INTERNATIONAL SIIV CONGRESS. PALERMO (ITALY).
- Damsere, D., Ebel, B., Mock, C., Afukaar, F., Donkor, P., & Kalowole, T. 2019. Evaluation of the effectiveness of traffic calming measures on vehicle speeds and pedestrian injury severity in Ghana. *Traffic Injury Prevention*.
- Daniel, B. D. 2012. The influence of width of road humps on operating speed. Faculty Of Civil And Environmental Engineering, Malaysia.
- Daniel, B. D. 2012. The influence of width of road humps on operating speed. Faculty Of Civil And Environmental Engineering, Malaysia.
- Department of Transportation, O. 2020. *Traffic Manual*. Bureau of Traffic Management. Oregon (USA), City of Portland.
- Dixon, J. 1986. *Tires, Suspension, and Handling*.
- Edwing, R. 2001. Impact of traffic calming. *Transportation Quarterly*.
- Elumala, R., & Suresh, P. 2017. Identifying Speed Hump, a Traffic Calming Device, as a Hotspot for Environmental Contamination in Traffic Affected Urban Roads. *ACS Omega*, Vol 2, p. 5434–5444.
- Emad Khorshid, M. A. 2004. A numerical study on the optimal geometric design of speed control humps. *Engineering Optimization*, Vol 36, No.1. Department Of Mechanical Engineering, Kuwait University.
- Fitzpatrick, K., Brewer, M., & Parham, A. 2003. Left-Turn and In-Lane Rumble Strip Treatments for Rural Intersections. Report No. FHWA-TX-04-0-4278-2, Texas Department of Transportation, Austin, TX.
- Fwa, T. F., & Liaw, C. Y. 1992. Rational approach for geometric design of speed-control road humps. *Transportation research record* 1356 pp 66-72, National Research of Singapore.
- García, A., Torres, A., Romero, M., & Moreno, A. 2011. Traffic Microsimulation Study to Evaluate the Effect of Type and Spacing of Traffic Calming Devices on Capacity. 6th International Symposium on Highway Capacity and Quality of Service. Stockholm, Sweden.
- Giffod, R. 1973. Road humps should be dug up: the case against.
- Griffin M.J. 1990. *Handbook of Human Response*. Southpark, UK.
- Gunwoo, L., Shinhye, J., Cheol, O., & Keechoo, C. 2013. An evaluation framework for traffic calming measures in residential areas. *Transportation Research Part D* 25 68.76, Korea.

- Harder, K., Bloomfield, J., & Chihak, B. 2006. Stopping Behavior at Real-World Stop-Controlled Intersections With and Without In-Lane Rumble Strips. Report No MN/RC-2006-42, Submitted to Minnesota Department of Transportation, St. Paul, M.
- Hassen, D., Miladi, M., Slim Abbes, M., Caglar Baslami Sli, S., Chaari, F., & Haddar, M. 2017. Road profile estimation using the dynamic responses of the full vehicle model.
- Heloisa M. Barbosa, M. R. 2000. A model of speed profiles for traffic calmed roads. Transportation Research Part A 34.
- Hernan Gonzalo-Orden, H. P.-A. 2018. Effects of traffic calming measures in different urban areas. Xiii Conference Of Transport Engineering, Cit 2018. Spain.
- Herrstedt, et al. 1991. Speed Reducers. Urban Traffic Areas-part 7.
- Hessling, J., & Zhu, P. 2008. Analysis of vehicle rotation during passage over speed control road humps. International conference on intelligent computation technology and automation.
- Heydinger, G. 1999. Measured vehicle inertial parameters-NHTSA's Data Through November 1998.
- Horn, K. (s.d.). A guide to roundabouts (two lane). State of Florida: Department of Transportation.
- International Organization for Standardization. 1986. ISO2631: Evaluation of human exposure to whole-body vibration.
- Jagerbrand, A., Johansson, M., & L., T. 2018. Speed responses to speed humps as affected by time of day and lights on residential road. MDPI Sweden.
- Kennedy, J., Gorell, R., Crinson, L., Wheeler, A., & Elliot, M. 2005. Psychological traffic calming. Prepared for Traffic Management Division Department for Transport TRL REPORT TRL641.
- Khairum, S. R., Hamsa, A., Mohdzin Bin, M., & Mansor, I. 2016. A theoretical overview of road hump effects on traffic noise in improving residential. World Conference On Transport Research. Shanghai.
- Khorshid, E., & Alfares, M. 2004. A numerical study on the optimal geometric design of speed control humps. Engineering Optimization, Vol 36, No.1. Department Of Mechanical Engineering, Kuwait University.
- Khorshid, E., & Alfares, M. 2007. Model refinement and experimental evaluation for optimal design of speed humps. Int. J. Vehicle Systems Modelling and Testing, Vol. 2, No. 1.

- Kirkpatrick, S. 1996. Tentative guidelines on the provision of speed breakers for control of vehicular speeds on minor city. The Indian Roads Congress.
- Klyne, M., Mie(Augt), C., & Maitpm, M.1998. The effect of edge lining on vehicle speeds through roundabouts and mid-block blisters. Proc.Instn.Cin.Engrs,Mun. Engr.127, 170-173.
- Krylov, V. 1998. Traffic calming and associated ground vibrations. Proceedings of the Institute of Acoustics, 41-8.
- Lamberti, R., & Abate, D. (s.d.). Il laboratorio sicurezza stradale (interventi planimetrici e ottici).
- Latoya, J., & Nedzesky, A. 2003. A comparative study of speed humps, speed slots and speed cushions.
- lightDome. (s.d.). Tratto da <http://www.instrada.eu/documenti/lightDome/Le%20Strade%20%20Gli%2>
- Lockwood, I. 1997. ITE Traffic Calming Definition. ITE Journal, 22.
- Mansfield Neil J. 2005. Human Response to vibration. Taylor & Francis Ltd.
- Marek, J., & Walgren, S. 1993. Mid-block speed control:chicanes and speed humps.
- Margaret Parkhill, P. R. 2001. Updated guidelines for the design and application of speed humps.
- Margaret Parkhill, P. R. 2001. Updated guidelines for the design and application of speed humps.
- Mhanna, M., Sadek, M., & Shahrour, I. 2011. Prediction and mitigation of traffic induced ground vibrations in an urban zone. WIT Transactions on The Built Environment, Vol 116.
- Mhanna, M. M. S. 2011. Study of traffic induced ground vibrations using a combined finite difference model . 20ème Congrès Français de Mécanique.
- Moreno, A., Garcia, A., & Romero, M. 2011. Speed table evaluation and speed modelling for low-volume crosstown roads. Transportation Research Record Journal Of The Transportation No 2203 , USA, p. 85-93.
- Moreno AT & García, A. 2013. Use of Speed Profile as Surrogate Measure: Effect of Traffic Calming Devices on Crosstown Road Safety Performance. Accident Analysis and Prevention, p. 23-32. doi:10.1016/ j.aap.2012.10.013.
- Namee, S., & Witchayangkoon, B. 2011. Crossroads vertical speed controll devices:suggestion from observation. International Transaction Journal Of Engineering, Managment, Applied Sciences & Technologies, Thailand.

- Oke, S., Salauz, T., Adeyefaj, O., Akanbi, O., & Oyawale, F. 2007. Mathematical Modelling of the Road Bumps Using Laplace Transform. *International Journal of Science & Technology* Volume 2. No 2., p. 129-141.
- Pahansen De Alwis. 2014. *Methods for shock and vibration evaluation applied on offshore power boats*. Stockholm, Sweden.
- Parkhill, M., Sooklall, P. R., Geni, M., & Bahar, P. 2001. Updated guidelines for the design and application of speed humps.
- Pau, M. 2001. Do speed bumps really decrease traffic speed? an italian experience.
- Persaud, B., Retting, R., Garder Per, E., & Lord, D. 2006. *Observational Before-After Study of the Safety Effect of U.S. Roundabout Conversions Using the Empirical Bayes Method*.
- Philip, A., & Weber, P. 1998. Toward a north american geometric design standard for speed humps. *Ite Journal*.
- Philip A. Weber, J. P. 2000. Toward a canadian standard for the geometric design of speed humps. *It Journal*.
- Pyne, H., Dougherty, M., Carsten, O., & Tight, M. 1995. *A Simulator Based Evaluation of Speed Reduction Measures for Rural Arterial Roads*. Working Paper 434, April. University of Leeds.
- Recommendations on the Design and Use of Engineering Safety Measures*. 2010. RISEP. Lithuanian Road Administration under the Ministry of Transport and Communications; p. 123.
- Ribeiro, P. J. 2015. *Evaluation of the vehicle dynamics, energy and environmental impacts of traffic calming measures*. Thesis to obtain the Master of Science Degree in Environmental Engineering. June. Lisbona, Spagna.
- Riviera, P., Bassani, M., & Dalmazzo, D. 2010. Field investigation on the effects on operating speed caused by trapezoidal humps. 90th TRB Annual Meeting.
- Russell, E., & Godavarthy, R. 2010. *Mitigating Crashes at High-Risk Rural Intersections with Two-Way Stop Control*. Report No. K-TRAN: KSU-06-4, Jan. Bureau of Materials and Research, Kansas Department of Transportation, Topeka,.
- Sahoo, P. 2009. *Geometric design of speed control humps in Bhubaneswar City*. *International Journal Of Advanced Technology In Civil Engineering*, Department Of Civil Engineering, Bhubaneswar, Odisha, India.
- Sayer, I., & Parry, D. 1994. *Speed control using chicanes*. Project Report 102, Transport Research Laboratory, Crowthorne, Berkshire.

- Shauna, H., Keith, K., Gary, T., & S., D. 2002. Temporary speed hump impact evaluation. Final Report, Center For Transportation Research And Education.
- Siti, S., & Hamsa, A. K. 2016. A study on the effects of road humps in reducing speed along local roads in residential areas. *Journal Of The Malaysian Institute Of Planners Volume Xiv, Malaysia*, p. 55-66.
- Smith, D., Knapp, K., & Dr. Hallmark, S. 2002. Speed impacts of temporary speed humps in small Iowa cities.
- T. F. Fwa, C. Y. 1992. Rational approach for geometric design of speed-control road humps. *Transportation research record 1356*, p. 66-72, National Research of Singapore.
- Tajudeen, A., Adebayo, O., & Sunday, A. 2004. Vehicle speed control using road humps. *Transport Vol Xix No3, University Of Ibadan, Nigeria*, p. 130-136.
- Talaat, A., & I., H. H. 2017. Effect of speed humps characteristics on pavement condition. *Journal Of Traffic And Transportation Engineering, Cjang'an University Egypt*.
- Talaat, A.-W., & Hassan Hashim, I. 2017. Effect of speed humps characteristics on pavement condition. *Journal Of Traffic And Transportation Engineering, Cjang'an University Egypt*.
- Toplak, S., Sever, D., Ivanič, A., Mohorić, M., & Lubej, S. 2016. Effect of traffic calming measures on ground-borne vibrations in residential areas - the Slovenian experiences. 7th AAAA Congress on Sound and Vibration. Ljubljana, Slovenia.
- Traffic Calming Guidelines, The South Carolina Department of Transportation (SCDOT). 2009. p. 35.
- Traffic Engineering South Carolina Department of Transportation. 2006. Traffic Calming Guidelines...reducing the speed and volume of traffic to acceptable levels.
- Transport, D. f. 2005. Rumblewave Surfacing. Department for Transport, Rumblewave Surfacing, Traffic Advisory Leaflet 1/05, Jan. Department for Transport, London, U.K., p. 6.
- Van Houten, R., & Van Hutten, F. 1987. The Effects of a Specific Prompting Sign on Speed Reduction. *Accident Analysis & Prevention*, p. 115-117. doi:10.1016/0001-4575(87)90030-3.
- Vlahogianni, E. 2006. Some empiric relations between travel speed, traffic volume and traffic composition in urban arterials. *Transportation*.
- Waltz, F., Hoefliger, M., & Fehlmann, W. (s.d.). Speed Limit Reduction from 60 to 50 km/h and Pedestrian Injuries. *Proceedings of the Twenty-Seventh Step Car*

- Crash Conference. International Research Council on Biokinetics of Impacts (IRCOBI) (p. 311-318). Warrendale, PA: Society of Automotive Engineers.
- Watts, G., & Krylov, V. 2000. Ground-borne vibration generated by vehicles crossing road humps and speed control cushions. *Applied Acoustics* 59, 221-236.
- Webster, D., & Layfield, R. 1998. Traffic Calming-Sinusoidal, H And S Humps. Transport Research Laboratory, Report 377.
- Werner, T. 201). Do speed humps help reduce vehicular speeds, volumes, and motorist accidents. San Jose State University.
- Ziolkowski, R. 2014. Speed profile as a tool to estimate traffic calming measurese efficiency. *Journal Of Civil Engineering And Architecture*, Volume 8, No.12 (Serial No.85), USA.

## APPENDIX A

The iterative process HIC calculation can be automated using a Matlab script below

```
clear all
close all
clc
%dati
t=xlsread('40 TFFM',1,'A2:A542');
a_tot=xlsread('40 TFFM',1,'B2:B542');
s_f=0.001;%SCALE FACTOR TO USE INDEXES AS A NUMBER
```

### % HIC COMPUTATION

```
for i = 1:length(t)
for j = 1:length(t)
HIC(i,j)=((((trapz(a_tot(i:j)))/((j-i+1)))^2.5)*(((j-i+1)*s_f))));
end
end
[HIC_max,I]=max(HIC(:));
[T_1,T_2]=(ind2sub(size(HIC),I));
T1=T_1*(s_f*1000); % milliseconds
T2=T_2*(s_f*1000); % milliseconds
dt_HIC_max =(T2-T1); % milliseconds
```

### %CALCULATION OF THE HIC 15

```
for i = 1:length(t)
for j = 1:length(t)
if (j-i+1)== 15
HIC_15(i,j)=HIC(i,j);
end
end
end
HIC_max_15=max(HIC_15);
[HIC_max_15,I]=max(HIC_15(:));
[T1__15,T2__15]=ind2sub(size(HIC_15),I);
T1_15=T1__15*(s_f*1000);%milliseconds
T2_15=T2__15*(s_f*1000);%milliseconds
```

### %CALCULATION OF THE HIC 36

```
for i = 1:length(t)
for j = 1:length(t)
if (j-i+1)== 36
HIC_36(i,j)=HIC(i,j);
end
end
end
HIC_max_36=max(HIC_36);
[HIC_max_36,I]=max(HIC_36(:));
[T1__36,T2__36]=ind2sub(size(HIC_36),I);
T1_36=T1__36*(s_f*1000);%milliseconds
T2_36=T2__36*(s_f*1000);%milliseconds
```

## APPENDIX B

### B.1 Historical excursus

In the 1950s and 1960s, the number of cars throughout Europe grew almost exponentially and the resulting traffic caused severe pressure on the entire road network, posing a threat to the quality of life in the city. To solve the capacity problems of the road network, which caused congestion, new lanes were added or new roads were built that reached and crossed the urban centers. Thus traffic congestion had become a more important concern than safety. It was thought to widen the streets to the detriment of pedestrians and cyclists who saw the public space available to them shrink. But wider roads induced motorists to increase speed, with greater exposure and risk to pedestrians at crossings.

At the end of the 1950s, traffic became so intense that some areas were unliveable, so people started thinking about safety. It was thought that the solution to eliminate conflicts between cars and vulnerable users was to separate traffic flows from users by classifying the road network in terms of function and capacity. But this created problems in existing urban areas which were redesigned and reorganized to make them more pleasant while leaving the possibility for cars to drive at reduced speeds. These speed reductions were possible thanks to the use of physical devices (such as narrowings, bumps, chicanes) which acted as obstacles for motorists (Lamera, 2000).

This solution, known as the "Woonerf design" (Collarte, 2012), is considered the emblem of traffic calming techniques. The Woonerven was officially approved by the Dutch government in 1976 and in the following decade, the idea spread to many other countries such as Germany, Sweden, Denmark, England, France, Japan, Israel, Austria and Switzerland.

The Woonerf solution presented critical issues such as high cost and low speed that could not be spread on a large scale. In the Netherlands, an attempt was made to evaluate whether the design principles of the Woonerven could be adapted to measures applicable to a wider range of roads and with lower costs, comparisons were made and the introduction of traffic moderation measures was envisaged as a type of intervention linked to costs and benefits.

The application of Traffic Calming techniques to residential areas took the name of "Section 40 areas" in Denmark, "Tempo 30" in Germany and "Zone 20 mph" in Great Britain.

The Germans decided in the 1980s to experiment with the application of traffic calming measures over a larger area. The results obtained were a reduction in speed in the face of traffic volumes that remained unchanged, the severity of accidents was reduced (De Pauw, Daniels, Thierie, & Brijs, 2014), air pollution decreased as well as the noise. These findings encouraged many cities around the world to do the same. At the beginning of the 1980s, Norway also felt the need for a policy to reduce the speed and traffic of crossing in the centres; Denmark also carried out an experiment. Thus, access gates, chicanes, roundabouts and other traffic moderation measures were introduced in the urban centres of the cities, resulting in a reduction in speed, accidents and atmospheric pollution, all at a much lower cost than the construction of new roads. Experimental programs were also launched almost simultaneously in France, the Netherlands and England. New devices were designed to capture the attention of motorists at the entrance to sensitive areas: differentiated flooring, coloured signs, lighting, etc.

Many nations have therefore moved to promote successful projects that aimed, as is the case today, at favouring the development of the non-motorized component. To encourage this alternative mobility, it is advisable to create comfortable and pleasant urban environments for pedestrians and cyclists so that they can use them in everyday life and not. In fact, it has been experienced that the perception of risk is significant for the choice of the mode of travel for both adults (Washington, Hawort, & Schramm, 2012); (Pooley, et al., 2013); (Chataway, Kaplan, Nielsen, & Prato, 2014); (Mertens, et al., 2016) and for children (Lorenc, Brunton, Oliver, Oliver, & Oakley, 2008); (Timperio, et al., 2006); (Carver, et al., 2005); (Carver, Timperio, Hesketh, & Crawford, 2010); (Christie, et al., 2011).

The traffic enhancement devices, despite having improved general safety, have limitations and generate problems in:

1. Buses: tend to increase travel times, can generate passenger discomfort and increase the wear of the mechanical parts of the buses.
2. Emergency services: can adversely affect the response times of emergency vehicles (fire and ambulance services). To be efficient, these services must use the fastest routes, rather than the shortest ones.
3. Cyclists: due to the high heights of the devices, they can experience discomfort when travelling on them.
4. Vehicle occupants, disabled or elderly: especially those with spinal problems, may find the measures, often especially vertical ones, more uncomfortable and more difficult to pass than more able people.

Traffic calming devices can be classified according to their effect in measures of:

- volume controls are used to reduce the amount of vehicles crossing a road.. These include total or partial road closures, deviations of various types (diagonals, etc.), central obstacles or barriers and forced curved islands.
- speed control including speed humps, speed bumps, raised areas (pedestrian crossings and intersections), roundabouts, chicanes, narrowings, etc. These measures through the variations of horizontal or vertical alignment and through narrowing of the carriageway reduce speeds of drivers.

Particularly the speed moderation tools can be further classified from a geometric point of view into:

- vertical devices that use the force of vertical acceleration aimed at containing excess speed;
- horizontal devices that use the force of lateral acceleration to reduce speed;
- psycho-perceptive devices used to moderate speed, without intervening on the geometry.

Field experiences have shown that vertical and horizontal devices tend to be more effective in reducing speeds. Below is only a brief overview of traffic calming with an elevation effect

### **Vertical devices**

Vertical speed control measures are one of the most effective forms of vehicle speed reduction. These devices are designed to reduce discomfort and minimize delays to service vehicles by covering, at times, only part of the width of the road.

Vehicles transiting on a localized irregularity of the road profile undergo a strong vertical acceleration due to the dynamic interaction between vehicle and irregularity. This acceleration causes a strong disturbance in the driver who is thus forced to reduce speed.

It is evident that, in order to operate an effective and continuous control of the speed of the vehicles, it is necessary to establish in series a certain number of such devices according to a specific spacing.

According to most of the studies and regulations, it has been seen that these devices can be classified into different categories listed below.

- **Speed humps**

The term "speed humps" is generic. Road bumps are elevations of the carriageway having different shapes and sizes to suit different positions and situations.

They are built in a bituminous conglomerate or rubber and have different profile trends, used in different countries. In Europe and Canada, the shapes are mainly trapezoidal or sinusoidal, in America sections with parabolic and circular development (arc of circle) are used (Department of Transportation, 2020).

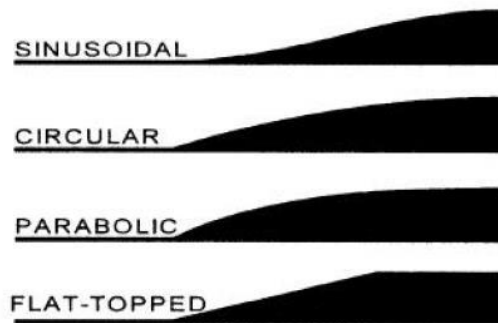


Figure B.1 Possible forms of speed humps

The geometry of the road bump can influence the degree of discomfort experienced by road users and the subsequent speed control effect.

Depending on the desired speed reduction, devices are inserted in series with a spatial gap defined a priori.

Bumps are the most used devices because they have proven effective in controlling speeds and are generally applicable to most road tracks.

The bumps can be classified into speed humps and speed bumps.

The substantial difference between speed humps and speed bumps concerns their length, as the former has a greater extension than speed bumps.

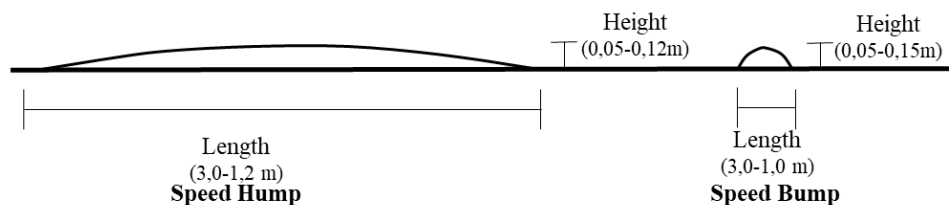


Figure B.2 Difference between a speed hump and a speed bump

Speed bumps are devices with a length of a few tens of cm, generally 30 cm, they are very common and easy to install that can be made of bituminous conglomerate or prefabricated plastic material. The height of such devices generally varies between 3 inch (7.62 cm) and 4 inch (10.16 cm).



*Figure B.3 Speed bump example*

Speed humps, on the other hand, are devices with a length of a few meters, they can vary between 12 feet (3.65 m) and 22 feet (6.70 m), also in this case the height varies between 3 inches (7.62 cm) and 4 inches (10.16 cm).



*Figure B. 4 Speed hump example*

These devices have innumerable advantages and disadvantages shown in the table.

Advantages	Disadvantages
<ul style="list-style-type: none"> <li>- the reduction in speed is influenced by the type of vehicle and the size of the bump (height, length and ramp gradient for flat humps);</li> <li>- reduction of accidents (about 60%);</li> <li>- reduction of traffic flows (about 25%);</li> </ul>	<ul style="list-style-type: none"> <li>- due to the vertical acceleration depending on the speed, the type of vehicle and the design of the bump, it causes annoyance to the drivers of the vehicles;</li> <li>- the discomfort of drivers and passengers on buses, ambulances and commercial vehicles is usually greater than that of cars</li> </ul>

<ul style="list-style-type: none"> <li>- bumps and raised joints can improve the appearance of a road if designed and built to a high standard;</li> <li>- on the bumps you could park avoiding loss of space;</li> <li>- if the back of the hump is flat it can be used as a crossing point for pedestrians;</li> <li>- minimal impact on snow clearing vehicles;</li> <li>- using bumps of reduced height reduces the inconvenience for passengers and bus drivers as well as reducing the travel times of the service vehicles. Even if this leads to an increase in the speed of cars.</li> </ul>	<p>(Herrstedt, 1991), even if the former pass through them at reduced speed;</p> <ul style="list-style-type: none"> <li>- the bumps increase the travel times of buses and emergency vehicles causing delays to the emergency services;</li> <li>- the reduction of the traffic flow on the section where the devices are applied can generate an increase of the vehicular flow on the surrounding untreated roads;</li> <li>- they can increase noise and vibration levels especially if there is a significant flow of commercial vehicles in the traffic flow;</li> <li>- bumps to be easily identified must be marked and illuminated;</li> <li>- poorly designed systems can lead to the aggressive behaviour of the driver who can be led to brake abruptly, increasing the noise and polluting emissions of individual vehicles;</li> <li>- such systems require sidewalk-to-sidewalk drainage for rainwater disposal.</li> </ul>
---	---

• **Speed table and raised crosswalks**

They are elevations of the road surface, connected to this thanks to connecting ramps (with a maximum gradient of 10%), which are positioned in correspondence with areas to be protected at high speeds or with the presence of pedestrian crossings.

Speed tables are elevations that reach about 22 feet (10-12 m) in length, which is longer than normal vehicles and 3 inches (7.62 cm) in height. They have a trapezoidal shape with a flat central back, joined laterally with two sinusoidal ramps.

The device can be made with asphalt, concrete, stamped asphalt or concrete, or other moulded materials.



*Figure B. 5 Raised crosswalks example*

The raised crosswalks is a device used for pedestrian crossing. This is usually longer and higher than the speed table to get to the curb level.

Such devices should be equipped with edge warning devices for the blind. This warning should be provided by means of a tactile surface.

They are built in bituminous conglomerate, rubber or more often brick (Department of Transportation, 2020).

From experience it has been noted that it is appropriate to impose an upper limit for the length (maximum 50 feet) of speed tables or raised crosswalks, otherwise, they lose their effectiveness.

Advantages	Disadvantages
<ul style="list-style-type: none"> <li>· speed reduction;</li> <li>· better definition of pedestrian areas;</li> <li>· self-application;</li> <li>· reduction of conflicts between vehicles and pedestrians.</li> </ul>	negative impact on emergency services (for example, ambulance, fire and police), slowing down response times and affecting the comfort of the patients transported.

## B.2 Effects of frequency on the human body

It is important to understand the concept of resonance, if the vibration has a very low frequency then the mechanical structure will move as a single unit, if instead the vibration has a high frequency the structure is isolated from the vibration itself. Between these two limit conditions there is a range of frequencies in which there will be a particular one in which the effect of the vibration will be maximized; this frequency is called the resonance frequency of the structure. To ensure that the vibrations are not too high at this frequency, the structures and the human body are dampened. Therefore, it responds differently to solicitations based on the frequency of the vibration and the natural frequency of vibrating. As for all mechanical structures, the human body also reacts differently as a function of frequency, especially for low frequencies it behaves as a single homogeneous mass, while for higher frequencies it behaves as a set of susceptible masses (of relative motion ) connected to each other by elastic elements such as muscles and dissipative elements such as cartilages. More specifically, the parts of the human body react differently depending on the frequencies, and each has its own resonance frequency. For example, the legs have a vibration frequency of 2 Hz, the abdomen has a frequency of 4-8 Hz, the chest a higher frequency around 50-100 Hz, the upper limbs frequencies ranging from 5 to 50 Hz, the head and the eyeball frequencies ranging from 20 to 90 Hz.

Hence, the level of stress induced by the vibration depends not only on the amplitude but also on the frequency. That is why it is sometimes preferred to describe vibration in the frequency domain rather than in the time domain. To do this, the

Fourier transform (FFT) is used in which a random signal is broken down into a series of simple sinusoidal signals, once passed in this domain the result will be a frequency response spectrum in which there will be frequencies to which the respective amplitudes are associated. The transition from the time domain to the frequency domain in the cases of the sinusoidal signal, multi-sinusoidal signal and random signal (using Mathcad) is reported below. In fact, you can see the result deriving from the transformation obtained by inserting the sinusoidal signal in the time domain and then passing it to the frequency domain with the FFT command.

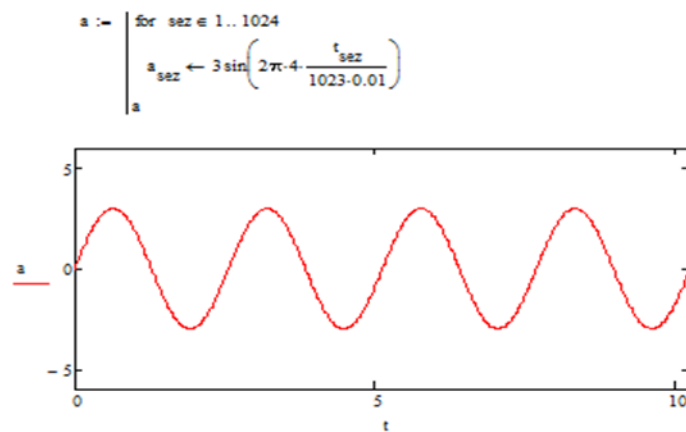


Figure B. 6 Signal as a function of time of a sinusoid

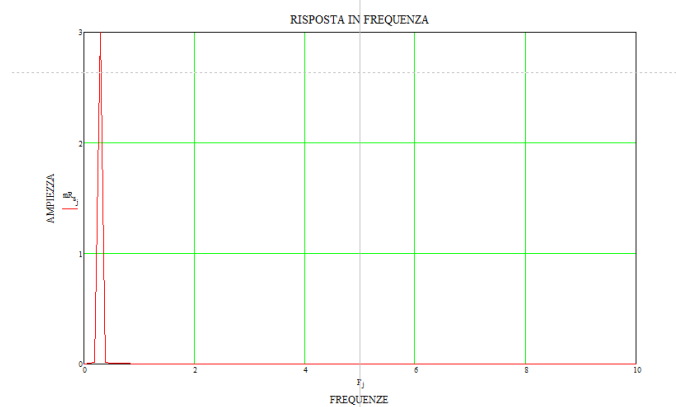


Figure B.7 Signal as a function of frequencies for a sine wave

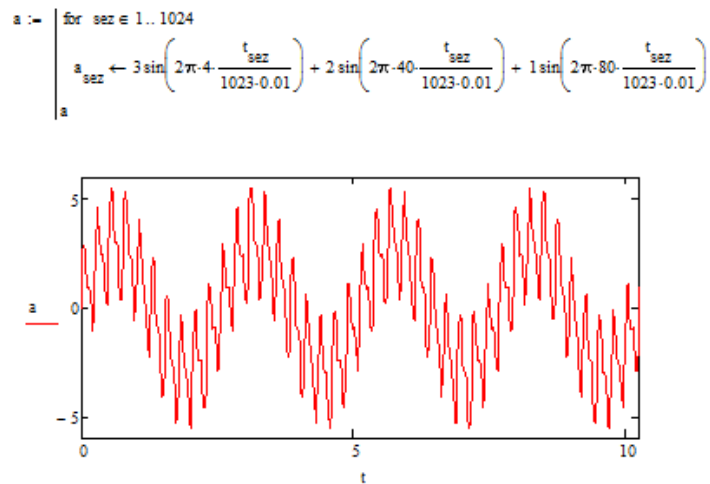


Figure B. 8 Time domain signal for a multi-sine wave

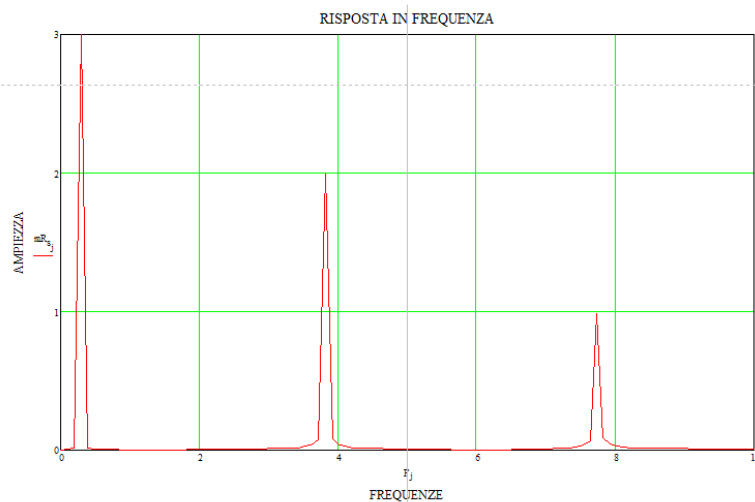


Figure B. 9 Signal in the frequency domain for a multi-sine wave

It can be noted that the difference between a sinusoidal and a multi-sinusoidal signal lies in the fact that a sinusoidal signal, in the frequency domain, has a peak with a value equal to its amplitude in correspondence with its own frequency, equal to 0.39 Hz; in the second case, a linear combination of three sinusoids with three different frequencies and amplitudes is observed. Three peaks of amplitude equal to 3.2 and 1 can be noted precisely in correspondence with the three frequencies at 0.39 Hz, 3.91 Hz and 7.82 Hz.

If, on the other hand, a random signal is evaluated, a representation of the signal in the time and frequency domain is obtained as shown below.

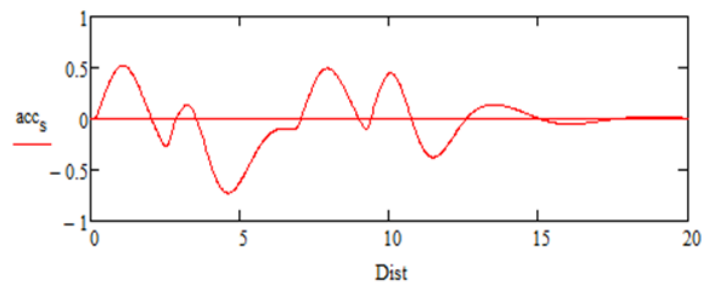


Figure B. 10 Random signal as a function of time

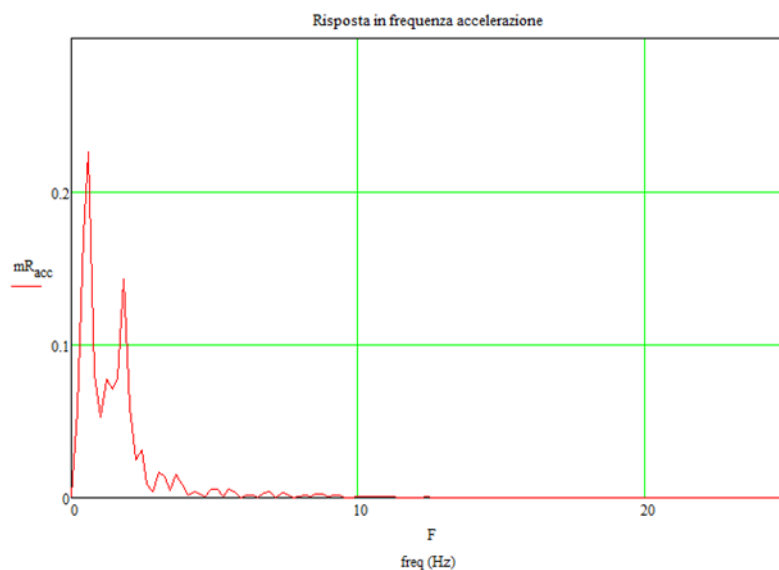


Figure B. 11 Random signal according to the frequencies

This spectrum will have a shape with a very irregular profile, therefore a representation in octave bands is preferred, thus dividing the frequency domain into bands. This concept is borrowed from acoustic physics, in which to represent a random sound the discretization is made to have a frequency spectrum with less irregularity, in short, a smoothed profile. The most used bands are those of octave and third of an octave. Each octave band has the particularity of having constant the ratio between the amplitude ( $df$ ), that is the difference between the upper and lower cut-off frequency, and the central frequency, equal to 0.707. The lower cut-off frequency of the  $i$ -th band corresponds to the upper cut-off frequency of the  $i$ -th-1 band. The one-third octave band has the ratio between the amplitude ( $df$ ) and the central frequency equal to 0.232; the centre frequency in both cases is given by the square root of the product between the lower cut-off frequency and the upper cut-off frequency. In the octave band, the lower frequency of the  $i$ -th band is double the lower frequency of the previous ( $i$ -th-1)

band. But in the one-third octave band, it is no longer double but there is an increase of a factor of 1.26. Ultimately, to find the lower value of the next band considering a band of an octave, multiply by 2, while for the band of a third of an octave, multiply by the cube root of 2. To represent this domain for n-th octave bands, one should make the nth root of the lower frequency to find the lower frequency of the next band.

The human body is exposed to deterministic or random waves, subdivided into stationary movements (in which the statistical properties do not change over time) or into non-stationary movements (when the statistical properties over time change).

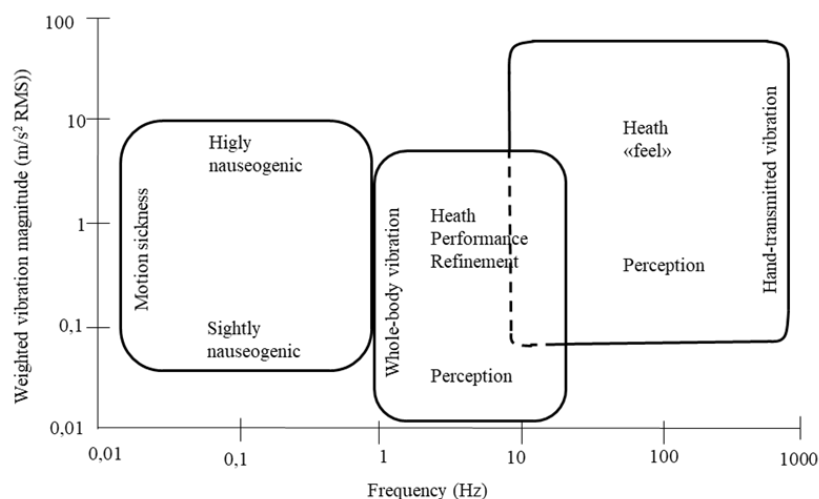
It is important to first understand how the three kinematic quantities are perceived as the frequency varies. For example, if you are on the top floor of a building and it begins to oscillate due to the strong wind, the movement is perceived but it is difficult to perceive the speed and acceleration. Similarly, if you look at a fan and touch the base, you notice the acceleration but cannot identify the movement.

The human body is exposed to different types of waves, both in amplitude and frequency. For example, a sine wave with a magnitude of 1 m/s<sup>2</sup> of RMS and a frequency of 0.2 Hz, i.e. a period of r seconds, has a peak-to-peak amplitude value of 2 m; this wave could represent the vertical oscillation which can be found on a ship trip. While with the same acceleration magnitude with a frequency of 1 Hz the peak-to-peak amplitude will be 70 mm; motion that can be found on a train journey. Always with the same magnitude with an oscillation of 5 Hz, you will have a peak-to-peak amplitude of 3 mm; this acceleration can be found during a road trip on an old car. With higher frequencies, always with the same magnitude, it becomes difficult to perceive the displacement; in fact at 20 Hz the vibration gives the sensation of being in a helicopter even if it has a peak-to-peak amplitude of 0.2 mm.

The effects on the human body vary according to the frequency and amplitude of the vibration. It is known that the effects on the whole body (WBV) for very low frequencies, therefore prolonged periods, are nauseating and increase with increasing amplitude while moving towards even lower frequencies can lead to motion sickness (a neurological disorder that some individuals subsequently experience rhythmic displacements during motion, for example on a ship). Furthermore, it may be difficult to maintain correct posture and loss of precision in gestures and manual activities. Motion sickness is a combination of unpleasant symptoms such as dizziness, nausea and vomiting that occur as a result of repetitive movements. It is a neurological disorder that derives from the contrasting interpretation of the signals coming from the vestibular, visual and proprioceptive systems. The signals that our brain receives, if there were any malformations of the vestibular system, could be discordant for the

different organs of perception, so once they reach the brain these signals come into conflict. For example, during a trip by car or by ship, the eyes send the signal that you are moving to the brain, but being seated, the other receiving organs send a different signal, this contrast is precisely the triggering cause of motion sickness, properly called movement disease. It often occurs during a trip, in fact, it is also known as seasickness or car sickness; in most cases, symptoms improve as the body adjusts to the conditions causing the problem. For example, if motion sickness occurs during a stay on a cruise ship, the malaise can improve within a few days. If, on the other hand, the vibrations have high frequencies, it can have effects on the parts in contact that can generate numerous injuries. Among the best known are the vascular lesions that can occur according to the secondary form (Raynard's phenomenon, commonly known as white finger syndrome); neurological lesions can present with neuropathies, hypoesthesia, reduction of thermal sensitivity and precision, moreover, an impairment of the sensory component can arise. Musculoskeletal lesions can be chronic-degenerative tendon or osteoarticular lesions. These damages occur precisely because at high frequencies our body does not react as a single mass but in a distinct way, therefore mechanically injuries can be created at the points of contact, as the parts of the body do not move asynchronously. Therefore, during a high-frequency vibration, there are elongations or shortenings that affect the state of health.

In general, vibrations with low frequencies, between 1 Hz and 20 Hz, have more relevant effects on the whole body while vibrations with high frequencies, between 10 Hz and 100 Hz have greater effects on the contact parts (Mansfield Neil J., 2005).



FigureB. 12 Effects on the human body as a function of frequency

The organs that make up the human body send different motion detection signals (because each system reacts differently to vibrations) which are combined and once they arrive at the brain they are assimilated and a cognitive model of the movement environment is generated. It has been observed that the visual system is very sensitive to oscillations at low frequencies, this allows us to see a relative displacement of objects that move with high periods; while the vestibular system is very sensitive to high-frequency oscillations because the semi-circular canals and the vestibule are sensitive to rotational and linear acceleration. The somatic system can be divided into three elements (kinesthetic, visceral and cutaneous) each of which receives the signals through the receptors found in muscles, joints, tendons or terminations present in the skin layers. Sometimes exposure to shocks or transients can be heard through the vibrations of the vehicle structure, above 20 Hz (high frequencies) the vibrating surfaces can act as amplifiers causing the perception of sound.

The problem of identifying vibration perception thresholds is a very complex problem, in fact, over the years numerous researches have been conducted in the laboratory exposing individuals to sinusoidal signals to evaluate the perception threshold of each.

It has been found that seated subjects, as in the case of drivers, exposed to vertical sinusoidal vibrations are able to perceive vibrations with a frequency of 5 Hz up to 0.01 m/s<sup>2</sup> RMS, while with vibrations having frequencies below 1 Hz and above 10 Hz the threshold perception rises to values of 0.03 m/s<sup>2</sup>, in general the human body is more sensitive to vibrations included in a frequency range between 4 Hz and 8 Hz.

For horizontal sinusoidal vibrations, on the other hand, the most perceptible vibration is always the one with a frequency of 1 Hz, while vibrations with higher frequencies have a perception threshold that increases up to 0.4 m/s<sup>2</sup> RMS at a frequency of 80 Hz.

These results have been developed, as mentioned before, on seated individuals, but in reality, it is also possible to travel in a supine or standing position, such as ships, rescue vehicles, military operations, or more commonly standing on buses, trains, subways. Therefore, studies have also been conducted that consider different positions in which it has been shown that there is not a big distinction of perception compared to the case of sitting position. The graphical representations of the perception thresholds are shown below.

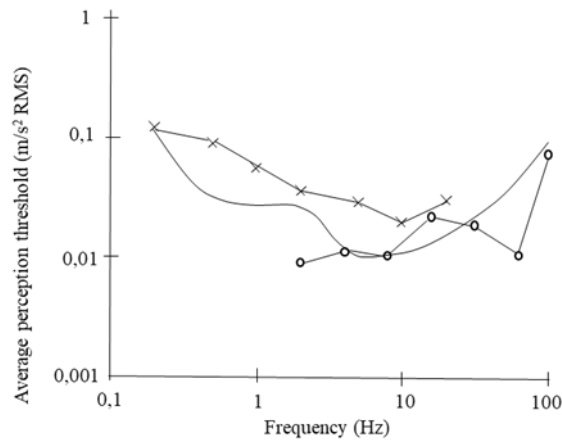


Figure B. 13 Perception thresholds for vibrations for vertical sinusoidal oscillations as a function of frequency

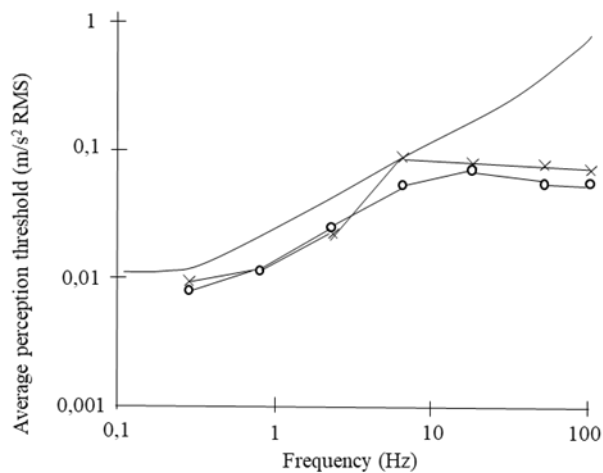
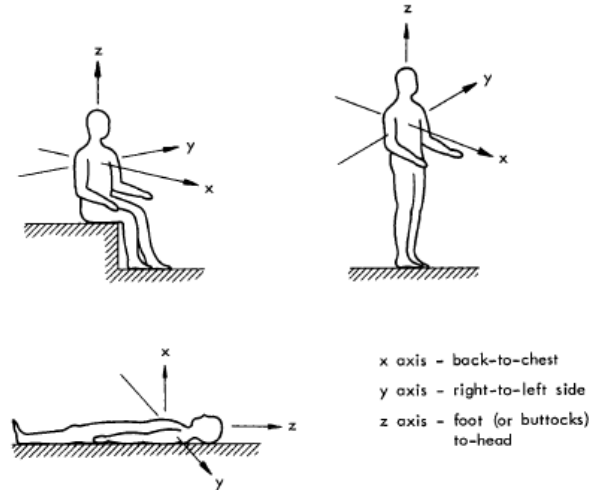


Figure B. 14 Perception threshold for horizontal sinusoidal vibrations as a function of frequency

Assuming that the response of the human body varies according to the frequencies, to determine the RMS or the eVDV it is advisable to weigh the quantities in a different way according to one's own frequency. Then weighting curves were identified by which a factor to be multiplied by the respective size was associated with each frequency band. This multiplication factor will be less than unity for frequencies outside the range between 4 and 8 Hz; it is conceivable that moving away from these frequencies, the body is not affected by these vibrations, therefore the multiplicative factor decreases. One can qualitatively imagine a bell curve. Before evaluating these curves it must be emphasized that the human body reacts differently also depending on the direction from which the vibrations come, therefore it is appropriate to define the Cartesian axes. The ISO 2631 standard defines an orthogonal system for a seated

person: the z axis that goes from the feet to the head, the x axis that goes from the back to the chest, the y axis that goes from right to left.



The acceleration evaluated is that along the z axis, therefore the components along the other two axes are neglected. The multiplicative factors as a function of the central frequency relative to a third of an octave and the multiplicative factors for the transverse vibrations referred to the x and y axes are reported below.

*Table B. 1 Multiplication factors for longitudinal and transverse vibrations*

Center frequency of the 1/3 octave band	Multiplication factor for longitudinal vibrations	Multiplication factor for transverse vibrations
1	0.5	1
1.26	0.56	1
1.6	0.63	1
2	0.71	1
2.6	0.80	0.8
3.16	1	0.63
4	1	0.5
5	1	0.4
6.3	1	0.316
8	1	0.25
10	0.80	0.2
12.5	0.63	0.16
16	0.50	0.125
20	0.40	0.1
26	0.316	0.08
31.6	0.25	0.063
40	0.20	0.06
50	0.16	0.04
63	0.125	0.0315

80	0.10	0.025
----	------	-------

The body is more sensitive to transverse vibrations, especially if between 1 and 2 Hz. On a graphic level, by superimposing the transverse and vertical vibrations, a translation is observed.

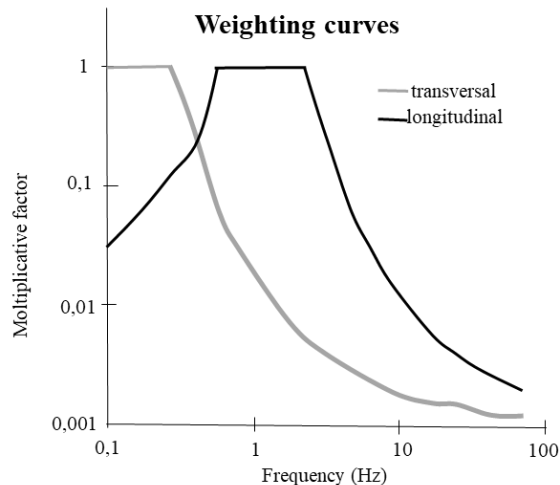


Figure B. 15 weighting curves for longitudinal and transverse vibrations

In the most general case, in which the components along x and y are also considered, the simultaneity along the 3 axes of vibration should have been taken into account, therefore the acceleration should be weighed along the 3 directions to then have a single acceleration value by applying the following equation:

$$a = \sqrt{(1.4a_{xw})^2 + (1.4a_{yw})^2 + a_{zw}^2} \quad \text{B'.1}$$

By applying a multiplication factor equal to 1.4 to the transverse accelerations, these can be uniformed to the longitudinal ones.

## B.2.1 International standard relating to exposure to vibrations

The reference standard for assessing the exposure of the human body to vibrations is the ISO 2631 standard (International Organization for Standardisation, 1986), drawn up in 1978 but subsequently updated several times, in fact there are more recent versions, in 1985, in 1997 and the last revision in 2014. Here are some basic passages to then highlight some similarities with the BS 6473 standard (British Standard institution, 1984), implemented in England by ISO 2631. In Italy, on the other hand,

the problem of vibrations was implemented in the legislative decree of no 81/2008, or "consolidated text on safety at work" which assesses the risk of exposure to vibrations in work field. The reference technical standards are UNI EN ISO 5349 for the arm-hand system and UNI 2631 for the vibrations transmitted throughout the body.

### B.3 Exemplary models of vehicles

In order to evaluate the disturbance induced on the driver when crossing the bump, it is necessary to schematize the vehicle with a simplified model. In this work, different models were considered which will be analyzed in detail below.

The quarter car model is used to represent a portion of the vehicle.

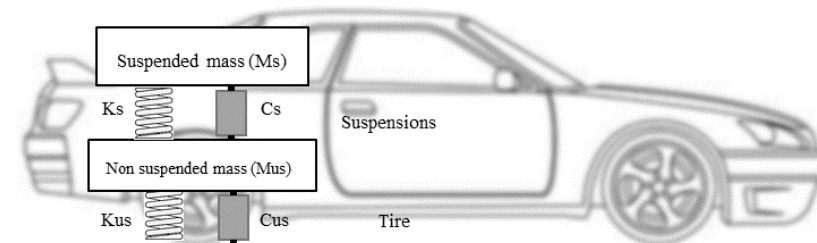


Figure B16 Quarter car model diagram

This model, with two degrees of freedom, sees the vehicle schematized with a spring ( $k_{us}$ ) supporting an unsprung mass ( $M_{us}$ ), representing the tire, connected via an elastic spring ( $k_s$ ) and a viscous damper ( $c_s$ ) to a sprung mass ( $M_s$ ), which represents the vehicle. The two degrees of freedom are the vertical displacements of the two masses.

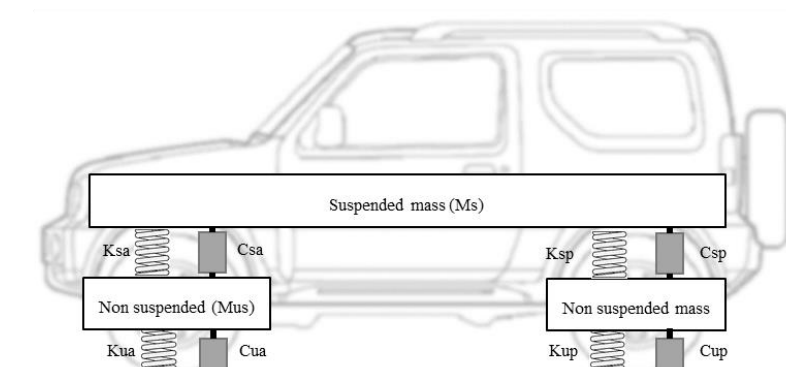


Figure B. 17 Half car model diagram

The model with four degrees of freedom, on the other hand, is schematized with a rigid suspended rod, which is the mass of the vehicle ( $M_s$ ), connected by means of

elastic springs ( $k_{sa}$ ,  $k_{sp}$ ) and viscous dampers ( $c_{sa}$  and  $c_{sp}$ ) with two masses unsprung, the tires ( $M_{ua}$  is the mass of the front tire and  $M_{up}$  the mass of the rear tire), connected to the ground by means of elastic springs ( $k_{ua}$ ,  $k_{up}$ ) and viscous dampers ( $c_{ua}$ ,  $c_{up}$ ).

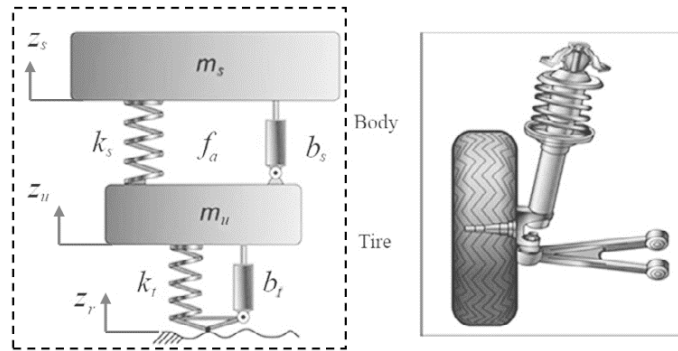


Figure B. 18 Spring-damper diagram representing the tire

In this diagram, the degrees of freedom are 4, there are three vertical displacements of the three masses (the two tires and the rigid rod) and, in addition, there is rotation around the center of gravity  $\mathcal{G}$ . The rotation around its own transverse axis is considered because, compared to the previous scheme, pitching can occur.

Since the phenomenon of pitching was present, it was necessary to evaluate the moment of inertia for the rigid rod, which is somewhat complicated due to the particular shape of the car body. In this discussion, the problem has been simplified by obtaining the moment of inertia by approximating the vehicle body to a rigid rod having a length equal to the total length of the vehicle. Remember the formula for the moment of inertia  $J$  ( $\text{kg m}^2$ ):

$$J = m i^2 \tag{B'.0.2}$$

where  $m$  represents the suspended mass of the entire vehicle excluding the masses of the front and rear axles, while  $i$  is the radius of inertia calculated as the moment of inertia divided by its area, remembering that the moment of inertia for a rectangular section is equal to:

$$M = \frac{BH^3}{12} \tag{B'.0.3}$$

Going to make this relationship it turns out that the radius of inertia "i" is equal to:

$$i = \frac{H^2}{12} \tag{B'.0.4}$$

Therefore the moment of inertia  $J$  will be given by the following definitive formula:

$$J = m \frac{H^2}{12} \quad B'.0.5$$

where the quantity H represents the full length of the vehicle.

In order to evaluate the accuracy of this simplification, assuming that the car body is a rigid rod, the moment of inertia that comes out of this formula was compared with the moment of inertia obtained experimentally.

To do this, 40 cars were taken from the entire vehicle fleet (Heydinger, 1999) from which the data relating to the mass, length and experimental values of the moment of inertia J are available ( $\text{kg m}^2$ ). For each vehicle, the moment of inertia was calculated using the equation B'.0.5 above as a function of mass and length.

The following graph places on the abscissa axis the moment value obtained experimentally and on the ordinate axis the moment obtained from the formula, from this it is clear how close the approximation of the vehicle body to a rigid rod is to reality, it can be in fact observe that the points approach the bisector line of the quadrant.

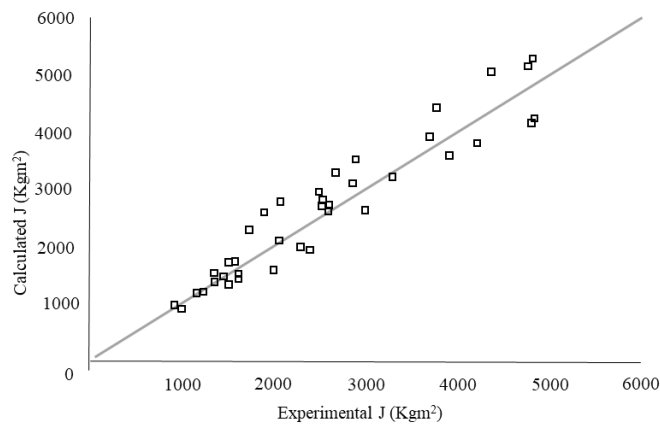


Figure B. 19 Comparison of experimental moment of inertia and calculated moment of inertia

This makes it possible to assume the value of the moment of inertia J ( $\text{kg m}^2$ ) as the product of the suspended mass and the radius of inertia as a function of the total length of the vehicle.

For the evaluation of the length of the vehicle footprint, on the other hand, the following relationship was used:

$$\pi r_i^2 \rho_g = F_v \quad B'.0.6$$

where the unknown is the radius of the footprint area (m), while  $F_v$  is the vertical discharge on the single wheel calculated as a quarter of the total mass of the vehicle and  $p_g$  is the tire inflation pressure (2 bar = 202650 N/m<sup>2</sup>). Therefore the radius of the footprint area is:

$$r_i = \sqrt{\frac{F_v}{2\pi p_g}} \quad B'.0.7$$

The footprint area is then double the radius of the footprint area, below is a summary table of the sizes listed so far for each type of vehicle:

	<b>weight (kg)</b>	<b>F<sub>v</sub> (N)</b>	<b>r (m)</b>	<b>D (m)</b>
<b>A</b>	940	2305.35	0.060176	0.12
<b>C</b>	1090	2673.225	0.064799	0.14
<b>D</b>	1707	4186.418	0.081091	0.16
<b>E</b>	2450	6008.625	0.097149	0.20

Furthermore, the values shown in the following table have been entered to represent the driver and the vehicle seat in the model.

Elastic stiffness of the seat (N / m)	10000
Linear coefficient of kinematic viscosity of the front suspension (N s/m)	500
Mass of seat and driver (kg)	100

It has been estimated that the distance between the driver and the centre of gravity is approximately 0.3 m, this is because the centre of gravity is generally located near the gear lever, located approximately 0.3 m from the driver's seat.

### **B.3.1 Description of mathematical models**

The quarter-car model is simpler as the car, which schematized with a suspended mass, interacts with the elevation profile through a viscous damper and elastic spring, and is also connected to the unsprung mass through a viscous damper and an elastic spring.

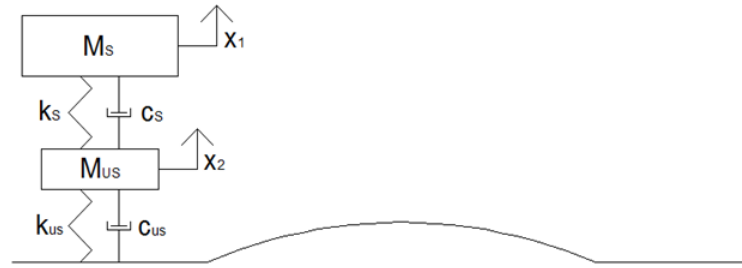


Figure B. 20 quarter-car model

From the analytical point of view, the solution of the problem is obtained through a system of differential equations:

$$[M] \ddot{X} + [C]\dot{X} + [K]X = \{Y\} \quad B'.0.8$$

Where:

[M]= mass matrix

[C]= damping matrix

[K]= matrix of elastic stiffnesses

{Y}= vector terms known

By operating a change of variables, the system of n second-order differential equations becomes a system of 2n first-order differential equations:

$$\{X\} = \begin{bmatrix} z_s \\ \dot{z}_s \\ z_u \\ \dot{z}_u \end{bmatrix} \quad B'.0.9$$

In which:

\$z\_s\$ is the height of the suspended mass (m),

\$\dot{z}\_s\$ is the velocity of the suspended mass (m/s),

\$z\_u\$ is the height of the unsprung mass (m),

\$\dot{z}\_u\$ is the velocity of the unsprung mass (m/s),

A system of first order differential equations is obtained:

$$\{\dot{X}\} = [A]\{X\} + \{B\}h_v \quad B'.0.10$$

where \$h\_v\$ represents the filtered share of the profile by the moving average operator. This system is solved by a numerical method for successive iterations; the response of the system in the i-th point is the sum of a free response of the system in the previous position (i-1) and the forced response of the input between the intervals (i-1 and i).

$$R_i = R_{i-1} + R_{(i-1,i)} \quad B'.0.11$$

The system of differential equations becomes:

$$\{\dot{X}\} = [A]\{X\} + \{B\}S_{ps} \quad B'.0.12$$

where  $S_{ps}$  represents the slope of the filtered profile (constant for each section). The closed form solution is as follows:

$$x_i = e^{A(\frac{\Delta}{V})} * x_{i-1} + A^{-1} * \left( e^{A(\frac{\Delta}{V})} - I \right) * B * u \quad B'.0.13$$

Where:

$e^{A(\frac{\Delta}{V})}$  represents the answer in i-1;

$A^{-1} * \left( e^{A(\frac{\Delta}{V})} - I \right) * B * u$  represents the forced response

By solving the system of differential equations, the vector  $\{X\}$  is evaluated with which it is possible to determine the slopes and the relative variations for each section, of the suspended and unsprung mass. Subsequently, from the values of the slopes it is possible to reconstruct the profile of the suspended and unsprung mass, thus deriving this profile with respect to time, speed and acceleration are obtained.

The matrices used for the resolution are the following:

$$A = \begin{bmatrix} 0 & 1 & 0 & 0 \\ -k_2 & -c & k_2 & c \\ 0 & 0 & 0 & 1 \\ \frac{k_2}{\mu} & \frac{c}{\mu} & \frac{-(k_1 + k_2)}{\mu} & \frac{-c}{\mu} \end{bmatrix}$$

$$B = \begin{bmatrix} 0 \\ 0 \\ 0 \\ \frac{k_1}{\mu} \end{bmatrix}$$

In the matrices all quantities are divided by the suspended mass, where:

$k_1$  ratio between the elastic stiffness of the tire and the suspended mass (N/m);

$k_2$  ratio between the elastic stiffness of the suspensions and the suspended mass (N/m);

$c$  ratio between the linear viscosity coefficient of the suspension and the suspended mass (Ns/m);

$\mu$  ratio between the unsprung mass and the suspended mass.

In this model, the linear viscosity coefficient of the tire is neglected as it appears to be very modest compared to the other quantities.

In addition to the characteristics of the vehicle, the altimetric profile (represented graphically on the Cartesian plane) and the speed must therefore be entered as input data.

It is then necessary to arbitrarily determine a spatial sampling step to which a corresponding sampling time step will be associated by means of the velocity. Having to operate in the range of frequencies between 0.5 Hz and 80 Hz, a step of 0.02 m was chosen in order to better represent the phenomenon. In fact, as can be seen from the following table, for low speeds information is lost for high frequencies for which it is not possible to sample having a very low maximum sampling frequency ( $f_s$ ), of a few tens of Hz.

Speed (Km/h)	Speed (m/s)	$\Delta=0.02$ m		$\Delta=0.05$ m		$\Delta=0.1$ m	
		$t_{int}$ (s)	$f_s$ (Hz)	$t_{int}$ (s)	$f_s$ (Hz)	$t_{int}$ (s)	$f_s$ (Hz)
5	1.388889	0.0144	69.44444	0.036	27.77778	0.072	13.88889
10	2.777778	0.0072	138.8889	0.018	55.55556	0.036	27.77778
15	4.166667	0.0048	208.3333	0.012	83.33333	0.024	41.66667
20	5.555556	0.0036	277.7778	0.009	111.1111	0.018	55.55556
25	6.944444	0.00288	347.2222	0.0072	138.8889	0.0144	69.44444
30	8.333333	0.0024	416.6667	0.006	166.6667	0.012	83.33333
35	9.722222	0.002057	486.1111	0.005143	194.4444	0.010286	97.22222
40	11.11111	0.0018	555.5556	0.0045	222.2222	0.009	111.1111
45	12.50000	0.0016	625.0000	0.004	250.0000	0.008	125.0000
50	13.88889	0.00144	694.4444	0.0036	277.7778	0.0072	138.8889
55	15.27778	0.001309	763.8889	0.003273	305.5556	0.006545	152.7778
60	16.66667	0.0012	833.3333	0.003	333.3333	0.006	166.6667
65	18.05556	0.001108	902.7778	0.002769	361.1111	0.005538	180.5556
70	19.44444	0.001029	972.2222	0.002571	388.8889	0.005143	194.4444

On the other hand, it was not possible to use a sampling step lower than 0.02 m because in that case important information would have been lost at low frequencies, having to use a very high elementary df.

To calculate the  $f_s$  as a function of the spatial sampling step and the velocity, the integration interval ( $t_{int}$ ) was first calculated as a ratio between the sampling step ( $\Delta$ ) and speed, then the  $f_s$  as the inverse of the sampling interval.

$$t_{int} = \frac{\Delta}{v} = \frac{1}{f_s} \quad B'.0.14$$

For example, proceeding at a speed of 5 Km/h (1.38 m/s) and a spatial step of 0.1 m, the sampling frequency is equal to 13.88; this frequency does not allow to evaluate the whole phenomenon in the frequency range of interest.

Entering the characteristics of the vehicle, the speed and the altitude profile through the system of differential equations, the result is a time history of the displacements of the suspended and unsprung mass. Velocity and acceleration were derived as an incremental ratio of displacement through numerical integration:

$$v_i = \frac{x_i - x_{i-1}}{t_{int}} \quad B'.0.15$$

$$a_i = \frac{v_i - v_{i-1}}{t_{int}} \quad B'.0.16$$

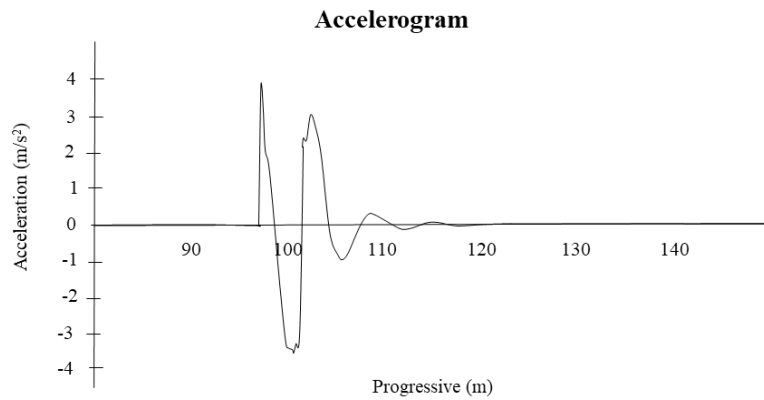


Figure B. 21 Acceleration as a function of space-time

The Half-car model was then analyzed which has four degrees of freedom, namely: the vertical displacement of the suspended mass, the rotation of the suspended mass (representative of the pitching phenomenon), the vertical displacement of the front unsprung mass and unsprung mass rear. In this model the suspended mass is not a point body but a rigid rod. The rigid member in physics is a one-dimensional body whose parts are subject to a rigidity constraint, i.e. a body that is stationary or moving never deforms.

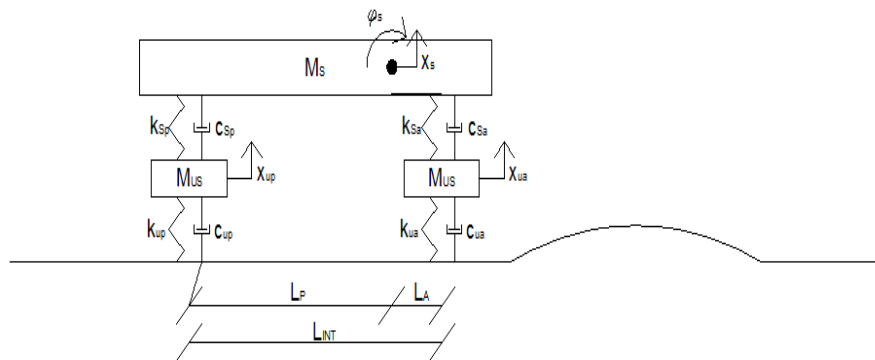


Figure B. 22 Half-car model

Mathematically, the resolution is similar to that used in the quarter-car model, in fact, the matrices of elastic stiffness and viscous dampers have been constructed. Also in this case the viscous dampers of the tires are neglected, furthermore, the distances between the front axle and the rear axle are measured with respect to the center of gravity of the rigid rod (the rod schematizes the vehicle body) in which the mass is concentrated suspended.

The matrices used are shown below:

$$M = \begin{bmatrix} m_s & 0 & 0 & 0 \\ 0 & J_s & 0 & 0 \\ 0 & 0 & m_{ua} & 0 \\ 0 & 0 & 0 & m_{up} \end{bmatrix}$$

$$K = \begin{bmatrix} -(k_a + k_p) & k_p L_p - k_a L_a & k_a & k_p \\ k_p L_p - k_a L_a & -(k_a L_a^2 + k_p L_p^2) & k_a L_a & -k_p L_p \\ k_a & k_a L_a & -(k_a + \epsilon_a) & 0 \\ k_p & -k_p L_p & 0 & -(k_p + \epsilon_p) \end{bmatrix}$$

$$C = \begin{bmatrix} -(c_a + c_p) & c_p L_p - c_a L_a & c & c_p \\ c_p L_p - c_a L_a & -(c_a L_a^2 + c_p L_p^2) & c_a L_a & -c_p L_p \\ c_a & c_a L_a & -c_a & 0 \\ k_p & -k_p L_p & 0 & -c_p \end{bmatrix}$$

In which this symbolism represents:

$m_s$  is the mass of the suspended rigid rod (kg);

$m_{ua}$  is the mass of the front axle (kg);

$m_{up}$  is the mass of the rear axle (kg);

$J_s$  is the moment of inertia of the rigid member;

$k_a$  is the elastic stiffness of the front suspension (N/m);

$k_p$  is the elastic stiffness of the rear suspension (N/m);

$L_a$  is the distance between the front axle and the center of gravity of the rigid rod (m);

$L_p$  is the distance between the rear axle and the center of gravity of the rigid rod (m);

$\epsilon_a$  is the elastic stiffness of the tire (N/m);

$\epsilon_p$  is the elastic stiffness of the tire (N/m);

$c_a$  is the kinematic viscosity coefficient of the front axle (N<sup>2</sup>/m);

$c_p$  is the kinematic viscosity coefficient of the rear axle (N<sup>2</sup>/m);

Also in this case a change of variables was carried out passing from a system of  $n$  second-degree differential equations to a system of  $2n$  first degree differential equations.

Consequently, vectors are obtained which represent the displacements of the three masses and the rotation. By way of example, the overlapping time histories of the displacements of these masses as they pass over a generic bump are reported below:

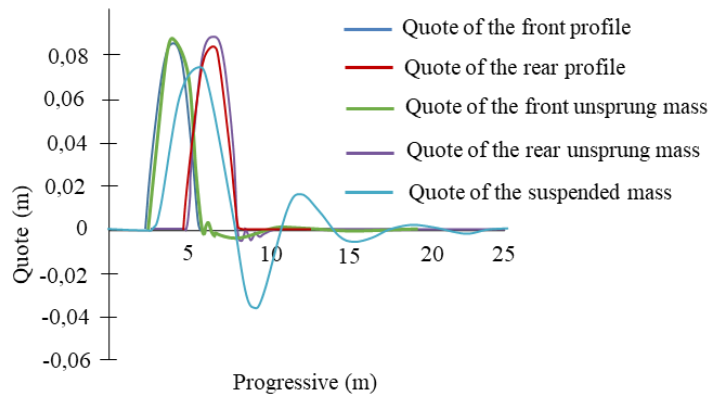


Figure B. 23 time-history of the movements of the masses

It is observed that the suspended mass begins to move when the front axle begins to cross the impact and that there is a time lag between the displacement of the front and rear unsprung mass; this delay corresponds to the ratio between the length of the step and the speed with which the crossing of the bump is simulated. What happens in the first ten meters is shown graphically below:

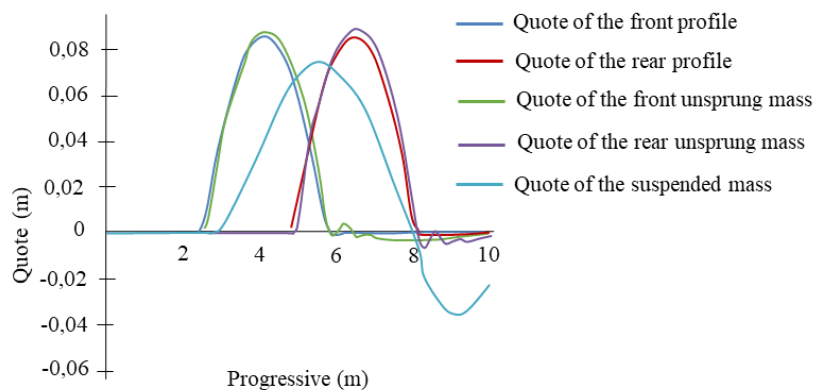


Figure B. 24 time history of the vertical displacements of the masses

It can be seen that the suspended masses differ little from the road profile while the trend of the suspended mass has a lower peak than the relative peaks of the unsprung masses, moreover there is a phase shift due to the dampers; even if from the graph it is not possible to perceive, there is a small undulation, small displacements of the rear

unsprung mass, even before the rear axle begins to cross the bump, which is explained by the fact that the rear axle is connected via the rigid rod to the front axle.

As in the case of the quarter-car, by deriving this representation of the displacements with respect to time, it is possible to obtain the speeds and accelerations as a function of time by making the incremental ratio of the displacements with respect to time and then going to make the ratio incremental speed with respect to time:

$$v_i = \frac{x_i - x_{i-1}}{t_{int}} \quad B'.17$$

$$a_i = \frac{v_i - v_{i-1}}{t_{int}} \quad B'.18$$

Below is an accelerogram of the mass suspended in the time domain on a generic bump:

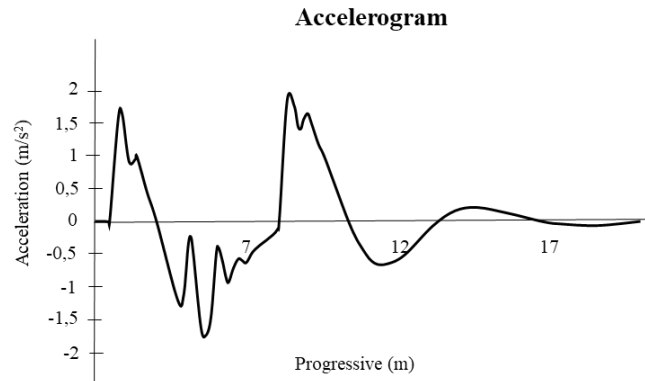


Figure B. 25 acceleration as a function of time

The 5 degrees of freedom model is more complex than the first two models, it consists of a model similar to the Half-car model with the addition of another degree of freedom, namely the vertical displacement of the driver. Therefore, compared to the Half-car it is necessary to construct matrices of inertia, stiffnesses and dampers of size  $5 \times 5$ , in which to insert new input data such as the total mass of driver and seat, the elastic stiffness of the seat, the kinematic viscosity coefficient of the seat and the distance between this mass and the center of gravity of the rigid rod which always represents the suspended mass.

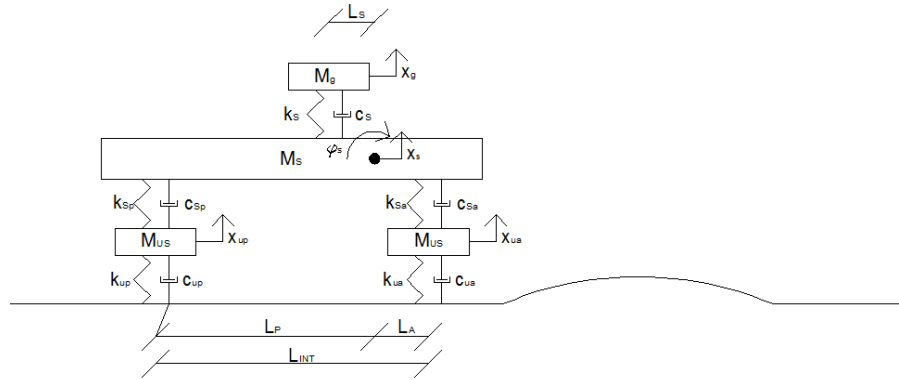


Figure B. 26 5 dof model

Below are the matrices used to solve the problem:

$$M = \begin{bmatrix} m_s & 0 & 0 & 0 & 0 \\ 0 & J_s & 0 & 0 & 0 \\ 0 & 0 & m_{ua} & 0 & 0 \\ 0 & 0 & 0 & m_{up} & 0 \\ 0 & 0 & 0 & 0 & m_g \end{bmatrix}$$

$$K = \begin{bmatrix} -(k_a + k_p + k_s) & k_p L_p - k_a L_a + k_s L_p & k_a & k_p & k_s \\ k_p L_p - k_a L_a + k_s L_p & -(k_a L_a^2 + k_p L_p^2 + k_s L_s^2) & k_a L_a & -k_p L_p & -k_s L_s \\ k_a & k_a L_a & -(k_a + \epsilon_a) & 0 & 0 \\ k_p & -k_p L_p & 0 & -(k_p + \epsilon_p) & 0 \\ k_s & -k_s L_s & 0 & 0 & -k_s \end{bmatrix}$$

$$C = \begin{bmatrix} -(c_a + c_p + c_s) & c_p L_p - c_a L_a + c_s L_s & c_a & c_p & c_s \\ c_p L_p - c_a L_a + c_s L_s & -(c_a L_a^2 + c_p L_p^2 + c_s L_s^2) & c_a L_a & -c_p L_p & -c_s L_s \\ c_a & c_a L_a & -c_a & 0 & 0 \\ k_p & -k_p L_p & 0 & -c_p & 0 \\ c_s & -c_s L_s & 0 & 0 & -c_s \end{bmatrix}$$

In which:

$m_s$  is the mass of the suspended rigid rod (kg);

$m_{ua}$  is the mass of the front axle (kg);

$m_{up}$  is the mass of the rear axle (kg);

$J_s$  is the moment of inertia of the rigid member (Nm<sup>2</sup>);

$k_a$  is the elastic stiffness of the front suspension (N / m);

$k_p$  is the elastic stiffness of the rear suspension (N / m);

$L_a$  is the distance between the front axle and the center of gravity of the rigid rod (m);

$L_p$  is the distance between the rear axle and the center of gravity of the rigid rod (m);

$\epsilon_{to}$  is the elastic stiffness of the tire (N / m);

$\epsilon_p$  is the elastic stiffness of the tire (N / m);

$c_a$  is the kinematic viscosity coefficient of the front axle (N s / m);

$c_p$  is the kinematic viscosity coefficient of the rear axle (N s / m);

$m_g$  is the total mass of the driver and seat (kg);

$k_s$  is the elastic stiffness of the seat (N / m);

$c_s$  is the kinematic viscosity coefficient of the seat (N s / m)

$L_s$  is the distance of the driver from the center of gravity of the rigid rod (m);

In this way, it is possible to derive the vertical displacements in the driver's time domain and by deriving twice with respect to time, the vertical acceleration that the driver undergoes is obtained.

### **B.3.2 Comparison between the 5 dof model and the decoupled 4 + 1 dof**

In this work, the different results were compared between the model in which the driver is coupled to the half-car model (studied as a 5-degree-of-freedom model) and the result of the decoupled model (in which the 4-degree model is first solved. of freedom (half-car) then the one degree of freedom model is solved with the output).

To evaluate the differences between the two approaches, two different cars (belonging to segments A and E) were used on a parabolic bump (12 feet in length and 3 inches in height) and a trapezoidal bump (22 feet in length and 3 inches in height). height).

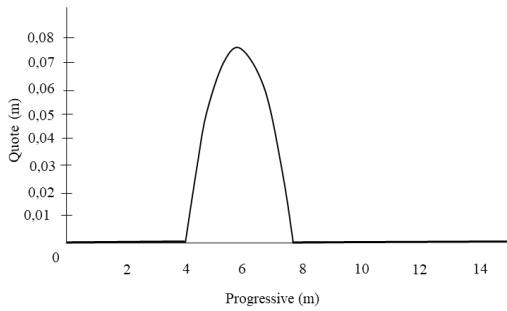


Figure B. 27 Speed hump (12 fett, 13 inch)

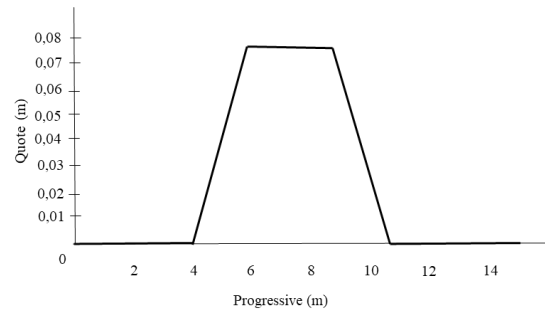


Figure B.28 Speed table (22 feet, 3 inch)

Below are the tables (V-RMS) and (V-eVDV) and the respective diagrams in which the RMS and eVDV values will be compared as the speed varies in a range between 0 km/h and 60 km/h for one type of vehicle with the coupled and uncoupled system. The fourth column shows the difference in absolute terms between the two approaches. In the tables and graphs, the values referring to the coupled model will be indicated with 5 while the values referring to the decoupled model will be indicated with 4 + 1.

**Vehicle A on parabolic profile**

Speed	RMS 5	RMS 4 + 1	%
5	0.01806	0.01859	2.854386
10	0.062699	0.074848	16.23113
15	0.095435	0.185764	48.62598
20	0.154671	0.258177	40.09099
25	0.241654	0.285548	15.3716
30	0.331264	0.350528	5.495703
35	0.419579	0.44925	6.604535
40	0.443006	0.486668	8.971724
45	0.523131	0.583491	10.34461
50	0.521649	0.583628	10.6196
55	0.572794	0.648268	11.64232
60	0.588158	0.642141	8.406646

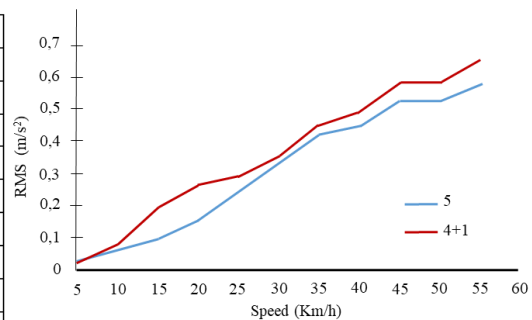


Figure B. 29 RMS comparison between coupled and decoupled approaches

Speed	eVDV 5	eVDV 4 + 1	%
5	0.032432	0.032115	0.975238
10	0.112595	0.131264	14.22256
15	0.157861	0.321575	50.91003
20	0.259622	0.431077	39.77372
25	0.40442	0.459297	11.94808
30	0.548292	0.564011	2.787066
35	0.690285	0.727047	5.056379
40	0.724237	0.788791	8.183917
45	0.848879	0.943661	10.04406
50	0.826654	0.932682	11.3681
55	0.881628	1.015002	13.14029
60	0.899371	0.989082	9.070204

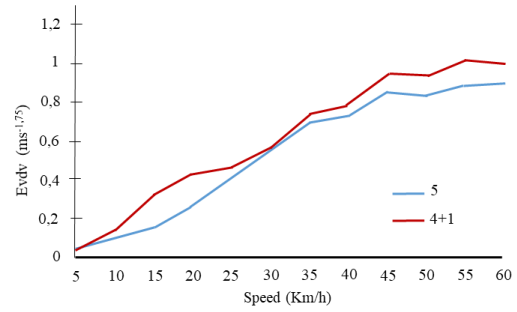


Figure B. 30 eVDV comparison between coupled and decoupled approaches

**Vehicle A on trapezoidal profile:**

Speed	RMS 5	RMS 4 + 1	%
5	0.01258	0.014665	14.22002
10	0.052206	0.051438	1.470782
15	0.089093	0.126901	29.79298
20	0.137171	0.160418	14.49167
25	0.219281	0.206383	5.881768
30	0.331242	0.328417	0.852813
35	0.457776	0.496712	7.838772
40	0.523941	0.601343	12.87159
45	0.650021	0.769658	15.54427
50	0.685204	0.820982	16.5384
55	0.799839	0.972367	17.74307
60	0.822625	0.979805	16.04199

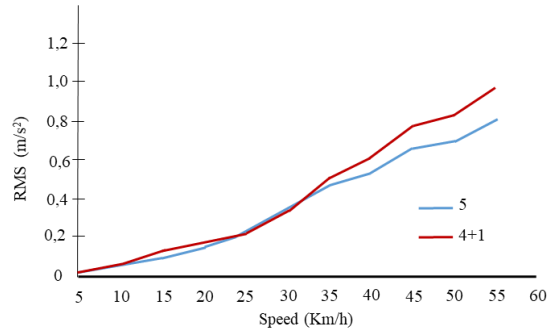


Figure B. 31 RMS comparison between coupled and decoupled approaches

Speed	eVDV 5	eVDV 4 + 1	%
5	0.021526	0.027202	20.86558
10	0.098918	0.098136	0.790688
15	0.158044	0.231152	31.62764
20	0.230447	0.278832	17.35281
25	0.369664	0.350513	5.180534
30	0.568492	0.549654	3.313602
35	0.77898	0.835716	6.788905
40	0.885896	1.007836	12.09921
45	1.072339	1.268914	15.49162
50	1.098704	1.322708	16.93523
55	1.25856	1.535031	18.0108
60	1.275302	1.512571	15.68648

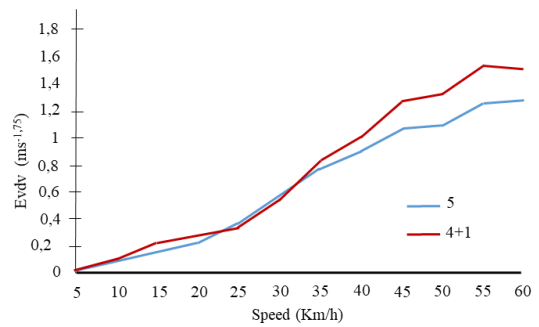


Figure B. 32 eVDV comparison between coupled and decoupled approaches

**Vehicle E on parabolic profile:**

Speed	RMS 5	RMS 4 + 1	%
5	0.014867	0.014762	0.701493
10	0.081682	0.07416	9.208774
15	0.162298	0.170476	4.796678
20	0.213442	0.215428	0.921924
25	0.251655	0.216777	13.85932
30	0.286999	0.232505	18.98764
35	0.326721	0.278264	14.83131
40	0.328173	0.299585	8.711331
45	0.380675	0.36024	5.368207
50	0.377486	0.368367	2.415546
55	0.417948	0.422143	0.993892
60	0.426839	0.417848	2.106327

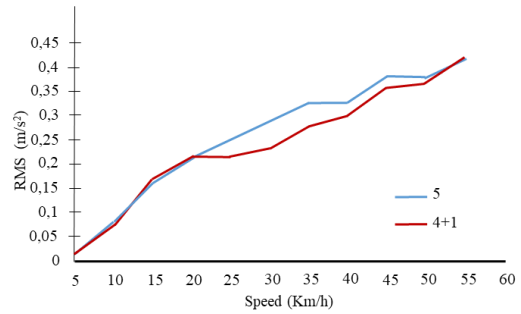


Figure B. 33 RMS comparison between coupled and decoupled approaches

Speed	eVDV 5	eVDV 4 + 1	%
5	0.024392	0.025737	5.224521
10	0.153848	0.134227	12.75331
15	0.295007	0.296014	0.340019
20	0.377164	0.359859	4.588163
25	0.436619	0.357825	18.04641
30	0.490982	0.373204	23.9883
35	0.552263	0.44027	20.27892
40	0.545249	0.468105	14.14842
45	0.615377	0.557019	9.48318
50	0.604525	0.563234	6.830362
55	0.657783	0.643249	2.209481
60	0.65624	0.634177	3.36203

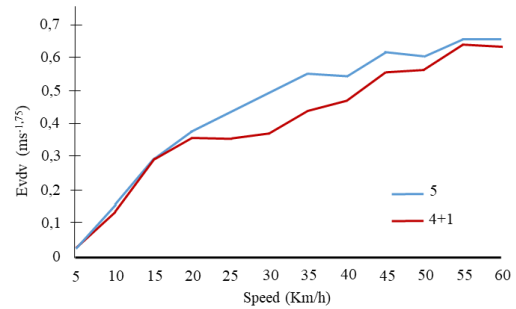


Figure B. 34 eVDV comparison between coupled and decoupled approaches

**Vehicle E on trapezoidal profile:**

Speed	RMS 5	RMS 4 + 1	%
5	0.012851	0.013336	3.643059
10	0.079599	0.075655	4.955444
15	0.132203	0.156289	15.41167
20	0.174427	0.1791	2.608851
25	0.216608	0.182017	15.96948
30	0.281886	0.242517	13.96621
35	0.364862	0.337505	7.498048
40	0.40399	0.395512	2.098409
45	0.491702	0.500824	1.821418
50	0.515668	0.533547	3.351048
55	0.604182	0.632913	4.539389
60	0.622748	0.647236	3.783486

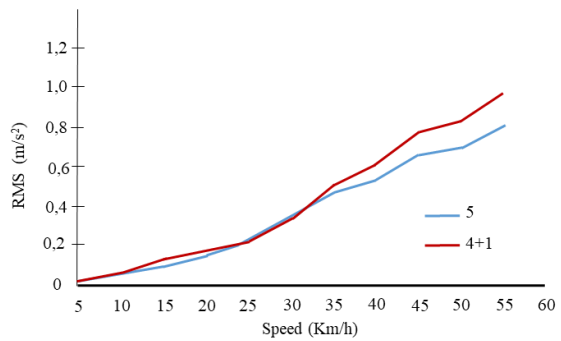


Figure B. 35 RMS comparison between coupled and decoupled approaches

Speed	eVDV 5	eVDV 4 + 1	%
5	0.02199	0.024045	8.544972
10	0.155163	0.147474	4.955444
15	0.242702	0.285514	14.99463
20	0.31386	0.318039	1.314223
25	0.382079	0.317424	16.92189
30	0.494358	0.414773	16.0986
35	0.639476	0.574048	10.23153
40	0.683368	0.663014	2.978418
45	0.810318	0.800901	1.162138
50	0.834029	0.845137	1.314349
55	0.953022	0.994261	4.147667
60	0.959996	0.998965	3.900943

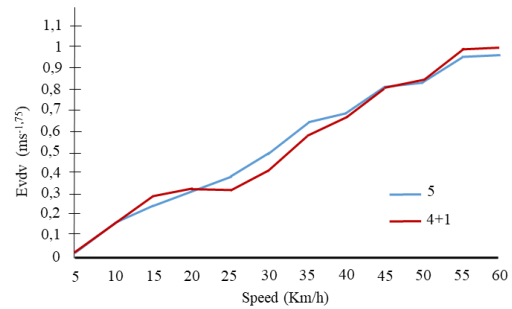


Figure B. 36 eVDV comparison between coupled and decoupled approaches

It is noted that the difference between the two approaches for each vehicle on each bump is minimal, in percentage terms, there is a difference of about 10%. It is observed that the results concerning vehicle A in the decoupled model give greater results, both in terms of RMS and eVDV, compared to the coupled model, this discrepancy increases with increasing speed. By analyzing vehicle E, however, it can be seen that the maximum discrepancy occurs in a speed range between 20 km/h and 35 km/h. However, compared to vehicle A, the greatest results are observed from the coupled model. Therefore it can be concluded that the two methods give different albeit comparable results for each type of vehicle.

There has also been an interest in evaluating the differences between the two methods, rather than in terms of RMS and eVDV, in the frequency-acceleration (f-acceleration) diagrams. As an example, only a few graphs are shown for each type of vehicle:

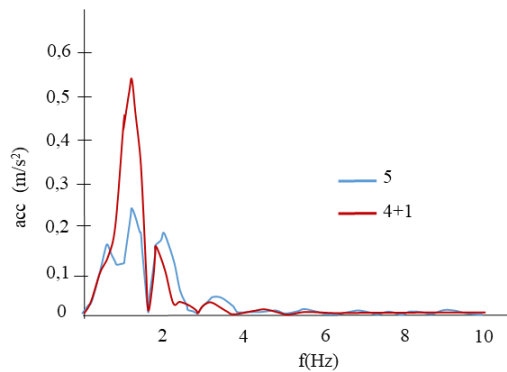


Figure B. 37 Accelerations in the frequency domain for vehicle A on a parabolic bump at 15 km/h

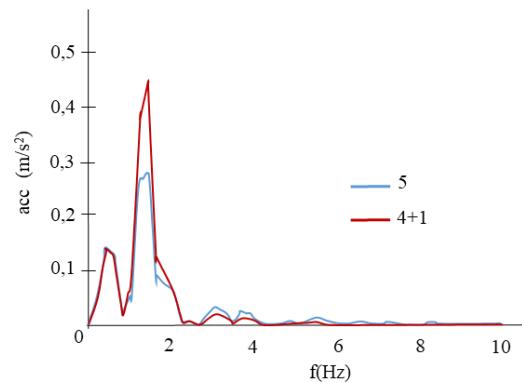


Figure B. 38 accelerations in the frequency domain for vehicle A over a trapezoidal bump at 15 km/h

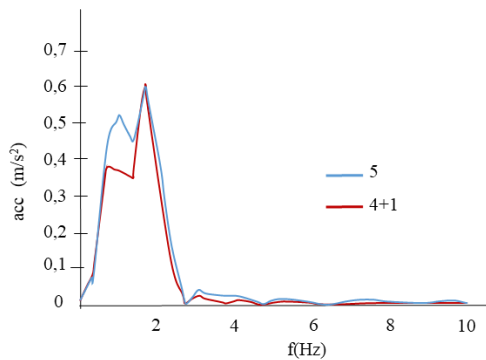


Figure B. 39 Accelerations in the frequency domain for vehicle E over a parabolic bump at 25 km/h

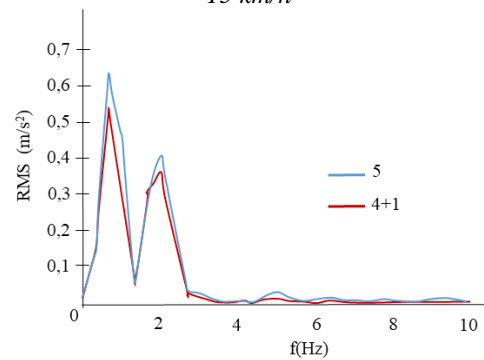


Figure B. 40 Accelerations in the frequency domain for vehicle E over a trapezoidal bump at 25 km/h

From these graphs it can be observed that the shape is qualitatively similar in both models, changing the values of R.M.S results in peaks falling in the same frequencies.

## References

- Carver, A., Salmon, J., Campbell, K., Garnett, S., Baur, L., & Crawford, D. 2005. Perceptions of the local neighborhood and walking and cycling among adolescents. *Am. J Health Promot.* 20, 139–147.
- Carver, A., Timperio, A., Hesketh, K., & Crawford, D. 2010. Are children and adolescents less active if parents restrict their physical activity and active transport due to perceived risk? *Social Sci. Med.* 70 (11), 1799–1805.
- Chataway, E., Kaplan, S., Nielsen, T., & Prato, C. 2014. Safety perceptions and reported behavior related to cycling in mixed traffic: a comparison between Brisbane and Copenhagen. *Transp. Res. Part F: Traffic Psychol. Behav.* 23, 32–43.

- Christie, N., Kimberlee, R., Towner, E., Rodgers, S., Ward, H., Sloney, J., & al., e. 2011. Children aged 9-14 living in disadvantaged areas in England: opportunities and barriers for cycling. *J. Transp. Geogr.* 19 (4), 943–949.
- Collarte, N. 2012. The Woonerf Concept “Rethinking a Residential Street in Somerville”. Master of Arts in Urban and Environmental Policy and Planning | Tufts University.
- De Pauw, E., Daniels, S., Thierie, M., & Brijs, T. 2014. Safety effects of reducing the speed limit from 90km/h to 70km/h. *Accid. Anal. Prev.* 62, 426–431.
- Harwood, D. 1993. Use of Rumble Strips to Enhance Safety. NCHRP Synthesis of Highway Practice 191, Transportation Research Board, Washington, DC.
- Lamera, G. 2000. Tratto da Accessibilità e sicurezza sulle strade: [www.digilander.iol.it/progetti2000](http://www.digilander.iol.it/progetti2000)
- Layfield, R. 1998. The effectiveness of speed cushions as traffic calming devices. TRL (Transport Research Laboratory, PTRC P381 (UK).
- Lorenc, T., Brunton, G., Oliver, S., Oliver, K., & Oakley, A. 2008. Attitudes to walking and cycling among children, young people and parents: a systematic review. *J. Epidemiol. Community Health* 62 (10), 852–857.
- Mertens, L., Compennolle, S., Gheysen, F., Deforche, B., Brug, J., Mackenbach, J., & al., e. 2016. Perceived environmental correlates of cycling for transport among adults in five regions of Europe. *Obes. Rev.* 17, 53–61.
- Pooley, C., Horton, D., Scheldeman, G., Mullen, C., Jones, T., Tight, M., & al., 2013. Policies for promoting walking and cycling in England: a view from the street. *Transp. Policy* 27, 66–72.
- Timperio, A., Ball, K., Salmon, J., Roberts, R., Giles-Corti, B., Simmons, D., & al. 2006. Personal, family, social, and environmental correlates of active commuting to school. *Am. J. Prev. Med.* 30 (1), 45–51.
- Traffic Manual. (s.d.). Bureau of Traffic Management. City of Portland, Oregon (USA).
- UNI EN 1463. 1998. “Prestazioni della segnaletica orizzontale per gli utenti della strada”. Ente Italiano di Normazione.
- Washington, S., Hawort, N., & Schramm, A. 2012. Relationships between self-reported bicycling injuries and perceived risk of cyclists in Queensland. *Transp. Res. Rec.: J. Transp. Res. Board* 2314 (1), Australia, 57–65.

